Vol. 181, March 31, 1986
Complete in one issue

ISSN 0003-2670

ANALYTICA CHIMICA ACTA

International journal devoted to all branches of analytical chemistry

ELSEVIER

ANALYTICA CHIMICA ACTA

International journal devoted to all branches of analytical chemistry
Revue internationale consacrée à tous les domaines de la chimie analytique
Internationale Zeitschrift für alle Gebiete der analytischen Chemie

PUBLICATION SCHEDULE FOR 1986

	J	F	M	A	M	J	J	A	S	O	N	D
Analytica Chimica Acta	179	180	181	182 183/1	183/2 184	185	186	187	188	189	190	191

Scope. *Analytica Chimica Acta* publishes original papers, short communications, and reviews dealing with every aspect of modern chemical analysis both fundamental and applied.

Submission of Papers. Manuscripts (three copies) should be submitted as designated below for rapid and efficient handling:

Papers from the Americas to: Professor Harry L. Pardue, Department of Chemistry, Purdue University, West Lafayette, IN 47907, U.S.A.

Papers from all other countries to: Dr. A. M. G. Macdonald, Department of Chemistry, The University, P.O. Box 363, Birmingham B15 2TT, England. Papers dealing particularly with computer techniques to: Professor J. T. Clerc, Universität Bern, Pharmazeutisches Institut, Baltzerstrasse 5, CH-3012 Bern, Switzerland.

Submission of an article is understood to imply that the article is original and unpublished and is not being considered for publication elsewhere. Upon acceptance of an article by the journal, authors will be asked to transfer the copyright of the article to the publisher. This transfer will ensure the widest possible dissemination of information.

Information for Authors. Papers in English, French and German are published. There are no page charges. Manuscripts should conform in layout and style to the papers published in this Volume. Authors should consult Vol. 170 for detailed information. Reprints of this information are available from the Editors or from: Elsevier Editorial Services Ltd., Mayfield House, 256 Banbury Road, Oxford OX2 7DH (Great Britain).

Reprints. Fifty reprints will be supplied free of charge. Additional reprints (minimum 100) can be ordered. An order form containing price quotations will be sent to the authors together with the proofs of their article.

Advertisements. Advertisement rates are available from the publisher.

Subscriptions. Subscriptions should be sent to: Elsevier Science Publishers B.V., Journals Department, P.O. Box 211, 1000 AE Amsterdam, The Netherlands. Tel: 5803 911, Telex: 18582.

Publication. *Analytica Chimica Acta* appears in 13 volumes in 1986. The subscription for 1986 (Vols. 179–191) is Dfl. 2730.00 plus Dfl. 312.00 (p.p.h.) (total approx. US $1126.70). All earlier volumes (Vols. 1–178) except Vols. 23 and 28 are available at Dfl. 231.00 (US $85.56), plus Dfl. 15.00 (US $5.56) p.p.h., per volume.

Our p.p.h. (postage, packing and handling) charge includes surface delivery of all issues, except to subscribers in the U.S.A., Canada, Japan, Australia, New Zealand, P.R. China, India, Israel, South Africa, Malaysia, Thailand, Singapore, South Korea, Taiwan, Pakistan, Hong Kong, Brazil, Argentina and Mexico, who receive all issues by air delivery (S.A.L. — Surface Air Lifted) at no extra cost. For the rest of the world, airmail and S.A.L. charges are available upon request.

Claims for issues not received should be made within three months of publication of the issues. If not they cannot be honoured free of charge.

For further information, or a free sample copy of this or any other Elsevier Science Publishers journal, readers in the U.S.A. and Canada can contact the following address: Elsevier Science Publishing Co. Inc., Journal Information Center, 52 Vanderbilt Avenue, New York, NY 10017, U.S.A., Tel: (212) 916-1250.

0003-2670/86/$03.50

Printed in The Netherlands

ANALYTICA CHIMICA ACTA
VOL. 181 (1986)

ANALYTICA CHIMICA ACTA

International journal devoted to all branches of analytical chemistry

ELSEVIER Amsterdam–Oxford–New York–Tokyo

Anal. Chim. Acta, Vol. 181 (1986)

0003-2670/86/$03.50

Printed in The Netherlands

Analytica Chimica Acta, 181 (1986) 1—26
Elsevier Science Publishers B.V., Amsterdam — Printed in The Netherlands

Review

THE KALMAN FILTER IN ANALYTICAL CHEMISTRY

STEVEN D. BROWN[a]

Department of Chemistry, Washington State University, Pullman, WA 99164-4630 (U.S.A.)

(Received 9th July 1985)

SUMMARY

During the past ten years, the means by which more information can be extracted from experimental data have become an important area of research in analytical chemistry. Digital filters have been demonstrated to have a number of applications to analytical problems. These techniques typically involve a least-squares fit of experimental data to some model of the process being filtered. One method for filtering experimental data is based on the Kalman filter, a recursive, linear digital filter first developed for use in navigation, but now used in many fields. This paper discusses the implementation of Kalman filters in analytical chemistry. The principles of state-space digital filtering are reviewed, and the development of state/space models is discussed. Discussion is focused on the discrete Kalman algorithms. Two examples are provided to demonstrate the operation of the discrete Kalman filtering algorithm. Similarities between Kalman filtering and weighted least-squares methods are considered, and the specific advantages and disadvantages of linear and nonlinear Kalman filtering approaches are evaluated. To illustrate the range of problems which benefit from use of the filter, a comprehensive literature survey of the application of Kalman filtering to chemical problems is provided.

The availability of low-cost, high-performance computers is prompting analytical chemists to reconsider the ways in which they examine data. Instrumental responses are now routinely available in digital form, which simplifies application of techniques such as background subtraction, Fourier-domain noise removal and peak integration. One data-analysis technique which is ideally suited to use with a small, high-performance computer is the Kalman filter. This digital filtering technique, first reported in 1960 [1], has been used extensively in fields such as navigation and hydrology, in which its ability to extract parameters from noisy data and to model complex systems is well established [2, 3]. Over the past ten years, several research groups have taken advantage of the unusual properties of the Kalman filter to solve problems in analytical chemistry. Despite its increasing use, however, the filter is not well recognized. This paper provides background on filtering con-

[a]Present Address: Department of Chemistry, University of Delaware, Newark, DE 19716, U.S.A.

0003-2670/86/$03.50

cepts necessary to the understanding of the properties of the Kalman filter, introduces one form of the filter and reviews applications of the filter in analytical chemistry. Papers in print prior to October, 1985 are included in this review.

FILTERING IN THE TIME AND FREQUENCY DOMAINS

Many modern digital filters are described in "state-space notation". To explain this notation, and to define some concepts essential to a clear understanding of the Kalman filter, a brief overview of filtering is necessary.

The purpose of filtering is to separate one component of a signal from another. Generally, filtering is done to reduce the effects of noise while minimizing the distortion of those characteristics of the signal that contain the desired information, such as peak shape or peak height. Electrical filters, for example, are often specified to pass signals of a given frequency range, while rejecting signals outside that range. This specification is convenient for removal of signal components traditionally considered as noise, as these components are often also specified in terms of their frequency characteristics. The frequency-domain formulation analyzes filters in terms of integral equations involving continuous or discrete Laplace and Fourier transforms [4, 5]. Filters described in this manner can be either analog or digital.

The concept of "filtering" is far from new in chemistry. Most chemists are familiar with frequency-domain descriptions of active or passive RC electrical filters based on resistors and capacitors, and used for the removal of electrical noise from some instrumental signal [6]. The introduction of the Savitzky-Golay polynomial digital filter [7, 8] and the Fourier filter [9] demonstrated the feasibility as well as the advantages of improving (smoothing) data in a computer rather than in some analog network. Like RC analog filters, these digital filters are often described in the frequency domain [6—9]. More recently, it has been recognized that filtering methods may be useful in many areas of analytical chemistry besides the removal of noise from some signal. Many of these applications are based on the special properties of the Kalman filter, a time-domain-based digital filter. For example, it is possible to compensate for drift in an instrumental response, to provide rapid separation of overlapping responses, to decide how and when to measure some response, and to remove extraneous components from some instrumental response by using time-domain filtering. These filtering methods can also be used to evaluate the quality of models describing chemical processes.

State-space notation

Responses generated by analytical instrumentation are generally some sort of data sequence in the time domain. Filters for these time series are best described in time domain as well; in many cases, description of these filters in the frequency domain is difficult or impossible. Filtering in the time domain is most often described in terms of differential or difference equations,

instead of equations based on the continuous or discrete integral transforms which are used in the commoner frequency-domain approaches. Time-domain approaches have evolved a specialized terminology; much of that terminology is used in this review, so that the interested reader may continue easily with some of the extensive literature on Kalman filtering. The problem being studied is called the "system". Mathematical description of this system in a time-domain "state-space" offers a number of mathematical and notational advantages over the frequency-domain approach [10, 11]. One is the ability to take the past behavior of the system into account. In the integral transform description of a filter, the initial conditions must be zero, and the filter equations yield only the immediate response of the system to some input, essentially an "input/output" description, without any effects caused by memory of the past behavior. By incorporating non-zero initial conditions, the past history of the system can be specifically included in the filter design. Other advantages include the explicit incorporation of time-dependent variables in the system model and the ability to provide for modelling of multiple inputs and outputs in a systematic fashion.

An important concept in state-space modelling is the definition of a state. Any set of variables which defines the past history of a system is said to be a state for the system. More precisely, the state of a system at some time, t_0, is the amount of information at t_0, which, together with the input (if any) at t_0, uniquely determines the output for all times $t > t_0$. The choice of state variables is arbitrary; because any set can be converted to another set by a linear transformation, any set of quantities sufficient to describe completely the dynamics of the system is satisfactory. A state vector, $\mathbf{X}$, can be represented by one or more artificial functions; it need not contain state variables which are experimentally observable, or even ones which are constant over time, but it must predict accurately the temporal behavior of the process being filtered. The number of state variables needed fully to describe a system is called the order of a system; if a system is described by an Nth order difference equation, N independent initial conditions are needed completely to define the output of the system, and there must be N state variables in the state vector [10].

In the time domain, filtering of an instrumental response, and the related processes of smoothing and prediction, can be represented as illustrated in Fig. 1. The general notation for time-domain estimation is $\hat{X}(k|j)$, where X is the quantity to be estimated and where k and j are indices which indicate at which point in time the estimate is being made, and how much of the data is being used to make the estimate, respectively. The superscript $\hat{}$ is used to indicate an estimated quantity. Filtering makes use of all prior information available for the system, as well as the present information obtained from a measurement, to generate a filtered response for each measurement as the signal evolves in time. This is indicated by the notation $\hat{X}(k|k)$, because all data obtained up through measurement k ($j = k$) are used to estimate X at point k. This is sometimes called an a posteriori estimate, because data

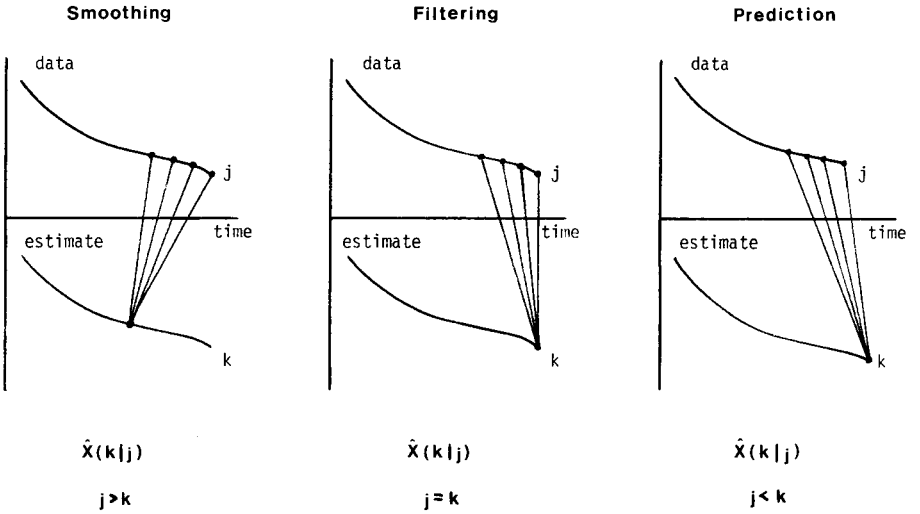

Fig. 1. Smoothing, filtering and prediction in the time domain.

obtained at point k are used to estimate a filtered quantity at point k, making the estimate "after the fact" of the measurement. Prediction uses information available up through measurement j to predict the outcome of the measurement which will be made at k, where $j < k$. If the value for j happens to be 1 less than k, the notation is $\hat{X}(k|k-1)$, signifying a "one-step-ahead" prediction of the measurement to be made at point k. Such a prediction is called an a priori estimate, because the estimate is made before the measurement. Filtering and prediction are quite closely related, and both are often used in digital "filters". Smoothing involves a very different approach; all available data are used to obtain estimates for quantities at each point where data were collected. In this case, $j > k$ in the expression $\hat{X}(k|j)$. While smoothing can also involve a digital filter, application of the digital filter is delayed until the experiment is complete. Both filtering and prediction can be done "on-line", while data are being collected. Smoothing is done off-line, however, as all data are used to improve the estimate for each state [6—12].

Filter weighting

A key element in the design of a digital filter is the weighting function used to evaluate how much emphasis should be given to current data, and how much to prior data. Linear filters use weighted linear combinations of past and present data to filter the current measurement. Weights need not be constant but can vary with the amount of data available for use in the filter. These weights are often chosen to minimize a "cost function" given by the average squared difference between the filter estimates for a signal and the true value for that signal. Filters using this weighting scheme are called minimum variance estimators, for reasons discussed below. It is also possible to design filters to minimize other cost functions [10—12].

One way to generate the time-dependent weighting function is to compute new weights for all previous data each time a new measurement becomes available. This approach becomes difficult as the number of data processed by the filter becomes large. A simple example illustrates this. Suppose that it is necessary to obtain the average of a stream of data, X_i, where $i = 1, 2, 3 \ldots n$. An obvious approach involves acquiring the data, then calculating the mean as usual, and doing this each time new data are acquired. In essence, an estimate is obtained for some true mean by recalculating the expression for the mean of n measurements, $\hat{m}_n$, where

$$\hat{m}_n = 1/n[X_1 + X_2 + X_3 + \ldots + X_n] \tag{1}$$

each time a new measurement X becomes available. Clearly, the weighting function $1/n$ changes as n increases.

An alternative approach is available, however. Equation 1 can be written as

$$\hat{m}_n = 1/n \sum_{i=1}^{n} X_i = 1/n \sum_{i=1}^{n-1} X_i + 1/nX_n \tag{2}$$

or, after rearranging,

$$\hat{m}_n = (n - 1/n)\hat{m}_{n-1} + (1/n)X_n \tag{3}$$

In Eqn. 3, the new estimate for the mean is obtained from the old estimate (obtained on the $n - 1$ data values previously available) as modified by information provided by the new data, which is weighted by the value $1/n$. Both approaches represent simple, linear filters for estimating the mean of a set of noisy measurements. There are some important differences, however. The first filter "algorithm", as it might be called, requires storage of the estimated value of m as well as all the n values of X, and it requires $n!$ additions, and n divisions. Requirements for the second algorithm are quite different: 2 storage locations (one for $\hat{m}$ and one for X_n), n additions, $2n$ multiplications and $2n$ divisions. Clearly, the second algorithm is more efficient than the first, however, because no redundant computations are needed, and the second approach can be continued ad infinitum without a growing data-storage problem. The second algorithm uses a recursive mode of operation. The key to the recursive method is the use of the results of a previous calculation step to aid in the evaluation of results for the present step. Like the first algorithm, it filters a data stream with use of weighting functions. In both cases, the weight given to new data decreases as n increases. Unlike the first algorithm, however, the second algorithm requires an initial guess for m_{n-1} to start the calculation (when $n = 1$); such a requirement is typical of all recursive calculations. From this example, it should be apparent that a recursive calculation of filter weights offers a number of advantages over other approaches; this recursive calculation of filter weights is one of the characteristics of the Kalman filter, serving to distinguish it from other state-space filters, such as the Wiener filter, in which weighting functions must be precomputed [10].

THE KALMAN FILTER

The Kalman filter algorithm is a series of equations that solve the general, linear filtering problem in state-space. There are many versions of the Kalman filter, each differing in the details of the actual calculations done, or in the assumptions made [10—13]. Several mathematically rigorous introductions which cover various forms of the Kalman filter are available in the engineering literature (e.g., [14]). In this introduction, only one form of the filter is discussed in detail, namely the discrete filter algorithm first given by Kalman [1]. For discussion of other discrete Kalman filter algorithms or continuous Kalman filter algorithms, see [11—13]. All versions of the filter use a linear "model" of the system, which is constructed of state variables as described below, along with a sequence of weighted measurements made on the system, to obtain improved (filtered) estimates for the state variables. The various versions of the Kalman filter differ in the way they perform the weighting and propagation calculations. Most discussions of the Kalman filter, including this one, present it in terms of time as the discrete, independent variable, but any convenient parameter can be used, provided that certain noise restrictions are satisfied. For example, the data and state variables might be in terms of potential or wavelength, instead of time.

Discrete-time models

The development of a system model is probably the most important step in Kalman filtering. The model is essentially a mathematical representation of the system being studied. The discrete Kalman filter requires a linear, discrete model. The system being modelled might be naturally discrete, as in the example above. Otherwise, it is necessary to use a system which is obtained from sampling of some other, continuous system, as when analog data are converted to digital form. The system modelled in the filter could also be a linearized version of a more complex, nonlinear system, as discussed below.

Regardless of how the system represented by the model in the Kalman filter comes to be linear and discrete, state-space notation requires that the same general form be used. Two difference equations given in terms of a vector containing the filter states describe the model. One defining equation for the model is the system dynamics equation, which describes the time dependence of the states of the filter. For a linear system which is observed at the discrete point in time, t_k, $k = 1, 2, 3, \ldots$, the system dynamics are described by the vector difference equation given by Eqn. 4 in Table 1. (All the symbols used are defined in Table 2.) In Eqn. 4, $\mathbf{X}(k)$ is the $n \times 1$ system state vector at time t_k. The system state vector $\mathbf{X}$ contains the state variables; these are the quantities which will be estimated ("filtered") through the application of the Kalman filter to the system data. The quantity, $\mathbf{F}$, is an $n \times n$ matrix, called the system dynamics matrix, which describes the time dependence of the model states in the absence of any external, noisy input. By connecting $\mathbf{X}$ at time, t_{k-1}, to $\mathbf{X}$ at time t_k, it provides a route by which

TABLE 1

The linear, discrete Kalman filter algorithm

System dynamics:	$\mathbf{X}(k) = \mathbf{F}(k, k-1)\mathbf{X}(k-1) + \mathbf{G}(k-1)\mathbf{w}(k-1)$	(4)
Measurement model:	$\mathbf{Z}(k) = \mathbf{H}(k)\mathbf{X}(k) + \mathbf{v}(k)$ (vector form)	(5)
	$Z(k) = \mathbf{H}^T(k)\mathbf{X}(k) + v(k)$ (scalar form)	(6)
Noise assumptions:	$E[\mathbf{w}(k)\mathbf{w}(j)^T] = \mathbf{Q}^{\delta}jk$	(7A)
	$E[\mathbf{v}(k)\mathbf{v}(j)^T] = \mathbf{R}^{\delta}jk$	(7B)
Initial conditions:	$E[\mathbf{X}(0)] = \mathbf{X}_0$	(8A)
	$E[(\mathbf{X}(0) - \mathbf{X}_0)(\mathbf{X}(0) - \mathbf{X}_0)^T] = \mathbf{P}_0$	(8B)
Other assumptions:	$E[\mathbf{w}(k)\mathbf{v}(j)^T] = 0$ for all j, k	(9)
State estimate extrapolation:	$\mathbf{X}(k\|k-1) = \mathbf{F}(k, k-1)\mathbf{X}(k-1\|k-1)$	(10)
Error covariance extrapolation:	$\mathbf{P}(k\|k-1) = \mathbf{F}(k, k-1)\mathbf{P}(k-1\|k-1)\mathbf{F}(k, k-1)^T + \mathbf{G}(k-1)\mathbf{Q}(k-1)\mathbf{G}(k-1)^T$	(11)
State estimate update:	$\mathbf{X}(k\|k) = \mathbf{X}(k\|k-1) + \mathbf{K}(k)[\mathbf{Z}(k) - \mathbf{H}(k)\mathbf{X}(k\|k-1)]$	(12)
Error covariance update:	$\mathbf{P}(k\|k) = [\mathbf{I} - \mathbf{K}(k)\mathbf{H}(k)]\mathbf{P}(k\|k-1)$	(13)
Kalman gain matrix:	$\mathbf{K}(k) = \mathbf{P}(k\|k-1)\mathbf{H}^T(k)[\mathbf{H}(k)\mathbf{P}(k\|k-1)\mathbf{H}^T(k) + \mathbf{R}(k)]^{-1}$	(14)

a one-step-ahead prediction of the state vector, from t_{k-1} to t_k, is accomplished. Because this matrix can be time-dependent, it is written as a function of the two times involved. The $n \times 1$ vector $\mathbf{w}(k-1)$ contains random noise, sometimes called modelling noise. The effect of this modelling noise on the propagation of the state vector from t_{k-1} to t_k is given by the $n \times n$ matrix, G. The product $\mathbf{G}(k-1)\mathbf{w}(k-1)$ provides a way to add a random component to the manner in which the state vector changes over time. Because random fluctuations are allowed (but not required) in the dynamics of the model, it is called stochastic. Models with a predictable (nonrandom) behavior with time are called deterministic, because knowledge of states at one time implies that the states can be determined at all other times.

The second defining vector difference equation for the filter model relates the state vector to the observable (measurable) $m \times 1$ vector quantity, Z. This equation, called the measurement model, is given as Eqn. 5 in Table 1. There, $\mathbf{H}(k)$ is an $m \times n$ matrix, and $\mathbf{v}(k)$ is an $m \times 1$ vector. The matrix H is called the observation matrix because it relates the filter model states to the observable quantities Z at some time t_k. The vector, v, describes the measurement noise present in Z. Because the measurement model structure anticipates data in vector form, accommodating simultaneous data from multiple

TABLE 2

Symbols used in the Kalman filter equations

Symbol	Type	Function
$\mathbf{f}(k, k-1)$	$n \times n$ matrix	system dynamics matrix (nonlinear filter)
$\mathbf{F}(\mathbf{X}(k-1), k-1)$	$n \times n$ matrix	system dynamics matrix (linearized form of **f**)
$\mathbf{F}(k, k-1)$	$n \times n$ matrix	system dynamics matrix (linear filter)
$\mathbf{G}(k-1)$	$n \times n$ matrix	system noise matrix
$\mathbf{h}(k)$	$n \times n$ matrix	observation matrix (nonlinear filter)
$\mathbf{H}(\mathbf{X}(k\|k-1)$	$n \times n$ matrix	observation matrix (linearized form of **h**)
$\mathbf{H}(k)$	$n \times n$ matrix	observation matrix (linear filter)
$\mathbf{I}$	$n \times n$ matrix	identity matrix
$\mathbf{K}(k)$	$n \times n$ matrix	Kalman gain matrix
k	scalar	index for discrete time
$\mathbf{P}(k\|k-1)$	$n \times n$ matrix	estimated covariance matrix (a priori estimate)
$\mathbf{P}(k\|k)$	$n \times n$ matrix	estimated covariance matrix (a posteriori estimate)
$\mathbf{P}_0$	$n \times n$ matrix	initial guess for **P**
$\mathbf{Q}$	$n \times n$ matrix	covariance of model noise
$\mathbf{R}$	$n \times n$ matrix	covariance of measurement noise
$\mathbf{v}(k)$	$n \times 1$ vector	noise in measurement
$\mathbf{w}(k)$	$n \times 1$ vector	noise in system model
$\mathbf{X}(k\|k-1)$	$n \times 1$ vector	estimated filter state vector (a priori estimate)
$\mathbf{X}(k\|k)$	$n \times 1$ vector	estimated filter state vector (a posteriori estimate)
$\mathbf{X}_0$	$n \times 1$ vector	initial guess for **X**
$\mathbf{Z}(k)$	$n \times 1$ vector	measurement
$\nu(k)$	$n \times 1$ vector	innovation sequence vector
Operations		
$\mathbf{X}^T$	transpose of vector **X**	
$\mathbf{H}^{-1}$	inverse of matrix **H**	
$E[\ldots]$	expectation value	
δ_{ij}	Kronecker delta (1 when $i = j$, 0 when $i \neq j$)	

sensors, or from multidimensional data sets is straightforward. Single measurements are also easily handled. In that case, the measurement model reduces to Eqn. 6 in Table 1, where $\mathbf{H}^T(k)$ is a row vector ($1 \times n$), and $\mathbf{v}(k)$ is a scalar. The definitions of all symbols and operations are collected in Table 2.

The properties of the noise sequences, $\mathbf{w}(k)$ and $\mathbf{v}(k)$, are especially important to the proper operation of the Kalman filter. Both noise processes are assumed to be independent, white-noise sequences, each with zero mean. The second-order statistics for these processes are given as Eqns. 7A and 7B in Table 1. The matrix quantities, **Q** and **R**, contain the variances of the modelling and the measurement noise, respectively. The noise assumptions insure that the estimated quantitites obtained from the filter will be statisti-

cally unbiased. If, in fact, the noise sequences which occur in the filter are found to meet these assumptions, the resulting minimum variance estimates obtained from the Kalman filter are guaranteed to be optimal, in that no other linear estimator can be expected to produce estimates with smaller variances. It is possible that some other, nonlinear estimator may produce estimates with smaller variances, however. When, in addition to the requirements listed above, the noise sequences **w** and **v** are found to have a Gaussian distribution, the resulting minimum variance estimates obtained from the Kalman filter are the best possible estimates; in this case, no other estimator, linear or nonlinear, can produce estimates with smaller variances [10—13]. For this reason, Kalman filtering is sometimes called optimal filtering.

Most of the noise requirements given above pose little problem in applying the Kalman filter. In analytical chemistry, the term $\mathbf{G}(k-1)\mathbf{w}(k-1)$ in Eqn. 4, can be taken as zero because most of the dynamic models used in chemistry are deterministic, and not random, except on a molecular level; these random contributions are too small to be important in most work. For a deterministic model, **Q**, **w** and **G** are all zero. Random fluctuations occur in the measurement process, however, and the measurement noise sequence, **v**, cannot be similarly neglected. The diagonal elements of the **R** matrix contain variances for the errors associated with the analytical measurements made to obtain **Z**; for optimal filtering to be possible, these errors must have zero mean and a gaussian distribution. The criterion of a zero mean for measurement error is one which is easily consistent with the desired performance of a procedure, though it is not always possible. Having errors with either a white distribution or a normal distribution is less simple for an analyst to control. In practice, however, measurement errors of the types commonly experienced in analytical chemistry often come close to satisfying the noise requirements discussed above, and they do not seem to cause significant deterioration of filter performance [15]. Finally, it should be noted that there is no need to define the noise or the states in terms of time as the independent variable. In fact, if the noise requirements discussed above can be met, then any convenient parameter can be used as the independent variable in the filter model.

The flexibility of the state-space model is one of the major advantages to the use of the Kalman filter. Modelling of time-dependent phenomena, such as chemical reactions, is very straightforward as a consequence of the system dynamics equation. The random component of the system model even permits inclusion of drift. Of special interest, however, is the ease with which the measurement model can be adapted to chemical problems. Either theoretical or empirical relations can be used to relate measurable quantities to the model states through the **H** matrix. For example, **H** might consist of several row vectors, each of which describes an entire visible spectrum by representing it as a series of molar absorptivities. This matrix could then relate the measured absorbances at the different wavelengths to filter states, which might be given in terms of component concentrations. Here, the filter

model is based on experimentally-obtained responses for pure component species. A filter using this empirical model could be useful in rapid deconvolution of overlapped spectra, as shown in Fig. 2. Filter models can be based on mathematical relations relating measurable quantities to filter states, as well. This feature provides for direct testing of theoretical model expressions by experiment, and for improving the quality of experimental data through use of a well established theory, provided that one is available. Figure 3 shows the theoretical measurement model constructed for the mathematical analysis of the response obtained from two competitive first-order reactions, where both reactions generate the same product, but at different rates. The states here are time-dependent concentrations of all species involved in the reaction. Although only a scalar absorbance measurement and single wavelength

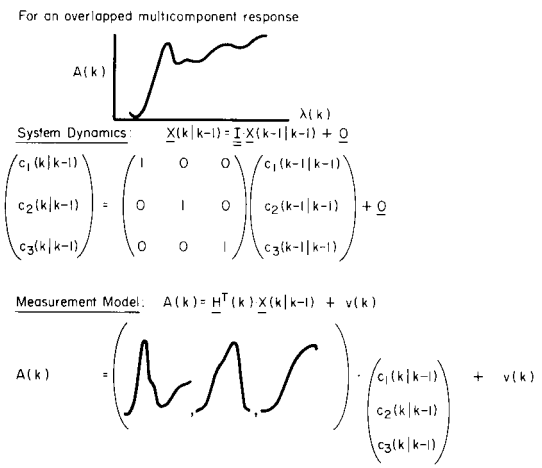

Fig. 2. An empirical state-space model: spectral resolution in multicomponent quantitation.

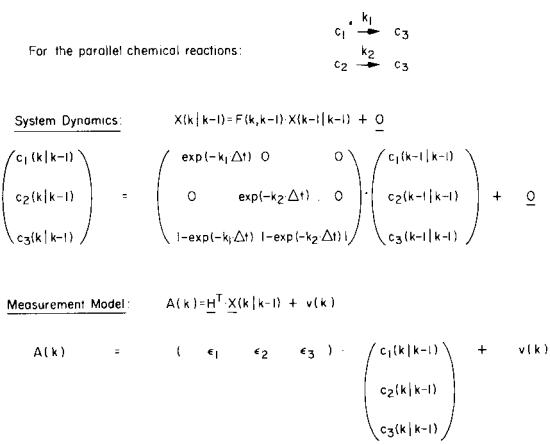

Fig. 3. A theoretical state-space model: chemical kinetic

responses (a vector $\mathbf{H}^T$) are indicated in the model illustrated, it is simple to extend this model to include multiple measurements (perhaps a spectrum) and multiple responses in **H** [by providing empirical (experimental) spectra of species 1, 2 and 3]. A significant advantage of the state-space method is the ease with which mixed theoretical-empirical models, or other complex models can be put into the filter algorithm.

The discrete Kalman filter

From the model structure defined above, a recursive filter can be developed [1]. The results of that development are given here.

The filter is used to estimate recursively both the model state vector, **X**, and the error associated with that state estimate. The error is calculated by the expression

$$\mathbf{P} = E[(\mathbf{X} - \hat{\mathbf{X}})(\mathbf{X} - \hat{\mathbf{X}})^T] = E[\mathbf{e}(k)\mathbf{e}^T(k)] \tag{15}$$

where $E[\ldots]$ indicates an expectation value, and where $\mathbf{e}(k)$ is defined as the estimation error, $\mathbf{X}(k) - \hat{\mathbf{X}}(k)$, at point k. The expression in Eqn. 15, a vector product, produces a covariance matrix, $\mathbf{P}(k)$, with the diagonal elements being the variances of the state variables, while the off-diagonal elements are the covariances. It is tacitly assumed in Eqn. 15 that the estimation error has a zero mean. The goal of filtering is to minimize some measure of the estimation error for the states used in the model; minimization of the size of the diagonal elements in this matrix accomplishes minimization of the mean square estimation error [10—13].

Equations 8—14 in Table 1 summarize the equations and initial conditions which are the Kalman filter algorithm.

Because the filter is set up as a recursive calculation, the initial guesses, $\mathbf{X}(0)$ and $\mathbf{P}(0)$, are required to start the filter and to enter the recursive loop. These initial guesses are used as the estimated values prior to the filtering of the first measurement, as indicated by the equations

$$\mathbf{X}(1|0) = \mathbf{F}(1, 0)\mathbf{X}(0) = \mathbf{F}(1, 0)E[\mathbf{X}(0)] \tag{16}$$

$$\mathbf{P}(1|0) = \mathbf{F}(1, 0)\mathbf{P}(0|0)\mathbf{F}^T(1, 0) \tag{17}$$

where the notation (1|0) is as discussed above. These are a more explicit form of Eqns. 8A and 8B in Table 1. The first measured response is used in the filter at this point.

A linear combination of the noisy measurement and the a priori estimate is used in the filter, as indicated by Eqns. 12 and 13 in Table 1. These two equations produce the filtered, a posteriori estimates. The $n \times n$ matrix $\mathbf{K}(k)$ used in these two equations is the Kalman gain matrix, actually a formula for calculating the optimal filter weights which produce the minimum variance fit of the model to the data. If Z is a scalar, as in Eqn. 6, the gain reduces to a vector quantity. It is apparent from the equations in Table 1 that the Kalman gain can be precomputed for use in applications in which real-time

processing of data is desirable, because it depends only on the **F** and **P** matrices, both of which are known prior to beginning the filtering process. In Eqn. 12, the term in brackets is called the innovation, where, in general

$$v(k) = \mathbf{Z}(k) - \mathbf{H}^T(k)\mathbf{X}(k|k) \tag{18}$$

As the difference between the actual and the predicted measurement, the innovation is a measure of the new information available in the measurement $\mathbf{Z}(k)$. The innovation also can be thought of as a "point-wise residual" associated with the filtering process [10—13]. Equation 12 thus updates the state vector by a weighted correction term. The size of the correction depends on the quality (accuracy) of the previous a priori estimate. The covariance matrix is updated to reflect information provided in the measurement by Eqn. 13 in Table 1.

Once the updates for the state vector and the covariance matrix have been obtained, the whole sequence begins again. Now, the a posteriori estimates for **X** and **P**, made after the first measurement has been filtered, are projected ahead to generate a priori estimates for the second measurement. Another one-step prediction is performed, using the transition matrix (Eqn. 10). The contribution of **w**(2) is ignored because it has a zero mean and is not correlated with the previous **w** value, as indicated by Eqn. 9. The covariance matrix is also projected ahead by one-step prediction, as indicated by Eqn. 11 in Table 1. The second measurement is made and the a priori estimates made in Eqns. 10 and 11 are corrected to reflect the new information present in the measurement, generating new a posteriori (filtered) estimates, as described above. Once again, new a priori estimates are generated from these estimates by one-step prediction, and the whole process repeats, continuing as long as new data are available for processing. The process, which can be regarded as a series of prediction-correction steps, is illustrated in Fig. 4.

Examples of Kalman filtering

To illustrate the manner in which these equations are used, the calculations performed with the filter are presented for two relatively straightforward examples.

The first example is chosen so that the filter operations can be done manually. The system dynamics and measurement models are given by the scalar equations

$$X(k) = 0.5X(k-1) \tag{19}$$

$$z(k) = X(k) + v(k) \tag{20}$$

This model might describe a continuous extraction, in which the distribution coefficient is 1.0. It happens that v is normally distributed, with zero mean, and a variance of 0.1. The initial guess for X, $X(0)$, is taken as 0, and its variance as 20. The observations $z(1) = 10.0$, $z(2) = 5.1$, and $z(3) = 2.5$ have been obtained. It is desired to find the best estimate for the value of X after three

extraction steps, $X(3|3)$, and its associated error $P(3|3)$, based on these data.

Equations 10—14, given in Table 1, can be used to obtain estimates for X before and after each extraction step. Application of these equations generates the results given in Table 3. The updated estimates, based on the three measurements available, are $X(3|3) = 2.47$ and $P(3|3) = 4.76 \times 10^{-3}$, which gives a result of 2.47 ± 0.07 for X after the third extraction. The estimated error has significantly decreased with the filter applied to just three measurements, as indicated by the drastic change in P. The Kalman gain also decreases over the three measurements; this change reflects the decrease in the size of the estimated error variance. The results in Table 3 parallel the process outlined in Fig. 4 in that estimates of X are improved and their associated errors have become smaller, as new data are processed.

The second example is more complex; it involves the estimation of the concentrations of all species involved in the parallel first-order reactions $C_1 \rightarrow C_3$; $C_2 \rightarrow C_3$ in which efforts to measure the response (e.g., absorbance) due to species C_3 involve interference from responses caused by C_1 and C_2. The state/space model for this system is described in Fig. 4. Estimates of all species concentrations are sought at all times in which a response has been measured. This problem is similar to those which occur in many kinetic methods [16] and in pharmacokinetic experiments [17]. This particular problem was chosen to illustrate filtering because it is not easily suited to simple, linear least-squares data processing, although it can be cast into a form suited for nonlinear regression (in which the initial concentrations are estimated, instead of the species concentrations as a function of time). The problem is made linear and easily solved through use of the Kalman filter, however. The Kalman filtering approach also offers the advantage of specifying the errors associated with the fit; although estimates of error can be obtained from a nonlinear regression, they usually require additional computation. All filter calculations reported here were done in PASCAL on a Sanyo MBC-555 computer equipped with 128K of random access memory. For this problem,

TABLE 3

Results from the extraction example

Step	X	K	P	z
(0|0) (initial guess)	0.0		20.0	
(1|0)	0.5		5.0	
Measurement 1		0.9800		10.0
(1|1)	9.81		0.1000	
(2|1)	4.91		0.0250	
Measurement 2		0.2000		5.1
(2|2)	4.95		0.0200	
(3|2)	2.47		0.0050	
Measurement 3		0.0476		2.5
(3|3)	2.47		0.0048	

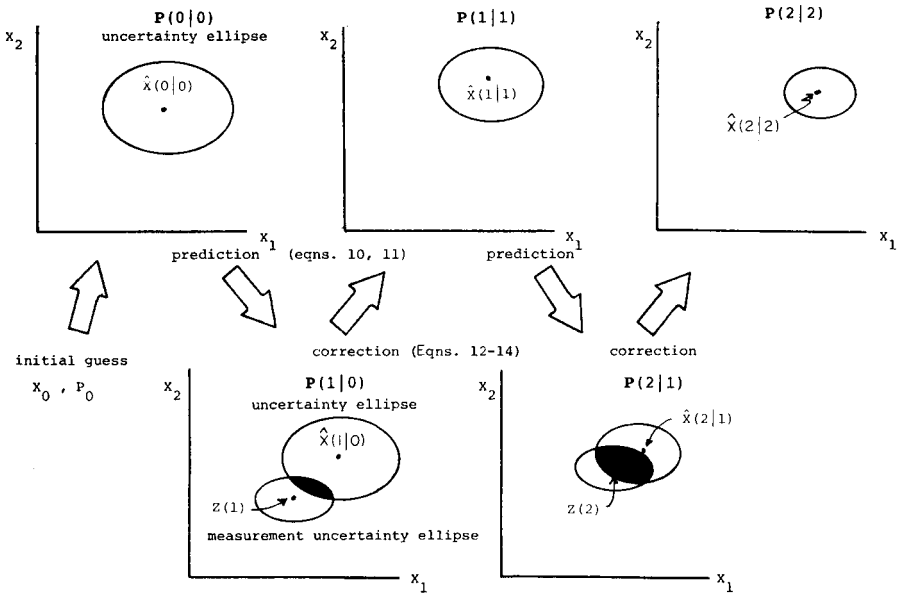

Fig. 4. Data processing by the Kalman filter showing the operation of the filter for a two-state, scalar measurement model.

two data sets, each with 50 synthetic measurements, were created by adding the responses for the individual components, taking into account the changes caused by chemical kinetics. Random noise was added to obtain a maximum signal-to-noise ratio of 1000. The parameters used to generate the synthetic data used for the filtering process are summarized in Table 4.

Results for this system are given in Table 5, and the evolution of the estimates in time is provided in Fig. 5. In run one (Fig. 5A), estimates for the states quickly settle to correct values. Run two, in which it is more difficult to distinguish between the two pathways, requires more measurements for the estimates to settle (Fig. 5C). In both cases, the innovation sequence

TABLE 4

Parameters used to simulate kinetic data[a]

Run	Kinetic constants (s^{-1})	Response factors	Initial conc.
1	$k_1 = 1.0 \times 10^{-2}$	$H_1 = 25$	$C_1 = 0.10$
	$k_2 = 3.0 \times 10^{-4}$	$H_2 = 35$	$C_2 = 0.10$
		$H_3 = 15$	$C_3 = 0.00$
2	$k_1 = 1.0 \times 10^{-3}$	$H_1 = 10$	$C_1 = 0.10$
	$k_2 = 3.0 \times 10^{-2}$	$H_2 = 15$	$C_2 = 0.05$
		$H_3 = 100$	$C_3 = 0.00$

[a]In all cases, the maximum signal-to-noise ratio was 1000, and the time interval was 3 s.

TABLE 5

Results from filtering of simulated data with model in Fig. 3.

Run	Species	Initial guess		Estimated conc.[a] (at t = 150 s)
		X	P	
1	1	0.0	1.0×10^{-2}	$2.24(\pm 0.01) \times 10^{-2}$
	2	0.0	1.0×10^{-2}	$9.46(\pm 0.4) \times 10^{-2}$
	3	0.0	1.0×10^{-4}	$8.44(\pm 0.9) \times 10^{-2}$
2	1	0.0	1.0×10^{-2}	$8.14(\pm 0.02) \times 10^{-2}$
	2	0.0	1.0×10^{-2}	$5.88(\pm 0.00) \times 10^{-4}$
	3	0.0	1.0×10^{-4}	$6.81(\pm 0.00) \times 10^{-2}$

[a]For run 1 at t = 150, the true concentrations are 2.23×10^{-2}, 9.56×10^{-2}, and 8.20×10^{-2}, respectively. For run 2 at t = 150, the true concentrations are 8.60×10^{-2}, 5.88×10^{-4}, and 6.34×10^{-2}, respectively. The numbers in parentheses are the estimated standard deviations, obtained from the covariance matrix P. In both runs, the measurement variance used in the filter was 1.0×10^{-5}.

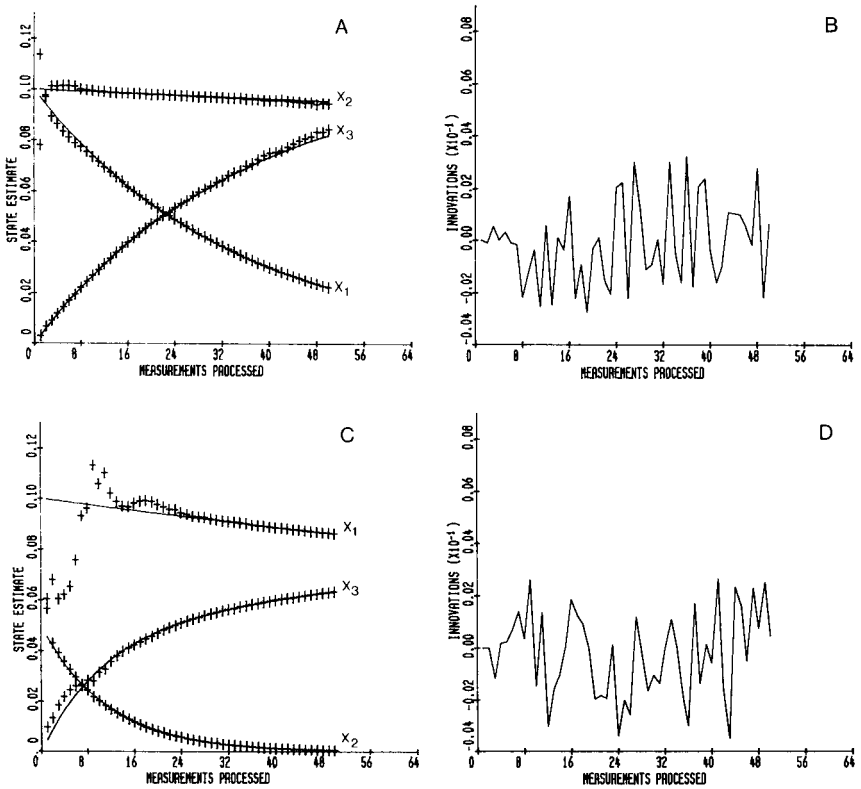

Fig. 5. Evolution of filter states for filtering of noisy kinetic data. (—) True concentration; (X) estimated concentration. (A) Change of species concentrations with time for run 1. (B) Filter innovations for fitting of run 1. (C) Change of species concentrations with time for run 2 in Table 3. (D) Filter innovations for fitting of run 2.

generated by the filter remains small and random (Figs. 5B and D); as required for good filtering, it is centered about zero.

Nonlinear estimation with the Kalman filter

Although the Kalman filter was developed for use with linear models, many of its applications have dealt with nonlinear problems. These problems often require the use of models with nonlinear system dynamics, nonlinear measurement models, or both. The model equations used in the Kalman filter in that case are Eqns. 21 and 22 of Table 6, where f and h are nonlinear functions of the state X. Table 6 also lists the equations which define an "extended Kalman filter", a form of the Kalman filter which is often applied to nonlinear problems [10—13]. The reader can verify that when the system dynamics and measurement model equations are linear, the extended filter reduces to the conventional Kalman filter.

TABLE 6

The extended, discrete Kalman filter algorithm

System dynamics:	$\mathbf{X}(k) = \mathbf{f}(k, k-1)\mathbf{X}(k-1) + \mathbf{G}(k-1)\mathbf{w}(k-1)$	(21)
Measurement model:	$\mathbf{Z}(k) = \mathbf{h}(\mathbf{X}(k\|k), k) + \mathbf{v}(k)$	(22)
Noise assumptions:	$E[\mathbf{w}(k)\mathbf{w}(j)^T] = \mathbf{Q}^{\delta}jk$	(23A)
	$E[\mathbf{v}(k)\mathbf{v}(j)^T] = \mathbf{R}^{\delta}jk$	(23B)
Initial conditions:	$E[\mathbf{X}(0)] = \mathbf{X}_0$	(24A)
	$E[(\mathbf{X}(0) - \mathbf{X}_0)(\mathbf{X}(0) - \mathbf{X}_0)^T] = \mathbf{P}_0$	(24B)
Other assumptions:	$E[\mathbf{w}(k)\mathbf{v}(j)^T] = 0$ for all j, k	
	f, h are continuous in $\mathbf{X}$ near $\hat{\mathbf{X}}$	(25)
State estimate extrapolation:	$\mathbf{X}(k\|k-1) = \mathbf{f}(\mathbf{X}(k-1), k-1)$	(26)
Error covariance extrapolation:	$\mathbf{P}(k\|k-1) = \mathbf{F}(\mathbf{X}(k-1), k-1)\mathbf{P}(k-1\|k-1)\mathbf{F}(\mathbf{X}(k-1), k-1)^T + \mathbf{Q}(k-1)$	(27)
State estimate update:	$\mathbf{X}(k\|k) = \mathbf{X}(k\|k-1) + \mathbf{K}(k)[\mathbf{Z}(k) - \mathbf{h}(\mathbf{X}(k\|k), k)]$	(28)
Error covariance update:	$\mathbf{P}(k\|k) = [\mathbf{I} - \mathbf{K}(k)\mathbf{H}(\mathbf{X}(k\|k-1))]\mathbf{P}(k\|k-1)$	(29)
Gain matrix:	$\mathbf{K}(k) = \mathbf{P}(k\|k-1)\mathbf{H}^T(\mathbf{X}(k\|k-1)) [\mathbf{H}(\mathbf{X}(k\|k-1))\mathbf{P}(k\|k-1)\mathbf{H}^T(\mathbf{X}(k\|k-1)) + \mathbf{R}(k)]^{-1}$	(30)
Definitions:	$\mathbf{F}(\mathbf{X}(k), k) = \left.\frac{\partial \mathbf{f}(\mathbf{X}(k), k)}{\partial \mathbf{X}(k)}\right\|_{\mathbf{X}(k) = \hat{\mathbf{X}}(k)}$	(31)
	$\mathbf{H}(\mathbf{X}(k\|k-1)) = \left.\frac{\partial \mathbf{h}(\mathbf{X}(k\|k-1), k)}{\partial \mathbf{X}(k\|k-1)}\right\|_{\mathbf{X}(k\|k-1) = \hat{\mathbf{X}}(k\|k-1)}$	(32)

Use of the extended filter requires a linearization of the **f** and **h** matrices in Eqns. 27 and 28. This forces a linearized form of the model in the Kalman filter. The method for accomplishing this linearization is conceptually straightforward; the elements of the matrices are expanded as a Taylor's series in the state variables, and truncated after the linear term. Because such an expansion must be performed around some value, a choice must be made. In the extended Kalman filter, the expansion of these matrices is performed around the current estimate for the state vector, $\hat{\mathbf{X}}(k)$. Thus, the linearized model matrices **F** and **H** are defined as indicated in Eqns. 31 and 32 of Table 6.

Using this expansion about the current estimate for the state vector requires the real-time calculation of the gain matrix, $\mathbf{K}(k)$, as can be seen from Eqn. 30 in Table 6. If, instead of the current state estimate, some prespecified "nominal path vector" is used for the expansion, the need for extensive real-time calculation can be avoided. Specifying a nominal path provides a tremendous computational advantage, as the gains $\mathbf{K}(k)$ can be computed off-line and stored prior to filtering. The cost, of course, is a decrease in filtering accuracy, as the prespecified vector is not as close to the actual behavior of the states as is $\hat{\mathbf{X}}$. This variant of the extended filter is called a "linearized Kalman filter" [11, 18]. Equations for the linearized Kalman filter are otherwise the same as for the extended Kalman filter.

Because the propagation of the extended Kalman filter covariance matrix defined in Eqn. 29 is only an approximation to the propagation of the true covariance matrix, as defined in Eqn. 11, neither the extended nor the linearized Kalman filters are guaranteed to produce optimal (minimum variance) estimates. Actual performance must be evaluated by Monte Carlo simulations [11, 13]. Nevertheless, the extended Kalman filter is usually the first method tried for nonlinear filtering. Some applications discussed below illustrate its use in analytical chemistry.

Relationship between Kalman filtering and deterministic least squares

Kalman filtering is sometimes called least-squares filtering. This is a misnomer, because the criterion used in the Kalman filter is minimum mean square error, and not the squared, deterministic error. There is some connection between the Kalman filter and ordinary, deterministic least squares, however, as is demonstrated below [19].

For an overdetermined set of m equations in some quantity, **X** (an $n \times 1$ vector, where $m > n$), given in matrix form

$$\mathbf{MX} = \mathbf{b} \tag{33}$$

where **M** is a known $m \times n$ matrix, and **b** is a known $m \times 1$ vector, no solution for **X** exactly satisfies all of the equations. The best solution is defined to be that which minimizes the weighted sum of the squared residuals, namely

$$(\mathbf{MX}_{\text{opt}} - \mathbf{b})^T\mathbf{W}(\mathbf{MX}_{\text{opt}} - \mathbf{b}) = \mathbf{e}^T\mathbf{We} \tag{34}$$

where the weighting matrix is taken as symmetric and positive definite. The variance-weighted solution to this problem is

$$\mathbf{X}_{opt} = [(\mathbf{M}^T\mathbf{W}\mathbf{M})^{-1}\mathbf{M}^T\mathbf{W}]\,\mathbf{b} \tag{35}$$

For the same problem, the Kalman filter solution is easily obtained. The state vector, **X**, is taken as constant, so that the system dynamics equation is

$$\mathbf{X}(k) = \mathbf{I}\mathbf{X}(k) + \mathbf{0} \tag{36}$$

where **I** is the identity matrix. The measurement model is given by Eqn. 6; here, $\mathbf{Z}(k)$ and $\mathbf{H}(k)$ are equivalent to **b** and **M** in the deterministic problem above. Because time is unimportant, all measurements can be treated as if they occur simultaneously. This effectively causes filtering in "batch" mode. And, because no a priori knowledge of **X** or **P** is assumed, $\mathbf{X}_0$ is taken as **0**, and $\mathbf{P}_0$ as ∞. The Kalman gain is calculated as

$$\mathbf{K}_0 = (\mathbf{H}^T\mathbf{R}^{-1}\mathbf{H})^{-1}\mathbf{H}^T\mathbf{R}^{-1} \tag{37}$$

and the Kalman filter estimate of **X** at $t = 0$ is found to be

$$\mathbf{X}_0 = [(\mathbf{H}^T\mathbf{R}^{-1}\mathbf{H})^{-1}\mathbf{H}^T\mathbf{R}^{-1}]\,\mathbf{Z}_0 \tag{38}$$

This is identical to the result found above for $\mathbf{X}_{opt}$ by the variance-weighted linear least squares, with $\mathbf{R}^{-1}$ acting as the variance weight matrix **W**.

This example illustrates several important points. First, the requirement of constant system dynamics limits the Kalman filter model to those simple, deterministic, time-independent systems which allow a measurement sequence to yield a system of overdetermined equations. While this restriction is needed for least-squares optimization, it is not essential for use of the Kalman filter, because a stochastic system dynamics model could have been used instead of Eqn. 36. The ability to handle complex, time-dependent models in a simple, direct manner distinguishes the Kalman filter from other digital filters. Second, the requirement that the filter be run using no prior information about **X** and assuming infinite initial covariances again limits the filter. Although such assumptions are required for least-squares optimization, the usual situation in analytical chemistry is that some knowledge of the system is available prior to optimization. This information is easily incorporated into the Kalman filter via the initial conditions of the recursive loop. The use of prior information by the Kalman filter is another of its distinguishing characteristics. Finally, this example demonstrates that the results of a deterministic optimization (by linear least squares) and a stochastic optimization (by Kalman filtering) can coincide, provided that certain restrictions are met. All of these restrictions are imposed on the model and initial conditions used by the Kalman filter. The solution to the deterministic least-squares optimization problem can therefore by considered a subset of Kalman filtering.

Limitations of Kalman filtering

The small size of the code needed to implement the Kalman algorithm and the recursive nature of the estimation process enable the filter to be used in

very complex systems [20]. Filters exist for systems up through order 50 (requiring 50 state variables); filters using 10—20 state variables are rather common [2, 11]. The main factors limiting the effectiveness of Kalman filtering are all associated with filter divergence, a phenomenon which occurs when the covariances estimated by the filter are larger than predicted by theory [11, 13]. In some cases, these errors can become very large. Divergence has three common sources: computer round-off problems, modelling errors, and system observability problems.

In any numerical procedure, computer round-off error can cause difficulties as the calculations become more involved. The Kalman filter propagation of the covariance matrix (Eqn. 11) is probably the part of the filter calculation that is most prone to round-off error, particularly when measurements are relatively noise-free (the components of **R** are small). Round-off error can cause this matrix to become semidefinite, or even indefinite. Several steps have been proposed to insure that this matrix remains symmetric and positive definite [11]. Several authors [11—13] have recognized that an improved equation can be derived for propagation of covariance, namely

$$\mathbf{P}(k|k) = [\mathbf{I} - \mathbf{K}(k)\mathbf{H}(k)] \cdot \mathbf{P}(k|k-1) \cdot [\mathbf{I} - \mathbf{K}(k)\mathbf{H}(k)]^T + \mathbf{K}(k)\mathbf{R}\mathbf{K}^T(k) \quad (39)$$

This equation is much less prone to round-off error than Eqn. 11. Other approaches for reducing round-off effects exist as well; one method that involves the propagation of the "square root" of the covariance matrix rather than the direct propagation of the covariance matrix has been found to be particularly effective in stabilizing the filter [21]. Square-root filters have a significantly larger computational burden than the algorithm given earlier, however. This limits their real-time use.

Errors in modelling are commoner and more serious than round-off error. These occur when the filter model was designed to expect the system to behave in one manner, but, in fact, the system behaves in some other way. These errors have the effect of forcing the filter to fit data to the wrong model. Modelling errors can arise from fairly subtle causes: e.g., the small, unnoticed (and therefore unmodelled) drift of an instrumental response with time. These errors are often negligible. Occasionally, gross modelling error can be seen: for example, large model errors occur if a model used for multicomponent filtering omits one or more of the states needed to describe all of the components actually present. Much effort has gone into the development of reliable methods for compensation of modelling errors in Kalman filtering, and several fairly general methods are available. These methods are classified as "adaptive" Kalman filters, as they provide a way for the model to adapt somewhat to the level of the innovations sequence; in this way, state-space models may be altered to reflect the system more accurately [11, 13, 18, 22, 23].

The third major source of filter divergence occurs when one or more states are not observable. Physically, this means that in a time-dependent system, some of the state variables, or their linear combinations, cannot be deter-

mined from measurements made on the system. If the unobserved parts of the model are unstable, the filter estimates for the states and for the errors in the state estimates may also be unstable, and filter divergence can occur. When the system is time-independent, multiple measurements can always be made, and a series of overdetermined equations can be solved for the state variables as in the least-squares example above. The problem of observability is not as easily circumvented in underdetermined, time-dependent systems, however. To insure that the states used in the time-dependent model can, in fact, be determined from filtering a series of measurements, an observability criterion [11—13] must be met: for a discrete nth order system, the information matrix

$$\mathbf{In}(n, 1) = \sum_{i=1}^{n} \mathbf{F}^T(i, n)\mathbf{H}^T(i)\mathbf{R}^{-1}(i)\mathbf{H}(i)\mathbf{F}(i, n) \tag{40}$$

must be positive-definite [11, 13]. This implies that it is possible to acquire information (and to decrease estimation error variance) about states that are, at the beginning of the process, completely unknown. If the model is stationary, i.e., if the noise statistics are constant over time, a related observability criterion can be used instead of the one given above. In this case, the observability matrix

$$\mathbf{M} = [\mathbf{H}^T|\mathbf{F}^T\mathbf{H}^T|(\mathbf{F}^T)^2\mathbf{H}^T| \ldots |(\mathbf{F}^T)^{n-1}\mathbf{H}^T] \tag{41}$$

must have a non-zero determinant, which is certain if and only if the matrix is of rank n [11]. Both criteria are most easily applied to systems of low dimensionality; fortunately, such systems are common in the modelling of chemical systems. In the chemical kinetics example given above (a stationary model) the observability matrix is

$$\begin{bmatrix} H_1 & AH_1 + DH_3 & A^2H_1 + (AD + D)H_3 \\ H_2 & BH_2 + EH_3 & B^2H_2 + (BE + E)H_3 \\ H_3 & H_3 & H_3 \end{bmatrix}$$

where H_i is the ith component of the $\mathbf{H}^T$ vector, and where $A = \exp(-k_1\Delta t)$, $B = \exp(-k_2\Delta t)$, $D = 1 - A$, and $E = 1 - B$. This matrix is of rank 3 only if A is not equal to B, if $H_1 + H_2$ is not equal to H_3, and if H_3 is not zero. This is equivalent to saying that there are three independent variables in this system only if all three produce a response, either directly or through a chemical reaction, and if the two reaction rates are not exactly equal. This conclusion is consistent with requirements established by a statistical experimental design [17] and also with "chemical intuition". The results shown in Fig. 5 demonstrate one effect of observability: the system used in run 1 is more observable than that of run 2, because the kinetic constants differ more. Not surprisingly, the state estimates track correct results much more quickly in run 1 than in run 2. For systems of high dimensionality, it may not be practical to compute either the information or the observability matrix, however. In these cases an off-line error analysis is needed [11, 18].

APPLICATIONS OF KALMAN FILTERS IN ANALYTICAL CHEMISTRY

The application of Kalman filters to analytical chemistry has centered on four problems to date: removal of noise from a spectral or voltammetric response, resolution of overlapped spectral or voltammetric peaks, instrumental drift compensation, and model identification and improvement. Each is discussed below.

Noise removal

Because filtering is strongly associated with removing noise from a signal, it is not surprising that the first chemical applications used the Kalman filter to remove noise from responses. Kelly and Harris [24, 25] used a filter quite similar to the Kalman filter to estimate parameters for gas chromatographic peaks in the presence of noise. Their filter used a maximum-likelihood criterion for obtaining optimal estimates of peak-shape parameters. Brubaker et al. [26] used polynomial and scalar state models in the development of Kalman filters for removal of noise from mass spectrometric data. Their time-varying, scalar implementation of the filter was very efficient at removing noise and at separating overlapping responses in the data. Seelig and Blount [27–29] used the extended Kalman filter to remove noise from data obtained by anodic stripping voltammetry. Two filter models were used: a single-measurement (current), single-state (concentration) model, and a two-measurement (current and potential), five-state (current, concentration, corrected potential, and two parameters describing a linear, non-Faradaic current function) model [27]. The two-measurement, five-state model accurately estimated concentrations even at signal-to-noise ratios near 1. Errors associated with the modelling of Faradaic and non-Faradaic components of the current were found not to degrade filter performance appreciably [28, 29]. Even with the two-measurement, five-state model, which used a linearized approximation of a fairly complex, nonlinear model, some real-time application of the Kalman filter was possible. The simpler one-measurement, one-state model was found to give results similar to those produced by the more complex filter.

Peak resolution

The commonest use of the filter has been for separation of overlapped peaks. Poulisse [30] first used the Kalman filter to identify the number of components present in an overlapped ultraviolet-visible spectrum. Later, Didden and Poulisse [31] extended this work to show that component concentrations could also be obtained; as many as ten components were resolvable from overlapped, synthetic spectra. Brown and Brown [32] applied the filter to separation of various overlapped voltammetric responses. Models used in this study, as well as in the studies by Poulisse, were based on experimental data obtained on pure components. A systematic study of the filter resolving power showed that peaks of similar size could be completely

resolved, regardless of the degree of overlap. The effect of model error and system observability were also discussed. This study was extended by Scolari and Brown [33], who determined the resolving power of Kalman filtering for closely overlapped square-wave responses, where component peak height ratios were substantially different from 1. The primary limitation was found to be the linearity of the measurement model. Overlapped square-wave voltammetric responses obtained in flow-injection systems have also been resolved by use of Kalman filters; results are similar to those found in static systems [34]. The Kalman filter was also used to resolve highly overlapped photoacoustic spectra for calculation of stability constants [35], and for assay of pigments [36] and analgesics [37] by direct spectrophotometry.

Detection and compensation of instrumental drift

The use of the Kalman filter for compensation of drift in the responses obtained from analytical instrumentation is a logical extension of its use for drift compensation in navigation [38]. Linear drift was removed effectively by including it as extra state variables in the model used for the resolution of multicomponent spectra [39]. Of course, instrumental drift is seldom strictly linear, as Thijssen et al. have recognized [40]. They developed a model for random drift by combining a random constant, a random walk, and a random ramp; this drift model was applied to the situation in which drift occurs in the calibration of a spectrophotometric method. Results from the application of the drift correction to simulated flow-injection data were quite promising. A criterion was developed for deciding whether to recalibrate or to measure the next unknown. The method requires prior knowledge of measurement noise variance and the system covariance matrix for use with the filter, but use of this or a similar approach to compensate for drift in real data is likely soon. Thijssen et al. [41] extended this work to include optimal designs for the calibration scheme. More recently, they used off-line fixed-interval smoothing to improve the on-line estimates made in the presence of drift. Both the on-line estimator and the off-line estimator used Kalman filters [42]. In batch processing, the abrupt changes in sample which occur between batches can be regarded as a form of drift, too. This drift can be modelled, and a Kalman filter can be used to reduce the variance of the measurements made on the process. In some cases, the variance is reduced by a factor of 2 [43, 44]. Other workers have coupled the Kalman filter with the generalized standard addition method to devise a recursive system for calibration and for removal of additive interferences [45]. A test made on the averaged innovation provides a route for detection, but not the correction, of instrumental drift and other deviations from the linear model which is assumed in the generalized standard addition method. The detection of drift and the automated recalibration of method are important first steps in the design of intelligent instrumentation.

Another way of approaching calibration problems is with information theory. Maximizing the information available from a measurement or a cali-

bration is important to the design of an assay. A recent application [46] used the Kalman filter, in conjunction with information theory, to identify the optimal places for measurements in a complex system. For example, to measure four components from multiwavelength spectrophotometric data, assuming that known, pure spectral data are available at 30 wavelengths, of which 6 are to be selected, classical optimization requires that 600000 4×4 determinants be calculated to find the best set of wavelengths. The procedure based on Kalman filtering requires less than 500 separate calculations of a set of equations relating the information to the system covariance matrix, a much simpler task. Another application has used the Kalman filter to aid in the selection of optimal wavelengths for precision enhancement in multicomponent quantitation [47].

Model identification and improvement

The Kalman filter can be applied to identify parameters used in models of various physical processes. This is a convenient way to obtain thermodynamic and kinetic constants, for example. Kalman filtering is particularly useful for studies of chemical kinetics, as the example given above demonstrates. The application of the extended Kalman filter to systems, the spectral responses of which are perturbed by chemical reactions, has been reported by Rutan and Brown [48, 49]. One study demonstrated the use of filtering in resolving a perturbed spectrum into its unperturbed component spectra [48]. The time dependence of the perturbation was used to obtain the first-order rate constant for the chemical reaction that occurred. A second study applied the Kalman filter to data acquired by a rapid-scanning spectrometer [49]. The time-dependent behavior of the entire spectrum was used to estimate rate constants for an enzyme reaction and the initial substrate concentration. Results from this approach were compared with an approach using the filter to analyze a single, perturbed spectrum (as in the above study) as well as with the usual least-squares approaches. This "three-dimensional" filtering is found to work as well as the Kalman filtering approach discussed above, and both approaches based on Kalman filtering were superior to those based on linear or nonlinear least squares.

Brown et al. [50] have also used the extended Kalman filter in conjunction with an explicit finite-difference digital simulation to model an irreversible electron transfer as measured by linear scan voltammetry. The digital simulation model depended on the heterogeneous charge-transfer rate constant and the transfer coefficient. The filter adjusted these parameters in the simulation "on the fly" best to describe the voltammetric data. The use of potential as the independent variable in the filter provided a direct route for observing the dependence of the transfer coefficient on potential, an observation which is otherwise not experimentally straightforward. Coupling of a finite difference simulation model to the difference equations used in the filter is direct and it provides a unique route for study of models for very complex chemical processes.

It is also possible to couple the Kalman filter with control algorithms, so that the data being processed may alter the way in which future data are collected. The application of a Kalman filter to a simple acid-base titration suggests one such coupling [51].

Several recent papers report the use of adaptive Kalman filters to improve models used in analytical chemistry. The adaptive Kalman filter uses the properties of the noise sequences defined in the filter model (Eqns. 7A and 7B above) to allow changes in the model, so that the model better describes the experimental data. It is possible to create additional state variables or correct existing state variables in this fashion. A recent review discusses one of the different approaches to adaptive filtering, and briefly summarizes the applications of adaptive filtering in analytical chemistry [52]. Brown et al. [53] demonstrated the use of the Kalman filter in the processing of voltammetric data obtained on a metal/ligand complex system, in which homogeneous kinetic effects perturbed the model. The adaptive filter, done manually in this early work, modelled the known electrochemical response, and allowed resolution of the component attributed to the free metal. This component had overlapped another one attributed to free metal produced from dissociation of the metal/ligand complex during the electrochemical measurement. Rutan and Brown [54] demonstrated a more automated adaptive filter for correction of spectral and electrochemical models used in multicomponent quantitation. They discussed the details of adaptive Kalman filtering, and discussed some limitations of the technique. An extension of this work coupled the adaptive filter to the simplex algorithm, making the adaptive filter completely automated [55]. This work demonstrated the use of adaptive filtering for compensation of interferences which are not included in the system model used for multicomponent quantitation. Resolution of spectral responses from severely overlapped background components is demonstrated, even when the peak ratio of unmodelled interferences to analyte reaches 14.

CONCLUSIONS

The application of Kalman filtering techniques to the analysis of chemical data offers a number of advantages. One is the possibility of explicitly including time in the model; this permits the modelling of drift, of reaction kinetics and of time-dependent inputs (e.g., titrations) in a straightforward manner. These methods are simple and fast enough to permit their use on most analytical instruments, and they are applicable to most analytical methods. Their use encourages a re-evaluation of how chemical data are collected. It may be advantageous to use the diagnostic capabilities of a Kalman filter to establish how a measurement is to be made, and to identify the optimal time and place for the measurement, so that chemical information is most efficiently extracted. Toward that goal, it should be noted that coupling of information theory and filtering was achieved long ago by means of maxi-

mum likelihood and other approaches; Kalman filters which maximize information (rather than minimize variance) are common [46, 48, 56].

Several aspects of Kalman filtering seem likely for study in the near future. One is the area of adaptive filtering, where better adaptive filters may aid in the examination of data where good, but not excellent models are available. The surface has only been scratched in this area. A second involves the use of filters as controllers, where the aim is automatic calibration and drift removal. Again, much remains to be done. The third area is the "inverse problem", i.e., identifying appropriate models for analytical processes by application of filtering to experimental data. The great gains made in the computation power of small and medium-sized computers may be of tremendous assistance in this area, because parallel filters and even sequential filters may find application.

This work was supported by the Division of Chemical Sciences, of the U.S. Dept. of Energy under grant DE-FG06-84ER13202. The author is indebted to past and present members of his research group who have contributed to many of the applications of Kalman filtering. Special thanks go to T. F. Brown and S. C. Rutan. Helpful critical comments on this manuscript were provided by T. F. Brown, D. M. Caster, and C. A. Scolari. T. F. Brown also assisted with the development of the PASCAL filtering program used in the kinetics example.

REFERENCES

1 R. E. Kalman, Trans. ASME, Ser. D: J. Basic Eng., 82 (1960) 34.
2 C. L. Chiu (Ed.), Applications of Kalman Filter to Hydrology, Hydraulics and Water Resources, Stochastic Hydraulics Program, Dept. of Civil Engineering, University of Pittsburg, Pittsburg, PA, 1978.
3 P. Eykhoff, System Identification, Wiley-Interscience, New York, 1974, Chap. 12.
4 A. Antoniou, Digital Filters: Analysis and Design, McGraw-Hill, New York, 1979.
5 B. Gold and C. M. Rader, Digital Processing of Signals, McGraw-Hill, New York, 1969.
6 P. D. Willson and T. H. Edwards, Appl. Spectrosc. Rev., 12 (1976) 1.
7 A. Savitzky and M. J. E. Golay, Anal. Chem., 36 (1964) 1627; 44 (1972) 1906.
8 M. U. A. Bromba and H. Ziegler, Anal. Chem., 51 (1979) 1760; 53 (1981) 1583; 55 (1983) 648; 56 (1984) 2052.
9 G. Horlick, Anal. Chem., 44 (1972) 943.
10 M. D. Srinath and P. K. Rajasekaran, An Introduction to Statistical Signal Processing with Applications, Wiley-Interscience, New York, 1979.
11 A. Gelb (Ed.), Applied Optimal Estimation, MIT Press, Cambridge, MA, 1974.
12 A. Sage and J. L. Melsa, Estimation Theory with Applications to Communications and Control, McGraw-Hill, New York, 1971.
13 A. H. Jazwinski, Stochastic Processes and Filtering Theory, Academic Press, New York, 1970.
14 I. B. Rhodes, IEEE Trans. Autom. Control, AC16 (1971) 688.
15 T. F. Brown, Dissertation, University of Washington, 1982.
16 H. B. Mark and G. A. Rechnitz, Kinetics in Analytical Chemistry, Wiley-Interscience, New York, 1968, Chap. 5.
17 L. Endrenyi (Ed.), Kinetic Data Analysis, Plenum Press, New York, 1981.

18 R. G. Brown, Introduction to Random Signal Analysis and Kalman Filtering, Wiley, New York, 1983.
19 H. W. Sorenson, IEEE Spectrum, 7 (1970) 63.
20 J. M. Mendel, IEEE Autom. Control, AC16 (1971) 748.
21 P. G. Kaminski, A. E. Bryson and S. F. Schmidt, IEEE Autom. Control, AC16 (1971) 727.
22 R. J. Fitzgerald, IEEE Autom. Control, AC16 (1971) 736.
23 R. K. Mehra, IEEE Autom. Control, AC17 (1972) 693.
24 P. C. Kelley and W. E. Harris, Anal. Chem., 43 (1971) 1170.
25 P. C. Kelley and W. E. Harris, Anal. Chem., 43 (1971) 1184.
26 T. A. Brubaker, F. N. Cornett and C. L. Pomernacki, Proc. IEEE, 63 (1975) 1475.
27 P. F. Seelig and H. N. Blount, Anal. Chem., 48 (1976) 252.
28 P. F. Seelig and H. N. Blount, Anal. Chem., 51 (1979) 327.
29 P. F. Seelig and H. N. Blount, Anal. Chem., 51 (1979) 1129.
30 H. N. J. Poulisse, Anal. Chim. Acta, 112 (1979) 361.
31 C. B. M. Didden and H. N. J. Poulisse, Anal. Lett., 13(A1) (1980) 921.
32 T. F. Brown and S. D. Brown, Anal. Chem., 53 (1981) 1410.
33 C. A. Scolari and S. D. Brown, Anal. Chim. Acta, 166 (1984) 253.
34 C. A. Scolari and S. D. Brown, Anal. Chim. Acta, 178 (1985) 239.
35 S. C. Rutan and S. D. Brown, Anal. Chem., 55 (1983) 1707.
36 A. van Loosbroek, H. J. G. Debets and D. A. Doornbos, Anal. Lett., 17(A8) (1984) 677.
37 A. van Loosbroek, H. J. G. Debets and P. M. J. Coenegracht, Anal. Lett., 17(B9) (1984) 779.
38 J. D. Salisbury, J. Inst. Navigation, 20 (1973) 190.
39 H. N. J. Poulisse and P. Engelen, Anal. Lett., 13(A14) (1980) 1211.
40 P. C. Thijssen, S. M. Wolfrum, G. Kateman and H. C. Smit, Anal. Chim. Acta, 156 (1984) 87.
41 P. C. Thijssen, G. Kateman and H. C. Smit, Anal. Chim. Acta, 157 (1984) 99.
42 P. C. Thijssen, G. Kateman and H. C. Smit, Anal. Chim. Acta, 173 (1985) 265.
43 H. N. J. Poulisse and R. T. P. Jansen, Anal. Chim. Acta, 151 (1983) 433.
44 R. T. P. Jansen and H. N. J. Poulisse, Anal. Chim. Acta, 151 (1983) 441.
45 B. Vangedinste, J. Klaessens and G. Kateman, Anal. Chim. Acta, 150 (1983) 71.
46 P. C. Thijssen, Anal. Chim. Acta, 162 (1984) 253.
47 P. C. Thijssen, L. J. P. Vogels, H. C. Smit and G. Kateman, Z. Anal. Chem., 320 (1985) 531.
48 S. C. Rutan and S. D. Brown, Anal. Chim. Acta, 167 (1985) 23.
49 S. C. Rutan and S. D. Brown, Anal. Chim. Acta, 175 (1985) 219.
50 T. F. Brown, D. M. Caster and S. D. Brown, Anal. Chem., 56 (1984) 1214.
51 P. C. Thijssen, N. H. M. DeJong, G. Kateman and H. C. Smit, Anal. Chim. Acta, 170 (1985) 265.
52 S. D. Brown and S. C. Rutan, NBS J. Res., 90 (1985) 1.
53 T. F. Brown, D. M. Caster and S. D. Brown, NBS Spec. Pub., 618 (1981) 163.
54 S. C. Rutan and S. D. Brown, Anal. Chim. Acta, 160 (1984) 99.
55 S. C. Rutan and S. D. Brown, Anal. Chim. Acta, 167 (1985) 39.
56 G. J. Bierman, IEEE Trans. Aerosp. Electron. Syst., AES9 (1973) 28.

Analytica Chimica Acta, 181 (1986) 27—36
Elsevier Science Publishers B.V., Amsterdam — Printed in The Netherlands

BAYESIAN CALIBRATION

JASHVANT D. UNADKAT[a], STUART L. BEAL[b] and LEWIS B. SHEINER*[b]

Division of Clinical Pharmacology, Schools of Medicine and Pharmacy, University of California, San Francisco, CA 94143 (U.S.A.)

(Received 29th April 1985)

SUMMARY

Two methods of analyzing calibration data are compared: the familiar least-squares method and an empirical Bayes method. The least-squares method uses the information obtained from the current calibration run but ignores all information obtained from previous runs. The empirical Bayes method uses the current information plus summarized information from past calibration runs, e.g., estimates of the means and variances of the parameters. Both methods are applied to simulated and real data. The empirical Bayes method is defined for any number of calibration standards, while the definition of the least-squares method requires modification when the number of standards is less than the number of parameters. The absolute error in predicting unknown analyte concentrations is used as a measure of goodness of calibration. When only one or two standards are used, the Bayes method results in better calibration than the least-squares method; e.g., with one standard, the average error with the Bayes method is at least 30% less than that with the least-squares method. The Bayes method is most useful when (i) run-to-run variation in calibration parameters is small (yet large enough to warrant regular calibration), (ii) residual error is significant, and (iii) it is desirable to use few calibration standards.

Calibration plots, both linear and nonlinear, are routinely generated in analytical laboratories for various assays. A commonly adopted mode of calibration is to generate a calibration graph over the range for which quantitative estimates of unknown analyte concentrations are required. This approach is costly if it requires the use of a large number of calibration standards. This paper describes an empirical Bayes method for processing calibration data that is applicable to both linear and nonlinear calibration. The method can be more efficient than the usual methods because it uses fewer standards to achieve similar precision.

Processing of calibration data usually proceeds as follows. Two sets of data (x_j, y_{1j}), $j = 1, \ldots, n$, and (x_0, y_{2j}), $j = 1, \ldots, m$, are available, where the y_{1j} and y_{2j} are responses of an assay system, and x_j, $j = 1, \ldots, n$, and x_0 are true analyte concentrations. The x_j, $j = 1, \ldots, n$ are the concentra-

---

[a]Present address: Department of Pharmaceutics, University of Washington, Seattle, WA, U.S.A. [b]Also Department of Laboratory Medicine, School of Medicine, University of California, San Francisco, CA 94143, U.S.A.

0003-2670/86/$03.50

tions of the calibration standards. The y_{1j} are the responses used to estimate the parameters of the calibration curve. The y_{2j} are used, along with the estimated calibration curve, to estimate x_0, the unknown concentration of analyte in a new sample. The x,y data are linked by the relationships

$$y_{1j} = f(\mathbf{P}, x_j) + \epsilon_{1j} \tag{1a}$$

$$y_{2j} = f(\mathbf{P}, x_0) + \epsilon_{2j} \tag{1b}$$

where the ϵ_{uj} are independent, mean zero, random errors, f is the form of the standard graph, and $\mathbf{P}$ is the vector of parameters of $\mathbf{f}$.

The classical approach to estimating x_0 is first to obtain an estimate, $\hat{\mathbf{P}}$, of $\mathbf{P}$ by fitting Eqn. 1(a) to the first set of data using weighted least-squares, and secondly to estimate x_0 from the second set of data by using

$$\hat{x}_0 = f^{-1}(\hat{\mathbf{P}}, \bar{y}_2) \tag{2}$$

where $f^{-1}(\mathbf{P}, a)$ is the value of x such that $f(\mathbf{P}, x) = a$, and $\bar{y}_2$ is the mean of the y_{2j}. This approach makes no use of data other than those in the two data sets.

In contrast, a Bayesian framework for the linear calibration problem is presented by Hoadley [1]. He postulated a prior probability distribution on x_0. This prior knowledge of the possible values for x_0 is used to modify the second step of the classical procedure. Although Hoadley's approach also assumes that parameters for each calibration graph arise from a prior distribution of possible values, this distribution is assumed to be so diffuse that virtually any finite parameter values are equally likely. Therefore, the first step of the classical procedure is not importantly changed. Later, Hunter and Lamboy [2] presented alternative Bayesian approaches, but continued to use an uninformative prior distribution for $\mathbf{P}$.

This paper focuses on a prior distribution on $\mathbf{P}$, with special emphasis on nonlinear calibration plots. This prior distribution is derived by using (rather than ignoring) information from past calibrations. To do so, a modified classical approach is adopted. The past and present calibration data are combined by use of an empirical Bayes procedure to yield an estimate, $\tilde{\mathbf{P}}$, of $\mathbf{P}$. This estimate is then used instead of $\hat{\mathbf{P}}$ in Eqn. 2 to yield $\tilde{x}_0$, another estimate of x_0. A prior distribution for x_0 is not considered. It is only for the special case of linear standard graphs curves that the approach of either Hoadley or Hunter and Lamboy can be combined with the empirical Bayes approach described here.

METHODS

To contrast the least-squares and empirical Bayes approaches, real calibration data for a drug assay (kindly supplied by SYVA Corporation, Palo Alto, CA) are used, as well as simulated data based on the real data. The goodness of calibration of the two methods is evaluated by comparing the precision of their estimates of "unknown" concentrations.

In this section, the form of the calibration plot used in this study is first described. The two approaches are then defined by specifying how each produces an estimate, $\hat{\mathbf{P}}$ and $\tilde{\mathbf{P}}$, respectively, of the vector of calibration curve parameters. Next, the real data are described. Finally, the simulated data and the studies conducted with them and with the real data are detailed.

A modified logistic function is used as the form of the calibration curve. The expected value of a response of the assay system to a sample with known analyte concentration, x, is

$$f(\mathbf{P}, x) = \{\mathbf{P}_1/[1 + \exp(-Q)]\} + \mathbf{P}_2 \tag{3}$$

where $Q = \mathbf{P}_3 + \mathbf{P}_4[\ln(x) + \mathbf{P}_5 x]$. For reasons explained below, the parameter, $\mathbf{P}_5$, is treated as a known constant, the value of which does not vary from run-to-run.

Estimators of P

The least-squares estimator of P. The ϵ_{uj} of Eqn. 1(a, b) are assumed to be statistically independent with zero mean and with variance σ^2. With this assumption, an estimate of $\mathbf{P}$ is traditionally obtained by using ordinary (unweighted) least squares. The least-squares (LS) estimate of $\mathbf{P}$ is that value of $\mathbf{P}$ minimizing the expression

$$O_{\mathrm{LS}}(\mathbf{P}) = \sum_{j=1}^{n} [y_{1j} - f(\mathbf{P}, x_j)]^2 \tag{4}$$

The validity of the constant variance assumption and the use of unweighted least squares with the present data are supported by the observed homogeneous distribution of residuals about the fitted curve (Eqn. 3).

When n, the number of y_{1j}, is less than 4, the number of effective calibration curve parameters, Eqn. 4 has no unique minimum with respect to $\mathbf{P}$. For such cases, the least-squares estimator is here redefined as follows: $\hat{\mathbf{P}}_1, \ldots, \hat{\mathbf{P}}_n$ are the values minimizing Eqn. 4 with $\hat{\mathbf{P}}_{n+1}, \ldots, \hat{\mathbf{P}}_4$ fixed to certain values, $\hat{\theta}_{n+1}, \ldots, \hat{\theta}_4$. These fixed values are elements of the prior mean of $\mathbf{P}$, obtained as described in the next section. As will be seen in the results section, the inter-curve standard deviation of the $\mathbf{P}_k$ decreases with k, so it is natural to fix the $\hat{\mathbf{P}}_k$'s as indicated.

The empirical Bayes estimator of P. In this approach, $\mathbf{P}$ is assumed to arise from a multivariate normal prior distribution with mean $\theta = (\theta_1, \ldots, \theta_4)$ and covariance matrix Ω. The residual errors, ϵ_{uj}, are assumed to be normally distributed with zero mean, and variance σ^2. Using Bayes rule, the mode of the posterior distribution for $\mathbf{P}$, given the y_{1j} (for $j = 1, \ldots, n$) is $\tilde{\mathbf{P}}$, the value of $\mathbf{P}$ minimizing the expression

$$O_{\mathrm{EB}}(\mathbf{P}) = \sum_{j=1}^{n} \{[y_{1j} - f(\mathbf{P}, x_j)]^2/\sigma^2\} + \sum_{k=1}^{4} \sum_{l=1}^{4} (\mathbf{P}_k - \theta_k)\omega^{kl}(\mathbf{P}_l - \theta_l) \tag{5}$$

where ω^{kl} is the k,lth element of Ω^{-1}. The first term on the right-hand side of Eqn. 5 is simply proportional to the usual sum of squared deviations of observations from predictions, as in the least-squares function (Eqn. 4). To get a better idea of what the second term on the right-hand side of Eqn. 5 means, observe that, if all covariances $\omega^{kl}(k \neq l)$ were zero, the term would be $\sum_{k=1}^{4} [(\mathbf{P}_k - \theta_k)^2/\omega_{kk}]$, which is termwise proportional to the simple sum of squared deviations of the elements of $\mathbf{P}$ from their "predictions" (prior means). The minimum of Eqn. 5 is defined no matter what the value of n; no ad hoc modification is required when the number of parameters in $\mathbf{P}$ exceeds the number of calibration standards. When $n = 0$, the minimum of Eqn. 5 clearly occurs when $\mathbf{P} = \theta$, its prior mean. As n increases, the relative contribution of the first summation in Eqn. 5 increases, and the empirical Bayes estimator tends towards the least-squares estimator given in Eqn. 4. For modest n, the relative magnitudes of σ^2 and Ω determine the compromise between the two extremes: the noisier the observations (large σ^2), the more $\tilde{\mathbf{P}}$ tends towards the prior mean; and the more diffuse the prior distribution ("large" Ω), the more $\tilde{\mathbf{P}}$ is determined by the calibration data.

To apply this method, values for the parameters, θ, Ω and σ^2 are required. These are obtained by analysis of an index group of I sets of calibration data, arising from I previous calibration runs, and assumed to be representative of a population of runs that includes the current one. One way to estimate the parameters is as follows: $\mathbf{P}_i$ denotes the true value of $\mathbf{P}$ for the calibration curve giving rise to the ith index data set. First, Eqn. 4 is used to estimate $\mathbf{P}_i$ for each of the I data sets separately. This results in estimates, $\hat{\mathbf{P}}_i$, $i = 1, \ldots, I$. Secondly, the mean of the $\hat{\mathbf{P}}_{ik}$ estimates θ_k, while the sample covariance matrix of the $\mathbf{P}_i$ estimates Ω. Finally, the quantity, $\hat{\sigma}^2$, is estimated from $I^{-1}(n-4)^{-1} \sum_{i=1}^{n} O_{\mathrm{LS}}(\hat{\mathbf{P}}_i)$. In fact, a somewhat more sophisticated approach (using the computer program NONMEM [3]) was used to estimate θ, Ω, and σ^2. The approach has been discussed elsewhere [4].

Two additional points regarding the empirical Bayes method are of note. First, this Bayes method is not limited to the case that σ^2 is a constant. If the variance of ϵ_{1j} varies with j, σ^2 in Eqn. 5 is simply replaced by that variance (or an estimate of it). Secondly, in principle, neither the data needed for calibration (by either method) nor the data used to estimate the population parameters (by the Bayes method) need include replicate responses at any standard concentrations. To the extent that replicates are available, however, they may contribute additional information, e.g., in estimating the population parameter, σ^2.

The real data

The real data consist of data from 25 calibrations. Concentrations of standards were 0, 1, 2, 4, 8, and 16 in arbitrary units. For all 25 runs, duplicate assay responses were present at all analyte concentrations except 0 and 1, for

which duplicates were only sometimes present. The responses ranged from 436 to 473 and from 711 to 790 for analyte concentrations 0 and 16, respectively. Figure 1 illustrates a typical calibration; the solid line is the fit obtained with Eqn. 3.

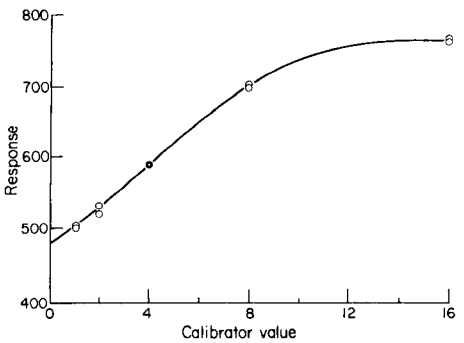

Fig. 1. Typical calibration data: (○) observed values; (—) value predicted from best-fit standard curve (Eqn. 3).

Studies with simulated and real data

Simulated data. Estimates $\hat{\theta}$, $\hat{\Omega}$ and $\hat{\sigma}^2$ were obtained by analyzing all the data from all 25 real calibration runs using NONMEM (Table 1). Individual sets of calibration data from 100 calibration runs were simulated. The ith set was simulated by first choosing $\mathbf{P}_i$ randomly from a multivariate normal distribution with mean $\hat{\theta}$ and covariance $\hat{\Omega}$. Six responses, $y_{ij}, j = 1, \ldots, 6$ corresponding to $x_j = 0, 1, 2, 4, 8, 16$, were generated by first computing a "true" y_{ij} using Eqn. 3 (with $\mathbf{P}_i$ chosen as above) and then adding to it a random "error" chosen from a normal distribution with mean 0 and variance σ^2 [5, 6].

Several subsets of calibration data, none greater than size three, were obtained from each full set of calibration data by choosing different subsets of standards. For example, one subset included only the standard at concentration 2; another, two standards, at concentrations 2 and 8. The 100 subsets corresponding to each choice of a combination of standards are here referred to collectively as a particular simulation. Each simulation was processed by both the least-squares and empirical Bayes methods.

The ability to predict concentrations of unknown analytes using the parameter estimates $\hat{\mathbf{P}}_i$ or $\tilde{\mathbf{P}}_i$ (the subscript i now refers to the ith data subset of a given simulation) is measured by computing an "average" goodness of calibration measure over the 100 subsets. A goodness of calibration measure for a given subset is defined as the average distance between the true concentration (x_0) and the predicted (or estimated) concentration, $\hat{x}_0$ ($\tilde{x}_0$) for a typical set of values of x_0. The set of values used here are $x_0 = 2$, 4 and 8. The value of m (see paragraph above Eqn. 1) is taken to be 1, and y_2 is computed without added random error. Therefore, $\hat{x}_0$ ($\tilde{x}_0$) corresponds to the

mode of the distribution of estimated concentrations that would result from using the estimated calibration curve for an unknown with true concentration x_0.

The goodness of fit measure for each subset of a simulation is defined as the average (across the three assessment points, x_{01}—x_{03}) of the absolute values of the errors expressed as a percentage (E) of $\hat{x}_0$ ($\tilde{x}_0$):

$$E = (100/3) \sum_{j=1}^{3} |(z_j - x_{0j})/x_{0j}| \tag{6}$$

where $z_j = \hat{x}_{0j}$ or $\tilde{x}_{0j}$. The mean (EM) of the above E values across the 100 subsets of the simulation is the final goodness of calibration measure used herein.

Real data. Essentially the same procedure as described for the simulated calibrations was followed for the real data. Some differences, necessitated in part by the restricted amount of real data available, are noted below.

The set of 25 standard-curve data sets was randomly divided into five distinct subsets (S_1—S_5). Each subset was removed from the complete data set leaving a depleted remainder subset (S_1'—S_5'). Each depleted subset was processed with NONMEM and parameter estimates, $\hat{\theta}_l$, $\hat{\Omega}_l$, and $\hat{\sigma}_l^2$, corresponding to S_l' (for $l = 1, \ldots, 5$) were obtained. The estimates, $\hat{\theta}_l$, $\hat{\Omega}_l$, and $\hat{\sigma}_l^2$, were used as the values of the prior mean and variance in the empirical Bayes analysis of data from S_l, the lth (original) subset. This procedure was followed so that real data used to estimate the parameters of the prior sets differed from that used by the empirical Bayes method.

A complete set of actual y values, corresponding to $x = 0, 1, 2, 4, 8, 16$, was chosen randomly from each real calibration data set (in S_l) for use as the y_{1j}. The remaining (duplicate) y values at $x = 2, 4, 8$ were used as assessment points. Again, different subsets of the y_{1j} were used by the two methods in different simulations. For each simulation, for each l, the goodness of calibration measure (E; Eqn. 6) was computed, using the assessment data, for each of the five real standard-curve data sets in S_l. The final measure (EM) was computed as previously, except that the average was over the 25 subsets, five from each of the subsets S_1—S_5. In this case, the individual values, $\hat{x}_0$ and $\tilde{x}_0$, used to assess goodness of calibration are not the modes of the distributions of estimated concentrations.

RESULTS

Figure 1 illustrates the fit of the logistic-type model (Eqn. 3) to all of the data from a typical real calibration curve. That the model is appropriate for the data is supported by the homogeneous random scatter of residuals about the curve (Fig. 2, in which residuals are shown for only three curves for clarity) as well as by the small absolute size of the residuals (typically 1—3 units), relative to the size of a typical response (ca. 600 units).

The estimates of the mean parameters, θ, and the run-to-run standard devi-

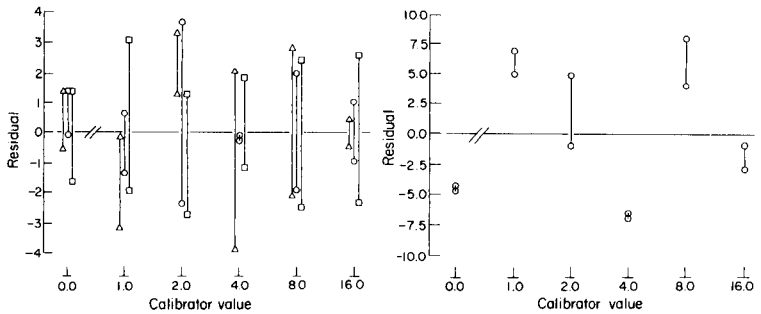

Fig. 2. Plot of residuals obtained for three calibration curve data sets fitted by Eqn. 3. The abcissa is logarithmic, whereas the ordinate is in units of the measured response. The vertical lines connect residuals from duplicate standards. The three distinct calibrations are indicated by different symbols, and their pairs of residuals are deliberately offset for clarity.

Fig. 3. Plot of residuals from fit of an incorrect model to data shown in Fig. 1. Format as for Fig. 2.

ations, and covariances, and the residual standard deviation, σ, from all of the real data, are given in Table 1. The estimates of the run-to-run standard deviations show that the parameters vary little between curves. For example, the coefficient of variation of P_2 is only ca. 2%. In fact, the coefficient of variation of P_5 (not shown) is so small that P_5 was assumed to be a constant, the value of which is known to equal the estimated mean, $\hat{\theta}_5$. It should also be noted that the standard deviation of the P_k decreases with k. The estimate, $\hat{\sigma}$, shows that a typical residual error (1σ) is only a small percentage (0.5%) of a typical response.

The goodness of calibration measure (EM), the difference in this measure between the two methods of calibration, and the statistical significance of the difference for the simulation and real studies are listed in Table 2. Table 2 presents only the results from a selected set of simulations. Although calibration schemes using two standards with identical concentrations can be studied via simulations, they cannot be studied with the real data available here, because these had only two responses for each standard. Therefore, results of simulations with two identical standards are not presented. In both Tables 1 and 2, the optimal subsets (of sizes one and two) of standard(s), for each scheme, as determined by the smallest value of EM, are marked by a superscript d.

DISCUSSION

For a calibration scheme that uses only one standard, the results of the simulation study (Table 2) indicate that when the standard concentration yielding the best performance for both methods ($x = 4$) is used, the empirical Bayes method reduces the estimation error of a typical unknown sample by almost 40% relative to the least-squares method.

TABLE 1

Estimates of mean parameter values and run-to-run standard deviations and covariances[a]

Parameters	Mean value ($\hat{\theta}_k$)	SD ($\hat{\omega}_{kk}^{1/2}$)	Covariances ($\hat{\omega}_{kl}$)		
			P_2	P_3	P_4
P_1	294.0	10.90	29.1	0.966	−0.0225
P_2	457.0	8.93		−0.149	0.0879
P_3	−2.63	0.16			−0.00496
P_4	0.455	0.036			

[a]Standard deviation of residual error ($\hat{\sigma}$) = 3.24.

TABLE 2

Goodness of calibration[a] when simulated and real data are processed by the least-squares and empirical Bayes methods for various standard subsets

Standards used	Least-squares	Empirical Bayes	Mean difference[b]	p[c]
Simulated data				
2	15.33	4.14	11.9	<0.001
4	6.47[d]	3.90[d]	2.57	<0.001
8	6.72	5.18	1.54	<0.001
16	8.59	6.13	2.46	<0.001
0, 8	5.02	4.77	0.252	<0.025
1, 8	3.12	3.02	0.099	<0.100
2, 8	3.00[d]	2.72[d]	0.285	<0.025
1, 16	5.70	4.90	0.800	<0.001
2, 16	4.39	3.82	0.570	<0.001
8, 16	25.5	4.22	21.3	<0.001
Real data				
2	9.04	5.27[d]	3.96	<0.025
4	7.69	5.84	1.86	<0.100
8	7.31[d]	6.32	0.984	<0.400
16	9.24	6.48	2.76	<0.050
0, 8	5.00	5.48	−0.475	<0.050
1, 8	4.75	4.72	0.027	>0.500
2, 8	3.84[d]	3.65[d]	0.189	<0.500
1, 16	5.44	5.27	0.163	<0.400
2, 16	5.01	4.95	0.050	>0.500
8, 16	23.72	5.13	18.60	<0.001

[a]EM (see Methods). [b]Mean difference in E (Eqn. 6); least-squares minus empirical Bayes. [c]Probability value by the (paired) t-test. [d]Optimal standards.

For a calibration scheme using two standards, although the empirical Bayes method continues to do better than the least-squares method, the reduction in estimation error is only 9% for the optimal case ($x = 2, 8$). The reason for this small difference between the two methods is that as the number of standards increases, the effect of the prior distribution on the parameter estimates decreases, so that the two estimators become more similar.

When $n \geqslant p$ (where p is probability), estimates $\hat{\mathbf{P}}$ and $\tilde{\mathbf{P}}$ are theoretically closer, the smaller the number of unknown parameter variance of the residual error. In the real data set, the residual error had coefficient of variation $\approx 0.5\%$, whereas in other data sets it could be as much as 5—10%. Additional simulations showed that when the value of σ^2 was increased ten-fold (so that the RSD was increased to ca. 1.7%), the EM from the empirical Bayes method is less than the EM from the least-squares method by more than 30% for the optimal two-standard case ($p < 0.001$).

The fact that the results of the analysis of the real data show the same order of magnitude of the difference in EM, between the two methods, as do the results of the simulations, adds credence to the simulation results. The lack of statistical significance of the real-data results is partly offset by the almost uniformly apparent better performance of the empirical Bayes method over the entire range of subsets of standards.

From the studies reported here it is concluded that the empirical Bayes method can result in better calibration than the least-squares method if the number of standards is small and/or if the magnitude of residual error is large. Alternatively, use of the empirical Bayes method will reduce the number of standards required to achieve a specified critical magnitude of calibration error. Use of the empirical Bayes method can also protect against bad design of the calibration study. For instance, when standards at 8 and 16 are used, the EM for the empirical Bayes method is six-fold smaller than the EM for the least-squares method (Table 2).

An exception to the above occurs when the model is incorrect. In that case, the weighting given by the Bayes method to the prior distribution is inappropriate, and the method may not be useful. For example, Fig. 3 shows a residual plot from the fit of a model different from that given by Eqn. 3 to the same data as shown in Fig. 1. The systematic trend of the paired residuals clearly indicates a poor fit. When this incorrect model was used with the real data, the empirical Bayes method performed no better, and in some cases worse, than the least squares method. Several selected results of this analysis are presented in Table 3.

In conclusion, when the run-to-run variability in calibration parameters is small yet large enough to warrant regular calibration, and when the residual error is significant, and when it is desirable for any reason to use few standards, the Bayesian calibration method presented here offers distinct advantages over the least-squares method if prior study shows that the functional form chosen to represent the standard curve is correct. Moreover, the empirical Bayes method provides a framework for further development. For example, if the index group of calibration data sets consists of data sets from

TABLE 3

Goodness of calibration for various standard subsets, when real data are processed by both methods with an incorrect model

Standards	Least-squares	Empirical Bayes
8	16.1	11.83
1, 8	9.57	10.93
1, 16	8.52	11.87

different laboratories, then interlaboratory variability in the mean and variance of calibration curve parameters can also be taken into account in a Bayesian framework, and just as a calibration scheme can be optimized for a specific run by using data on inter-run variability, so it can be optimized for a specific laboratory by using data on inter-laboratory variability.

This work was supported in part by NIH Grants GM 26676 and GM 26691, and by the SYVA Corporation.

REFERENCES

1 B. Hoadley, J. Am. Stat. Assoc., 65 (1970) 356.
2 W. G. Hunter and W. F. Lamboy, Technometrics, 23 (1981) 323.
3 S. Beal and L. B. Sheiner, Am. Stat., 34 (1980) 118.
4 S. Beal and L. B. Sheiner, Technical Report of the Division of Clinical Pharmacology, University of California at San Francisco, 1980.
5 P. Lewis, A. Goodman and J. Miller, IBM Systems J., 8 (1969) 135.
6 G. E. P. Box and M. Muller, Ann. Math. Stat., 29 (1958) 610.

Analytica Chimica Acta, 181 (1986) 37—49
Elsevier Science Publishers B.V., Amsterdam — Printed in The Netherlands

SIMULTANEOUS CORRELATION CHROMATOGRAPHY, A NEW TECHNIQUE APPLIED TO CALIBRATION IN HIGH-PERFORMANCE LIQUID CHROMATOGRAPHY

H. C. SMIT*, C. MARS and J. C. KRAAK

Laboratory for Analytical Chemistry, University of Amsterdam, Nieuwe Achtergracht 166, 1018 WV Amsterdam (The Netherlands)

(Received 19th September 1985)

SUMMARY

Simultaneous correlation chromatography (SCC) is introduced as a technique capable of analyzing several different samples simultaneously on the same chromatographic column. The theoretical basis of the technique is outlined and a computer simulation demonstrates the feasibility of the method. The advantages and potential of the technique are discussed. The technique is applied experimentally in a calibration procedure for high-performance liquid chromatography. During the calibration, unknown sample and calibration standards are processed under the same conditions, resulting in very accurate calibration. Other applications are outlined.

The basic principles of correlation chromatography have been established for a considerable time [1—3] and several applications have been reported, particularly in trace determinations, gas chromatography and high-performance liquid chromatography (HPLC) [4—8]. Another interesting application is the use of correlation chromatography in continuous gas analysis, e.g., with pyrolysis techniques [9].

Correlation chromatography belongs to the family of multiplex methods and is essentially statistical in nature. It cannot be considered as a real separation method; the correlogram is calculated from a (pseudo)random input signal and from the resulting very complex detector signal. Although the components passing the detector are unresolved, a correlogram analogous to a conventional chromatogram is obtained. In other words, it is possible to measure a chromatogram from a sample without a physical separation. Nevertheless, the retentive properties of the column have to be the same as in common chromatography.

The question arises whether it is possible to analyze ("separate") more than one sample at the same time in one column by applying the same principles. The following reasoning looked promising. Suppose that two (or more) different samples are injected simultaneously, each controlled by a random input pattern, suitable for correlation chromatography but mutually completely uncorrelated. Then completely independent correlograms should be

0003-2670/86/$03.50

obtained even if the same components are present in the different samples. Such multiplex procedures would greatly improve the efficiency of chromatography. In practice a big problem arises. It is necessary to use pseudo-random binary sequences (PRBS) to reduce the measurement time and the estimation error to acceptable values. However, completely uncorrelated pseudo-random patterns cannot be generated, which means that the suggested procedure is impracticable. A possible solution is described, which obviates this problem at the cost of time. Some experiments on the simultaneous determination of two components are known [10, 11]. In this paper, a generalization for more samples and a practical application are presented. The basic principle is the use of only one long PRBS, but with a time shift equal to an integral number of chromatogram durations but different for each sample. Computer simulation shows the practicality of the method and results of practical experiments are given. The possibilities and limitations of this new method are discussed.

THEORY OF CORRELATION CHROMATOGRAPHY

For convenience, the principles and theory of common correlation chromatography, including definitions of relevant quantities, are outlined briefly. This theoretical basis will be used to explain the principles of simultaneous correlation chromatography (SCC).

In common correlation chromatography, the sample is not injected as a single pulse, but according to a PRBS [12]. A PRBS is a binary noise with a specific length (the sequence length) of $2^m - 1$ periods controlled by a clock, $m \in N$, the only two levels being $+1$ and -1 or 1 and 0. The periodic nature of the PRBS input signals yields low estimate variance of the evaluation of statistical quantities like correlation functions if taken over an integral number of sequences. Besides, the levels can be used to control simple on-off valves, corresponding to the "injection" of sample and mobile phase. The output from the detector is a summation of all the chromatograms resulting from the injections; straightforward interpretation of the detector signal is impossible. However, taking the cross-correlation function $R(t_1, t_2)$ of the injection pattern $x(t)$ (the PRBS) and the detector signal $y(t)$ yields a correlogram identical to a chromatogram obtained from a single injection if certain conditions are fulfilled. By definition,

$$R_{xy}(t_1, t_2) = E[x(t_1)y(t_2)] \tag{1}$$

where $E[\,]$ denotes the expected value of the expression between the brackets. Under stationary conditions, Eqn. 1 can be rewritten as $R_{xy}(\tau) = E[x(t - \tau)\, y(t)]$. In practice, discrete signals are used:

$$R_{xy}(k) = (1/M) \sum_{j=1}^{M} x_{j-k} y_j \tag{2}$$

It can be proved that the cross-correlation function $R_{xy}(\tau)$ is only equivalent to the chromatogram obtained from a single injection if the autocovariance function (ACVF) of the input signal is approximately impulse-shaped [3]. The ACVF is defined by $R_{xx}(t_1, t_2) = E[x(t_1)x(t_2)]$. Under stationary conditions the ACVF is $R_{xx}(\tau) = E[x(t-\tau)x(t)]$. In practice,

$$R_{xx}(k) = (1/M) \sum_{j=1}^{M} x_{j-k} x_j \tag{3}$$

In correlation chromatography, the shape of the ACVF of the input signal can be considered as the shape of a (virtual) single injection resulting in the correlogram. The ACVF of a PRBS is a triangle with a basewidth of two clock periods (Fig. 1). The sample is injected many times during the length of the chromatogram, therefore the signal-to-noise ratio is dramatically increased compared with normal chromatography based on single injection. This is one of the most important advantages of correlation chromatography. A disadvantage is that more time is always needed because all the injected components must pass the detector during the correlation procedure. The consequence is the extension of the correlation time with at least one extra sequence, the pre-sequence.

SIMULTANEOUS CORRELATION CHROMATOGRAPHY

The basic principle of SCC is the simultaneous determination of n different samples on the same column by using multiplex techniques. The basis of the SCC technique is the use of a PRBS with a length equal to the sum of the durations of the n different chromatograms. This PRBS is used to control the input of each sample to the column, but the start position in the PRBS is different. Each sample starts at a specific place with start positions s_1, s_2, ... s_n, respectively. The result is a combination of shifted versions of the same PRBS, each version $x(t - s_i)$ being the injection pattern of sample i. If the response of the column (chromatogram) to a normal inpulse-shaped injection is $h_i(t)$, then the output signal resulting from sample i can be calculated as a convolution of the input signal and the impulse response of

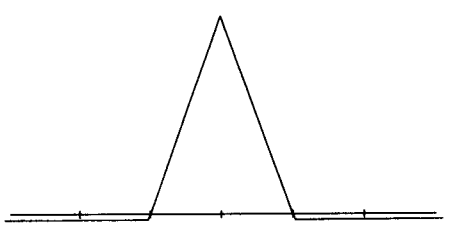

Fig. 1. The autocovariance function of a PRBS (virtual injection).

the system:

$$y_i(t) = x(t - s_i) * h_i(t) \quad \text{or} \quad y_i(t) = \int_0^\infty h_i(\tau)x(t - s_i - \tau)\mathrm{d}\tau \tag{4}$$

The total output signal is a summation of the output signals of the n samples:

$$y(t) = \sum_{i=1}^{n} y_i(t) \tag{5}$$

Substituting Eqn. 5 in Eqn. 1 gives

$$R_{xy}(t_1, t_2) = E[x(t_1) \sum_{i=1}^{n} y_i(t_2)] \tag{6}$$

Interchanging the expected value and the summation procedure gives

$$R_{xy}(t_1, t_2) = \sum_{i=1}^{n} E[x(t_1)y_i(t_2)] \tag{7}$$

Substituting Eqn. (4) in Eqn. 7 yields

$$R_{xy}(t_1, t_2) = \sum_{i=1}^{n} E[x(t_1) \int_0^\infty h_i(\tau)x(t_2 - s_i - \tau)\mathrm{d}\tau] \tag{8}$$

This gives

$$R_{xy}(t_1, t_2) = \sum_{i=1}^{n} \int_0^\infty h_i(\tau)E[x(t_1)x(t_2 - s_i - \tau)]\,\mathrm{d}\tau \tag{9}$$

Correlation of $x(t)$, in this case a PRBS, and the i shifted PRBS injections $x(t - s_i)$ will give i shifted ACVFs ${}^iR_{xx}$:

$${}^iR_{xx}(t_1, t_2 - s_i - \tau) = E[x(t_1)x(t_2 - s_i - \tau)] \tag{10}$$

Equations 9 and 10 give

$$R_{xy}(t_1, t_2) = \sum_{i=1}^{n} \int_0^\infty h_i(\tau){}^iR_{xx}(t_1, t_2 - s_i - \tau)\mathrm{d}\tau \tag{11}$$

If $x(t)$ is stationary, then

$${}^iR_{xx}(t_1, t_2 - s_i - \tau) = {}^iR_{xx}(t_2 - s_i - \tau - t_1) = {}^iR_{xx}(t - s_i - \tau) \tag{12}$$

Hence,

$$R_{xy}(t) = \sum_{i=1}^{n} \int_0^\infty h_i(\tau){}^iR_{xx}(t - s_i - \tau)\mathrm{d}\tau \tag{13}$$

Equation 13 can be written as a sum of convolutions:

$$R_{xy}(t) = \sum_{i=1}^{n} {}^{i}R_{xx}(t - s_i) * h_i(t) \tag{14}$$

This means that the cross-correlation function is a summation of i convolutions, each convolution resulting from a sample. The convolutions can be considered as the outputs caused by the virtual inputs ${}^{i}R_{xx}(t - s_i)$ and the impulse responses $h_i(t)$ as being the chromatograms of the samples. The input ${}^{i}R_{xx}(t - s_i)$ is a shifted ACVF of the PRBS, in effect the virtual injection of the sample. This means that in the correlogram the response of the sample, the chromatogram, can be found directly after the virtual injection time. The time between these virtual injections has to be large enough to avoid overlap of the responses of the samples in the total correlogram. Besides, all the correlograms of the samples must fit in the total correlogram. These demands lead to the following conditions:

$$M\Delta T > \sum_{i=1}^{n} l_i \tag{15}$$

and

$$|s_{i+1} - s_i|\Delta T > l_i \tag{16}$$

where M is the sequence length of the PRBS, ΔT the clock period in seconds, n the number of samples, l_i the length in seconds of the chromatogram of sample i, and s_i the shift of the PRBS of sample i expressed in clock periods.

These principles of simultaneous chromatography are illustrated in Fig. 2. The technique is shown for three samples with the same chromatogram length and a short sequence length, in this case 31 clock periods. The PRBS is divided into three parts to determine the starting points of the three shifted injection patterns, one for each sample. The resulting injection patterns for the samples are also shown in Fig. 2. The injection procedure corresponds to three different virtual injections, positioned at the beginning, at one third and at two thirds of the total sequence length (Fig. 2). No overlap of the three sample correlograms occurs in the total correlogram, provided that the time between two virtual injections is equal to, or greater than, the chromatogram length of the samples. The correlograms of the three samples can be found respectively in the first, the second and the third part of the total correlogram. Figure 3 shows the results of a computer simulation.

EXPERIMENTAL

One of the problems with practical experiments in simultaneous chromatography is the injection of the samples. The independent simultaneous random injections of more than one sample into the column must not influence the performance of the chromatographic system. If this condition is not

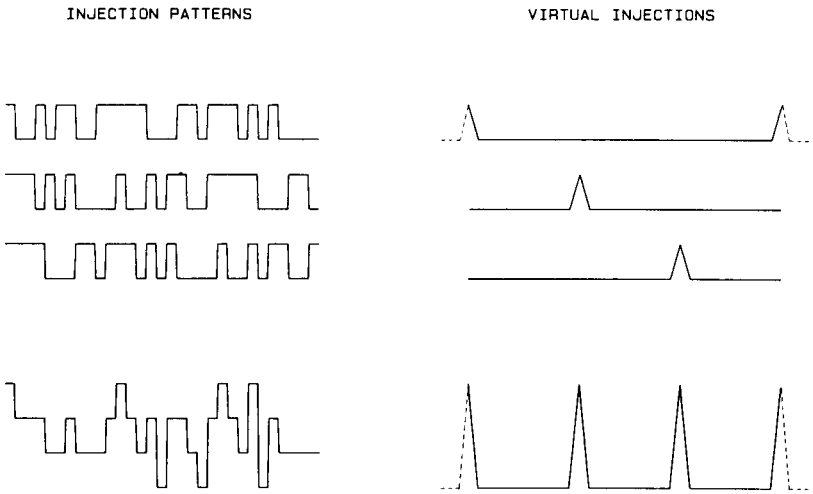

Fig. 2. SCC of three samples with equal chromatogram length. The three upper lines show the shifted injection patterns and the shifted virtual injections of the three samples; the bottom lines shows the injection pattern and the virtual injection in the case of SCC. Dividing the clock period into sub-clock-periods is not taken into account.

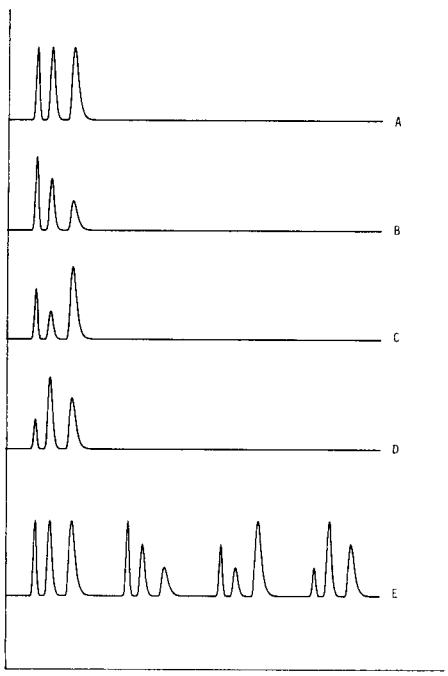

Fig. 3. A simulation of SCC with four samples. Curves A, B, C and D show the single correlograms and curve E the result of SCC.

fulfilled, correlation noise and ghost peaks can be expected and the separation can be affected; this problem will be addressed in a later paper.

The first experiments with SCC were done with HPLC. The injection principle is the same as described in earlier publications concerning common correlation chromatography [8]. Four reservoirs are used, which means that three samples can be measured simultaneously; the fourth tube contains the eluent. The equipment is outlined in Fig. 4. The outlets of the reservoirs are connected to the column by a home-made arrangement with very narrow-bored tubing. The samples and the eluent are separated from the pump by electromagnetic valves and freely movable plungers. A driving liquid, generally water, moves the plunger forward if the valve is open and the corresponding sample or the eluent flows into the column. This construction allows the application of commercially available valves without special specifications concerning corrosion resistance, inertness and low dead volumes. If either eluent or one sample is fed into the column, as is usual in common correlation chromatography, the flow will not be disturbed. The situation is different in the case of SCC. In the chosen example with three samples, possibly two or three samples have to be injected simultaneously into the column. In each case the flow in the column has to be kept constant. This problem was tackled as follows. Sample can be injected during the total clock period, but it is also possible to inject sample only during a (variable) part of the period; which part is not important. It does not matter at what time in a clock period the sample is injected into the column. Of course, reducing this "duty cycle" implies reducing the amount of the injected sample. The mentioned problem of simultaneous injection can then be solved by subdividing the clock period into n parts if n samples have to be analyzed. Each part can be

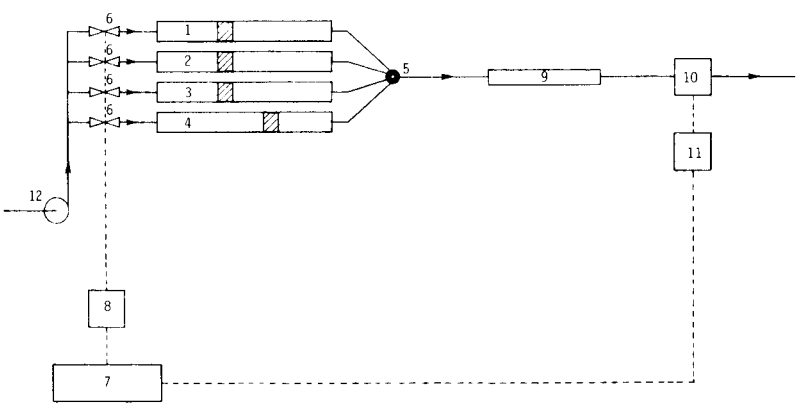

Fig. 4. Schematic diagram of a SCC system with three sample reservoirs. (1, 2, 3) Sample reservoirs; (4) eluent reservoir; (5) home-made joint; (6) electromagnetic valves (Lucifer 121, Model A54), stainless steel, 24 V; (7) microcomputer; (8) valve driver; (9) column; (10) u.v. detector, 254 nm (Spectra-Physics SP8300); (11) amplifier and low-pass filter; (12) pump (Spectra-Physics 740B).

used for the injection of a particular sample; depending on the momentary binary level of the PRBS, sample or eluent is fed into the column by switching the corresponding valves. The electromagnetic valves are controlled by a microprocessor system via power amplifiers. This system generates the shifted pseudo-random binary sequences. The same microprocessor [13] is used for data acquisition. After being amplified, filtered by an anti-aliasing filter and digitized, the detector signal is stored on tape. An off-line correlation program, developed in this laboratory and run on a HP-1000 computer, yields the different correlograms (chromatograms). Thus the concentrations of the components of each sample can be determined by data processing afterwards.

RESULTS

At first sight, SCC looks very promising for reducing the analysis time (routine analysis) because of the simultaneous processing of several samples. However, the need to correlate an integral number of sequences, at least one (long) PRBS length, implies an extension of the analysis time and eliminates the time advantage of simultaneous injection. However, it is not necessary to use a complete pre-sequence; the length of the longest chromatogram is sufficient. Of course, the dramatic noise-reduction property of the correlation procedure still holds. Nevertheless, very interesting applications can be found by using the property that in SCC all samples are "separated" under exactly the same conditions.

A chromatographic system is never stable and quantitative chromatographic analysis is never free from deterministic or random errors. This emphasizes the necessity of regular calibration, and in case of random errors there will be uncertainty in the establishment of the calibration curve. Furthermore, calibration parameters always drift slowly and in analytical practice regular recalibration is essential. Because of its properties, SCC can reduce the errors and greatly improve the accuracy of the calibration. Sample and calibration standards can be measured simultaneously on the same chromatographic system under the same conditions. Therefore, this application was chosen for the first experiments. The following chromatographic conditions were selected: A Supelco LC-8DB column (5 μm; 15 cm long, 4.6 mm i.d.) was used with a methanol/water eluent (84% v/v methanol) at a flow rate of 1 ml min^{-1}.

Three different samples, each composed of naphthalene, anthracene and 1,2-benzanthracene, were prepared (Table 1). The concentrations of naphthalene and 1,2-benzanthracene were halved for the successive samples, while the anthracene concentration was kept constant. Anthracene was used as the internal standard to correct for variations in the injected volumes of the different samples. The normal chromatogram of one of the samples is shown in Fig. 5A. In the SCC experiment, a PRBS with a length of 127 clock periods was used; the starting points of the injection patterns of the samples were shifted over one third of the PRBS length. The clock period of 9 s was divided

TABLE 1

The concentrations of naphthalene, anthracene and 1,2-benzanthracene in the three samples used for SCC

Compound	Concentration (mg l^{-1})		
	1	2	3
Naphthalene	7.690	3.845	1.922
Anthracene	0.320	0.320	0.320
1,2-Benzanthracene	2.152	1.076	0.538

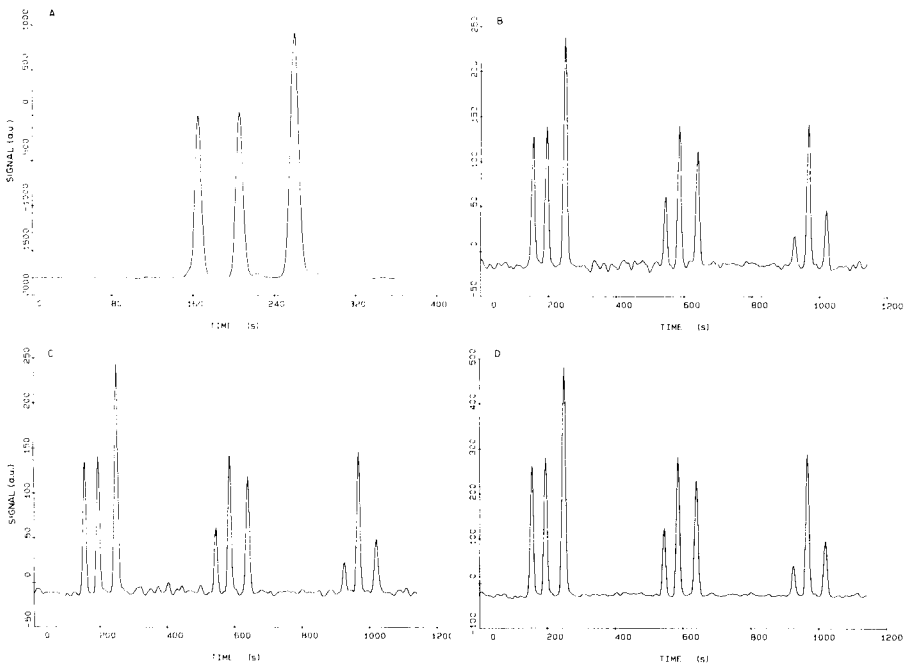

Fig. 5. Results: (A) normal chromatogram for sample 1; (B) simultaneous correlogram 1; (C) simultaneous correlogram 2 (bits inverted); (D) the sum of simultaneous correlograms 1 and 2. Signals are given in arbitrary units.

into 3 sub-clock-periods of 3 s each. The complex signal of the detector was filtered by a low-pass filter with a cut-off frequency of 0.1 Hz to prevent aliasing, and was digitized with a frequency of 0.33 Hz, which resulted in 1 data point for each sub-clock-period. The data obtained were processed afterwards on the HP-1000 minicomputer by the mentioned correlation program. Results are shown in Fig. 5B and C. The "chromatograms" of the different samples appear, as expected, in the first third, the second third and the last third of the correlogram, respectively. With one exception, the chosen

experimental conditions were similar for both correlograms; the bits of the PRBS were inverted, i.e., an injection during a certain level of the PRBS in the first case corresponds to no injection (eluent) in the other case. Obviously, the method works quite well in practice. The rather "noisy" baseline can be explained by the experimental injection system. The sample reservoirs and plungers were partly from an older construction, resulting in a non-ideal injection and therefore noise-like ghost peaks on the baseline. The development of an appropriate injection system will certainly improve the baseline, as will be proved by the results of the following experiment, which will be explained fully in a later paper. The correlograms of Fig. 5B and C are averaged, with the result shown in Fig. 5D. The *S/N* ratio of this addition of the two correlograms is much better than could be expected from the averaging of two independent noise recordings. This implies that most of the baseline "noise" is deterministic and mainly originates from the imperfect injection system. An extensive treatment of the origin of spurious peaks with a noise-like appearance in correlation chromatography will be given later.

To evaluate the parameters of the peaks, a fitting procedure was applied to the correlograms using a non-linear regression software package with a Fraser-Suzuki peak model [14]. The peak areas were calculated (Table 2) and corrected for systematic errors with the internal standard (anthracene). The values obtained are shown in Table 3. The calibration graphs for naphthalene and 1,2-benzanthracene are shown in Fig. 6A—D. Of course, only three points are available for each calibration line. Assuming linearity, the best approximating line is determined by using the least-squares approach. Table 4, showing the correlation coefficients, gives an impression of the goodness of fit. One can conclude that despite the noisy baseline the fit is extremely good. Obviously, the system is linear in the chosen range, but more interesting is the conclusion that SCC allows very accurate quantification. The effects of both deterministic disturbances and random noise are greatly reduced by the simultaneous determination of calibration standards and the noise-reducing property of the correlation procedure, respectively.

TABLE 2

The peak areas for the three samples in correlograms 1 and 2

	Peak areas (a.u.)[a]					
	Correlogram 1			Correlogram 2		
	1	2	3	1	2	3
Naphthalene	1.598	0.831	0.401	1.595	0.788	0.378
Anthracene	1.736	1.782	1.851	1.678	1.732	1.803
1,2-Benzanthracene	3.100	1.557	0.695	3.083	1.588	0.795

[a]Arbitrary units.

TABLE 3

The peak areas and the corrected peak areas for naphthalene and 1,2-benzanthracene

Compound	Sample[a]	Correlogram 1		Correlogram 2	
		Area[b]	Corrected area[b]	Area[b]	Corrected area[b]
Naphthalene	1	1.598	0.921	1.595	0.951
	2	0.831	0.466	0.788	0.455
	3	0.401	0.217	0.378	0.209
1,2-Benzanthracene	1	3.100	1.786	3.083	1.837
	2	1.557	0.874	1.588	0.917
	3	0.695	0.375	0.795	0.441

[a]Concentrations are given in Table 1. [b]Arbitrary units.

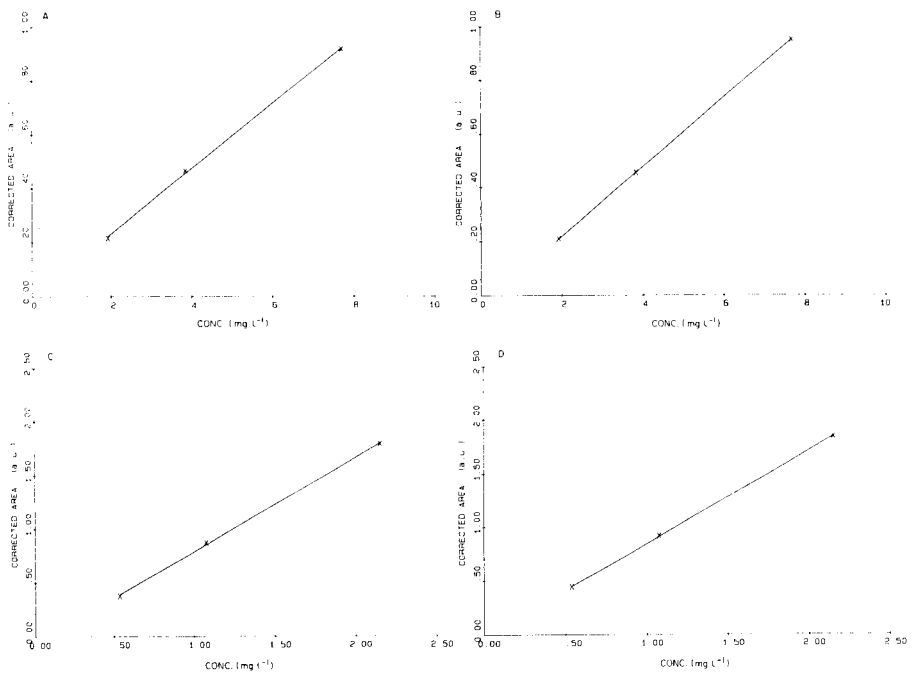

Fig. 6. Calibration graphs: (A) naphthalene obtained from simultaneous correlogram 1; (B) naphthalene obtained from simultaneous correlogram 2; (C) 1,2-benzanthracene obtained from simultaneous correlogram 1; (D) 1,2 benzanthracene obtained from simultaneous correlogram 2.

A good impression of the merits of the method is given by a comparison of the results of four successively independent experiments. The obtained calibration points are shown in Fig. 7. Although each calibration experiment yields an almost perfectly fitting linear calibration plot, the calibration points

TABLE 4

The correlation coefficients of the calculated calibration graphs

	Correlation coefficients	
	Correlogram 1	Correlogram 2
Naphthalene	0.99981	1.00000
1,2-Benzanthracene	0.99975	0.99997

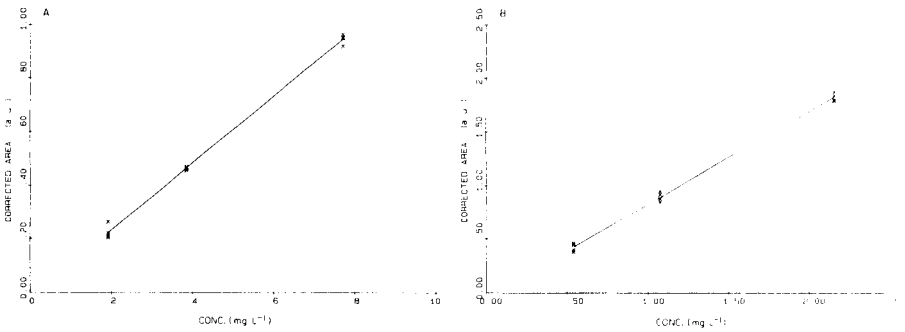

Fig. 7. Calibration points from four independent successive correlation experiments: (A) naphthalene; (B) 1,2-benzanthracene.

for the same concentration, measured successively, are distributed with rather large standard deviations, as could be expected with the imperfect system. Even with an imperfect experimental system, the first results are striking.

DISCUSSION

The SCC method proves to work well in practice. One may conclude that particularly the injection system has to be improved; the control signals and the data processing are not problematic. However, the demands placed on the mechanical parts (valves, flow system, etc.) are high. This can be considered as the most difficult point in correlation chromatography generally. In the case of SCC the demands are at least as high, and indeed the SCC system is more complicated, so that attention has to be given to the development of suitable high-precision injection systems. Nevertheless, even with the present experimental set-up the results of the calibrations are good, if suitable data processing is used afterwards. This gives an impression of the potential power of the method to increase the accuracy of the quantitative chromatographic analysis. The injection of eluent during a calibration is actually redundant, as the unknown sample can be injected instead of the eluent. The intersection of the calibration graph and the concentration axes then gives the unknown sample concentration directly.

Another possible application is the deconvolution of unresolved peaks. Of course, it is possible to estimate the peak parameters of the unresolved peaks by using, for instance, a non-linear regression approach with an appropriate model [14]. However, one of the problems is that in many cases the mutual influence of the components during the separation cannot be neglected. In other words, the system is non-linear in this respect. The absorption behaviour and consequently the peak shape change during the separation, depending on the local concentrations of the other components. This implies that a previously established model of the peak shape cannot be used, resulting in considerable systematic errors in the evaluation of the peak parameters. If the single components present in a mixture to be analyzed are determined simultaneously with the same components in a calibration mixture, then every component is influenced in the same way. The problem mentioned is then reduced to a simple linear combination of known peaks with unknown amplitudes. Work on this application of SCC is in progress.

The authors thank Mr. R. Mulder, Mr. P. Hoogerbrugge and Mr. R. Oostervink for their valuable contributions.

REFERENCES

1 K. Izawa, K. Furuta, T. Fujiwara and N. Suyama, Ind. Chim. Belge, 32 (1967) 223.
2 H. C. Smit, Chromatographia, 3 (1970) 515.
3 H. C. Smit, Journal A, 24 (1983) 145.
4 G. C. Moss, P. J. Kipping and K. R. Godfrey, in S. G. Perry (Ed), Proceedings of the 9th International Symposium on Gas Chromatography, Montreux, October, 1972, Applied Science Publ., Barking, 1973, p. 187.
5 R. Annino and J. Leone, J. Chromatogr. Sci., 20 (1982) 19.
6 C. Largeau and B. Espiau, J. Chim. Phys., 71 (1974) 1143.
7 H. C. Smit, T. T. Lub and W. J. Vloon, Anal. Chim. Acta, 122 (1980) 267.
8 J. M. Laeven, H. C. Smit and J. C. Kraak, Anal. Chim. Acta, 150 (1983) 253.
9 E. Urbas, M. Kaljurand and E. Küllik, J. Anal. Appl. Pyrolysis, 1 (1980) 213.
10 K. C. Ng and G. C. Moss, in Proceedings of Conference on Laboratory Automation, London, 1970, Institution of Electronic and Radio Engineers (1970), IERE Conf. Proc. No. 20, p. 197.
11 C. Largeau and F. Barras, Chromatographia, 12 (1979) 160.
12 A. C. Davies, IEEE Trans. Comput., C20 (1971) 270.
13 R. P. J. Duursma, H. Steigstra, R. G. Logchies and H. C. Smit, Anal. Chim. Acta, 144 (1982) 13.
14 P. J. H. Scheeren, P. Barna and H. C. Smit, Anal. Chim. Acta, 167 (1985) 65.

Analytica Chimica Acta, 181 (1986) 51—56
Elsevier Science Publishers B.V., Amsterdam — Printed in The Netherlands

CORRELATION GAS CHROMATOGRAPHY OF THERMAL DEGRADATION PRODUCTS OF THERMOSTABLE POLYMERS

E. KÜLLIK* and M. KALJURAND
Institute of Chemistry, Academy of Sciences of the Estonian SSR, Tallinn (U.S.S.R.)
(Received 12th March 1985)

SUMMARY

Correlation chromatography is applied to the investigation of the thermal degradation kinetics of polyimide film at temperatures up to 500°C. As the amount of gases evolved from the polyimide degradation below 450°C is low, it is difficult to measure by single injection or concentration of sample. Because of its detector noise-suppression properties, correlation chromatography is a practical alternative to single injections or sample concentration.

Studies of the composition of the gases evolved during the thermal degradation of thermostable and flame-retardant polymers at low temperatures (from ambient to 500°C) are of interest for several reasons. Frequently, the working temperature of polymers lies in this region. The kinetics of degradation at low temperatures is different from that at high temperatures and studies of the composition of degradation products provide valuable information on the degradation processes in this case.

The exact value of "low temperature" depends not only on the thermal stability of the polymer under study but also on the sensitivity of the analytical equipment used for the measurement of the amount of evolved gases. Gas chromatography is widely used for this purpose and so the limit of detection of the particular detector used for the evolved products determines the exact value of "low temperature" or temperature where degradation starts. For example, if the widely used thermal conductivity (TCD) and flame ionization (FID) detectors are considered, then this temperature will be completely different for FID and TCD. The TCD has a detection limit three orders higher than that of the FID. However, the degradation products contain several compounds that give no response on the FID (e.g., H_2, CO, CO_2, H_2O, NH_3) and this is why the use of TCD's is still important.

In this paper, an attempt is made to estimate the amount of the gases evolved during polymer degradation at low temperatures and the influence of some factors on it, by using the Arrhenius equation. It will be shown that the detection limit of the TCD is too high for this kind of measurement and that the use of the noise-suppression technique, correlation chromatography, is a good alternative to single injections of evolved gases into the chromatograph.

0003-2670/86/$03.50

THEORETICAL

Consideration is limited to the isothermal case to obtain equations in a concise form. Formally, the degradation process can be described by the so-called first-order Arrhenius equation:

$$dg(t)/dt = Z \exp(-E/RT)\,(g_0 - g(t)) \quad (1)$$

Here $g(t)$ is the amount of the gas evolved during degradation, t is time, g_0 is the total amount of the evolved gas, R is the gas constant, T is the heating temperature of sample and Z and E are kinetic parameters characterizing the sample (pre-exponential factor and activation energy). Although Z and E cannot be assigned to definite physical or chemical parameters of the polymer, Eqn. 1 fits the evolved gas curve, $g(t)$, quite well and Z and E values are available for a huge number of polymers from thermogravimetric measurements. This justifies the application of Eqn. 1 in the present study.

In the degradation experiment, samples are taken from the gas stream flowing through the reactor, so for the amount of sample, Δg, that is directed to the chromatographic column during the time, Δt, Eqn. 1 can be modified to give

$$\Delta g = g_0 Z \exp(-E/RT)\,\Delta t \quad (2)$$

As low-temperature pyrolysis is considered, it can be assumed that the polymer is only slightly degraded, which means that $g(t) \approx 0$. It follows from Eqn. 2 that the signal value depends linearly on the amount of the sample, g_0, and on the sampling time.

The sampling time, Δt, should be of the order of 1—2 s to maintain proper resolution of the chromatographic peaks. The total amount of the evolved gas, g_0, is equal to or less than the polymer weight. Several factors limit this value. They include the need for uniform temperature distribution of the sample, and the need for a low reactor volume to ensure rapid evacuation of the evolved products from reactors and exclusion of diffusion effects. It follows that the sample weight should not exceed 50 mg [1], usually the weight is 5—10 mg.

The influence of temperature is more complicated. Differentiating Eqn. 2 by T gives

$$\delta \Delta g/\Delta g = (E/RT)(\delta T/T) \quad (3)$$

It follows that small variations in temperature will be amplified by a factor of E/RT. For some thermostable polymers at temperatures when degradation starts, this factor can be as high as 50 [2], which makes it a source of large errors. In fact, Eqn. 3 explains quite clearly why interlaboratory reproducibility in pyrolysis gas chromatography is so difficult to achieve. Small variations in temperature produce great changes in the amount (and probably in the composition) of the evolved gases.

A numerical example emphasizes the problem. For the parameters Δt =

1 s, g_0 = 10 mg and $Z \exp(-E/RT) = 10^{-4}$ s^{-1}, which is a typical kinetic constant for the degradation reaction of polyimide fibres at temperatures below 400°C [2], the amount of sampled gas, Δg, is 10^{-3} mg, which is near the detection limit for the TCD.

Clearly, there are two main difficulties in measuring low gas streams from the thermal degradation of polymers. First, the signal level is too low and is corrupted by detector noise if proper experimental conditions are maintained. Secondly, random temperature fluctuations produce big variations in the sampled amount. A common way of dealing with low-level signals in chromatography is to concentrate the sample but this is inconvenient in the present case because many traps would be needed when the kinetics of the degradation process is of interest.

This situation is a good challenge to correlation chromatography [3—5]. Because of its noise suppression and averaging properties, correlation chromatography is able to overcome both the difficulties inherent to single-injection measurements. As it is a multiple-injection technique, the result is averaged over several hundred injections and thus the influence of the reactor temperature variations is decreased. Because correlation chromatography has a multiplex advantage, detector noise is suppressed [3]. A modern system for correlation chromatography permits decrease in the noise level by two orders of magnitude [4] and so the detection limit is greatly improved. The detector noise is reduced by a factor of $(n/2)^{1/2}$, where n is the number of injections made during the experiment. Because of input noise (variations in sample amount with varying temperature), however, some extra noise is generated to the decorrelated chromatogram; this is correlation noise. The standard deviation of the correlation noise is given by the formula [6] $S_{\Delta H} = a S_E/n^{1/2}$, where $S_{\Delta H}$ is the standard deviation of the correlation noise, S_E is the standard deviation of variations in the sample amount and a is a numerical factor depending on the sharpness of the chromatographic peak. For a narrow peak (peak width less than 1% of the total length of the chromatogram, this factor is usually 2—3. If variations in sample weight are, say, 50%, then the standard deviation of the correlation noise for n = 512 is about 5% of the chromatographic peak height.

Deterministic variations (degradation reactions in the pyrolysis oven) also generate correlation noise. The standard deviation of this noise depends on the rate of variations in sample weight. For 50% variations during the experiment and for n = 512, the standard deviation of the correlation noise is also about 5% of the chromatographic peak height [7].

Thus the overall result of a correlation chromatographic experiment cannot be considered only as simple averaging and correlation noise puts a limit to the applicability of such experiments.

EXPERIMENTAL

A 200-μl stainless steel reactor was used. The temperature of the reactor was programmed to 500°C. The carrier gas (helium) carries the degradation

products to the atmosphere or to the gas chromatographic column depending on the position of the two-position pneumatic sampling valve (a Pye-Unicam chromatographic valve). In all experiments, a polyimide film (PM-80) was used. The sample weight was approximately 30 mg. The volatile products evolved by the polymer degradation were analysed in a 1 m × 3 mm i.d. stainless steel column filled with the selective polymer sorbent Tepasorb (manufactured by the Pilot-Production Plant of the Institute of Chemistry, Estonian Academy of Sciences). The column temperature was 112°C. The separated components were detected by the TCD of a LHM-80 gas chromatograph. The signal from the TCD was amplified by an instrumentation amplifier and digitized by a 10-bit analog-to-digital converter (ADC). The amplifier and ADC were home-made.

An Apple IIe microcomputer was used as the digital correlator for correlation chromatography. The Apple IIe generates a pseudo-random binary sequence and (according to this sequence) sends commands to the sampling valve via its one-bit outputs. At the same time, the microcomputer acquires the digitized TCD signal. When the experiment has been completed, data are decorrelated by the fast Hadamard transform and the resulting chromatogram (or correlogram) is plotted on an Epson MX-80 printer. The Apple IIe is able to decorrelate a sequence with 2048 elements. The decorrelation and control programs are written in 6502 microprocessor machine language and in BASIC.

RESULTS

Figure 1 shows a typical output noise pattern from the TCD/amplifier/ADC system. From visual examination, this noise can be characterized as wide-

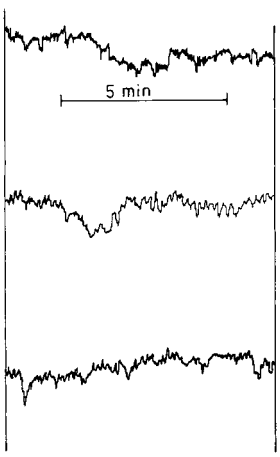

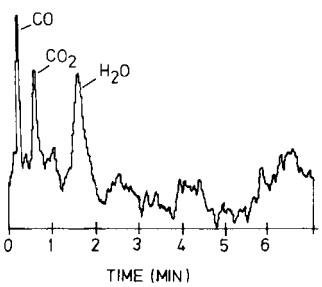

Fig. 1. Sample of TCD noise with a duration of 700 values.

Fig. 2. Correlogram of degradation products of polyimide degraded at 200°C.

band noise with a slow, randomly fluctuating mean. As can be seen, the low-frequency noise component causes serious problems in detecting wide chromatographic peaks of low amplitude.

In all experiments on correlation chromatography, a 127-element sequence was used with a 2-s digitizing interval. During a 4-h experiment with heating below 450°C, the polymer weight loss was about 6%. From this value, the average rate of gas evolution from the polyimide was estimated to be 10^{-7} g s^{-1}, which is near to the detection limit of the TCD used.

Figure 2 shows a typical correlogram of degradation products of the polyimide film. The elution order is CO, CO_2 and H_2O. This correlogram was recorded at a reactor temperature of 200°C.

It can be of interest to scan the whole temperature region to 500°C, at which extensive degradation of polyimides begins. The procedure was as follows: the temperature of the polyimide was raised by 20°C increments from ambient to 500° C. At each isothermal step, a correlogram was recorded. The length of one isothermal step was 20 min. The areas of the chromatographic peaks were measured for each individual compound at every reactor temperature. These areas served as a measure of the evolution rate of that compound at that particular temperature. Figure 3 shows the amounts of the gases evolved in each isothermal step. It is of interest to note that, despite its very high thermal stability, the polyimide evolves gases even below 450° C before degradation really begins. Evolution of water at 200—300° C was confirmed by mass spectrometric data [8].

Conclusion

Correlation chromatography can be used to determine the low-temperature thermal degradation kinetics of thermally stable polymers. While other techniques (sample concentration or single injection) fail, correlation

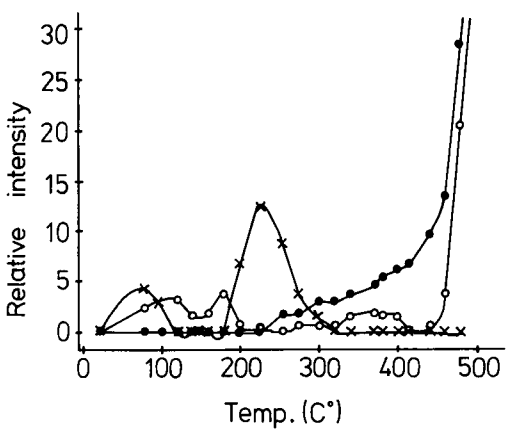

Fig. 3. Curves for the stepwise temperature-programmed degradation of a polyimide. Degradation product: (×) water; (○) CO; (●) CO_2.

chromatography can provide valuable information about the thermal behaviour of polymeric materials at low temperatures.

REFERENCES

1 L. Costa, G. Camino and L. Trossarelli, J. Chromatogr., 279 (1983) 125.
2 M. J. Bessonov (Ed.), Poliimidi, klass termostoikih polimerov (Polyimides a Class of Thermal Stable Polymers), Leningrad, Nauka, 1983, p. 130.
3 J. B. Phillips, Anal. Chem., 52 (1980) 468A.
4 H. Smit, Trends Anal. Chem., 2 (1983) 1.
5 M. Kaljurand and E. Küllik, J. Chromatogr., 171 (1979) 243.
6 M. Kaljurand and E. Küllik, J. Chromatogr., 186 (1979) 145.
7 M. Koel, M. Kaljurand and E. Küllik, Eesti NSV TA Toimetised, Keemia, 32 (1983) 125.
8 A. S. Teleshova, E. N. Teleshov and A. N. Pravdennikov, Visokomolekuljarnic soedinenija, A17 (1975) 134.

Analytica Chimica Acta, 181 (1986) 57—64
Elsevier Science Publishers B.V., Amsterdam — Printed in The Netherlands

SIMULTANEOUS HIGH-SPEED DATA ACQUISITION FROM TWO ATOMIC ABSORPTION SPECTROMETERS COUPLED TO A PDP-11 MINICOMPUTER

A. PARLOW[a], A. BOSCH, K. H. DEGENHARDT and U. ROESICK*

Hahn-Meitner-Institut für Kernforschung Berlin GmbH, Glienicker Str. 100, D-1000 Berlin 39 (Federal Republic of Germany)

(Received 9th September 1985)

SUMMARY

Two Perkin-Elmer 5000 atomic absorption spectrometers equipped with graphite furnaces are interfaced via serial CAMAC I/O ports to a PDP-11 computer running under the real-time operating system RSX-11M. This configuration permits simultaneous and independent processing of transient atomization signals from both spectrometers asynchronous to the program flow and without specific time-scheduling. As well as data collection routines, the software package contains subprograms for graphic representation and detailed evaluation of the signals. Various signal artefacts observed in the determinations of rubidium and cadmium are discussed.

Computer-based processing of time-resolved atomization signals in graphite-furnace atomic absorption spectrometry (a.a.s.) is now part of standard methodology. Most manufacturers of such equipment now offer a compatible computer with corresponding software. In some cases, these computers are built into the device and are used not only for data collection but also for operating the spectrometer optics, the graphite furnace and the sample changer [1]. Older equipment can also be connected to an external computer, provided that the spectrometer has an analog-to-digital converter and an appropriate interface for data output [2]. Such computer links have been described previously [3—14]. However, all these applications are single-user systems only. Recently developed operating systems for real-time application in a multi-user/multitask environment (e.g., the commercial RSX-11M, Digital Equipment Corp., and UNIX/RTU, Bell Laboratories, systems) make it possible to operate more than one spectrometer at the same time with the same computer. There are some advantages to such a multi-user system. As required, it can be expanded without great expense and every additional user has access to the whole configuration and to all available software components.

---

[a]Present address: Fachinformationszentrum Chemie GmbH, Steinplatz 2, D-1000 Berlin 12, F.R.G.

0003-2670/86/$03.50

EXPERIMENTAL

Hardware and operating system

Two Perkin-Elmer atomic absorption spectrometers (PE-5000 and PE-5000/Zeeman) were selected for the link. Both devices were equipped with graphite furnaces (HGA-400 and HGA-500, respectively), automatic sample changers (AS-40) and RS-232C communication interfaces. The laboratory computer used was a PDP 11/40 with a 256-kbyte main memory, two 10-Mbyte disc drives (RL02) and one TU10 magnetic tape. Later upgrading of the system with an 11/73 processor and a memory extension to 4 Mbyte is intended. Nine terminals and a graphic plotter (HP-7475A) were connected to the computer. Three of the terminals allowed high-resolution screen graphics to be displayed. The computer was linked to the mainframe (Siemens 7890) of the institute via a local X.25 network and to a CAMAC system [15] for real-time applications. The CAMAC dataway was connected to the PDP-11 unibus by a Borer 1533A crate controller; CAMAC 3340B communication interfaces (Kinetic Systems) were used for the serial data transfer. The computer was operated with the version 4.1 of RSX-11M. A Tektronix 834 data communication tester was used to test the communication link and for time measurements of interrupt handling.

Interfacing and interrupt handling

Figure 1 shows a block diagram of the coupling. The communication interfaces of both a.a.s. devices were operated in the so-called "high-speed

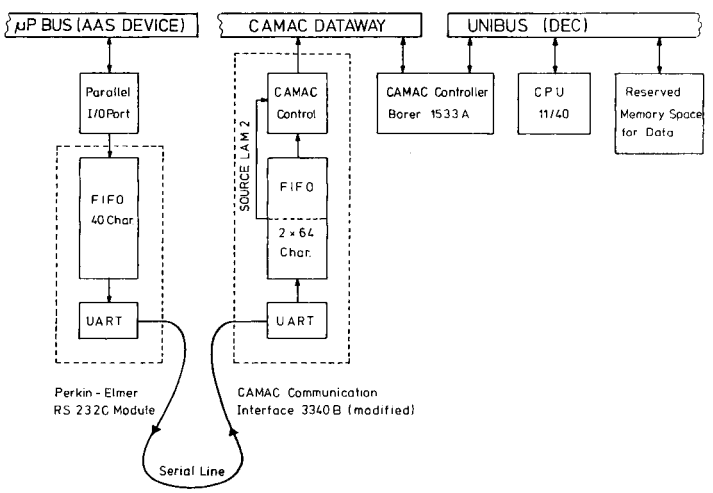

Fig. 1. Block diagram of the communication link between an atomic absorption spectrometer and the PDP-11 computer. FIFO, first-in-first-out memory; UART, universal asynchronous transmitter and receiver; LAM 2, CAMAC-interrupt signal released once the FIFO contains 64 characters.

one-way transfer mode" [2]. The beginning and time span of data recording were selected and fixed in advance in the temperature program of the graphite furnace. Once a data transfer had started, the spectrometer sent a digitized value in the form of 6 ASCII-characters to the computer every 20 ms. An additional linefeed was transferred every ten values. The baud rate on the communication link was 4800 bit s^{-1}.

At present, complications in coupling more than one spectrometer to the same computer arise from the asynchronous data transfer, because the transfer is not triggered by the receiver and it is impossible to stop a running transfer without loss of data. Therefore, it is necessary for the data relayed, to be accepted by the computer independently of its own current activity even if both spectrometers are transmitting at the same time. This is achieved by special interrupt handling. As can be seen in Fig. 1, the CAMAC communication interface is equipped with a 128-character FIFO buffer memory on the receiver side. In this buffer, transmitted data are stored first. The service request from the interface is given by an interrupt signal (LAM, look at me) on a particular line to the CAMAC controller. In the original logic of this module, the LAM signal is released either when FIFO is full or when a special terminating character (EOT, end of transmission) is detected. On reception of the interrupt signal a software event flag is set in the operating system of the computer and data transfer from the FIFO is initialized. After the FIFO has been read out by program instructions, the operating system waits for the next interrupt.

During the preparation of the computer linkage, it became obvious that the processing of the interrupt received from the filled-up FIFO took so long that further incoming data created a buffer overflow and were lost. However, this overflow could be avoided if the interface hardware was changed. After a slight modification, the interrupt was generated as soon as the buffer was half-full. So an additional buffer of 64 characters was available after the first 64 characters had been received and the maximum computer response time was extended in this way to 200 ms, before any data were lost. Readout of the FIFO was done in block mode, i.e., the whole buffer was emptied by only one program instruction. So the interrupt rate was maintained at a low level and the processor was kept free. As test measurements with simulated data showed, the time period between setting the LAM and reading the first character is 2 ms and another 5 ms pass before the half-full FIFO is emptied. During this time the computer is occupied only with this interface. A comparison between this time period and the maximum permitted response time of 200 ms shows that, with modified interface logic, data transfer from both spectrometers functions perfectly, provided that no other task takes precedence over data acquisition. This can be controlled, however, when appropriate priorities are set for the programs in question.

Data acquisition program and on-line processing

Because of the limitations of the computer used (maximum task size 64 kbyte, maximum available memory 180 kbyte), it was necessary to divide the program into two parts. The actual data collection program was kept small (24 kbyte) and memory-resident during a measurement cycle, with a data buffer for 1000 data points. The control task (54 kbyte) included the user interface, data conversion routines, file management and on-line data evaluation. This control task was called up only when needed, thereby opening space for other users. Most program parts were written in FORTRAN-IV; a few data-conversion routines were coded in MACRO-11 assembler.

The programs were organized as follows. So long as neither of the two spectrometers were transmitting data, the computer was available for other jobs. When an interrupt service request was detected, all tasks with lower priority were suspended and the interrupt was taken over. Once the data collection was finished, a special memory cell in the communication interface was checked for the transfer errors, i.e., parity errors, framing errors and buffer overflows. When the transfer was error-free, all characters representing the measured values were converted into real numbers and transformed into absorbance values. These values were stored with additional information on disc in specially designed spectra files and later on magnetic tape. Each measurement could immediately be evaluated on-line, which took about 4 s and gave information about the net absorbance in the peak maximum (A_{max}), the peak integral within preselected intervals ($A \times s$), the appearance time of the peak maximum (t_{peak}) and the quotient $A_{max}/A \times s$. This quotient was used as a test for the recognition of signal deformations. The final evaluation was made after completion of a series of analyses. For this purpose, additional programs were developed, e.g., to represent the signals graphically, to evaluate characteristic peak parameters, to manipulate the data numerically and to calibrate and evaluate standard addition measurements.

Several users can work with this system without disturbing each other's operation. Each user starts his own task on his own terminal with his own identification code and writes data into his own files. Attempts to use other person's files are recognized and forestalled. The reliability of the described data collection has been tested and checked with simulated data under worst-case conditions by using a Tektronix 834 communication tester. Currently, the program has been running error-free for more than one year.

RESULTS

The following four examples deal with signal artefacts observed during day-to-day measurements and the lack of consideration or misinterpretation of which might produce wrong analytical results. It should be emphasized that these artefacts are not connected in any way to the spectrometers used but are caused partly by the analytical method itself and partly by the

spectrometer design and might also occur with other atomic absorption equipment. Although the artefacts have different origins, a certain classification is possible. Thus a distinction was made between signal distortions caused by deviations in the baseline from the linear trend (examples 1 and 2) and signal distortions caused by erroneous lamp triggering (examples 3 and 4). Instrumental details of these measurements are summarized in Table 1.

Example 1 (Fig. 2) derives from attempts to develop a precise method for the determination of rubidium in biological fluids [16]. The example demonstrates the danger of an erroneous baseline subtraction. Looking at the rubidium signal in Fig. 2 (curve b), one would assume without hesitation a horizontal baseline under the signal and interpolate accordingly. However, as curve (a) in Fig. 2 demonstrates, the baseline shows a step-like deviation from a horizontal trend just at the interpolation interval. This deviation must be considered in the final evaluation procedure or the concentrations evaluated will be too low.

Example 2 (Fig. 3) shows that the Zeeman a.a.s. also has its limitations in compensating for nonspecific losses of light. The dotted output represented as (a) in Fig. 3 is the "cadmium" signal of a solution of high-purity sodium chloride. This solution was purified with APDC and chloroform by extraction and should not have contained any cadmium at all. The observed signal can be classified as an artefact because it is narrower and appears later than the real cadmium signal. It is caused by background absorption which is not compensated for. As shown in detail elsewhere [17], the effectiveness of the Zeeman compensation in the case of the PE 5000/Zeeman spectrometer depends not so much on the height of the background absorption signal or

TABLE 1

Instrumental settings for the determination of rubidium and cadmium in the examples described

Example	Rb in water	Cd in 0.1 M NaCl	Cd in water	Cd in amniotic fluid samples
Spectrometer	PE 5000	PE 5000/Zeeman	PE 5000/Zeeman	PE 5000/Zeeman
Wavelength/slit (nm)	780.0/1.4	228.8/0.7	228.8/0.7	228.8/0.7
Lamp	EDL[a] (6 W)	EDL (4 W)	EDL (4 W)/HCL (8 mA)	EDL (5 W)
Graphite tube	normal	pyro[b]	pyro[b]	pyro[b]
L'vov platform	no	yes	yes	yes
Matrix modification	no	yes[c]	no	yes[c]
Sample dilution	—	1:3	—	1:3
Injection volume (μl)	10	16	20	16
Ashing[d]	800/10/30	500/5/35	250/5/35	500/5/35
Atomization with gas stop	1900/0/5	1700/0/5	1700/0/5 and 2500/1/5	1700/0/5

[a]Electrodeless discharge lamp. [b]Pyrolytically coated. [c]0.5% (w/v) $(NH_4)_2HPO_4$. [d]Temperature (°C)/ramp(s)/hold(s).

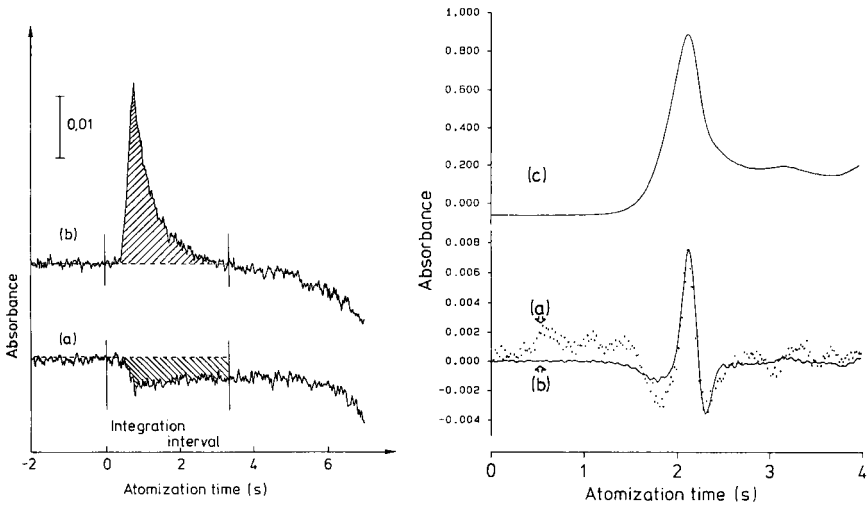

Fig. 2. Incorrect baseline subtraction demonstrated in the determination of rubidium by graphite-furnace a.a.s. (a) Baseline measured with high-purity water sample; (b) atomization signal of 0.05 ng Rb. Measurements were made without deuterium background compensation.

Fig. 3. Baseline deviations arising from insufficient background compensation by Zeeman a.a.s. in the determination of cadmium in purified 0.1 M NaCl. (a) Measured absorbance/time profile; (b) baseline calculated from the background signal [17]; (c) background signal. The "true" cadmium signal should occur between 0.5 s and 2.0 s.

on its steepness but on its curvature, i.e., all baseline distortions caused by uncompensated background absorption may be calculated from the second derivative of the background signal. Figure 3 (curve b) shows the result of this calculation. As can be seen clearly, the artefact computed from the background signal presented in Fig. 3 (curve c) corresponds well with the measured curve (a). The baseline is distorted most where the background signal has its maximum and therefore its sharpest curvature. Knowledge of this relationship can be supplied effectively during method development. For instance, falsifications arising from baseline deviation in measurement samples with high electrolyte content can be avoided by properly adjusting the dilution factor and injection volume.

Example 3 (Fig. 4) also shows an artefact which was observed in the determination of cadmium with Zeeman a.a.s., but only when a hollow-cathode lamp (HCL) was used with the maximum heating rate of the graphite furnace (Fig. 4B). The artefact is rectangular in shape and reproducible. It starts 0.13 ± 0.02 s before atomization begins and lasts for 0.65 ± 0.03 s. Values for A_{max} and $A \times s$ are $(34.5 \pm 1.8) \times 10^{-3}$ and $(18.0 \pm 1.1) \times 10^{-3}$ s, respectively. If this artefact had not been taken into account, the purified water would have been thought to be contaminated with 0.2 $\mu g\ l^{-1}$ cadmium. Parallel measurements of the same samples with an EDL under the

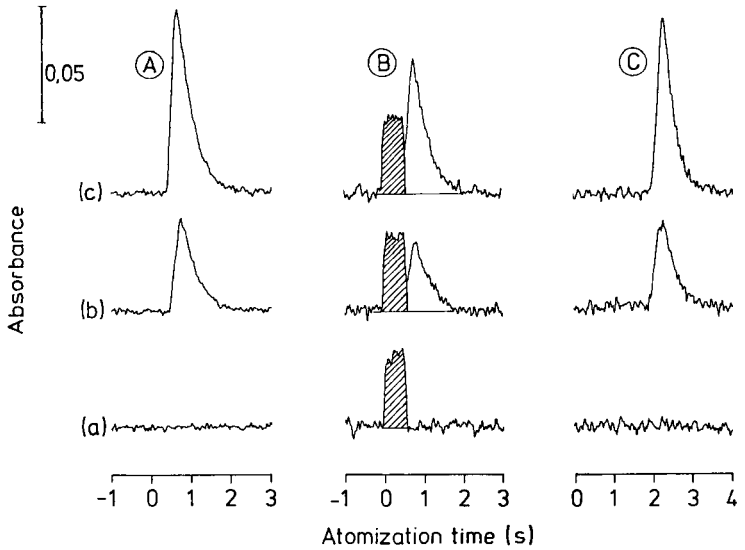

Fig. 4. Appearance of signal artefacts during furnace atomization with maximum power heating in cadmium determinations by Zeeman a.a.s.: (a) high-purity water; (b) after addition of 0.2 $\mu g\ l^{-1}$ Cd; (c) after addition of 0.4 $\mu g\ l^{-1}$ Cd. (A) Measurements with EDL and maximum power heating to 1700°C; (B) measurements with HCL and maximum power heating to 1700°C; (C) measurements with HCL and furnace heating to 2500°C at reduced power (ramp time 1 s).

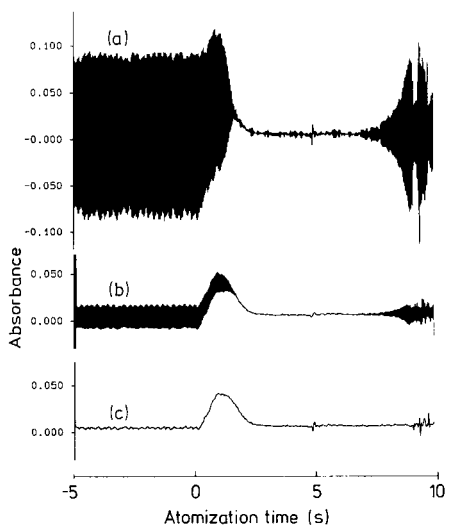

Fig. 5. Signal distortion originating from lamp instabilities in the determination of cadmium in amniotic fluid samples by Zeeman a.a.s. (a) Measured absorbance/time profile; (b) after smoothing by means of a quadratic 11-point least-squares polynomial filter [18]; (c) after smoothing by means of a symmetrical 3-point triangular filter function [18]. Atomization conditions are given in Table 1.

same atomization conditions (Fig. 4A) and with the HCL and slower heating rates in the atomization step (Fig. 4C) were without error and resulted in cadmium contamination levels below the detection limits of 0.01 $\mu g\ l^{-1}$ and 0.04 $\mu g\ l^{-1}$, respectively.

Example 4 (Fig. 5) shows the dramatic signal distortion that can be caused by a vibrating EDL. Resonance of this kind can destroy the lamp but can be stopped by reducing the power applied to the lamp. It is therefore important to recognize such resonance at all times, e.g., by on-line graphic representation of the signal just after measurement. It is usual to smooth the original data before representation because signal details can be hidden by signal noise. Here there is a possibility that, because of a wrong choice of smoothing, non-statistical noise can also be filtered out and lamp vibration will not be recognized. This is demonstrated in Fig. 5; trace (c) shows the same signal as trace (a) after the original data had been smoothed with a symmetrical 3-point triangular filter function [18]. In this case the better choice would be an equivalent Savitzky-Golay filter of the second order [18], because it is equally efficient in smoothing the random noise, but still shows the malfunction of the equipment (trace b).

REFERENCES

1 T. W. Barnard, Anal. Chem., 51 (1979) 1172A.
2 W. B. Barnett and R. D. Ediger, At. Absorpt. Newsl., 17 (1978) 125.
3 K. M. Aldous, D. G. Mitchell and F. J. Ryan, Anal. Chem., 45 (1973) 1990.
4 E. Lundberg and G. Johansson, Anal. Chem., 48 (1976) 1922.
5 R. D. Reid and E. H. Piepmeier, Anal. Chem., 48 (1976) 338.
6 W. B. Barnett and M. M. Cooksey, At. Absorpt. Newsl., 18 (1979) 61.
7 D. D. Siemer and J. M. Baldwin, Anal. Chem., 52 (1980) 295.
8 E. Lundberg and W. Frech, Anal. Chem., 53 (1981) 1437.
9 J. P. Erspamer and T. M. Niemczyk, Appl. Spectrosc., 35 (1981) 512.
10 M. Suzuki, K. Ohta and T. Yamakita, Anal. Chim. Acta, 133 (1981) 209.
11 D. C. McDonald and R. S. Neil, Anal. Chim. Acta, 138 (1982) 145.
12 K. Lum, D. Naranjit, B. Radziuk and Y. Thomassen, Anal. Chim. Acta, 155 (1983) 183.
13 M. T. C. de Loos-Vollebregt, R. A. M. Oosterling, F. B. Boudewijn and L. de Galan, At. Spectrosc., 4 (1983) 160.
14 R. Guevremont and J. Whitman, Anal. Chim. Acta, 154 (1983) 295.
15 IEEE (Ed.), CAMAC Instrumentation and Interface Standards, Wiley, New York, 1982.
16 D. Behne and D. Gawlik, unpublished work.
17 U. Roesick, A. Parlow and G. Fuerstenau, in B. Welz (Ed.), Fortschritte in der atomspektrometrischen Spurenanalytik, Vol. 2, Verlag Chemie, Weinheim, 1986, p. 225.
18 A. Savitzky and M. J. E. Golay, Anal. Chem., 36 (1964) 1627.

Analytica Chimica Acta, 181 (1986) 65—77
Elsevier Science Publishers B.V., Amsterdam — Printed in The Netherlands

DYNAMISCHE INTERPRETATION VON INFRAROTSPEKTREN

MICHAL JAMRÓZ und ZBIGNIEW LATEK
Institut der Industrielle Chemie, Rydygiera 8, 01-793 Warszawa (Polen)
ZDZISLAW HIPPE*
Technische Universität, W. Pola 2, 35-959 Rzeszów (Polen)
(Eingegangen den 8 der Februar 1985)

SUMMARY

(Dynamic Interpretation of Infrared Spectra) Results of investigation of an algorithm, based on a novel static-dynamic method, for interpretation of infrared spectra are presented. The IRSCAN-D algorithm can recognize 103 infrared-active substructures comprising C, H, N, O, S, halogen, P and Si atoms. The results indicate that the algorithm is efficient; roughly 97% of the substructures are correctly ascribed, with a surprisingly low number (60%) of false recognitions.

ZUSAMMENFASSUNG

Es werden Ergebnisse der Untersuchungen über einen Algorithmus zur Interpretation der Infrarotspektren nach einer neu entwickelten statisch-dynamischen Methode vorgestellt. Der Algorithmus IRSCAN-D erfasst 103 infrarotspektroskopisch aktive aus C, H, N, O, S, F, Cl, Br, I, P und Si bestehende Substrukturen. Eine hohe Wirksamkeit des beschriebenen Algorithmus wurde bewiesen, indem der Anteil von richtig erkannten Substrukturen etwa 97% beträgt, wobei nur wenige Substrukturen (60%) falsch zugeschrieben wurden.

Wichtige analytische Daten werden durch empirische Interpretation von Spektren erhalten, z.B. von IR-, UV-, Raman-Spektren, Protonenresonanz, oder ^{13}C-Kernresonanz-Spektren. Das Ergebnis einer solchen Interpretation ist eine Liste von Substrukturen, die vermutlich (mit einer gewissen Wahrscheinlichkeit) im untersuchten Molekül auftreten. Wir sprechen daher über das Erkennen von Substrukturen, einem in den Bereich der qualitativen analytischer Chemie, das als Grundoperation der komputergestützten Strukturbestimmung organischer Verbindungen gilt.

Unabhängig von der inneren Organisation von Informations-Systemen, die diesem Zweck dienen, und unabhängig von ihrem Wirkungsprinzip [1—4], lässt sich in jedem Fall ein Modul heraussondern, dessen grundsätzliche Aufgabe eben diese qualitative Analyse ist. Die bisherigen Erfahrungen in diesen Bereich weisen darauf hin, dass im allgemeinen (weitgehend unabhängig von der Art des Spektrums) drei Typen von Identifikationsalgorithmen angewandt werden [5], und zwar: (a) Vergleichsalgorithmus, auch library-search genannt; (b) Algorithmus des binären Identifizierungsbaumes; sowie (c) Matrix-Algorithmus.

0003-2670/86/$03.50

Der Algorithmus von Typ library-search lässt sich auf einen komputermässigen Vergleich des Spektrums einer unbekannten Substanz mit auf einem Informationsträger gespeicherten Bezugsspektren zurückführen. Grundsätzlich muss dabei die Codierung der Datenbasis genau normiert sein, und das Spektrum einer unbekannten Substanz muss vor dem Vergleichsprozess in gleicher Weise umgewandelt werden.

Bekannt sind Datenbasen, in denen Spektren (IR) in diskreter Form d.h. als linearer Vektoren bzw. zweidimensionale Matrizen beschrieben sind. Dies entspricht der Positions- bzw. der Positions- und Intensitäts-Angabe der Absorptions-Banden. Die Spektren können auch in quasi-analoger Form beschrieben werden, als zweidimensionale Matrizen mit grosser Elementenzahl (z.B. je 2 cm^{-1}). Es sind sogar Basen von Spektraldaten bekannt, die Informationen enthalten, die sich erst nach spezieller Verarbeitung (z.B. Fourier-Transformation) aus den IR-Spektren ergeben. Ein wesentliches Merkmal des Algorithmus vom Typ library-search ist die einfache Programmierung sowie Proportionalität der Suchzeit zur Zahl der Referenz-Spektren in der Basis. Der Algorithmus kann zwei Resultate erbringen. (1) Das Spektrum einer unbekannten Substanz besitzt ein genaues Duplikat unter den Bezugsspektren, dann entspricht die Struktur der Unbekannten den Struktur des Bezugsspektrums. Hier haben wir es also mit dem Erkennen der gesamten Struktur zu tun und nicht lediglich von Einzelelemente (Struktur-Fragmente, Substrukturen; ohne Möglichkeit genau zu bestimmen wie sie verbunden sind). (2) Hat des Spektrum der Unbekannten kein ihm genaue entsprechendes Bezugsspektren, so stützt sich das System auf die Spektrenähnlichkeit und die mit ihr korrelierte Strukturähnlichkeit. In diesem Fall lassen sich mindestens die chemische Klasse der untersuchten Substanz oder manche Substrukturen erkennen. Die Leistungsfähigkeit der Algorithmen vom Typ library-search erreichen einen gewissen Grenzwert, der von der Art der Formulierung von Identitäts- und Ähnlichkeits-Kriterien für Spektren und insbesondere von der Referenz-Daten-Basis abhängt. Da heute die grössten Bezugsdateien nicht mehr als $10—15 \times 10^4$ IR-Spektren umfassen, d.h. 0,8—1% bekannter chemischen Verbindungen, wird offensichtlich warum man nach allgemeineren Lösungen strebt, wie sie die anderen Identifizierungsalgorithmen darstellen.

Der Algorithmus vom Typ des binären Identifizierungsbaumes auch als Algorithmus hierarchischer Gruppierung bezeichnet, basiert auf der Formulierung von binären Fragen (zulässig sind nur Antworten JA oder NEIN) und ihrer Zusammenstellung in einer solchen Reihenfolge, die die besten Identifizierungsergebnisse für Substrukturen gewährleistet. Die Formulierung eines leistungsfähigen binären Klassifikators bildet hier das Grundproblem. Um dieses Problem zu veranschaulichen, bedienen wir uns eines elementaren Beispiels für das Erkennen einer Substruktur schematisch dargestellt in Abb. 1. Der binäre Klassifikator ist hier im Prädikat angegeben und lautet: "enthält das Spektrum eine Bande im Intervall . . . cm^{-1} mit der Intensität . . .?". Die Reihenfolge der Klassifikatoren, spielt hier eine wesentliche Rolle:

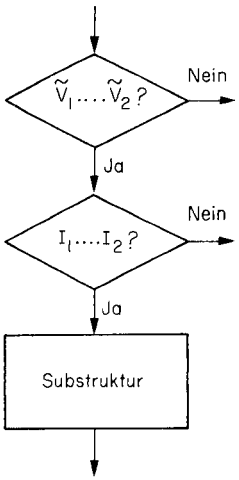

Abb. 1. Schema eines binären Klassifikators.

nach der Huffmanshen Regel [6] soll man zuerst über diejenigen Fragen entscheiden, die mit der grössten Wahrscheinlichkeit auftreten. Die Leistungsfähigkeit der Algorithmen vom Typ des binären Baums ist recht hoch bezogen auf die Menge der verarbeiteten Information. Die für eine Einzelidentifizierung notwendige Rechenzeit ist sehr kurz, die Schwierigkeiten beim Programmieren aber sind beträchtlich. Dieses Problem kann überwunden werden durch Selbstprogrammierung des Computers [7] indem das Programm zur Spektreninterpretation nach der Baum-Methode grösstenteils durch den Computer selbst vorbereitet wird. Ein anderes Problem, das hier unterstrichen werden muss, betrifft die Auswahl von binären Klassifikatoren. Es ergeben sich hier zwei Alternativen: entweder wird der binäre Klassifikator durch den Computer festgelegt, z.B. nach der Methode der Mustererkennung, oder der binäre Klassifikator wird vom Menschen vorgegeben, der Einscheid erfolgt also ausserhalb des Computers. Diese intuitive bzw. nach der "trial and error" Methode konzipierte Auswahl vom binären Klassifikatoren (binären Fragen) wurde mit Erfolg bei unzähligen Anwendungen eingesetzt, lange bevor diese Prozedur Mustererkennung genannt wurde.

Der Matrix-Algorithmus besitzt eine Struktur, die der des binären Algorithmus vom Typ Baum formell nahe steht. Der einzige Unterschied beruht darauf, dass die Spektruminterpretation durch sequentielle Interpretation der Banden erfolgt z.B. nach abnehmenden Wellenzahlen. Der Matrix-Algorithmus kann daher als computerisierte Korrelationstabelle angesehen werden, die eine sehr schnelle und, innerhalb der gegebenen Möglichkeiten, ausführliche Spektren-Analyse erlaubt. Ihr Resultat ist eine Liste von Substrukturen, die vermutlich in der analysierten Verbindung vorhanden sind. Selbstverständlich, kann die Liste der Substrukturen keine solchen Struktur-Fragmente enthalten, die spektral inaktiv sind. Ausserdem kann diese Liste

einen hohen Anteil von Substrukturen enthalten, die falsch zugeordnet wurden (die sog. überschüssigen Fragmente). Dies ist eine natürliche Konsequenz der Mehrdeutigkeit der Methoden der Spektralanalyse. Wesentlich ist hier die Tatsache, dass einer bestimmten Absorptionsbande (oder Absorptionsbanden) mit gleicher Wahrscheinlichkeit nicht eine, sondern mehrere Substrukturen zugeordnet werden können. Die Ergebnisse der binären Klassifikation werden in Matrixelementen den Substrukturen zugeordneten aufsummiert. Jedem Matrixelement entspricht eine genau bestimmte Substruktur, und der Zahlenwert des Elementes gibt die Wahrscheinlichkeit an, dass die entsprechende Substruktur in der analysierten Verbindung vorhanden ist. Der Vorteil einer solchen Darstellung liegt darin, dass die Werte der Matrixelemente von Substrukturen leicht manipulieren werden können, so dass die zusätzliche Informationen (ausser IR-Spektrum) über die Probe einfach und wirksam ausgenutzt werden können. Auf Grund einer Spektren-Analyse ohne Verwendung zusätzlicher Information wird beispielweise festgestellt, dass im untersuchten Molekül, mit gleicher Wahrscheinlichkeit Substrukturen wie "aromatischer Ring", "Oxiranring" und die "Gruppe P=O" auftreten können. Wenn dem Analytiker die Bedingungen der Synthese der untersuchten Verbindung bekannt sind, also die Art der gebrauchten Substrate, und er weiter weiss, dass die Reaktion, in der die untersuchte Verbindung entstanden ist, auf dem Angriff aromatischer Verbindungen beruht und weder eine phosphororganische Verbindung noch Phosphorsäure verwendet wurden, so lässt sich die Wahrscheinlichkeit der Anwesenheit der Substruktur "Aromatischer Ring" vergrössern (im Verhältnis zur Wahrscheinlichkeit "Oxiranring") und das Fragment "Gruppe P=O" völlig eliminieren (der Wert des entsprechenden Elementes in der Substruktur-Matrix zu nullen). Trotz solcher Eingriffe sind die Matrix-Algorithmen durch hohes Informationsrauschen (grosse Überschüsse fälschlich entdeckter Substrukturen) gekennzeichnet. Die genannten Probleme wurden erstmals gelöst mit der Anwendung des Algorithmus der dynamischen Interpretation von IR-Spektren, der im unsere Instituten entwickelt wurde.

EXPERIMENTELLER TEIL

Beschreibung des Algorithmus der Problemlösung. Definitionen der Begriffe

Der erarbeitete Algorithmus gestattet etwa 80 (IR-aktive) Substrukturen zu erkennen, aufgebaut aus den Atomen C, H, N, O, S, P, Si, X, wobei X für Halogene steht. Die Liste der erkennbaren Substrukturen ist in Tabelle 1 gegeben. Der Prozess der Problemlösung benutzt die von uns zusammengestellten Korrelationstabellen [8], die aufgrund von [9—14] sowie aufgrund eigener Erfahrungen aufgebaut wurden. In diesen Tabellen wird jede Substruktur mit einer möglicht grossen Zahl von diagnostischen Banden (bis zu 6) beschrieben, wobei jede Bande durch drei Parameter gekennzeichnet ist: (a) Lageintervall der Absorptionsbande (cm^{-1}), (b) Bereich seiner Intensität (%T) sowie (c) Grad der Banddiagnostizität (arbiträr im Intervall von 1 bis

10 angenommen). Wir setzen voraus, dass die Absorptionsbanden, die die jeweilige Substruktur beschreiben, als nicht-gleichwertvoll behandelt werden müssen. Die Absorptionsbanden, die die jeweilige Substruktur kennzeichnen, wurden willkürlich in drei Kategorien eingeteilt. (1) Banden, deren Anwesenheit unentbehrlich ist, um die entsprechende Substruktur zu erkennen, als notwendige Banden bezeichnet. Ihnen wurde ein Diagnostizitätgrad (D) des Bande von 10 bis 7 zugeordnet. (2) Banden, die in IR-Spektrum auftreten sollten, damit die aufgegebene Substruktur gut erkennbar ist, wurden als erwünschte Banden bezeichet. Ihnen wurde ein Diagnostizitätgrad D von 6 bis 4 zugeschrieben. (3) Banden, die zusätzlich die Anwesenheit einer gewünschten Substruktur bestätigen und sich durch kleine oder veränderliche Intensität oder diagnostische Mehrdeutigkeit auszeichnen. Sie wurden als ergänzende Banden bezeichnet und D auf 3 bis 1 gesetzt.

Der Diagnostizitätsgrad D einer Absorptionsbande in IR hängt auch davon ab, wieviel Substrukturen die Bande mit ähnlicher Intensität im untersuchten Spektralbereich indiziert. In der Tabelle 2 wurde die relative Abhängigkeit des Diagnostizitätsgrades D von den oben erwähnten Faktoren dargestellt. Die detaillierten Werte des Koeffizienten D für erkennbare Substrukturen wurden nach der "trial-and-error" Methode festgelegt. Der Mangel an Banden der ersten Kategorie (im interpretierten IR-Spektrum) im Bandensatz, der die jeweilige Substruktur kennzeichnet, deutet auf die Abwesenheit des entsprechenden Strukturmerkmals in der globalen Struktur der analysierten Verbindung hin. Das Fehlen einer erwünschten Bande dagegen (zweite Kategorie) oder einer ergänzenden Bande (dritte Kategorie), setzt entsprechend den Wert des Koeffizienten der Strukturidentifizierung herab. Die Tabelle 3 enthält beispielsweise Daten für die Substruktur —COOH. Das Erkennen der genannten Substruktur erfolgt auf Grund der Anwesenheit der Banden 1, 2 und 4 im untersuchten IR-Spektrum (notwendige Banden). Die Anwesenheit der Bande Nr. 3 im IR-Spektrum (erwünschte Bande) beeinflusst erheblich die Grösse des Identifizierungskoeffizienten. Der Einfluss der Anwesenheit der Banden Nr. 5 sowie 6 (ergänzenden Banden) auf die Grösse des Identifizierungskoeffizienten bleibt dagegen gering.

Wirkungsprinzip des Identifizierungsalgorithmus

Die Interpretation des IR-Spektrums einer unbekannten Substanz durch Erkennen der in ihr auftretenden Substrukturen erfolgt in zwei Etappen. In der ersten Etappe erfolgt die sogenannte statische Identifizierung. Sie beruht auf der Überprüfung ob für die in der Tabelle 1 genannten Substrukturen die charakteristischen Spektralmerkmale im IR-Spektrum der analysierten Substanz enthalten sind. Für jede auf diese Weise erkannte Substruktur wird der Identifizierungskoeffizient IF auf der Skala von 1 bis 100 errechnet. Die Grösse des Koeffizienten IF hängt vom Diagnostizitätsgrad der für die jeweilige Substruktur charakteristischen Banden ab, sowie von der Übereinstimmung ihrer Lage und Intensität mit Korrelationsdaten. Den grösseren Einfluss auf den Wert von IF üben Banden mit grossem Diagnostizitätsgrad D

TABELLE 1

Symbole von erkennbaren Substrukturen im Algorithmus

Nr.	Symbol	Nr.	Symbol
1	ARYL[a]	49	⊖>C=O[e]
2	ARYL-1	50	ARYL—OH[a]
3	ARYL-1,2	51	ALKYL—OH[a]
4	ARYL-1,3	52	(ALKYL)3—C—OH
5	ARYL-1,4	53	>C=N—OH
6	ARYL-1,2,3	54	ARYL—O—[a]
7	ARYL-1,2,4	55	ALKYL—O—[a]
8	ARYL-1,3,5	56	—O—CH3
9	PYRIDINE[a]	57	>C=C—O—
10	PYRIDINE-2	58	⊖>(C—O—C)<[e]
11	PYRIDINE-3	59	⊖>(C—C—C)<[e]
12	PYRIDINE-4	60	ARYL—NO2[a]
13	PYRIDINE-R1,R2	61	ALKYL—NO2[a]
14	ALKYL[a]	62	:N—NO2
15	—CH2—	63	—O—NO2
16	—(CH2)3—	64	—SO2NH2
17	>C—CH3	65	—SO2NH—
18	>C—(CH3)2	66	—O—SO2—O—
19	>C—(CH3)3	67	—SO3H
20	>C—CH=CH2	68	—SO2—
21	>C—C=CH2	69	>S=O
22	—CH=CH— (Z)	70	—SH
23	—CH=CH— (E)	71	ARYL—S—
24	>C=CH—	72	ALKYL—S—
25	>C=N—	73	>S=C—NH2
26	ARYL—NH2[a]	74	>S=C—NH—
27	ALKYL—NH2[a]	75	—C≡CH—
28	—NH2·HX[b]	76	—C≡N
29	ARYL—NH—	77	—S—C≡N
30	ALKYL—NH—	78	>C=C=O
31	ARYL—N:	79	>C=C=C<
32	ALKYL—N:	80	—N=C=O
33	ALKYL—N—(CH3)2	81	—N=C=S
34	—(C=O)—NH2	82	—N=C=N—
35	—(C=O)—NH—	83	—SO2—F
36	—(C=O)—N:	84	—SO2—Cl
37	—NH—(C=O)—NH2	85	ALKYL—(C=O)X[a]
38	—[O=C(—NH—)C=O]—	86	ARYL—(C=O)X[a]
39	ARYL—CHO[a]	87	X-ALKYL—NO2[a]
40	ALKYL—CHO[a]	88	ARYL-Cl[a]
41	—COOH	89	ARYL-BR[a]
42	—COO—[c]	90	ARYL-F[a]
43	—COO—[d]	91	ARYL-CF3[a]
44	H2N—C—COOH	92	ALKYL-Cl[a]
45	—[O=C(—O—)C=O]—	93	ALKYL-BR[a]
46	⊖—[O=C(—O—)C=O]—[e]	94	ALKYL-I[a]
47	ARYL—(C=O)—	95	>P—H u. ::P—H
48	ALKYL—C=O)—	96	—P=O u. >P=O

TABELLE 1 (Fortgestetzt)

Nr.	Symbol	Nr.	Symbol
97	—P=S u. ⩾P=S	101	⩾SI—C⩽
98	ALKYL—O—P< u. ALKYL—O—P::	102	ARYL—SI⩽
99	ARYL—O—P< u. ARYL—O—P::	103	⩾SI—O—
100	⩾SI—H		

[a]Generell. [b]X = Halogen. [c]Aryl ester. [d]Alkyl ester. [e]⊖ = Cyklisches unaromatisches System.

TABELLE 2

Abhängigkeit des Diagnostizitätsgrades D einer Absorptionsbande im IR von seiner Kategorie

Kategorie einer Absorptionsbande	Die Zahl der Substrukturen[a]	*D*
1. Notwendige Banden	1 bis 2 Substrukturen	10
	2 bis 3 Substrukturen	9
	3 bis 4 Substrukturen	8
	5 und mehr Substrukturen	7
2. Erwünschte Banden	2 bis 3 Substrukturen	6
	3 bis 4 Substrukturen	5
	5 und mehr Substrukturen	4
3. Ergänzende Banden	2 bis 3 Substrukturen	3
	3 bis 5 Substrukturen	2
	6 und mehr Substrukturen	1

[a]Die die Absorptionsbanden mit nahestehenden Spektralparametern besitzen mit Berücksichtigung der Intensität.

TABELLE 3

Substruktur —COOH (6 diagnostische Bänden)

Nr. des diagnostischen Banden	Bereich von Wellenzahlen (cm^{-1})	Durchlässigkeit kleiner als (%T)	*D*
1	2800—2400	60	9
2	1740—1650	10	8
3	1440—1410	40	4
4	1320—1270	40	7
5	1250—1170	50	1
6	950—900	50	3

aus. Eine notwendige Bedingung zum Erkennen einer Substruktur, die aliphatische unverzweigte oder verzweigte Ketten, bzw. aromatische Systeme enthält, ist die Anwesenheit von Banden im untersuchten IR-Spektrum, die für aliphatische oder aromatische Gruppierung charakteristisch sind [das heisst ein früheres Erkennen der Substruktur ALKYL (generell) oder ARYL (generell)]. Dementsprechend werden die Substrukturen ALKYL (generell) und ARYL (generell) gleich am Anfang erkannt, die Erkennung der übrigen Substrukturen dagegen bleibt in der statischen Identifizierung unwesentlich. Aus der statischen Identifizierung ergibt sich eine Menge von in den untersuchten Verbindung erkennbaren Substrukturen sowie entsprechenden Werten des Identifizierungskoeffizienten. In der zweiten Etappe der Interpretation, von uns dynamische Identifizierung genannt, erfolgt die erneute Mengenanalyse der Substrukturen aus der ersten Etappe nach der originalen Weise der Problemlösung, die auf dem Ausschliessen — für erkannte Substrukturen — charakteristischer Bänder aus dem interpretierten Spektrum beruht. Dieser Prozess, von uns Bandenblockierung genannt, hängt vom Diagnostizitätsgrad der jeweiligen Bande ab und erfolgt dann, wenn der Identifizierungskoeffizient IF für eine erkannte Substruktur den Wert grösser als 70 erreicht. In Spezialfällen kann die blockierte Bande, die arbiträr einer Substruktur zugeschrieben wurde, zur Identifizierung eines anderen strukturellen Fragments benutzt werden. Dies wird als Bandenentblockung bezeichnet. Dies ist nur dann möglich, wenn man der analysierten Substruktur andere hochdiagnostische Bänder unterordnen kann, und der vorher (in der ersten Etappe) errechnete Identifizierungskoeffizient IF grösser als 70 ist. Die Entblockung einer Bande wurde in den Algorithmus eingeführt aus der Einsicht, dass eine bestimmte Bande (Banden) im IR mehr als eine Substruktur repräsentieren kann. In der zweiten Etappe der Interpretation des Spektrums spielt die Reihenfolge der analysierten Substrukturen eine sehr wichtige Rolle. Sie wurde von uns experimentell auf Grund der für eine jeweilige Substruktur charakteristischen Bandenzahl und ihres Diagnostizitätsgrades festgelegt. Dies bedeutet, dass zuerst diejenigen Substrukturen erkannt werden, die mit vielen Bandern grosser Diagnostizität beschrieben sind, wobei dieser Prozess immer mit der Bestätigung der Anwesenheit von Absorptionsbanden beginnt, die für Substrukturen ALKYL (generell) sowie ARYL (generell) charakteristisch sind. Die Etappe der dynamischen Interpretation wird mit einem Informationsausdruck über die erkannten Substrukturen abgeschlossen, mit errechnetem Identifizierungskoeffizienten sowie mit der Charakteristik der Nutzung einzelner Banden (Blockieren-Entblockung).

Computerunterstützte Realisierung des Algorithmus

In Anlehnung an den dargestellten Algorithmus wurde das Programm (IRSCAN-D) in der Sprache FORTRAN-IV erarbeitet. Das Programm nimmt zusammen mit den Korrelationstabellen 12 kWorte (24 Bit pro Wort) ein. Das interpretierte IR-Spektrum wird in Form eines sogenannten Spektrumvektors dargestellt, in dem für jede Absorptionsbande Lage und Intensität

angegeben wird. Die Lage der Bande kann in folgenden Einheiten aufgeführt werden: (cm^{-1}) oder (μm), die Intensität dagegen kann durch den Werte der prozentuallen Durchlässigkeit oder der Absorption angegeben werden. Die Eingabedaten werden automatisch auf die inneren Einheiten (cm^{-1}, %T) umgerechnet und normalisiert. Die Umrechnung von Einheiten und die Normalisierung des Spektrums machen die Programmbenutzung von der Registrierungsweise des Spektrums unabhängig und kompensieren so gewissermassen die unrichtige Ausführung des IR-Spektrums.

Als zusätzliche Eingabedaten können ergänzende Informationen über die qualitative Zusammensetzung sowie über die in der untersuchten Verbindung auftretenden Substrukturen dienen (wenn der Analytiker über solche Informationen verfügt). Die für eine Spektruminterpretation notwendige CPU-Zeit ist sehr kurz (einige Sekunden). Die Korrelationstabellen stellen einen gesonderten Programmteil dar. Das Programm IRSCAN-D ermöglicht zusätzlich die Interpretation von Fragmenten von IR-Spektren. Die Interpretation von Spektrenfragmenten ergibt schlechtere Resultate, nichtsdestoweniger findet sie in diejenigen Analysen Gebrauch, in denen das Erhalten des IR-Spektrums in ganzen Spektralbereich unmöglich ist, z.B. wegen hoher Absorption des Lösungsmittels.

BEISPIEL UND DISKUSSION DER ERGEBNISSE

Beispiel für den Identifizierungsalgorithmus

Die Wirkung des oben beschriebenen Algorithmus wurde am Beispiel der Interpretation des IR-Spektrums von Milchsäure (Kat. Nr. SADTLER 2493, DMS 14167) dargestellt. Der Vektor dieses Spektrums sieht folgendermassen aus (cm^{-1}/%T):

3400/22	1637/60	1217/23	870/70
2990/35	1458/51	1126/05	822/58
2930/50	1412/53	1095/48	741/65
2620/63	1374/49	1046/42	640/60
1727/04	1277/46	922/66	

Auf Grund eines Datenvergleichs aus Korrelationstabellen mit spektralen Merkmalen des untersuchten Spektrums (statische Identifizierung) ergab sich eine Menge von 10 Substrukturen, die in der Tabelle 4 nach dem Wert des Identifizierungskoeffizienten IF geordnet sind. Für die ersten acht Substrukturen ist der Identifizierungskoeffizient IF grösser als 70 und aus diesem Grund können Absorptionsbanden dieser Substrukturen entweder (1) überhaupt nicht in Frage kommen beim Erkennen anderer Substrukturen (sog. Blockieren) oder (2) berücksichtigt werden, aber mit dem wesentlich kleineren Identifizierungskoeffizienten (sog. Entblockung).

Im Prozess der dynamischen Identifizierung wurden die Substrukturen in der in der Tabelle 5 geschilderten Reihenfolge analysiert. Die ersten drei Substrukturen wurden re-identifiziert mit gleichzeitigem Blockieren von

TABELLE 4

Ergebnis der statischen Interpretation des Spektrums von Milchsäure

Nr.	Entdeckte Substruktur	Charakteristische Spektralmerkmale (cm^{-1}/%T)	IF
1	—COO—(ALKYL ESTER)	1727/04; 1217/23; 1095/48	99
2	ALKYL (generell)	2930/50; 1458/51	98
3	ALKYL—OH (generell)	3400/22; 1412/53; 1095/48 (oder 1046/42); 922/66	93
4	—COOH	2620/63; 1727/04; 1412/53; 1277/46; 1217/23; 922/66	92
5	⩾C—CH3	2990/35; 1374/49	85
6	ALKYL—O— (generell)	1126/05	80
7	(ALKYL)3—C—OH	3400/22; 1126/05[a]	74
8	⊖⩾C=O	1727/04	70
9	—SO3H	1217/23; 1046/42[a]	68
10	⩾C=CH—	2990/35[b]; 1637/60[b]; 822/58	66

[a] Fehlen eines diagnostischen Bandes im Vektor des untersuchten Spektrums. [b] Bandenlage am Rande eines Intervalls.

insgesamt 10 Banden des untersuchten Spektrums. Die nächste Substruktur ALKYL-OH (gen) hat zwei unblockierte charakteristische Banden, was eine Entblockung der weiteren zwei Banden (1412; 922) zur Folge hat (partielle Deckung von Spektralbereichen für Schwingungen —COOH und ALKYL-OH (gen.)). Die Entblockung der Banden bewirkt eine Herabsetzung des Wertes des Identifizierungskoeffizienten der untersuchten Substruktur (siehe die Tabelle 6). Auch die Substruktur Nr. 8 ist re-identifiziert; die übrigen Substrukturen (Nr. 5, 6, 7, 9 und 10), die in der statischen Identifizierung erkannt wurden, sind im Prozess der dynamischen Identifizierung eliminiert worden, weil ihre charakteristischen Banden früher blockiert wurden. Nach dem Abschluss der Etappe der dynamischen Identifizierung verbleiben nur 5 aus 19 Banden des untersuchten Spektrums, die keiner erkannten Substrukturen zugeordnet wurden. Im Verlauf der durchgeführten Identifizierung des IR-Spektrums von Milchsäure ergab sich eine Menge von fünf Substrukturen, die nach dem Wert des Identifizierungskoeffizienten IF geordnet in der Tabelle 6 dargestellt sind.

Die Untersuchung der Wirksamkeit des Identifizierungsalgorithmus

Zur Einschätzung der Leistung des Algorithmus wurden folgende Koeffiziente verwendet. (1) Koeffizient SRP, der den prozentuellen Anteil der richtig erkannten Substrukturen an der Summe aller in IR-aktiven Substrukturen in der untersuchten chemischen Verbindung ausdrückt. (2) Koeffizient SRE, der den prozentuellen Anteil der fehlerhaft erkannten Substrukturen im Verhältnis zu den richtig erkannten Substrukturenzahl ausdrückt. (3) Koeffizient SPI, der als sogenannte Identifizierungswahrscheinlichkeit gilt. Dieser Koeffizient ist der Quotient der Summe von ıdentifizierungskoeffizienten

TABELLE 5

Verlauf der dynamischen Interpretation des Spektrums von Milchsäure

Nr.	Analysierte Substruktur	Blockierte Banden	Entblockte Banden	Übrige unblockierte Banden aus dem Spektrumvektor
1	ALKYL (generell)	2930; 1458	—	3400; 2990; 2620; 1727; 1637; 1412; 1374; 1277; 1217; 1126; 1095; 1046; 922; 870; 822; 741; 640
2	>C—CH3	2990; 1374	—	3400; 2620; 1727; 1637; 1412; 1277; 1217; 1126; 1095; 1046; 922; 870; 822; 741; 640
3	—COOH	2620; 1727; 1412; 1277; 1217; 922	—	3400; 1637; 1126; 1095; 1046; 870; 822; 741; 640
4	ALKYL—OH (generell)	3400; 1046 oder 1095	1412; 922	1637; 1126; 870; 822; 741; 640
5	>C=CH—	—	—	1637; 1126; 870; 822; 741; 640
6	—COO—(ALKYL ESTER)	—	—	1637; 1126; 870; 822; 741; 640
7	⊖>C=O	—	—	1637; 1126; 870; 822; 741; 640
8	ALKYL—O— (generell)	1126	—	1637; 870; 822; 741; 640
9	—SO3H	—	—	1637; 870; 822; 741; 640
10	(ALKYL)3—C—OH	—	—	1637; 870; 822; 741; 640

TABELLE 6

Schlussergebnis der Interpretation des Spektrums von Milchsäure

Nr.	Entdeckte Substruktur	IF
1	ALKYL (generell)	98
2	—COOH	92
3	—C—CH3	86
4	ALKYL—OH (generell)	85
5	ALKYL—O— (generell)	76

der richtig erkannten Substrukturen und der Summe von Identifizierungskoeffizienten aller durch den Algorithmus erkannten Substrukturen.

Die Interpretationsergebnisse für eine grosse Zahl (etwa 200) von zufällig aus verschiedene Klassen von organischen Verbindungen ausgewählten Verbindungen zeigen den sehr hohen Wirkungsgrad des dargestellten Algorithmus. Die genannten Koeffizienten betrugen (für die ganze Menge untersuchter Spektren) entsprechend: SRP = 97%, SRE = 60% und SPI = 70%. Auf Grund des gewonnenen experimentellen Materials darf man schlussfolgern, dass der erarbeitete Algorithmus der statisch-dynamischen Spektreninterpretation im IR ein sehr wirksames Erkennen von Substrukturen in organischen Verbindungen beliebiger Klasse ermöglicht. So wurde z.B. in der ganzen Menge von 200 interpretierten IR-Spektren nur in 30 Fällen eine der in der untersuchten chemischen Verbindung vorhandene Substruktur nicht erkannt, und für 30% der interpretierten Spektren wurde nicht mehr als eine Substruktur zusätzlich erkannt. Die Zahl der überschüssig erkannten Substrukturen war am grössten bei der Spektreninterpretation jener chemischen Verbindungen, die Substrukturen mit Atomen von Halogenen, P, Si enthalten. Dies ist hauptsächlich durch die kleine Zahl diagnostischer Banden für diese strukturellen Fragmente verursacht.

Ein kennzeichnendes Merkmal des erarbeiteten Identifizierungsalgorithmus (ausser grossen Arbeitsgeschwindigkeit des Programms) ist die Tatsache, dass er alle bisher bekannten Algorithmen übertrifft (z.B. Muster-Erkennunge-Methoden) in Bezug auf die Fähigkeit, Substrukturen in 97% richtig zu erkennen bei gleichzeitig ungewöhnlich geringer Erkennungsziffer überschüssiger Substrukturen (SRE = 60%). Nach Literaturangaben (z.B. [15]) führt gewöhnlich der Versuch, die Wirksamkeit von Identifizierungsalgorithmen dieses Typs um einige Prozente zu erhöhen eine drastische Vergrösserung der Zahl der im Überschuss entdeckten Substrukturen herbei (sogar um einige hundert Prozent). Man kann vermuten, dass der erarbeitete Algorithmus ein wirksames Werkzeug in der Strukturanalyse organischer Verbindungen sein wird.

Vorliegende Arbeit wurde im Rahmen des Problems MR-I-32 ausgeführt, koordiniert durch Warschauer Universität.

LITERATUR

1 L. A. Gribov, M. E. Elyashberg and V. V. Serov, J. Mol. Struct., 50 (1978) 371.
2 Z. Hippe, B. Dębska, J. Duliban and B. Guzowska-Świder, Anal. Chim. Acta, 133 (1981) 303.
3 S. Sasaki, H. Abe, I. Fujiwara, T. Yamasaki, Z. Hippe, B. Dębska, J. Duliban and B. Guzowska-Swider, Chem. Anal., 27 (1982) 171.
4 H. B. Woodruff and M. E. Munk, Anal. Chim. Acta, 95 (1977) 13.
5 Z. Hippe, Anal. Chim. Acta, 150 (1983) 11.
6 M. Dąbrowski, O teorii informacji, PZWS, Warszawa, 1974.
7 Z. Hippe and B. Dębska, Bull. Acad. Polon. Sci., Ser. Sci. Chim., 22 (1974) 551.

8 W. W. Simons, The Sadtler Handbook of Infrared Spectra, Heyden and Son, London, 1978.
9 IRSCOT — Infrared Structural Correlation Tables, Heyden and Son, London, 1965.
10 R. Mecke and F. Langerbucher, Infrared Spectra of Selected Chemical Compounds, Heyden and Son, London, 1964.
11 DMS — Documentation of Molecular Spectroscopy, Butterworths, London, 1967.
12 L. J. Bellamy, Advances in Infrared Group Frequencies, Methuen, Bungay, 1968.
13 H. A. Szymanski, Progress in Infrared Spectroscopy, Vol. 2, Plenum Press, New York, 1964.
14 N. L. Alpert, W. E. Keiser and H. A. Szymanski, Theory and Practice of Infrared Spectroscopy, Plenum Press, New York, 1970.
15 Z. Hippe, Trends Anal. Chem., 2 (1983) 240.

Analytica Chimica Acta, 181 (1986) 79—85
Elsevier Science Publishers B.V., Amsterdam — Printed in The Netherlands

ABSOLUTE MODELLING OF URBAN AEROSOL ELEMENTAL COMPOSITION BY FACTOR ANALYSIS

KRISTIAN KEIDING*

Environmental Engineering Laboratory, University of Aalborg, Department of Civil Engineering, Sohngaardsholmsvej 57, DK-9000 Aalborg (Denmark)

FINN PALMGREN JENSEN and NIELS Z. HEIDAM

National Agency of Environmental Protection, Air Pollution Laboratory, Risø National Laboratory, DK-4000 Roskilde (Denmark)

(Received 12th July 1985)

SUMMARY

Data on the elemental composition of urban aerosols from a Danish city are treated by R-mode factor analysis to identify and quantify contributions from different sources. The analysis produced a 6-factor solution. If it is assumed that all sources contributing to the total suspended particulates were determined, absolute calculations of emission profiles and source contributions are possible.

Factor analysis has been applied to aerosol data in order to derive receptor models for air-quality studies [1, 2]. The R-mode factor analysis, including varimax rotation, has been used successfully to demonstrate the influence of different sources on the variation of the observed variables [3—6]. So far, absolute calculations of the resulting emission profiles by this approach have been impeded by autoscaling because information on the mean values is lost. Thus only the observed variance has been modelled. The present work demonstrates that by introducing a normalization of the factor-scores, i.e., by assuming that the sum of factor-scores equals the total suspended particulate, this shortcoming of the method can be resolved.

METHOD

The fundamental assumption is a linear model relating ambient elemental concentrations to the contributions of different sources to the suspended particles by a matrix, A, containing the collection profiles of the p derived sources (collection profile is used here to distinguish the measured profile from the source emission profile):

$$x_t = Af_t + \epsilon_t \quad (1)$$

The concentration of element i at time t measured at the collection site is given by x_{it} and f_{jt} is the concentration of suspended particulate from source j. The source profile element a_{ij} is the ratio of the mass of element i to the

0003-2670/86/$03.50

mass of total suspended particles (TSP) originating from source j as measured at the collection site.

The stochastic residual, ϵ_t, is assumed to be normally distributed with a mean value of zero, thus

$$\bar{x} = \mathbf{A}\bar{f} + 0 \tag{2}$$

The autoscaling of x_t implies that the actual model used in factor analysis is

$$y_t = \mathbf{B}g_t + \delta_t \tag{3}$$

where $y_t = \mathbf{S}_x^{-1}(x_t - \bar{x})$ and $g_t = \mathbf{S}_f^{-1}(f_t - \bar{f})$. Here $\mathbf{S}_x$ and $\mathbf{S}_f$ are diagonal matrices containing the standard deviations. Estimation of the B matrix is done by R-mode factor analysis, involving varimax rotation; that permits the standardized source contributions, g_t, to be estimated [4].

Combining Eqns. 1 and 2 leads to

$$x_t - \bar{x} = \mathbf{A}(f_t - \bar{f}) + \epsilon_t \tag{4}$$

Combining Eqn. 3 with the definitions of y_t and g_t gives

$$x_t - \bar{x} = \mathbf{S}_x\mathbf{B}\mathbf{S}_f^{-1}(f_t - \bar{f}) + \mathbf{S}_x\delta_t \tag{5}$$

and thus the identity

$$\mathbf{A} = \mathbf{S}_x\mathbf{B}\mathbf{S}_f^{-1} \tag{6}$$

is established. $\mathbf{S}_f$ is so far unknown, but, by assuming that the sum of f_j equals TSP, $\mathbf{S}_f$ can be estimated.

The assumption

$$\mathrm{TSP}_t = \sum_j f_{j,t} + \epsilon_{\mathrm{TSP},t} \tag{7}$$

can similarly be expressed by

$$\mathrm{TSP}_t = \mathbf{A}_o f_t + \epsilon_{\mathrm{TSP},t} \tag{8}$$

where $\mathbf{A}_o$ contains a p-dimensional unit row vector a', and thus an expression equivalent to Eqn. 1 is obtained. Autoscaling of TSP_t leads to an expression analogous to Eqn. 3:

$$\mathrm{TSP}_t = s_{\mathrm{TSP}}^{-1}(\mathrm{TSP}_t - \overline{\mathrm{TSP}}) = \mathbf{C}_o g_t + \delta_{\mathrm{TSP},t} \tag{9}$$

where $\mathbf{C}_o$ consists of a one-dimensional row vector c', which can be estimated by multiple regression, as will be described in a later paper. Similarly to the derivation of Eqn. 6, the expression

$$a' = s_{\mathrm{TSP}}c'\mathbf{S}_f^{-1} \tag{10}$$

is obtained. Thus, since $a' = (1, 1, 1, \ldots\ldots)_p$

$$s_{f_j} = s_{\mathrm{TSP}}c_j \tag{11}$$

which with Eqn. 6 permits the calculation of each element in the emission

profile matrix A:

$$a_{ij} = s_{x_i} b_{ij} / (s_{TSP} c_j) \quad (12)$$

Once the A matrix has been established, estimation of the source contributions, f_t, is done by weighted linear regression. The weighting was done in order to minimize the residuals in the regression. This was achieved by weighting the data with the inverse of the residual variance from the factor analysis. Because the total variance of an element is s_{xi}^2, the residual variance is $(1 - h_i^2)s_{xi}^2$, where h_i^2 is the communality of element i. Thus the weight matrix is diagonal with elements $w_{ii} = (1 - h_i^2)s_{xi}^2$.

RESULTS

The elemental composition of the total suspended particles (TSP) was determined by proton-induced x-ray emission spectrometry. Filter samples were taken daily in the city of Odense (200,000 inhabitants). Mean values and standard deviations for the 15 most frequently occurring elements were estimated from 322 samples taken during 1983 (Table 1). The TSP was evaluated from the difference in weight between the exposed and unexposed filters. The filters were weighed under conditions of controlled temperature and relative humidity. Factor analysis with varimax rotation was applied to the elemental composition data. A 6-factor model fits the data well and the factor loadings (B matrix) as well as the communalities, h^2, are listed in Table 1. The same data were analyzed again, including TSP as a variable. As

TABLE 1

Mean values and standard deviations of observed variables, factor loadings of varimax-rotated principal factor analysis, and communalities

Element	$\bar{x}$	s_x	g_1	g_2	g_3	g_4	g_5	g_6	h^2
Al	476.7	471.7	0.837	0.170	−0.023	0.249	0.278	0.271	0.942
Si	1105.2	1280.7	0.886	0.149	−0.003	0.136	0.218	0.051	0.876
S	2038.3	1593.5	0.332	0.214	0.073	0.201	0.130	0.841	0.927
Cl	1884.8	2201.9	0.063	0.118	−0.987	0.048	0.009	0.033	0.995
K	325.0	405.5	0.428	0.111	−0.011	0.102	0.867	0.130	0.974
Ca	665.7	626.2	0.854	0.158	−0.142	0.341	0.093	0.148	0.922
Ti	64.2	58.7	0.884	0.187	−0.012	0.331	0.151	0.160	0.975
V	20.0	15.2	0.241	0.888	−0.107	0.297	0.094	0.136	0.974
Mn	18.7	17.5	0.776	0.266	−0.032	0.304	0.114	0.399	0.938
Fe	703.4	583.0	0.811	0.264	−0.009	0.413	0.152	0.256	0.986
Ni	7.7	6.2	0.243	0.886	−0.087	0.284	0.066	0.196	0.974
Cu	19.3	12.8	0.483	0.338	0.043	0.710	0.132	0.224	0.921
Zn	89.6	74.2	0.534	0.371	−0.066	0.425	0.003	0.451	0.812
Br	169.3	125.0	0.315	0.226	0.096	0.848	0.015	0.114	0.892
Pb	786.4	510.9	0.321	0.284	−0.016	0.839	0.117	0.171	0.932
TSP	65.45	41.45	0.675	0.335	−0.094	0.344	0.194	0.445	0.931

the factor loadings of the 15 elements were essentially unaffected by the inclusion of TSP in the analysis, it can be concluded that the TSP behaves virtually as an independent variable. Hence the factor loadings obtained for TSP are equivalent to the regression coefficients, c_j, in Eqn. 9 [7].

The factors were identified on the basis of the factor loadings as well as the seasonal variation of the standardized source contributions. The most dominating factor, g_1, is characterized by high loadings of Al, Si, Ti and Ca and is most pronounced in the summer months. Consequently, it is ascribed to wind-blown soil. However, fly ash from coal-fired plants will also contribute to this factor. Factor g_2 is dominated by vanadium and nickel and the high winter values conform with the interpretation of g_2 as coming from fuel-oil combustion. Factor g_3 is dominated by chloride and values are high in periods of high westerly winds; it can be ascribed to sea spray. Lead and bromine are dominant elements in factor g_4, which is associated with automobile exhaust. Factor g_5 is dominated by potassium and coupled weakly to the soil elements. The seasonal variation shows minor fluctuations throughout the year, except for the late summer months, in which very high values are found. The factor is therefore associated with suspended particulates emitted by straw fires in fields after harvesting. Finally, a long-range transport (LRT) factor is established on the basis of high sulphur loadings on factor g_6. High values were found in the spring and early summer months, when south-easterly winds prevail.

The resulting emission profiles were calculated according to Eqn. 12 (Table 2). The values obtained are in accord with similar values obtained with the same approach on data taken in parallel from three other stations in

TABLE 2

Estimated emission profiles (ng μg^{-1})

Element	Soil f_1	Fuel oil f_2	Marine f_3	Traffic f_4	Straw f_5	LRT f_6
Al	14.11	5.77	2.78	8.24	16.31	6.93
Si	43.72	14.82	4.14	13.46	37.43	3.82
S	18.92	24.56	−29.86	22.46	18.43	72.65
Cl	4.96	18.71	557.78	7.41	21.46	3.94
K	6.2	3.24	1.14	2.90	43.72	2.86
Ca	19.11	7.12	22.82	14.98	7.24	5.02
Ti	1.85	0.79	0.18	1.36	1.10	0.51
V	0.13	0.97	0.42	0.32	0.17	0.11
Mn	0.48	0.33	0.14	0.37	0.24	0.38
Fe	16.90	11.08	1.35	16.89	11.02	8.09
Ni	0.05	0.39	0.13	0.12	0.05	0.07
Cu	0.22	0.31	−0.14	0.63	0.21	0.16
Zn	1.11	1.98	1.26	2.21	0.03	1.81
Br	1.41	2.03	3.08	7.43	0.23	0.77
Pb	5.86	10.45	2.09	30.06	7.43	4.74

the same city. Compared with profiles used by other authors [8, 9], the profiles found here are much less distinct. This is attributed to the different concepts of emission and collection profiles, which will be discussed later.

The prime aim of this work was to demonstrate that the method used here permits calculation of the absolute source contributions. In Table 3, the model estimates of the ambient elemental concentrations from the TSP are compared with the observed values. The comparison is done in terms of variances and mean values, the former being expressed by the correlation coefficient between the observed and modelled values and the latter by comparing the means of model estimates and observed values. On average, the estimate of the mean values is 99.4% ± 6.7% and the average correlation coefficient between modelled and observed values is 0.9717. Thus a satisfactory fit is obtained by the model.

In Fig. 1A, the observed sulphur values are plotted against the modelled values. In this case, the modelled mean is 92% of the observed mean and the correlation between modelled and observed values is 0.9864. Thus a good fit for sulphur was obtained. In Fig. 1B, the differences between modelled and observed values are plotted against the observed values. It can be seen that the absolute values of the residuals increase as the observed values increase. Such behaviour of the residuals can normally be ascribed to incorrect weighting of the input data in the statistical treatment. In this study, it is considered to illustrate a violation of the requirement of normal distribution for the input variables. Work on finding better weighting functions is in progress, but within the scope of this work this is not a critical aspect.

TABLE 3

Comparison of model and observed values

Element	r	$\bar{x}_{obs}$ (ng m^{-3})	$\bar{x}_{mod}$ (ng m^{-3})	$\frac{x_{mod}}{x_{obs}} \times 100\%$
Al	0.9699	476.7	495.8	104
Si	0.9342	1105	987.8	89
S	0.9864	2038	1878	92
Cl	1.0000	1885	1883	101
K	0.9995	325.0	327.4	101
Ca	0.9657	662.7	662.3	100
Ti	0.9920	64.16	60.18	94
V	0.9916	20.01	19.49	97
Mn	0.9734	18.71	20.95	112
Fe	0.9962	703.4	716.1	102
Ni	0.9921	7.729	7.900	102
Ci	0.9679	19.29	19.10	99
Zu	0.8924	89.62	97.63	109
Br	0.9460	169.3	177.0	105
Pb	0.9806	786.4	759.2	97
TSP	0.9597	65.45	57.07	87

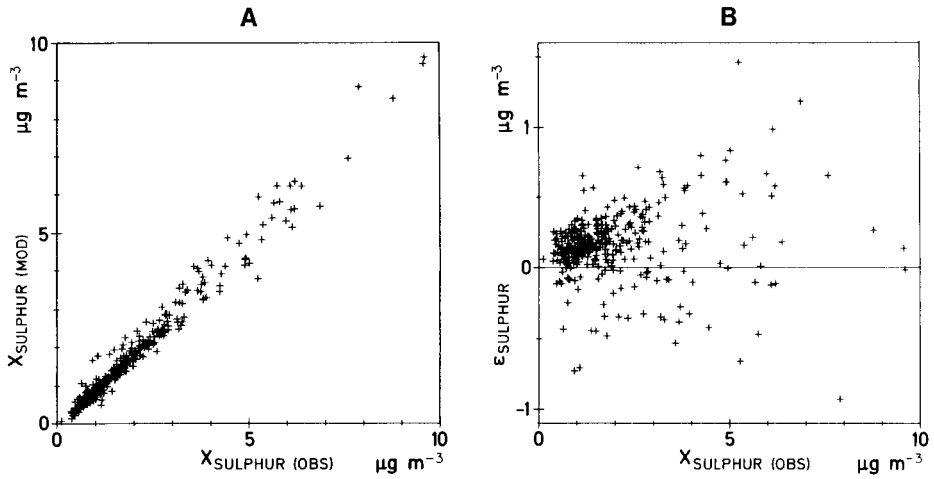

Fig. 1. (A) The model values for sulphur as a function of the observed values. (B) The residuals for sulphur as a function of the observed sulphur values.

DISCUSSION

It has been demonstrated above that, by including a normalization by $TSP_t = A_o f_t$, absolute calculations can be made after R-mode factor analysis. The physical understanding of the model is closely connected to the inherent orthogonality of the factors derived. This implies that the concept of collection profiles as used here includes both differences in source emission patterns and differences in atmospheric dispersion. This means that the collection profiles calculated here reflect statistical covariant incidents rather than express the chemical and physical modification of the corresponding emissions.

From the collection profile for automobile exhaust, it is recognized that aluminium is enriched with respect to silicon, in comparison with the soil factor. This is in accordance with the observation that road dust is enriched with aluminium [8] and the expectation that there is a high correlation between road dust, automobile exhaust and traffic intensity. Further, it can be calculated that 8% of the ambient lead concentration is related to the soil factor. As resuspension of particulates from automobile exhaust most likely will be governed by the same forces as wind erosion of soils, it seems reasonable to assume that this coupling is caused by resuspension of road dust with lead-containing particles from engine exhausts.

Reliable emission profiles are difficult to establish and, as shown, they must be expected to differ from the collection profiles resulting from receptor model studies. It seems more realistic, therefore, to pursue studies of this type rather than to attempt to fit incomplete emission profiles to the data, because some inferences as to the sources of the contributions appear to be possible.

The authors express their gratitude to Niels Pind, University of Aarhus, for additional computer calculations on the residuals, and for the plots. The authors thank Tenna Clausen for careful typing of this manuscript.

REFERENCES

1 T. G. Dzubay, R. K. Stevens, W. D. Balfour, H. J. Williamson, J. A. Cooper, J. E. Core, R. T. De Cesar, E. R. Crutcher, S. L. Daltner, B. L. Davis, S. L. Heisler, J. J. Shah, P. K. Hopke and D. L. Johnson, Atmos. Environ., 18 (1984) 1555.
2 R. C. Henry, C. L. Lewis, P. K. Hopke and H. J. Williamson, Atmos. Environ., 18 (1984) 1507.
3 D. F. Gatz, J. Appl. Meteorol., 17 (1978) 606.
4 N. Z. Heidam, Atmos. Environ., 18 (1984) 329.
5 K. Kemp, MST LUFT-A88, Risoe Natl. Lab., Denmark, 1984.
6 P. Van Espen and F. Adams, Anal. Chim. Acta, 150 (1983) 153.
7 N. Z. Heidam, Atmos. Environ., 16 (1982) 1923.
8 D. J. Albert and P. K. Hopke, Atmos. Environ., 14 (1980) 1137.
9 M. S. Miller, S. K. Friedlander and K. H. Hidy, in G. H. Hidy (Ed.), Aerosol and Atmospheric Chemistry, Academic Press, New York, 1972, p. 301.

Analytica Chimica Acta, 181 (1986) 87—96
Elsevier Science Publishers B.V., Amsterdam — Printed in The Netherlands

MINIGLASS, AN INTERACTIVE PROGRAM FOR THE EVALUATION OF STABILITY CONSTANTS OF METAL/LIGAND COMPLEXES FROM POTENTIOMETRIC DATA

A. IZQUIERDO* and J. L. BELTRAN

Department of Analytical Chemistry, Faculty of Chemistry, University of Barcelona, Diagonal 647, Barcelona 08028 (Spain)

(Received 7th August 1985)

SUMMARY

MINIGLASS is a microcomputer program for the treatment of pH titrations for evaluation of stability constants and adjustment of the parameters defining the titration curve. The program is written in PASCAL for the HP-200 computer series, and contains procedures for blank titrations, acidity constants and metal/ligand stability constants. Graphics support is provided for easy interaction with the user. The data files can be written by the editor of the operating system or can be created automatically from an automatic titration system. The program is tested for the determination of the formation constants of the well-studied Ni^{2+}/glycine system. The results obtained agree well with literature values.

A very widely used method of studying complex formation between metal ions and ligands with acid-base properties is based on the potentiometric titration with a pH electrode [1—3]. The titrimetric data are used to evaluate equilibrium constants by graphical methods in simple systems [1, 4] and calculated by computer programs in more general systems [2, 4, 5]. Most popular computer programs, e.g., LETAGROP [6], SCOGS [7], MINIQUAD [8], DALSFEK [9], were written for use on large computers because of the amount of information needed to calculate the "best" set of constants. However, the improvement of microcomputers in memory and speed has led to the appearance of several programs specifically designed for microcomputers, e.g., TITFIT [10], BEST [11] and MICMAC [12]. The function minimized in each program can be different: DALSFEK uses the e.m.f., SCOGS and TITFIT the volume of titrant, BEST and MICMAC the pH, and MINIQUAD the total analytical concentrations; in LETAGROP there is a choice of several functions ($\bar{n}$, e.m.f., or analytical hydrogen ion concentration).

Of course, the programs used in large computers are faster, but the direct interaction possible with the user of a personal computer is very useful in the definition of the "chemical model" of the system studied [10]. For this purpose, the program MINIGLASS described below has been designed to run on a personal computer; it is fully interactive and easy to learn. This new

0003-2670/86/$03.50

program is tested on the well-known Ni^{2+}/glycinate system, which has been used previously for comparison of methods [10, 13, 14].

THE MINIGLASS PROGRAM

MINIGLASS is a menu-driven and single-touch operation program, so that the instructions needed for the user are minimal. Another feature that simplifies use of the program is the graphical presentation: the results of calculations can be plotted on the screen (or plotter) as titration curves (experimental and calculated) or distribution of the residuals (error vs. $-\log [H^+]$).

The program is written in PASCAL for the Hewlett-Packard series 200 personal computers (working on the HP PASCAL operating system, version 2.1); translation to other computers should be easy, given the high compatibility between HP PASCAL and UCSD PASCAL. The compiled code uses about 64 kbytes of memory, but needs more memory for the data and arrays used (between 40 and 80 kbytes depending on implementation). In the present configuration, this program can run calculations from up to nine titrations and more than 600 experimental points.

MINIGLASS is designed for three different types of titration: a Blank procedure (strong acid with strong base) for the evaluation of pK_w and the acid and alkaline junction potentials, a PKAS procedure for the calculation of protonation constants, and a Complex procedure for complex formation equilibria. In the first two cases, the function to be minimized is the sum of squared residuals with respect to $-\log [H^+]$:

$$U = \sum (-\log[H^+]_{exp} + \log[H^+]_{calc})^2 \quad (1)$$

In the third case, this function can be selected or refinement with respect to the titrant volume added can be performed:

$$U' = \sum (V_{t,exp} - V_{t,calc})^2 \quad (2)$$

Of course, the three types of treatment can be applied in one general program, but a different procedure for each problem is preferred here to speed execution of the program.

Characteristics of the procedures

The Blank procedure. The theoretical free hydrogen ion concentration is calculated in this case by means of the charge balance in the solution being titrated. If V_0 ml of hydrochloric acid of concentration C_0 mol l^{-1} is titrated with V_t ml of sodium hydroxide (H_t mol l^{-1}), the charge balance at any point of titration will be:

$$[H^+] + [Na^+] = [Cl^-] + [OH^-]$$

Substituting $[OH^-]$, $[Cl^-]$ and $[Na^+]$ by their actual values, and making $V_{tot} = V_0 + V_t$ yields

$$[H^+] + (H_t V_t / V_{tot}) = (C_0 V_0 / V_{tot}) + (K_w / [H^+])$$

Rearrangement of this equation gives

$$[H^+]_{calc} = \{(C_0 V_0 - H_t V_t) + [(C_0 V_0 - H_t V_t)^2 + 4K_w V_{tot}^2]^{1/2}\}/2\, V_{tot} \quad (3)$$

The PKAS procedure. In this procedure, the algorithm proposed by Motekaitis and Martell [15] in the PKAS program is used, as it is specifically designed for acid-base equilibria. The advantage of this algorithm over another general algorithm (described below) is its faster execution, which is important for a microcomputer.

The only difference here is in the partial derivatives: in the present program they are taken with respect to $\ln[H^+]$ instead of $[H^+]$, to prevent negative values in the latter.

The Complex procedure. As noted previously, the refinement in metal/ligand complexes can be done in two ways: minimizing the sum of squared residuals (SSR) with respect to $-\log[H^+]$ or V_t. The user can select the working mode directly from the main menu, without interrupting the program execution, so that the results obtained from the two models can readily be compared in the search of the "best model". The calculations needed for both options are very similar, and so are contained in this single procedure. The mathematical background for the first case is as follows.

The equilibrium system contains n components and k species. The free concentration of component i is denoted as c_{li}, and by convention the hydrogen ion will always be the nth component. An array of stoichiometric coefficients cf is defined such that the coefficient of the ith component in the j species will be $cf_{j,i}$. If β_j is the formation constant for the species j, the concentration of this species in the equilibrium will be

$$S_j = \beta_j \prod_{i=1}^{n} c_{li}^{c_{j,i}} \quad (4)$$

$\vec{G}$ is defined as a vector which contains the theoretical mass balances for all the components. The mass balance for the ith component is

$$G_i = c_{li} + \sum_{j=1}^{k} cf_{j,i} S_j \quad (5)$$

To calculate the concentration of each species on the basis of the equilibrium constants, the free concentrations of the components are needed. The system then has n non-linear equations (the $\vec{G}$ vector) and n unknown quantities (the free concentrations in the equilibrium), which is solved by the iterative Newton method [16]. Defining a new vector $\vec{F}$ as the difference between the calculated and experimental total concentrations for each component ($\vec{T}$) gives

$$F_i = G_i - T_i$$

from which it is clear that the components $\vec{F}$ are equal to zero when the system of equations is solved.

The vector of the natural logarithms of the free concentrations of components is defined as $\vec{L}$ (e.g., $L_i = \ln c_{li}$). Differentiation of the $\vec{F}$ vector with respect to $\vec{L}$ gives the Jacobi matrix $|\mathbf{J}|$:

$$\mathbf{J}_{i,l} = \mathrm{d}F_i/\mathrm{d}L_l = \delta_{il}c_{li} + \sum_{j=1}^{k} cf_{j,i}\, cf_{j,l}\, S_j \tag{6}$$

where δ_{il} is the Kronecker delta, which is equal to 1 if $i = 1$, and zero otherwise. According to the iterative process, the values of the $\vec{L}$ vector in the $(m + 1)$ iteration will be equal to

$$\vec{L}_{m+1} = \vec{L}_m - \vec{F}_m\, |\mathbf{J}^{-1}|_m = \vec{L}_m - \vec{R}_m$$

The new vector $\vec{R}$ is defined as $\vec{R} = \vec{F}\, |\mathbf{J}^{-1}|$. Changing the elements of this vector by $R_i = \ln(\exp R_i)$, and making $L_l = \ln c_{li}$ yields

$$\ln(c_{li})_{m+1} = \ln(c_{li})_m - \ln(\exp R_i)_m$$

and finally

$$(c_{li})_{m+1} = (c_{li})_m / \exp(R_i)_m \tag{7}$$

This iterative cycle is repeated until the sum of absolute values of the elements of the vector $\vec{F}$ is less than 10^{-9}, which takes about 3—6 iterations. The advantage of taking derivatives with respect to the logarithms of the free concentrations is that the result of Eqn. 7 cannot be negative, so that the concentrations of the free components and complex species are always positive [17]. Once the solution for each point has been attained, the residual is defined by

$$D = -\log[\mathrm{H}^+] + \log c_{ln} \tag{8}$$

When the refinement is made with respect to the titrant volume, the iterative solution of the system is very similar to the above, but now is solved only for $(n - 1)$ components, because the free concentration of hydrogen ion is fixed. Once the free (theoretical) concentrations of the other components are known, the mass balance for the hydrogen ion is constructed: T_{h0} is defined as the initial total hydrogen ion concentration, and T_h the concentration at any point of the titration. Thus

$$T_h = (T_{h0}\, V_0 + H_t V_t)/(V_0 + V_t) = [\mathrm{H}^+] + \sum_{j=1}^{k} cf_{j,n} S_j \tag{9}$$

where H_t is >0 if the titrant is acidic, and <0 if alkaline. The right-hand side of this equation is the nth element of the $\vec{G}$ vector as defined in Eqn. 5. Rearranging Eqn. 9 gives

$$T_{h0}\, V_0 + H_t V_t = G_n\, (V_0 + V_t) \tag{10}$$

and

$$V_{t,calc} = (T_{h0} - G_n)\, V_0/(G_n - H_t) \qquad (11)$$

The result of Eqn. 11 is the theoretical titrant volume at any point in the titration. The residual is defined in this case by $D = V_{t,exp} - V_{t,calc}$.

In a single procedure, the theoretical values of $-\log[H^+]$ or V_t can be obtained with essentially the same calculations. This is possible by making the hydrogen ion the last component and by conducting the titrations with a single burette in which the titrant can be acid or base. The present implementation of this procedure allows the determination of stability constants for systems with up to four components, although this can be changed by re-dimensioning the arrays used.

Method of refinement

The parameters that can be refined with this program are the constants for protonation and complex formation, and the pK_w and liquid junction potentials. The values of the intercept (E_0') and the slope of the electrode (g), and the total initial concentrations of the reactants (including the titrant) are also adjustable parameters, so that this program is very useful in the search of systematic errors.

In the program, the Gauss-Newton iterative method is used [18—20] and will not be discussed here. In the present case, the derivatives needed are obtained numerically because of the variety of adjustable parameters. The iterative process of minimization is repeated until the relative change in SSR between two iterations is less than 0.1%. In the case of divergence in the refinement process, the method is modified to optimize the "shifts" of parameters, as described by Wentworth [21]. If after this, the SSR is reduced, the program turns to the Gauss-Newton method, but if convergence is not achieved, the refinement process is stopped and a warning message is displayed on the screen. In any case, the parameters taken are always those corresponding to the minimum in SSR.

Other features

With the MINIGLASS program, the user has several options to make the calculations easy. These options are available from the main menu, by pressing a single key. For example, there is a procedure for changing the parameters manually, which is useful if after a refinement cycle the results do not agree with experience. Another feature is the possibility of changing the experimental points being considered in the calculations, analogously to the MINIPOT program [22].

The Complex procedure contains options for adding or rejecting species (or changing the value of their formation constants) to see the effect on the titration curves before the refinement is started; it is thus possible to estimate if certain species have any significance or not. Otherwise, there is a species selector which can be set on or off as required. Of course, the special

feature of the Complex procedure is the possibility of changing the refinement mode. This option is also available from the main menu.

The data files used in MINIGLASS are "text" files, and are written by the user by means of the editor of the operating system. Another way to construct the data files is by using an automatic data acquisition assembly (the components are noted in the experimental part). The automatic titration system is controlled by a BASIC program, so that when the titration is finished, the program creates a data file in the floppy or Winchester disk of the computer allowing direct on-line data collection. The advantages of such a system are complete automation with minimal errors in data transcription.

EXPERIMENTAL

The program and automatic titration assembly were used to evaluate the stability constants for the Ni^{2+}/glycine system. First, the acidity constants for the glycinate ion were evaluated and then the complex formation with nickel ion was examined. In the first case, the total concentration of glycine ranged from 0.007 to 0.026 mol l^{-1}. In the complex formation titrations, the concentration of metal ion was between 0.0025 and 0.0119 mol l^{-1}, the ligand/metal ratio being between 2:1 and about 5:1. Table 1 lists the experimental conditions for each titration.

The ionic strength in all experiments was 1.00 mol l^{-1} in sodium chloride and the temperature was kept constant at 25 ± 0.1°C. All the reagents used were of analytical grade.

The equipment included an automatic burette (Metrohm E-415), a pH meter (Radiometer PHM-84) with a glass electrode (G202B) and a Ag/AgCl reference electrode (K801), and a Tectron Selecta thermostat.

For the calculations and automatic titration control, a Hewlett-Packard HP-9816S desk computer, with 768 kbytes of main memory, was used. External mass storage units were a 3 1/2-in. floppy disk (270 kbytes) and a Winchester fixed disk (15 Mbytes). Auxiliary equipment included the HP-7475A plotter and HP-82906A printer.

TABLE 1

Experimental conditions

Titration number	$[gly]_0$ (10^{-3} mol l^{-1})	$[Ni^{2+}]_0$ (10^{-3} mol l^{-1})	Ligand/metal ratio	Range of $-\log[H^+]$
1	6.96	—	—	1.7—10.6
2	13.23	—	—	1.8—10.2
3	26.46	—	—	2.1—10.7
4	12.02	2.49	4.83	2.9—9.6
5	10.80	5.33	2.02	2.9—9
6	21.60	5.33	4.05	3.6—9.7
7	33.29	8.71	3.82	2.9—9.6
8	24.05	11.88	2.02	3.3—8.3

The data acquisition unit was a HP-3421A, connected to the computer through a HP-IB interface, and equipped with eight analog inputs to read the data and eight digital outputs to drive the burettes. The data readings were taken from the recorder output of the pH meter.

Listings of the MINIGLASS program or copies on a 3 1/2-in. floppy disk for the HP-200 computer series are available on request to the authors.

RESULTS AND DISCUSSION

The experimental data were processed in two steps; first, the calculations were done by refining the formation constants separately for each titration, and then they were all processed together. Initial approximations for the stability constants were taken as the values of $-\log[H^+]$ or $-\log[gly^-]$ in the formation curves at the half-$\bar{n}$ points (see Figs. 1 and 2).

TABLE 2

Calculated stability constants

Titration number[a]	$\log \beta_{1mh}$[b]				
	101	102	110	210	310
1 p	9.652(3)	12.064(5)			
1 v	9.657(3)	12.064(3)			
1 h	9.652(3)	12.063(5)			
2 p	9.660(2)	12.076(5)			
2 v	9.659(3)	12.074(4)			
2 h	9.658(2)	12.074(5)			
3 p	9.657(3)	12.073(5)			
3 v	9.660(2)	12.070(3)			
3 h	9.656(3)	12.072(5)			
4 v			5.623(6)	10.356(5)	13.729(7)
4 h			5.624(3)	10.356(4)	13.731(5)
5 v			5.619(3)	10.338(3)	13.710(21)
5 h			5.625(2)	10.336(3)	13.740(11)
6 v			5.625(3)	10.367(3)	13.750(3)
6 h			5.619(3)	10.364(4)	13.745(5)
7 v			5.617(7)	10.340(6)	13.689(8)
7 h			5.621(5)	10.343(6)	13.693(7)
8 v			5.611(1)	10.328(1)	13.646(8)
8 h			5.613(1)	10.329(2)	13.646(7)
1–3 p	9.657(4)	12.072(9)			
1–3 v	9.660(1)	12.069(2)			
1–3 h	9.656(2)	12.070(3)			
4–8 v			5.615(2)	10.333(2)	13.709(3)
4–8 h			5.619(2)	10.341(2)	13.715(3)
Final values	9.657(3)	12.070(5)	5.620(5)	10.346(14)	13.708(39)

[a]p: Calculated by the PKAS procedure. v and h: calculated by the Complex procedure (V_t and $-\log[H^+]$, respectively). [b]The estimated standard deviation on the final digit is given in parentheses.

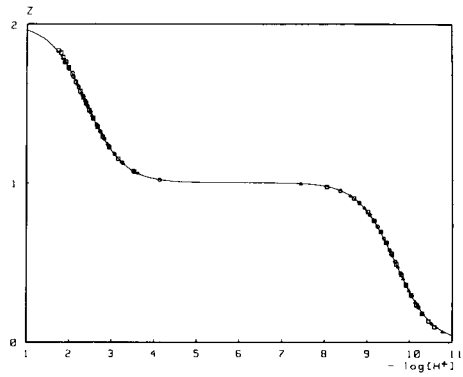

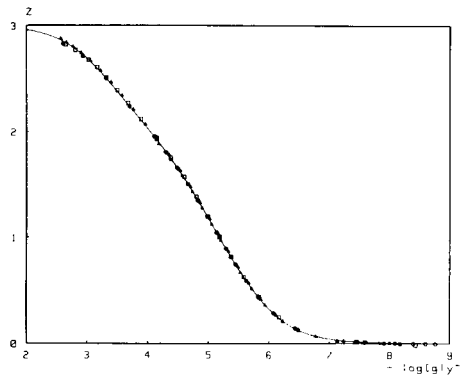

Fig. 1. Protonation curve of glycinate. Symbols: (□) titration 1; (○) titration 2; (△) titration 3. For clarity, only half of the total experimental points are plotted. The solid line is the theoretical curve plotted from the constants given in Table 2.

Fig. 2. Formation curve for the Ni^{2+}/glycinate system. Symbols corresponding to titration conditions in Table 1: (□) 4; (○) 5; (△) 6; (●) 7; (▲) 8. Only half the total points are plotted. The solid line is the theoretical curve.

The results obtained are shown in Table 2. Titrations 1—3 were used to evaluate the acidity constants of glycinate, and the values obtained by the different modes of calculation (by the PKAS and Complex procedures) agree well. The complex formation between glycinate and nickel was studied in titrations 4—8, with more than 210 experimental points. The refinement of three stability constants was possible in 4 iterations (about 10 min). Figure 3 shows the titration curves (experimental and calculated) and the distribution of residuals plotted by MINIGLASS for curves 4—8.

The final values for the protonation of glycinate and the formation of the Ni^{2+} complexes are given in Table 3, showing good agreement with those published in the literature.

To conclude, the MINIGLASS program combines the capability of calculations found in other programs written for large computers with the easy

TABLE 3

Comparison of results

Species l,m,h	Values of log β_{lmh}[a]		
	Ref. 10	Refs. 13, 14	This work
101	9.63	9.651(12)	9.657(3)
102	12.08	12.071(26)	12.070(5)
110	5.58	5.615(35)	5.620(5)
210	10.30	10.363(62)	10.346(14)
310	13.75	13.930(340)	13.708(39)

[a]With standard deviations, where available.

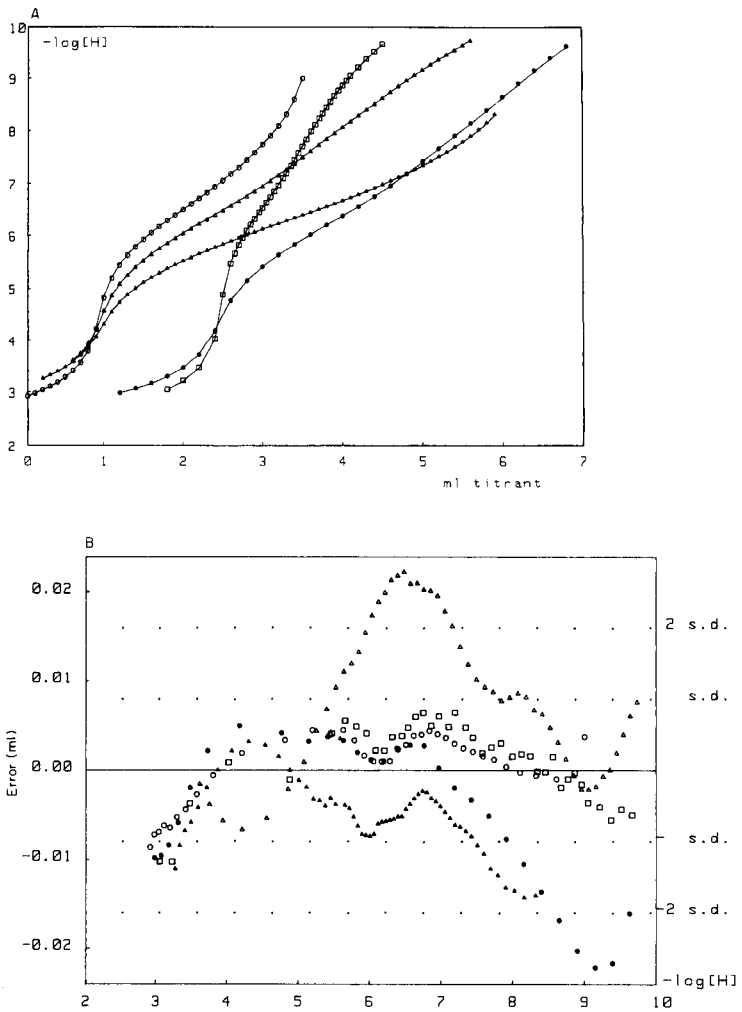

Fig. 3. (A) Experimental and calculated titration curves for titrations 4—8. (B) Distribution of residuals corresponding to titrations 4—8. Symbols as in Fig. 2.

access and direct interaction of microcomputers. In combination with the automatic data acquisition system, it provides a powerful tool for evaluation of stability constants.

REFERENCES

1 F. J. C. Rossotti and H. S. Rossotti, The Determination of Stability Constants, McGraw-Hill, New York, 1961.
2 F. R. Hartley, C. Burgess and R. M. Alcock, Solution Equilibria, Ellis Horwood, Chichester, 1980.

3 H. S. Rossotti, Chemical Applications of Potentiometry, Van Nostrand, London, 1969.
4 H. S. Rossotti, Talanta, 21 (1974) 809.
5 F. J. C. Rossotti, H. S. Rossotti and R. J. Whewell, J. Inorg. Nucl. Chem., 33 (1971) 2051.
6 L. G. Sillén, Acta Chem. Scand., 18 (1964) 1085.
7 I. G. Sayce, Talanta, 15 (1968) 1397.
8 A. Sabatini, A. Vacca and P. Gans, Talanta, 21 (1974) 53.
9 R. M. Alcock, F. R. Hartley and D. E. Rogers, J. Chem. Soc., Dalton Trans: (1978) 115.
10 A. D. Zuberbüler and T. A. Kaden, Talanta, 29 (1982) 201.
11 R. J. Motekaitis and A. E. Martell, Can. J. Chem., 60 (1982) 2403.
12 A. Laouenan and E. Suet, Talanta, 32 (1985) 245.
13 E. Bottari, A. Braibanti, L. Ciavatta, A. M. Corrie, P. G. Daniele, F. Dallavalle, M. Grimaldi, A. Mastroianni, G. Mori, G. Ostacoli, P. Paoletti, E. Rizzarelli, S. Sammartano, C. Severini, A. Vacca and D. R. Williams, Ann. Chim., 68 (1978) 813.
14 A. Braibanti, F. Dallavalle, G. Mori and B. Veroni, Talanta, 29 (1982) 725.
15 R. J. Motekaitis and A. E. Martell, Can. J. Chem., 60 (1982) 168.
16 B. P. Demidovich and I. A. Maron, Computational Mathematics, Mir, Moscow, 1981.
17 Ting-Po I. and G. H. Nancollas, Anal. Chem., 44 (1972) 1940.
18 A. Sabatini and A. Vacca, J. Chem. Soc., Dalton Trans: (1972) 1693.
19 W. H. Sachs, Technometrics, 18 (1976) 161.
20 E. Durand, Solutions Numeriques des Equations Algébriques, Tome II: Systèmes de Plusieurs Equations, Masson et Cíe, Paris, 1972.
21 W. E. Wentworth, J. Chem. Educ., 42 (1965) 96.
22 F. Gaizer and A. Puskás, Talanta, 28 (1981) 565.

Analytica Chimica Acta, 181 (1986) 97—106
Elsevier Science Publishers B.V., Amsterdam — Printed in The Netherlands

ROTATION IN SIMPLEX OPTIMIZATION

DONALD D. BURGESS
Department of Chemistry, McMaster University, Hamilton, Ontario L8S 4K1 (Canada)
(Received 13th August 1985)

SUMMARY

A modification of the modified simplex method of optimization was tested. This modification involves rotation of the simplex when the standard simplex motion by reflection, expansion and contraction, fails to lead to continued progress of the simplex. Two other methods and several kinds of rotation are compared for four response surfaces. Certain rotations are shown to be superior to others and to two previously reported operations that do not involve rotation.

The modified simplex method developed by Nelder and Mead [1] has found wide acceptance in the design of procedures in analytical chemistry. This algorithm has been further modified by several authors [2—9]. An important advantage of the modified simplex method is its ability to adjust its size and shape to accommodate the local shape of the response surface.

A problematic step in the modified simplex algorithm is the treatment of "failed" contractions. Reflection, expansion and contraction along a line joining the worst vertex of the most recent simplex and the centroid of the opposite face of this simplex are the basic operations of the modified simplex optimization method. These operations are designed to locate a new vertex that exhibits a response better than the response found for at least one of the vertices of the most recent simplex. Here, better means numerically greater or less, depending upon whether a maximum or a minimum is sought. Contraction is applied if reflection and expansion do not locate a better vertex. If contraction also does not yield a better vertex, failed contraction has occurred and the simplex cannot proceed using the basic operations. Various tactics have been proposed for dealing with failed contractions [1, 3, 8—10]. The difficulty lies in obtaining an operation that results in further progress by the simplex, that does not impair its ability to search in all directions and that does not quickly lead to new failed contractions or oscillation about the region where failed contraction occurred.

Operations proposed for use in the case of failed contractions include: (a) massive contraction of the simplex [1]; (b) rejection of the next-to-worst vertex, as developed by King [8] and described by Deming and Parker [9]; (c) a combination of reflection away from the next-to-worst vertex with expansion and contraction from the vertex obtained in the failed contraction

0003-2670/86/$03.50

towards the best vertex [3]; and (d) translation of the simplex so that its centre is placed at the best vertex [10]. The purpose of this study is to establish the merits of rotating the simplex upon failed contraction.

During optimization, it is desirable to satisfy three conditions. First, too rapid reduction in the size of the simplex must be avoided in order to prevent premature convergence. Second, the symmetry of the simplex should not be unnecessarily decreased, as this decreases its ability to move in some directions [4]. Third, on failed contraction, further progress requires motion in new directions because the directions already searched have proved unsuitable. Successful recovery from failed contraction is clearly more likely if several new directions can be examined quickly.

When massive contraction is used at failed contractions, neither the first nor the third of these conditions is met. Rejection of the next-to-worst vertex satisfies all three requirements but moves the simplex in only one new direction. Operation (c) described above can explore two new directions but symmetry is reduced when the reflected point is not retained. Simple translation of the simplex explores new directions to only a limited degree. Rotation of the simplex, however, results in the exploration of more than one new direction and preservation of simplex size and symmetry. Results reported by Gustavsson and Sundkvist [3] indicate that the exploration of new directions is particularly important.

EXPERIMENTAL

The simplex optimization program was executed using an IBM-PC microcomputer equipped with a numeric coprocessor. The program was written in the C language and all computations were done in double precision with fifteen significant figures.

A set of two convergence criteria was used [2]. The standard deviation of the responses at the vertices of the most recent simplex was first compared to a preset value (RTOL, response tolerance). If the standard deviation was smaller than RTOL, the response at the simplex centroid was obtained and the root-mean-square of the centroid and vertex responses was compared with RTOL. If it was less than RTOL, the optimization was halted. The conditions of non-convergence and critical non-convergence [6] correspond to differences of respectively 10 and 1000 times RTOL between the response at the best vertex and the true optimum response value. In the evaluation of expansions, the new vertex was compared with the reflected point [7].

The testing procedure of Gustavsson and Sundkvist [3] was used in this study. Four response functions were tested with eight different initial simplex sizes. For each combination of response function and simplex size, 100 optimizations were run with the initial location of the centroid of each simplex chosen by means of a random number generator. The same sequence of random numbers was used for each of nine methods for treating failed contractions. The maximum number of iterations was set to 500. All

optimizations were done with two adjustable parameters. The response functions were a two-dimensional paraboloid [6] ($-1000 < X < 1000$, $-1000 < Y < 1000$, RTOL = 10^{-4}), a least-squares fit [11] ($0 < X < 2$, $0 < Y < 2$, RTOL = 10^{-4}), Rosenbrock's function [12] ($-25 < X < 25, -25 < Y < 25$, RTOL = 10^{-5}) and a modification of Fletcher and Powell's helical valley [2] ($-100 < X < 100, -100 < Y < 100$, RTOL = 10^{-4}).

The results of these trials are shown in Figs. 2—6. These histograms are projections of three-dimensional data sets and are best viewed as sets of flat vertical plates placed at right angles to a flat horizontal plate. In all plots, more favourable results occur at smaller vertical distances and scheme numbers (see below) run from I at the front to IX at the back of each vertical plate. The initial simplex size, expressed as a percent of the variable parameter ranges, is represented by ISS %.

Schemes for failed contraction

Figure 1 outlines the operations tested.

Type I. The next-to-worst vertex was rejected. Reflection, expansion and contraction were done along a line passing through the next-to-worst vertex and the centroid of the opposite face of the simplex. This is Type A in the paper by Gustavsson and Sundkvist [3].

Type II. The worst point was rejected using the centroid and reflected point applied in type I. This is Type B in the paper by Gustavsson and Sundkvist [3].

Type III. The simplex was rotated by −90° about its centroid.

Type IV. The simplex was rotated by −90° about the best vertex.

Type V. The simplex was rotated by −90° about the worst vertex.

Type VI. The simplex was rotated by −90° about the next-to-worst vertex.

Type VII. The simplex was rotated about the worst vertex in order to place the simplex centroid on the line passing through the best and worst vertices.

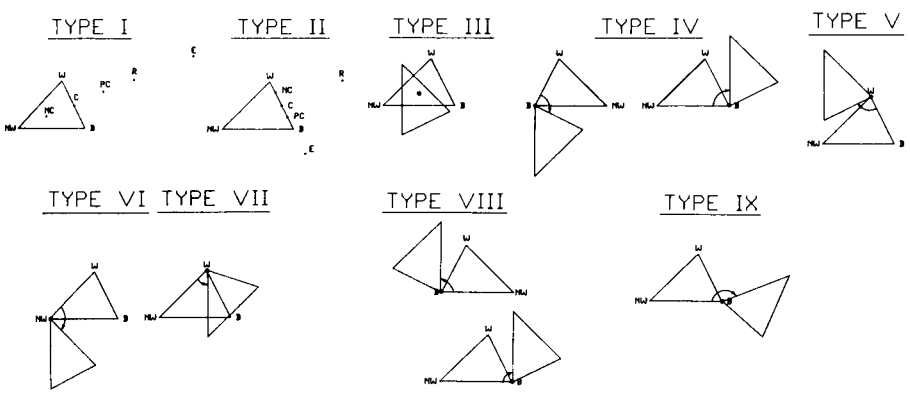

Fig. 1. Simplex rotation. C, Centroid. Vertices: B, best; W, worst; NW, next-to-worst. R, reflection; E, expansion; PC, positive contraction; NC, negative contraction.

Type VIII. The simplex was rotated by + or −90° about the best vertex so that rotation was in the same direction as a rotation of the next-to-worst vertex towards the worst vertex.

Type IX. The simplex was rotated in the same direction as for type VIII but by an angle that made the line that originally passed through the best and next-to-worst vertices parallel to a line through the next-to-worst vertex and the centroid of the opposite side.

Before the operations described above, the worst vertex was replaced by the vertex obtained on contraction. In Fig. 1, two views are shown for methods IV and VIII to illustrate the difference between them. The simple rotations were tried with angles of 45° but, as performance was worse, these trials are not included here.

RESULTS AND DISCUSSION

Gustavsson and Sundkvist [3] reported computational problems that resulted in unreasonably good performance for Rosenbrock's function, presumably as a result of failure properly to detect early fulfillment of the convergence criteria, and concluded that these problems could be overcome. The same behaviour was noted in this work but the cause has not been found even though their formulae were used in computing test values for convergence and double precision was used in the calculations. The results obtained in this work do, however, permit comparisons of different treatments of failed contractions.

Three aspects of performance used in comparing the nine operations at failed contractions were the number of function evaluations, the number of non-convergent optimizations and the number of failed contractions. The average number of evaluations indicates the efficiency of the method and the standard deviation indicates its consistency with respect to changing starting points. The number of non-convergent optimizations is related to the probability of accurately locating the true optimum. Failed contractions introduce a risk of early convergence or oscillation, as observed in many cases in the present work, and therefore are preferably avoided. The average and standard deviation of the number of failed contractions indicate the degree to which a method succeeds in this.

Two methods can be compared with respect to the number of function evaluations only if the number of non-convergences is similar for the two methods [2]. An optimization that terminates early naturally uses fewer evaluations than one that progresses further to locate the actual optimum. Figure 2 shows, for methods II, IV, and IX with Fletcher and Powell's function, that the introduction of rotations exacts only a small number of extra evaluations and does not seriously impair efficiency. The consistency of the number of evaluations (Fig. 3) was found to vary with success in avoiding non-convergent optimization, as would be expected.

The least-squares function and Fletcher and Powell's function yielded the

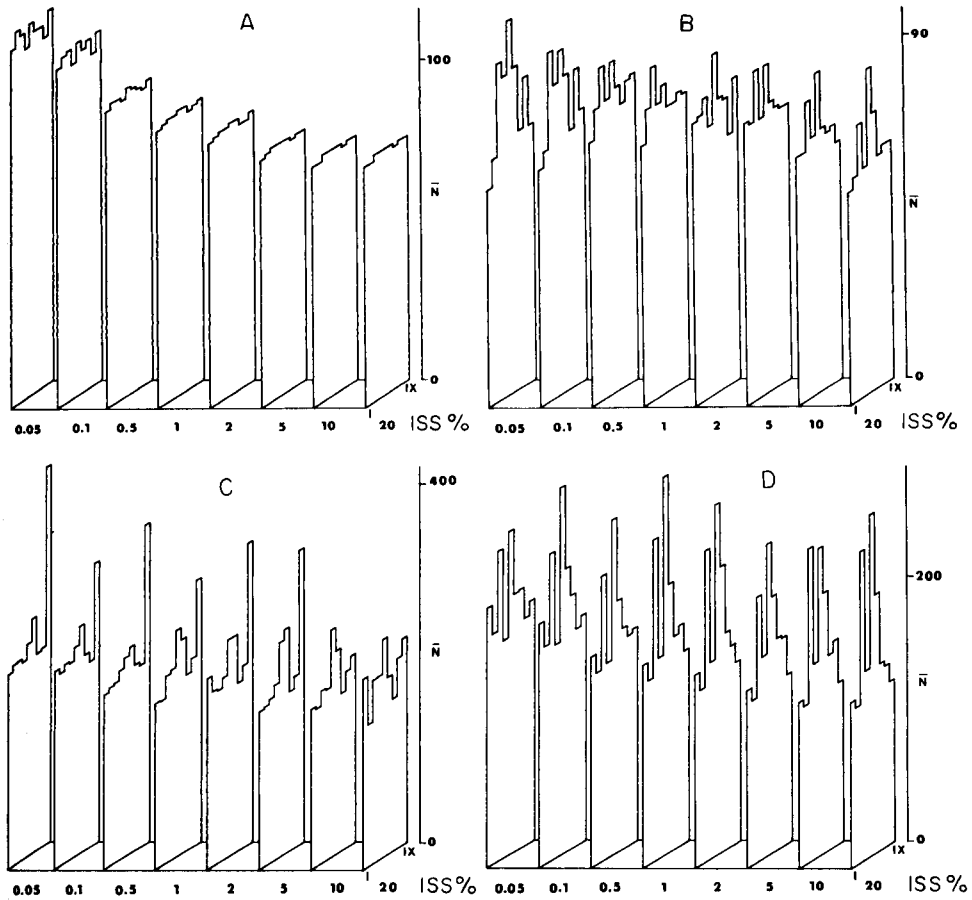

Fig. 2. Average number of function evaluations. Response functions: A, paraboloid; B, least squares; C, Rosenbrock's function; D, Fletcher and Powell's function.

most information concerning differences in the number of non-convergent optimizations. These results are given in Fig. 4. For the least-squares function, the rotation methods (III—IX) are clearly superior to methods I and II. Method II gave the fewest non-convergences with Fletcher and Powell's function. Of the rotation methods, IV and IX performed best. When both functions are considered, method IV gave the best accuracy. No non-convergent trials were encountered for the parabolic function.

Figure 5 gives the results found for the average number of failed contractions. Little variation was found for the paraboloid and least-squares functions. Methods III and VII gave the lowest numbers of failed contractions for Rosenbrock's function whereas methods IV, VIII and IX performed well for Fletcher and Powell's function. This pattern was repeated for the variability of the number of failed contractions (Fig. 6) except that

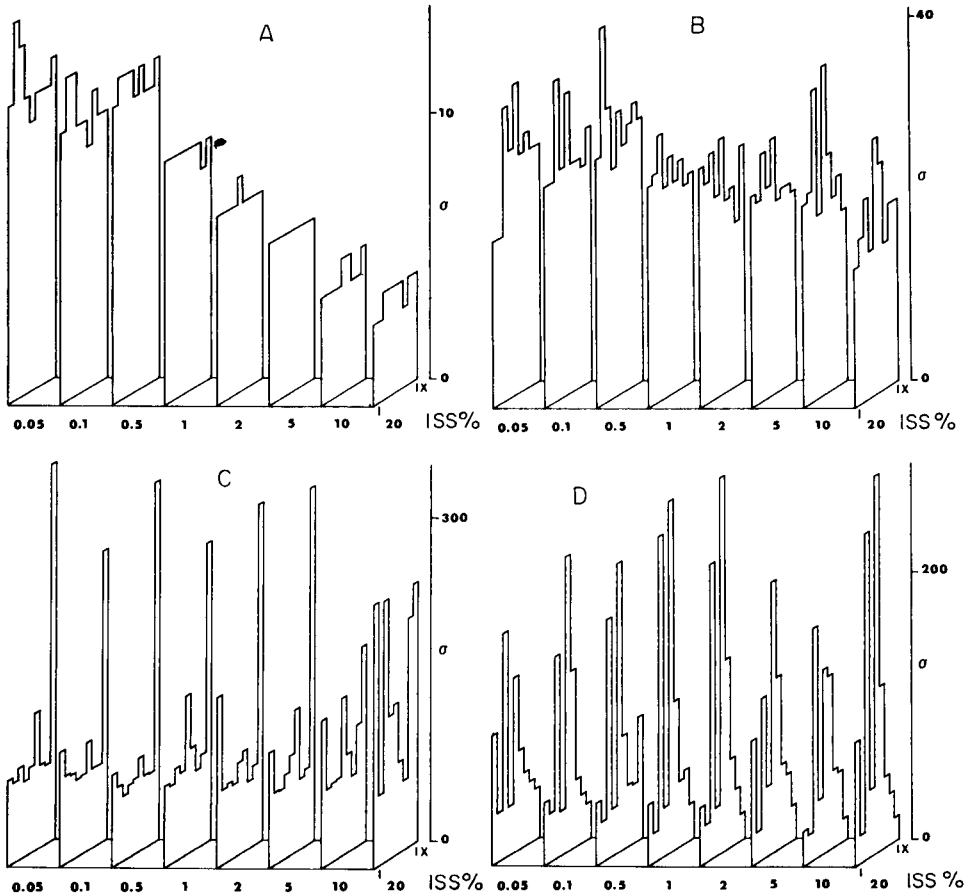

Fig. 3. Standard deviation of number of function evaluations. Response functions as in Fig. 2.

method II also showed low values for Fletcher and Powell's function. Overall, method IV showed the most favourable performance in avoiding failed contractions.

Of the rotation methods, rotation by $-90°$ about the best vertex gave the most satisfactory results. This method also compared favourably with the Type II operation, giving significantly fewer non-convergences for the least-squares function and only somewhat more for Fletcher and Powell's function. Figure 1 shows that both operations can explore the region adjacent to the best and worst vertices. Type II also explores a region beyond the best vertex in the opposite direction from the worst vertex. Type IV does this either directly or by subsequent reflection from a vertex placed near the previous worst vertex. The superior performance of these methods indicates that movement into these regions is desirable. The improved per-

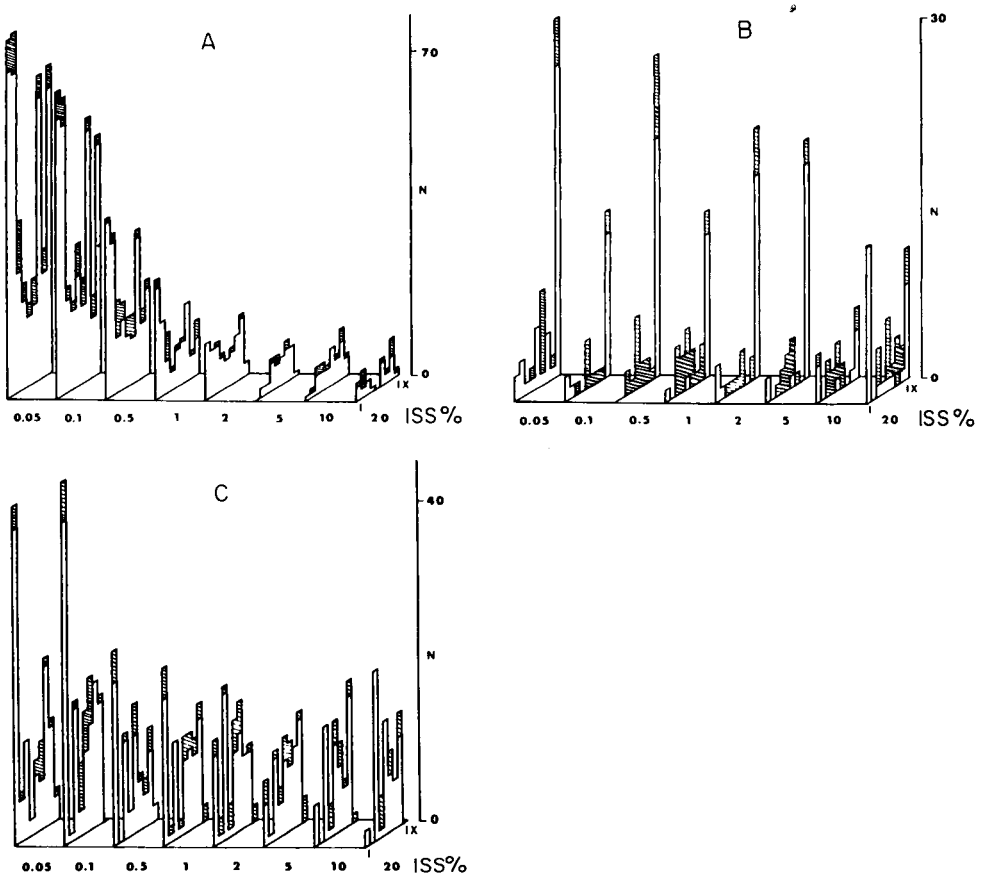

Fig. 4. Number of non-convergent optimizations. Shaded areas show the excess of non-convergent over critically non-convergent optimizations. Response functions: A, least squares; B, Rosenbrock's function; C, Fletcher and Powell's function.

formance of Type IV over Type II for the least-squares function indicates that, with at least some response surfaces, preservation of simplex symmetry at failed contractions is beneficial. Types II and IV explore similar directions, but Type IV preserves simplex symmetry while Type II often does not.

The inferior performance of methods VII, VIII and IX is, at first sight, surprising. If the simplex is of low symmetry, however, methods VII and IX change its position and orientation to only a small degree. Method IV results in rotation into one of two different regions, depending on the orientation of the simplex. Method VIII chooses only one of these. A trial in which rotations were made as in method VIII, but in the opposite direction, gave results similar to those of method VIII for the least-squares function and better than those of method IV for Fletcher and Powell's function. Here too, the anomaly was due to low simplex symmetry. Rotation at failed

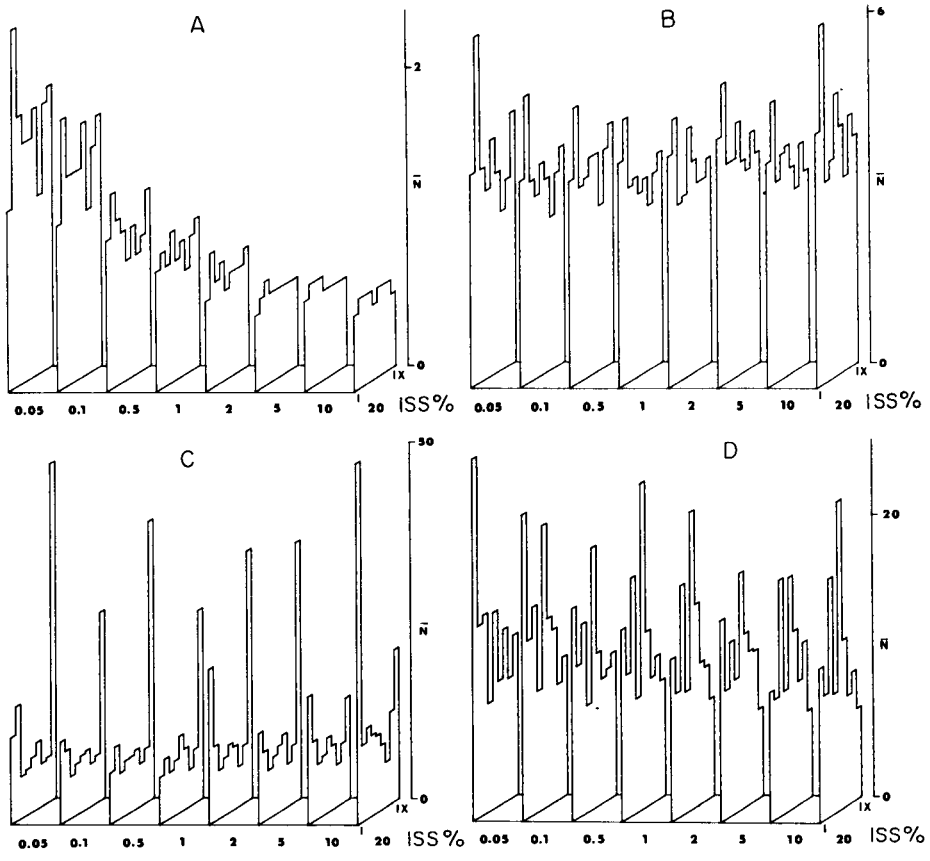

Fig. 5. Average number of failed contractions. Response functions as in Fig. 2.

contractions should therefore yield greater improvement if the simplex symmetry is controlled explicitly [6, 13].

For general use, the rotation operation must be extended to optimizations involving more than two adjustable parameters. Computation of the required rotation transformation requires the selection of an axis of rotation. As this study has shown that rotation about a vertex is satisfactory for two-dimensional simplexes, it is probable that an edge of a simplex of higher dimension would be suitable for the axis of rotation. Finding the best edge will require further study, but the observations made in this work suggest that either the edge connecting the best and worst vertices or the edge connecting the best and next-to-best vertices would be an appropriate choice. A disadvantage of simplex rotation over other operations is increased computational complexity. This may be particularly severe when many adjustable parameters are involved.

Rotation offers a conceptually straightforward means for redirecting

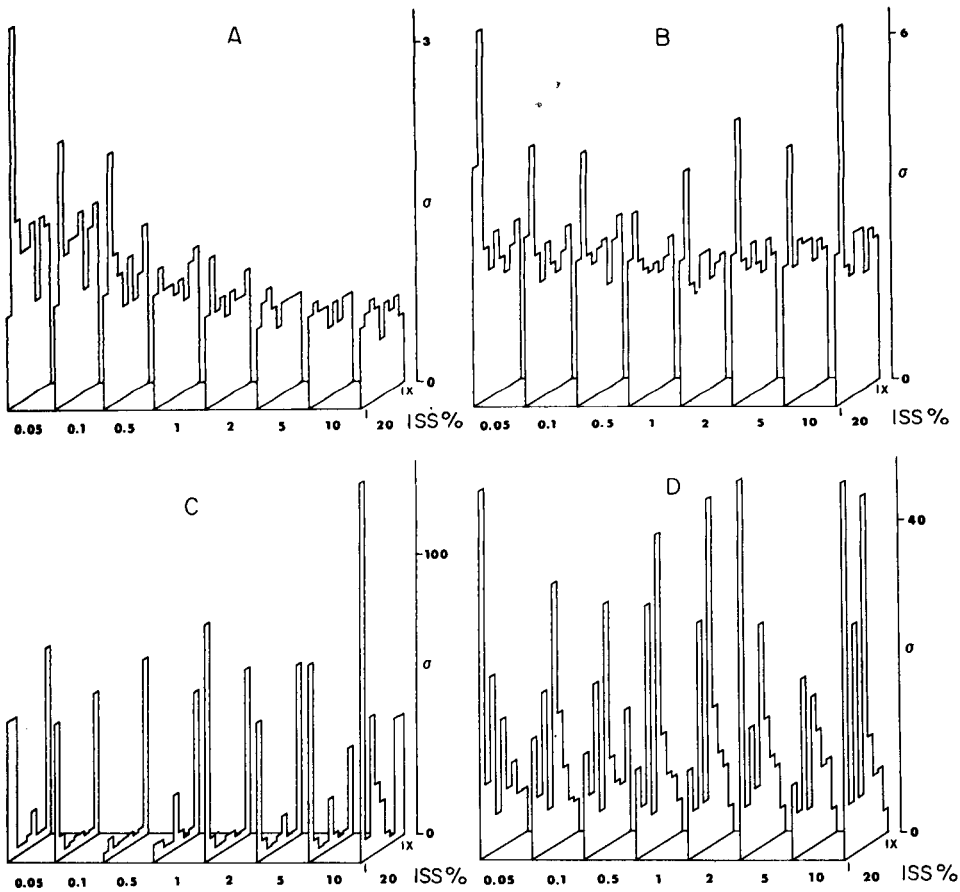

Fig. 6. Standard deviation of number of failed contractions. Response functions as in Fig. 2.

simplexes at failed contractions without sacrificing symmetry; it also lessens the problems of oscillation upon failed contraction that are observed when other schemes are employed.

REFERENCES

1 J. A. Nelder and R. Mead, Comput. J., 7 (1964) 308.
2 E. R. Aberg and A. G. T. Gustavsson, Anal. Chim. Acta, 144 (1982) 39.
3 A. Gustavsson and J.-E. Sundkvist, Anal. Chim. Acta, 167 (1985) 1.
4 P. F. A. van der Weil, R. Maassen and G. Kateman, Anal. Chim. Acta, 153 (1983) 83.
5 M. W. Routh, P. A. Schwartz and M. B. Denton, Anal. Chem., 49 (1977) 1422.
6 P. B. Ryan, R. L. Barr and H. D. Todd, Anal. Chem., 52 (1980) 1460.
7 P. R. Benyon, Appl. Stat., 23 (1974) 250.
8 P. G. King, Ph.D. dissertation, Emory University, Atlanta, GA, 1974.
9 S. N. Deming and L. R. Parker, CRC Crit. Rev. Anal. Chem., 7 (1978) 187.

10 R. R. Ernst, Rev. Sci. Instrum., 39 (1968) 998.
11 S. N. Deming and S. L. Morgan, Anal. Chem., 45 (1973) 278.
12 H. H. Rosenbrock, Comput. J., 3 (1960) 175.
13 P. F. A. van der Weil, R. Maassen and G. Kateman, Anal. Chim. Acta, 153 (1983) 83.

Analytica Chimica Acta, 181 (1986) 107—116
Elsevier Science Publishers B.V., Amsterdam — Printed in The Netherlands

AN IMPROVED SIMPLEX ALGORITHM FOR DEALING WITH BOUNDARY CONDITIONS

M. R. CAVE

British Geological Survey, Nicker Hill, Keyworth, Nottingham NG12 5GG (Great Britain)

(Received 4th October 1985)

SUMMARY

Two existing and one new method for dealing with boundaries in simplex optimization are tested on 2-, 3-, and 5-parameter test functions, each subject to five different boundary conditions. The performance of the new method is shown to be the most consistent over all conditions.

Simplex optimization has proved to be a useful tool in analytical chemistry as shown in a review of its earlier uses [1] and by more recent applications [2—6]. Since the introduction of the basic simplex method by Spendley et al. [7] as a generalized optimization method, several modifications have been tested [8—13] to try to improve the speed and accuracy of the optimization. These modifications have concentrated on varying methods for calculating the new vertex for each successive simplex move from existing vertices, given their respective responses. The results of this work show that the choice of method is very important, although there is another area of practical importance which has as yet received little attention, namely, the effect of boundary conditions.

The aim of the work described here is to test the two existing and one new method for dealing with boundary conditions, on 2-, 3- and 5-parameter test functions with a series of boundary conditions imposed on them.

THEORY

In simplex optimization of a multiparametric system, there will be constraints on each parameter which are usually set by physical restraints on instrumentation. During the optimization, however, it is quite common that the simplex procedure will arrive at a combination of parameter settings in which one or more parameters has exceeded its boundary condition. Nelder and Mead [8] used a simple solution to this problem by assigning an artificially low response to the straying vertex, which under the variable size rules [8] will cause the simplex to contract and move back within the boundary conditions. Using this method can cause a problem if the optimum

0003-2670/86/$03.50

setting of the parameter is close to or actually on the boundary condition. As the simplex tries to approach the optimum, it will be forced away by the boundary rule and then approach again from a different direction. This process may have to be repeated several times before the optimum is reached. As will be shown below, this can lead to an increase in the number of experiments required and loss of accuracy in defining the optimum.

This limitation was recognised by Routh et al. [9] who devised an alternative mode of dealing with boundary conditions, which was primarily designed to be used with their super modified simplex method [9, 10]. This method is illustrated in Fig. 1 for a two-parameter example (i.e., the simplex is a triangle) with the vertices B, Nw, and W representing the combinations with the best, next to worse, and worst responses, respectively. The normal simplex step would then be produced by reflecting the triangle B Nw W about the line B Nw to produce R which in this case would be in violation of the boundary condition. Routh et al. [9] suggested that the new vertex should be formed at R′ by correcting R back to a point just on the boundary condition, and then continuing with B Nw R′ as the new simplex. The main advantage of this method over the former is the ability to explore the factor space up to and including the boundary condition, which should prove more effective when the optimum is close to or on the boundary.

From the experimental results, which will be discussed in detail below, it was evident that it would be advantageous to combine in one method the ability to move back and approach the optimum from a different direction as in the first method, and the ability to search up to the boundary as in the second method. With reference to Fig. 2, the combined method only uses a corrected point R′ at the boundary to form the new simplex if the response at R′ is greater than at B. If this is not the case, then a negative contraction to form Nc is used. A further modification was also made to

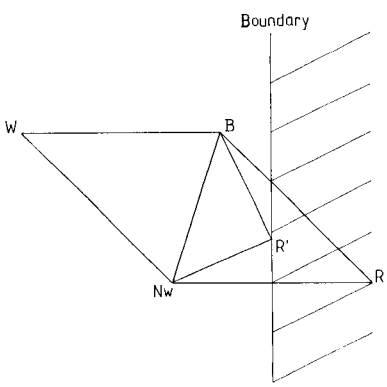

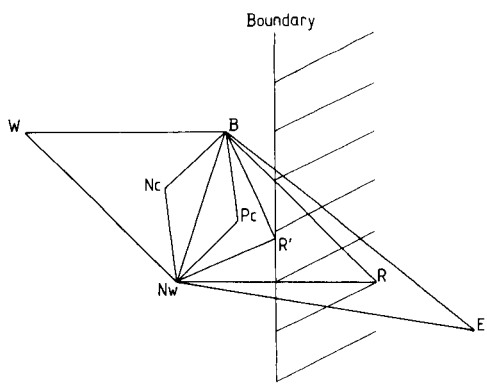

Fig. 1. Explanation of boundary rule 2. For symbols, see text.

Fig. 2. Explanation of combined boundary rule.

remove an anomaly which would have existed when this boundary method was used with the modified simplex method [8]. Normally, when R is formed if the response at R is greater than at B, then an expansion in the direction of R to form E would be performed. This would be pointless in the case of R′ as it would serve only to place E outside the boundary condition. In the combined method, therefore, when a corrected point R′ is formed with response greater than B, a positive contraction Pc is tried; if this produces a response greater than R′ a negative contraction Nc is tried, the better of the two responses from Nc and Pc being used to form the new simplex. If the response at Pc is less than that at R′, then R′ is used to form the new simplex. The three boundary methods described were then used to form three simplex algorithms based on the simplex method of Nelder and Mead [8] with the modifications suggested by Aberg and Gustavsson [11], and given the initials MSM, MSM1 and MSM2, respectively.

The three test functions used to evaluate the performance of the three methods are as follows:

$$\text{function } 1 = \cos X_1 + \cos X_2 \tag{1}$$

(optimum $X_1 = X_2 = 0°$; response = 2)

$$\text{function } 2 = \cos X_1 + \cos X_2 + \cos X_3 \tag{2}$$

(optimum $X_1 = X_2 = X_3 = 0°$; response = 3)

$$\text{function } 3 = \cos X_1 + \cos X_2 + \cos X_3 + \cos X_4 + \cos X_5 \tag{3}$$

(optimum $X_1 = X_2 = X_3 = X_4 = X_5 = 0°$; response = 5)

Well-behaved functions were chosen, as the main aim was to study performance at different boundary conditions rather than the effect of function complexity on the simplex methods.

Five sets of boundary conditions were chosen for the parameters in each function to try to simulate all the possible conditions occurring in practical situations: (I) $-180° \leqslant Xn \leqslant 180°$, the optimum being symmetrically placed between the two boundaries; (II) $-60° \leqslant Xn \leqslant 180°$, the optimum being slightly displaced towards one boundary; (III) $-10° \leqslant Xn \leqslant 180°$, the optimum being positioned very close to one boundary; (IV) $0° \leqslant Xn \leqslant 180°$, the optimum being positioned on the boundary; and (V) $20° \leqslant Xn \leqslant 180°$, the true optimum being positioned outside the boundary but with a local optimum on one boundary. All of the parameters in each function (represented as Xn for the general case) were subject to the same boundary conditions.

EXPERIMENTAL

The microcomputer system used was a Commodore 64 with a Commodore 1541 single disc drive unit and a Commodore MPS-801 dot matrix printer.

All programs were written in Commodore 64 BASIC; copies are available from the author on request.

Each simplex method was evaluated by using a method similar to that described by Ryan et al. [10] and Parker et al. [13]. For each function and set of boundary conditions, six initial starting sizes for the simplex were chosen (2, 10, 20, 40, 60, and 80% of the factor space). For each starting size, 100 randomly-generated coordinates were produced within the particular boundary condition being used. These coordinates and the procedure described by Yarbro and Deming [14] were used to construct the initial simplexes for each function, step size and boundary condition. The same set of initial simplexes for each function was used with each simplex method (MSM, MSM1 and MSM2).

The simplex optimizations for all functions were terminated when the standard deviation on the responses for the current simplex fell below 0.001. An expansion factor of 2 and contraction factor of 0.5 were used for each simplex method.

RESULTS AND DISCUSSION

The results of each optimization are reported in Table 1 in the manner of Ryan et al. [10], giving the average number of evaluations for each initial starting simplex, the relative standard deviation on the average number of evaluations for each initial starting simplex and the non-critical to critical non-convergence ratio. (A non-critical non-convergence is defined as one for which the simplex converges to a false optimum 10 times the termination criterion distant from the true optimum; a critical non-convergence is defined as one for which the simplex converges to a false optimum more than 1000 times distant.)

From these data, a performance value, similar to that used by Parker et al. [13], was calculated for each simplex and step size, which combined both speed and accuracy in one function. The performance function (P) is defined by $P = -\log(A)$, where A is the average number of evaluations. If critical or non-critical non-convergences occur, then P is defined as $P = -\log(A\ (10N)\ (100C))$, where N is the number of non-critical non-convergences and C is the number of critical non-convergences. This is a slightly modified version of the performance function used by Parker et al. [13], in that a negative rather than a positive logarithmic function is used. This then defines, more logically, the simplex method with the highest P value to be the best as opposed to the method with the lowest P value as suggested by Parker et al. By plotting the calculated P values against initial starting

---

Fig. 3. Comparison of the performance of MSM (○) and MSM1 (+) on the different functions for different boundary conditions. Functions: (A) 2-parameter; (B) 3-parameter; (C) 5-parameter. Boundary conditions: (a) −180° to 180°; (B) −60° to 180°; (C) −10° to 180°; (d) 0° to 180°; (e) 20° to 180°.

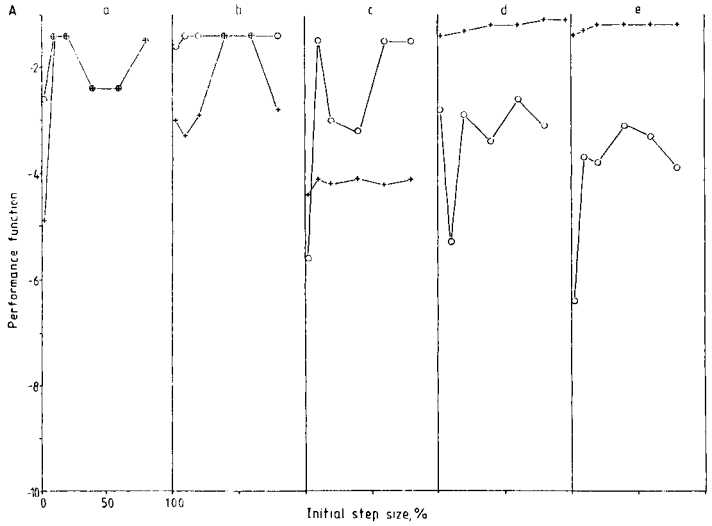
A
a
b
c
d
e
Performance function
-2
-4
-6
-8
-10
0
50
100
Initial step size, %

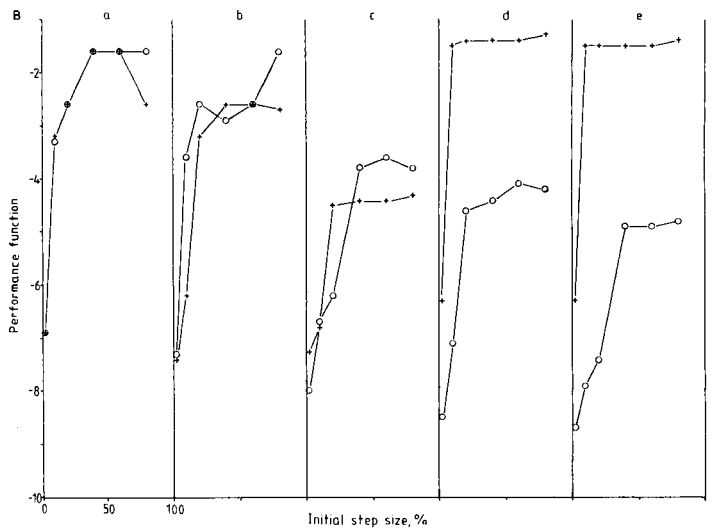
B
a
b
c
d
e
Performance function
-2
-4
-6
-8
-10
0
50
100
Initial step size, %

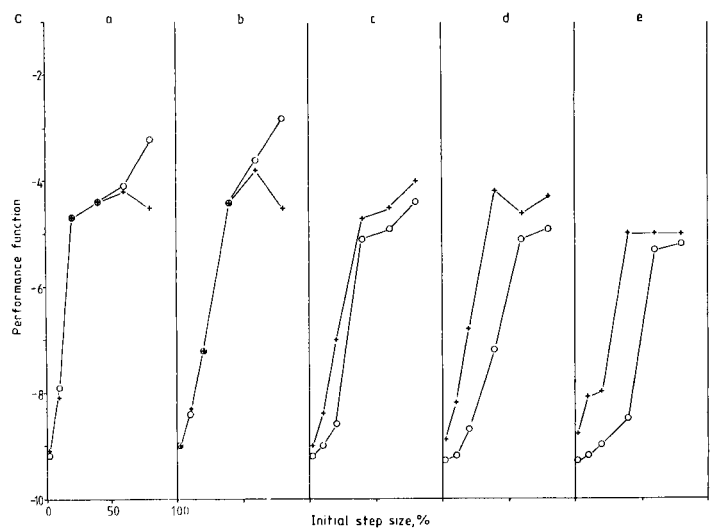
C
a
b
c
d
e
Performance function
-2
-4
-6
-8
-10
0
50
100
Initial step size, %

simplex size, graphical representations of the performance trends for each simplex method on each function and boundary condition can be obtained, as shown in Figs. 3 and 4. The results for methods MSM1 and MSM2 are plotted separately along with the corresponding data for MSM, the MSM data providing a reference point for comparison of methods.

Initial comparison of methods MSM and MSM1 (Table 1 and Fig. 3) confirmed that both speed and accuracy of determining the optimum were lost when MSM was used if the optimum condition lay close to or on the boundary conditions, and that MSM1 gave very good performance when the boundary conditions coincided with a local or global optimum. There were some reservations, however, as to the overall performance of MSM1 in that it tended to produce reduced performance compared to MSM (mainly because of increased inaccuracy in defining the optimum) at large initial sizes (60 and 80%) for all functions where the optimum was symmetrically placed and slightly displaced towards the boundaries, and for the 2- and 3-parameter functions when the optimum was close to but not on the boundary. The reason for this can perhaps be explained by referring to Fig. 1. The operation of the boundary condition rule in MSM1 when R′ is formed is, in effect, a positive contraction. If the initial starting simplex is large, covering most of the factor space, then the formation of R′ could well be a massive contraction which would lead to a premature collapse of the simplex procedure before it had arrived at the optimum, leading to a reduced performance. Similarly, if the optimum is close to a boundary, the simplex procedure would be continually "bumping" against the boundary contracting each time and again collapsing prematurely.

The results of the combined method MSM2 compared with MSM are summarized in Fig. 4. The success of this method is shown by the fact that for all bar one case at initial starting step sizes greater than 40%, MSM2 is as good as or outperforms MSM. In the one case where this is not so (Fig. 4A, c), an examination of the relevant data in Table 1 shows the difference to be due to an increased number of non-critical non-convergences at initial step sizes of 60 and 80% (8 and 10, respectively, compared with 0 and 0) which is only marginally less accurate.

For the 2- and 3-parameter functions, MSM2 behaves as a compromise method, producing marginally reduced performance over MSM1 at boundary conditions coinciding with the optimum, and improved performance over MSM1 at boundary conditions close to the optimum. For the 5-parameter function, less predictably, MSM2 produces the best performance of the three methods over all boundary conditions, even at boundary conditions where the optimum is not close to or on the boundary. The multidimensional geometry involved in this case minimizes the validity of interpretations of the relative merits of each method using 2-dimensional models.

Fig. 4. Comparison of the performance of MSM (○) and MSM2 (×) on the different functions for different boundary conditions. (A—C) and (a—e) as in Fig. 3.

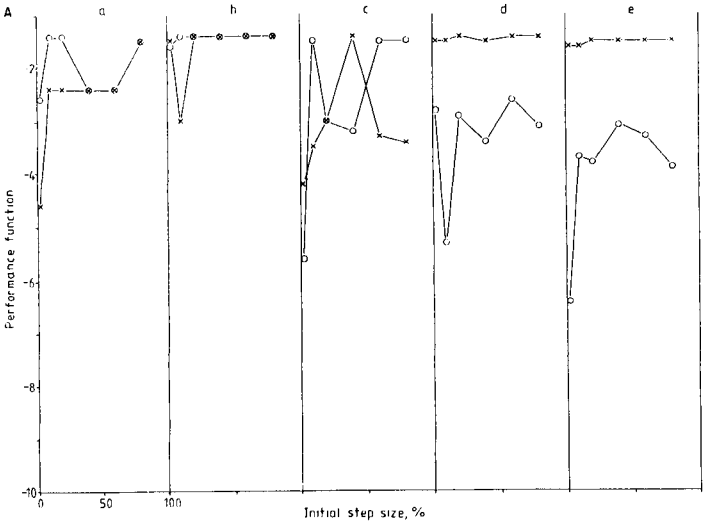
A
a
b
c
d
e
Performance function
-2
-4
-6
-8
-10
0
50
100
Initial step size, %

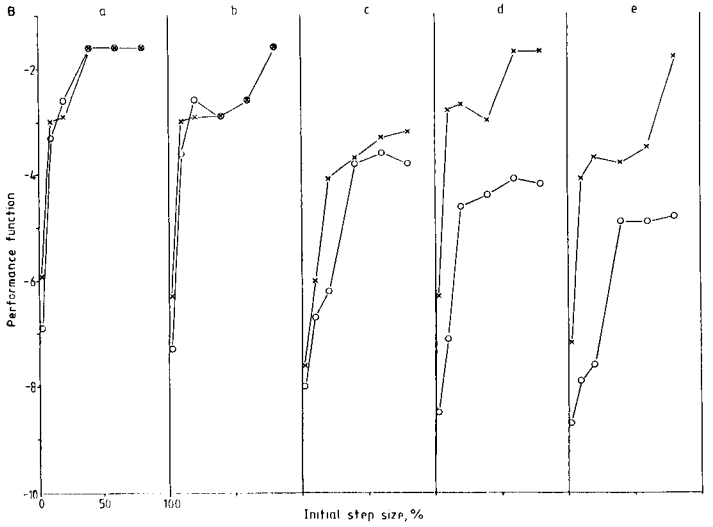
B
a
b
c
d
e
Performance function
-2
-4
-6
-8
-10
0
50
100
Initial step size, %

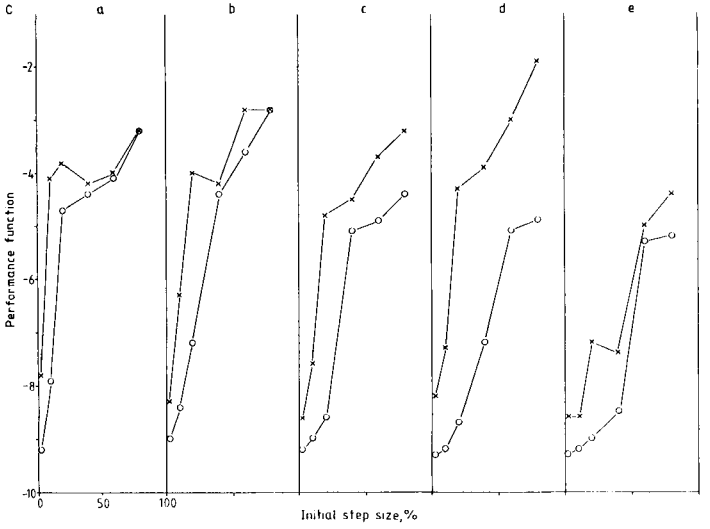
C
a
b
c
d
e
Performance function
-2
-4
-6
-8
-10
0
50
100
Initial step size, %

TABLE 1

Comparison of simplex methods for the 2-, 3- and 5-parameter functions

Boundary condns.	ISS[a] (%)	2-Parameters									3-Parameters		
		MSM			MSM1			MSM2			MSM		
		Av. no.[b]	RSD (%)	NC/C[c]	Av. no.[b]	RSD (%)	NC/C[c]	Av. no.[b]	RSD (%)	NC/C[c]	Av. no.[b]	RSD (%)	NC/C
I	2	36	29	1/0	36	30	2/1	35	31	1/1	81	44	15/6
	10	25	22	0/0	25	22	0/0	24	21	1/0	48	30	4/0
	20	24	16	0/0	24	16	0/0	24	16	1/0	42	27	1/0
	40	24	14	1/0	24	14	1/0	24	14	1/0	39	15	0/0
	60	26	13	1/0	26	13	1/0	26	13	1/0	41	14	0/0
	80	28	12	0/0	28	12	0/0	28	12	0/0	41	12	0/0
II	2	36	35	0/0	36	34	3/0	35	36	0/0	74	48	33/8
	10	27	32	0/0	27	37	7/0	25	29	4/0	51	41	8/0
	20	23	21	0/0	24	36	3/0	23	21	0/0	42	30	1/0
	40	24	15	0/0	24	15	0/0	24	15	0/0	39	22	2/0
	60	25	13	0/0	25	16	0/0	25	13	0/0	38	14	1/0
	80	27	16	0/0	33	29	2/0	28	16	0/0	42	15	0/0
III	2	46	33	4/2	29	21	81/0	36	24	41/0	95	35	70/15
	10	30	31	0/0	22	19	56/0	28	26	11/0	74	44	32/2
	20	30	24	3/0	20	21	80/0	27	21	4/0	64	39	24/1
	40	28	17	5/0	19	25	71/0	27	16	0/0	55	31	11/0
	60	29	17	0/0	19	25	81/0	27	16	8/0	50	26	8/0
	80	29	14	0/0	17	22	69/0	28	16	10/0	45	14	14/0
IV	2	58	34	1/0	25	19	0/0	34	25	0/0	114	32	82/35
	10	45	25	4/1	18	15	0/0	30	26	0/0	85	31	52/3
	20	41	23	2/0	16	17	0/0	26	22	0/0	77	24	52/0
	40	39	17	7/0	14	17	0/0	28	18	0/0	78	27	34/0
	60	40	17	1/0	13	11	0/0	25	23	0/0	71	2	19/0
	80	42	17	3/0	12	13	0/0	28	16	0/0	64	15	22/0
V	2	83	26	16/2	26	16	0/0	43	30	0/0	119	29	95/43
	10	68	23	8/0	20	16	0/0	36	35	0/0	110	27	88/8
	20	64	19	9/0	17	18	0/0	32	28	0/0	109	26	79/3
	40	62	16	2/0	15	17	0/0	33	23	0/0	102	25	70/0
	60	63	16	3/0	14	13	0/0	29	28	0/0	100	22	74/0
	80	63	18	13/0	14	14	0/0	30	16	0/0	91	15	71/0

[a]Initial simplex size. [b]Average number of evaluations. [c]Non-critical to critical non-

CONCLUSIONS

For the five different boundary conditions used it has been shown that major differences between the performance of the three simplex methods occur mainly when the optimum is close to or actually on the boundary. In practical situations it is unlikely that the true global optimum will be situated exactly on a boundary, although it may well be the case that it will be close to a boundary or that the boundary marks a local optimum. A case in which the physical restraints of instrumentation forced a local optimum at the boundary has been reported [15]; in a simplex optimization of an inductively-coupled plasma spectrometric system the maximum gas flow rate through the nebulizer tube was proving optimal until a tube with higher flow capacity was used, thus allowing a true global optimum to be found.

					5-Parameters								
M1		MSM2			MSM			MSM1			MSM2		
RSD (%)	NC/C^c	Av. no.[b]	RSD (%)	NC/C^c	Av. no.[b]	RSD (%)	NC/C^c	Av. no.[b]	RSD (%)	NC/C^c	Av. no.[b]	RSD (%)	NC/C^c
47	15/7	66	33	4/3	203	34	100/70	194	36	100/70	193	33	38/9
30	3/0	44	27	2/0	163	42	82/6	153	36	82/11	105	32	11/0
27	1/0	40	18	2/0	116	40	45/0	116	40	46/0	84	28	8/0
15	0/0	39	15	0/0	96	34	29/0	96	34	29/0	94	35	18/0
14	0/0	41	14	0/0	80	24	17/0	80	24	18/0	81	25	13/0
17	1/0	41	12	0/0	76	12	2/0	105	32	29/0	76	12	2/0
45	37/9	66	45	11/3	184	44	100/59	179	42	100/58	187	42	60/18
40	16/2	45	36	2/0	155	39	87/19	148	40	86/16	114	47	16/1
29	4/0	41	26	2/0	129	43	64/2	124	40	62/2	90	36	10/0
19	1/0	40	23	2/0	89	32	26/0	86	27	32/0	83	31	18/0
17	1/0	38	13	1/0	66	16	6/0	68	18	9/0	65	14	1/0
37	1/0	42	15	0/0	67	12	1/0	85	23	33/0	67	12	1/0
34	97/6	59	28	70/9	204	38	100/85	170	43	100/63	159	32	91/30
30	85/2	52	29	20/1	192	33	99/54	134	38	97/21	137	43	67/4
21	81/0	48	21	26/0	178	31	98/23	122	49	86/1	113	32	57/0
17	77/0	44	17	12/0	144	36	86/0	79	23	60/0	89	22	36/0
17	75/0	42	15	5/0	121	28	64/0	78	26	40/0	78	14	6/0
17	78/0	44	13	4/0	83	18	27/0	66	17	15/0	78	13	2/0
37	7/6	70	36	9/3	215	32	100/90	180	48	73/60	201	35	41/17
26	0/0	60	33	1/0	216	33	100/66	148	40	49/20	182	39	25/4
17	0/0	51	22	1/0	189	32	100/29	118	48	27/2	148	35	12/0
14	0/0	52	24	2/0	174	31	97/1	83	38	20/0	119	39	6/0
17	0/0	48	21	0/0	148	18	93/0	87	25	41/0	97	19	1/0
15	0/0	52	22	0/0	121	16	66/0	76	22	27/0	87	18	0/0
27	7/7	87	48	19/9	216	29	100/93	204	45	65/43	250	38	67/23
23	0/0	85	39	14/0	211	29	100/79	171	46	51/15	228	34	74/21
22	0/0	79	33	7/0	209	29	100/52	146	39	52/12	232	33	70/1
18	0/0	82	28	8/0	199	25	100/16	140	36	65/0	205	29	64/7
14	0/0	66	33	5/0	183	20	100/0	127	29	72/0	182	22	52/0
14	0/0	63	24	0/0	168	18	100/0	100	30	92/0	157	17	17/0

nvergence ratio.

The absolute data as reported in Table 1 are relevant only to the particular test functions used; the trends in performance, however, (Figs. 3 and 4) should provide a degree of guidance for practical situations. The MSM boundary method has been shown to work well as long as the optimum is placed away from boundary conditions. The very nature of an optimization experiment, however, lies in not knowing where the optimum is at the outset and, as already mentioned, physical restraints on instrumentation do not allow optimal settings and boundaries to be set at will. The combination of the two methods MSM and MSM1 produces an algorithm which is far less sensitive to the positioning of boundaries and perhaps should be universally adopted as the method of choice in simplex optimization work.

This paper is published with the approval of the Director, British Geological Survey (N.E.R.C.).

REFERENCES

1 S. N. Deming and L. R. Parker, Jr., CRC Crit. Rev. Anal. Chem., 7 (1978) 187.
2 C. F. Lam, A. Forst and H. Bank, Appl. Spectrosc., 33 (1979) 273.
3 L. Ebdon, M. R. Cave and D. J. Mowthorpe, Anal. Chim. Acta, 115 (1980) 179.
4 J. C. Berridge, Analyst (London), 109 (1984) 291.
5 D. D. Burgess and P. Hayumbu, Anal. Chem., 56 (1984) 1440.
6 S. C. Rutan and S. D. Brown, Anal. Chim. Acta, 167 (1985) 39.
7 W. Spendley, G. B. Hext and F. R. Himsworth, Technometrics, 4 (1962) 441.
8 J. A. Nelder and R. Mead, Comput. J., 7 (1964) 308.
9 M. W. Routh, P.-A. Swartz and M. B. Denton, Anal. Chem., 49 (1977) 1422.
10 P. B. Ryan, R. L. Barr and H. D. Todd, Anal. Chem., 52 (1980) 1460.
11 E. R. Aberg and A. G. T. Gustavsson, Anal. Chim. Acta, 144 (1982) 39.
12 A. Gustavsson and J.-E. Sundkvist, Anal. Chim. Acta, 167 (1985) 1.
13 L. R. Parker, Jr., M. R. Cave and R. M. Barnes, Anal. Chim. Acta, 175 (1985) 231.
14 L. A. Yarbro and S. N. Deming, Anal. Chim. Acta, 73 (1974) 391.
15 G. L. Moore, P. J. Humphries-Cuff and A. E. Watson, Spectrochim. Acta, Part B: 39 (1984) 915.

Analytica Chimica Acta, 181 (1986) 117—123
Elsevier Science Publishers B.V., Amsterdam — Printed in The Netherlands

THE DETERMINATION OF THALLIUM IN SEDIMENTS AND NATURAL WATERS

J. P. RILEY* and S. A. SIDDIQUI[a]

Department of Oceanography, University of Liverpool, P.O. Box 147, Liverpool L69 3BX (Great Britain)

(Received 18th October 1985)

SUMMARY

Thallium is determined in natural waters (including sea water) by first preconcentrating it by adsorption from oxidizing medium onto a strongly basic anion exchanger as the tetrachlorothallate(III) ion. After elution with sulphur dioxide and evaporation, thallium is estimated either by graphite-furnace atomic absorption spectrometry or by differential-pulse anodic stripping voltammetry. Relative standard deviations of 4% were found for both endpoints at thallium concentrations of 15 ng l^{-1}. There was good agreement between the results obtained by the two techniques. The technique is also applied to digests from deep-sea sediments.

Although attempts to detect thallium in sea water had been made by both Shaw [1] and Brooks [2], it was not until 1969 that its concentration was shown by neutron activation analysis to be about 9—16 ng kg^{-1} [3]. Values in this range have also been found by anodic stripping voltammetry (a.s.v.) by Batley and Florence [4]. Very recently, Flegal and Patterson [5] have re-investigated the problem by a stable isotope dilution procedure, taking care to minimize contamination in both sampling and the further analysis by the use of ultra-clean methods. They concluded that the oceanic concentrations of the element lay in the range 12—16 ng kg^{-1} and that its geochemical behaviour is similar to that of the alkali metals. As part of a programme of work here on the marine geochemistry of thallium, a method suitable for routine use has been developed for the analysis of sea water and sediment. The method depends on preconcentration of the element on an anion-exchange resin followed by specific elution and determination by electrothermal atomic absorption spectrometry or differential-pulse anodic stripping voltammetry.

Preconcentration of thallium

Because the concentrations of thallium in most natural waters are too low to be determined directly (<0.1 nM) it is necessary to preconcentrate the

[a]Present address: Centre of Excellence for Marine Biology, University of Karachi, Karachi-32, Pakistan.

0003-2670/86/$03.50

element before it can be quantified. For this purpose, some workers [6, 7] have used a dithizone/chloroform extraction procedure as a preliminary to determination by isotope dilution mass spectrometry. Thallium(III) is strongly adsorbed from chloride medium by strongly basic anion exchangers and this has been used as the basis for the preconcentration and specific separation of the element in the analysis of sea [3] and other natural waters [8]. Because of the simplicity of this technique and the fact that it can readily be used with large sample volumes it was adopted for the present work. Because the Deacidite FF resin used in previous work [3] was no longer available, radiochemical tests with ^{204}Tl were made with a 5 × 1-cm bed of an analogous resin, Duolite A-101D. These showed that the element was quantitatively (>99.3%) retained from sea water, which had been rendered 0.1 M with respect to hydrochloric acid and to which bromine water had been added to ensure that thallium(III) was present. Tests also confirmed that no thallium was eluted if the column was washed with 20 ml of water containing 1 ml of bromine water followed by 90 ml of 4 M nitric acid containing 2 ml of bromine water and a further 20 ml of water. Thallium was quantitatively eluted by 35 ml of saturated sulphur dioxide solution. The anion-exchange behaviour of several other elements under the same conditions was also examined. These showed (Table 1) that, although a number of other elements existing as oxy-anions or strongly bound chloro-anions were retained by the exchanger, these were mainly removed by the preliminary elution with water and 4 M nitric acid and were absent from the sulphur dioxide eluate.

TABLE 1

Ion-exchange behaviour of elements from sea water medium (0.1 M with respect to hydrochloric acid)

Element	Cd(II)	Co(II)	Cr(III)	Cu(II)	Fe(III)	Mn(II)
Weight (mg)	0.1	0.6	0.4	0.4	0.4	0.3
Retention (%)	97.7	1.3	0.2	8.0	3.1	1.0
Recovery (%) in 20 ml water	91.2	1.3	0.0	8.0	3.1	1.0
Recovery (%) in 90 ml 4 M HNO_3	3.5	0.0	0.0	0.0	0.0	0.0
Recovery (%) in 20 ml water	3.0	0.0	0.0	0.0	0.0	0.0
Recovery (%) in SO_2/water	0.0	0.0	0.0	0.0	0.0	0.0
Element	**Mo(VI)**	**Ni(II)**	**Pb(II)**	**Sn(II)**	**Zn(II)**	**Tl(III)**
Weight (mg)	0.3	0.4	0.8	1.0	0.2	0.001
Retention (%)	98.0	8.7	17.5	0.5	4.9	>99.5
Recovery (%) in 20 ml water	1.5	8.7	16.7	0.5	4.7	0.0
Recovery (%) in 90 ml 4 M HNO_3	0.0	0.0	0.8	0.0	0.0	0.0
Recovery (%) in 20 ml water	0.0	0.0	0.0	0.0	0.0	0.0
Recovery (%) in SO_2/water	0.0	0.0	0.0	0.0	0.0	>99.3

Determination of thallium by flameless atomic absorption spectrometry

Atomic absorption spectrometry (a.a.s.) was chosen for the determination of thallium in the concentrate because of its inherently high sensitivity. The flame version of this technique was used for this analysis of concentrates from natural waters by Korkisch and Steffan [8], but even with concentrates from 10-l samples they were unable to achieve a detection limit of better than 1 $\mu g\ l^{-1}$. Electrothermal a.a.s. has been used for the determination of thallium in a variety of materials, but has been shown to be subject to many interferences [9]; furthermore, it is insufficiently sensitive for the direct determination of the element in natural waters. It was, therefore, thought worthwhile to combine this technique with the preliminary specific anion-exchange preconcentration. Accordingly, the optimum furnace operating conditions for the determination of thallium were investigated. With the Instrumentation Laboratories instrument, these were found to be a pyrolysis temperature of 400°C and an atomization temperature of 2000°C. Under these conditions, a sensitivity of 0.02 ng ml^{-1} thallium was achieved for 1% absorbance.

Determination of thallium by anodic stripping voltammetry

Anodic stripping voltammetry provides a highly sensitive means of determining thallium and this has been used in its differential pulse mode, following pre-concentration, for the analysis of sea water [4]. The use of this technique was therefore investigated to provide a comparison with the atomic absorption procedure.

In preliminary experiments, differential-pulse a.s.v. was used to establish the optimum electrode system for the determination of 1 $\mu g\ ml^{-1}$ thallium at pH 8.2 (using the instrumental settings set out in the Experimental section). It was found that, although a mercury-coated rotating glassy carbon disc electrode gave a lower detection limit than either a hanging mercury drop electrode or a wax-impregnated electrode, the results obtained with it were very erratic. Because of its stability and reproducibility, the hanging drop electrode was selected. When the technique was applied to ion-exchange concentrates from 10-l samples of sea water and redistilled water, the a.s.v. recordings showed the presence of $\mu g\ l^{-1}$ levels of cadmium, copper and lead. The source of these metals was found to be the sulphur dioxide solution used to elute the thallium and probably originated from the sulphur dioxide canister or its needle valve. This difficulty was overcome, without loss of sensitivity for thallium, by masking by addition of ethylenediaminetetraacetic acid before the a.s.v. measurements. The contamination with these elements caused no interference in the atomic absorption spectrometric measurement.

EXPERIMENTAL

Reagents and solutions

Ion exchange column. Backwash Duolite A-101D (52-100 mesh) with water to remove fines and then digest it on a water bath twice with ten

times its volume of 2 M nitric acid. After washing several times by decantation with water, pour sufficient slurry of the resin into a 1-cm bore ion-exchange column to give a packed length of 5 cm.

Reagents. Water doubly distilled from a silica still is used for preparation of reagents, blanks and standards.

Hydrochloric acid (6.5 M) is distilled from a silica still. Hydrochloric acid (2 M) is prepared by dilution of the 6.5 M hydrochloric acid with water. Nitric acid (4 M) is prepared by dilution of concentrated nitric acid distilled in a silica still. Hydrofluoric acid is 40% (w/w).

Bromine water is prepared by saturating water with excess of bromine. Sulphur dioxide solution is prepared as required by saturation of water with sulphur dioxide. Sodium hydroxide solution (1 M) is prepared by dissolving 9.0 g of sodium hydroxide in water and diluting to 200 ml with water. For the ethylenediaminetetraacetic acid (EDTA) solution (0.1 M), 4.53 g of the tetrasodium salt is dissolved in 50 ml of water and the solution is diluted to 100 ml with water.

Standard thallium solution. A 100 μg ml^{-1} thallium solution is prepared by dissolving 0.0652 g of thallium(I) nitrate in water and diluting to 500 ml with water. This solution is used to prepare, as required, working standards containing 1 μg ml^{-1} Tl and 100 ng ml^{-1} Tl.

Instruments

An Instrumentation Laboratories Model IL 351AA/AE atomic absorption spectrometer fitted with a flameless atomizer (ILFA 455) and a hollow-cathode lamp was used for a.a.s. measurements. The absorbance was measured at 276.9 nm with a 0.5-nm bandpass and an atomization temperature of 2000°C.

For anodic stripping voltammetry, a Princeton Applied Research polarograph (model 174A) was fitted with a hanging mercury drop electrode, a platinum counter electrode and a silver/silver chloride reference electrode. The instrument was operated in the differential-pulse mode with a potential scan rate of 5 mV s^{-1}, a pulse modulation amplitude of 25 mV and a full scale response of 0.5 μA.

Analysis of natural waters

Preconcentration. Filter 10 l of the water sample through a 4-cm membrane filter having a pore diameter of 0.45 μm. To the filtrate, add 65 ml of 6.5 M hydrochloric acid and 20 ml of bromine water. Pass the resultant solution through the anion-exchange column at a flow rate not exceeding 5 ml min^{-1}. Wash the column with 25 ml of water containing 1 ml of bromine water, then with 90 ml of 4 M nitric acid containing 2 ml of bromine water, and finally with 25 ml of water containing 1 ml of bromine water. Discard the washings. Elute thallium with 35 ml of saturated sulphur dioxide solution and wash the column with 10 ml of distilled water. Combine the eluate and washings and evaporate to dryness in a silica beaker on a water bath.

Dissolve the residue in 0.1 ml of 4 M nitric acid, transfer the solution quantitatively to a 10 ml calibrated flask and dilute to volume with water. Carry a distilled water blank through the whole process.

Determination of thallium by atomic absorption spectrometry. Inject aliquots (20 μl) of the concentrate and blanks into the graphite tube of the electrothermal atomizer, programmed according to the manufacturer's instructions. Determine the absorbance at 276.8 nm, using an atomization temperature of 2000° C. Calibrate the technique by the method of standard additions using a sample which has been spiked with 2 ng ml^{-1} thallium.

Determination of thallium by anodic stripping voltammetry. Transfer 9 ml of the concentrate to a 10-ml volumetric flask. Carefully adjust its pH to 8.2 ± 0.3 by cautious addition of 1 M sodium hydroxide, add 100 μl of EDTA solution and dilute to volume with water. Transfer the solution to the polarographic cell and bubble with nitrogen for 5 min. Generate a mercury drop on the end of the capillary and adjust the speed of the stirrer so as to avoid formation of air bubbles. Plate thallium for 15 min at a potential of −750 mV. Switch off the stirrer and allow the solution to stand for 30 s. Strip the thallium, using the conditions outlined above. Calibrate by the standard addition procedure, making two successive additions of 10 μl of standard thallium solution containing 10 μg ml^{-1} thallium. Measure the resultant peak heights on the chart records. Obtain the corresponding blanks similarly.

Analysis of sediments

Accurately weigh about 0.5 g of the washed and dried (105°C) sediment into a 50-ml teflon beaker. Add to it 10 ml of 40% (w/w) hydrofluoric acid and 5 ml of concentrated nitric acid. Cover the beaker with a teflon lid and heat overnight on a boiling water bath. On the following day, remove the lid and allow the liquid to evaporate to dryness. Add 10 ml of 4 M nitric acid and then warm. If the residue does not dissolve completely, add a further 10 ml of hydrofluoric acid, cover and repeat the digestion. Evaporate the solution to dryness on the water bath and repeat the evaporation, first with two 10-ml aliquots of 4 M nitric acid, and finally with 10 ml of 6.5 M hydrochloric acid. Dissolve the residue in 4 ml of 6.5 M hydrochloric acid and dilute to 250 ml with water. Add 2 ml of bromine water and then proceed with the anion-exchange preconcentration process and determination as described for water samples.

RESULTS AND DISCUSSION

The recoveries of thallium by the a.a.s. and d.p.a.s.v. procedures were tested by analysing three 10-l aliquots of a sample of ocean water, after spiking two of them with 100 ng and 200 ng of thallium. The results of these experiments (Table 2) showed that excellent recoveries of spiked thallium were achieved by both techniques.

As a further check on the precision and comparability of the two methods,

TABLE 2

Recovery of thallium from 10-l aliquots of sea water after spiking with thallium

Thallium added (ng)	Thallium found (ng l^{-1})		Recovery (%)	
	D.p.a.s.v.	A.a.s.	D.p.a.s.v.	A.a.s.
0	9.5	9.3	—	—
100	19.2	18.9	97	96
200	29.4	30.2	99	104

TABLE 3

Replicate analysis of coastal sea and estuarine water samples for thallium

Location	Date	Thallium found (ng ml^{-1})		Mean (ng ml^{-1})	
		D.p.a.s.v.	A.a.s.	D.p.a.s.v.	A.a.s.
Meols	12/12/80	16.9	16.5	16.9	16.5
	9/1/81	17.8, 16.2, 17.0	17.6, 17.0, 17.9	17.0 ± 0.8	17.5 ± 0.5
	3/4/81	16.2, 17.3, 16.2, 16.8	17.5	16.6 ± 0.5	17.5
New Brighton	12/12/80	15.3, 15.4, 15.0	14.7, 15.5, 15.9	15.2 ± 0.2	15.4 ± 0.6
	9/1/81	15.5	14.8	15.5	14.8
	3/4/81	14.9, 15.9, 15.6, 17.1	17.7, 15.3, 15.2, 15.2	15.9 ± 0.9	15.8 ± 1.2

samples of inshore waters from the Irish Sea and Mersey Estuary were analysed. These showed a satisfactory correspondence between the results obtained by the two techniques (Table 3). The concentrations of thallium found lie close to the value of 18.7 ± 0.9 ng l^{-1} recorded for the Irish Sea by Matthews and Riley [3]. They are somewhat greater than those found for Australian inshore waters by Batley and Florence [4] (mean 13.1 ng l^{-1}), and more recently for open ocean surface waters by Flegal and Patterson [5] (mean 12.4 ng l^{-1}, range 11.3—15.3 ng l^{-1}).

The recovery of thallium from sediments was checked by analysing in replicate 0.5-g portions of a North Pacific manganese-rich sediment both alone and after spiking with 0.5 μg of thallium. This showed a thallium content of 1.67 ± 0.10 μg g^{-1} and, after spiking, of 2.62 ± 0.13 μg g^{-1}, corresponding to a recovery of 95% on the spike. The observed concentration of thallium is in excellent agreement with the value of 1.75 μg g^{-1} found in the same sample by neutron activation analysis [10]. As a further test of the method, thallium was determined in a series of sediments from the East Pacific. Satisfactory agreement was found between results obtained by the d.p.a.s.v. and a.a.s. techniques (Table 4).

TABLE 4

Analyses of deep sea sediments for thallium using d.p.a.s.v. and a.a.s. techniques

Station no.	Lat.	Long.	Depth (m)	$CaCO_3$ (%)	Thallium ($\mu g\ g^{-1}$)	
					D.p.a.s.v.	A.a.s.
East Pacific Rise						
SH1522	8°51'S	108°04'W	3147	80	0.08	0.05
SH1554	8°52'S	108°06'W	3022	68	0.07	0.05
Bauer Deep						
SH1576	10°09'S	101°04'W	4265	67	0.33	0.33
SH1583	8°22'S	101°27'W	4015	67	n.d.[a]	0.01
Galapagos Rise						
SH1561	11°09'S	92°10'W	4133	50	0.20	0.18
SH1562	11°16'S	91°07'W	3817	84	0.03	0.02
SH1572	11°10'S	89°59'W	3947	80	0.13	0.13
Peru Basin						
SH1566	11°42'S	85°32'W	4401	0	0.32	0.29
SH1567	11°47'S	85°05'W	4340	0	0.02	0.02
North Pacific						
Cusp 15p	37°15'N	143°07'W	5220	0	1.65	1.70

[a]n.d. = not determined.

The authors thank Dr. Helen Rowson for the gift of sediment samples and for providing data on their carbonate contents.

REFERENCES

1 D. M. Shaw, Geochim. Cosmochim. Acta, 2 (1952) 118.
2 R. R. Brooks, Analyst (London), 85 (1960) 745.
3 A. D. Matthews and J. P. Riley, Anal. Chim. Acta, 48 (1969) 25.
4 G. E. Batley and T. L. Florence, J. Electroanal. Chem., 61 (1975) 205.
5 A. R. Flegal and C. C. Patterson, Mar. Chem., 15 (1985) 327.
6 M. Murozumi and S. Nakamura, in Isotope Marine Chemistry, Uchida Rokakuho, Tokyo, 1980.
7 M. Murozumi, Jpn. Soc. Anal. Chem., 30 (1981) S19.
8 J. Korkisch and I. Steffan, Int. J. Environ. Anal. Chem., 6 (1979) 111.
9 W. Slavin, Graphite-furnace Atomic Absorption Spectrometry: A Source Book, Perkin-Elmer Corporation, Norwalk, Connecticut, 1984.
10 A. D. Matthews, Ph.D. Thesis, University of Liverpool, 1969.

Analytica Chimica Acta, 181 (1986) 125—137
Elsevier Science Publishers B.V., Amsterdam — Printed in The Netherlands

STUDIES WITH DITHIZONE
Part 26. The Interaction of Thallium(III) with Solutions of Dithizone in Organic Solvents

H. M. N. H. IRVING,*[a] A. H. NABILSI, A. MAWLEY and D. C. RUPAINWAR

Department of Inorganic and Structural Chemistry, University of Leeds, Leeds LS2 9JT (Great Britain)

CHERYL SACHT

Department of Analytical Science, University of Cape Town, Rondebosch 7700 (South Africa)

(Received 2nd July 1985)

SUMMARY

The strong oxidising capacity of thallium(III) dominates its reaction with solutions of dithizone (H_2Dz) in organic solvents. When carbon tetrachloride is used as solvent, the unstable thallium(III) complex $Tl(HDz)_3$ is found in the organic phase but it very quickly disproportionates to the thallium(I) complex [Tl(HDz)], and bis-1,5-diphenylformazan-3-yl-disulphide. This reaction is notably faster in chloroform, in which thallium(I) dithizonate is the first identifiable product. In contact with an acidic aqueous phase, thallium(I) dithizonate is reverted to regenerate dithizone in the organic phase and Tl^+ ions appear in the aqueous phase. Organic solutions of the disulphide disproportionate spontaneously by first-order kinetics to give an equimolar mixture of dithizone and the mesoionic compound, 2,3-diphenyl-2,3-dihydrotetrazolium-5-thiolate: this change is much slower in carbon tetrachloride than in the more polar chloroform and is catalysed by both Tl^+ and Tl^{3+}. If thallium(III) is present in excess, the mesoionic compound is the principal oxidation product of the dithizone although a dication may also be formed. The mesoionic compound does not react with thallium(I) but forms a water-soluble 2:1 complex with thallium(III); partition of this complex into the organic phase is uninfluenced by chloride ions. Because of the large number of competing reactions, the composition of the reaction mixture at any stage of the reaction between thallium(III) and dithizone depends on the relative concentrations of the components, the order in which they are brought together, the time elapsed after mixing, the pH of the aqueous phase, and the nature of the organic solvent.

The use of dithizone (1,5-diphenyl-3-mercaptoformazan; H_2Dz) to effect the extraction of thallium(I) into chloroform from aqueous solutions

$$Tl^+ + H_2Dz(org) \rightarrow H^+ + Tl(HDz)\ (org) \qquad (1)$$

in the pH range 10—12 is well documented and presents no difficulties [1—7]. The determination of thallium(I) as its dithizonate has recently been

[a]Present address: Department of Analytical Science, University of Cape Town, Rondebosch 7700, South Africa.

0003-2670/86/$03.50

improved [8] by applying the principle of reversion [1]. The liquid-liquid extraction of the organothallium(III) complexes, $(CH_3)_2Tl(HDz)$ and $(C_6H_5)_2Tl(HDz)$, into carbon tetrachloride is also possible at pH > 8.5 and 5—12, respectively [9]. These intensely coloured 1:1 complexes can be isolated as stable dark purple solids and the structure of the diphenylthallium-(III) complex which forms a 5-coordinate compound, $(C_6H_5)_2Tl(HDz) \cdot C_2H_5OH$, on recrystallization from ethanol has been established by single-crystal x-ray methods [27].

In complete contrast, the reactions between aqueous solutions of (hydrated) thallium(III) and solutions of dithizone in organic solvents are found to be extremely complicated and do not lend themselves to the determination of thallium in this oxidation state. It was stated early on that a yellowish-red primary thallium dithizonate could be extracted into carbon tetrachloride from solutions of thallium(III) at pH 3—4 [10]. Koroleff [11] concurred but implied that the reaction was incomplete because the cation had also oxidised the dithizone. The experiments described here have demonstrated that the course of the reaction is dominated by the powerfully oxidising capabilities of Tl^{3+} and complicated further by the fact that both Tl^{3+} and its reduction product Tl^{+} can react further with the resulting oxidation products of the dithizone.

When a solution of dithizone in chloroform (Fig. 1, spectrum 1) is added to an excess of Tl^{3+} ions in dilute perchloric acid at pH $\approx$ 1 in a separating funnel, there is an immediate change in colour from green to deep wine-red (spectrum 2). On shaking the two phases for 1 min, the organic phase changes colour to a pink-red (spectrum 3), and on standing in contact with the aqueous phase for 3—4 h further colour changes take place through orange to yellow (spectrum 4). Clearly, there is a whole series of consecutive and time-dependent reactions. Further experiments confirmed that they could be brought under observable control only by a careful choice of reagent concentrations.

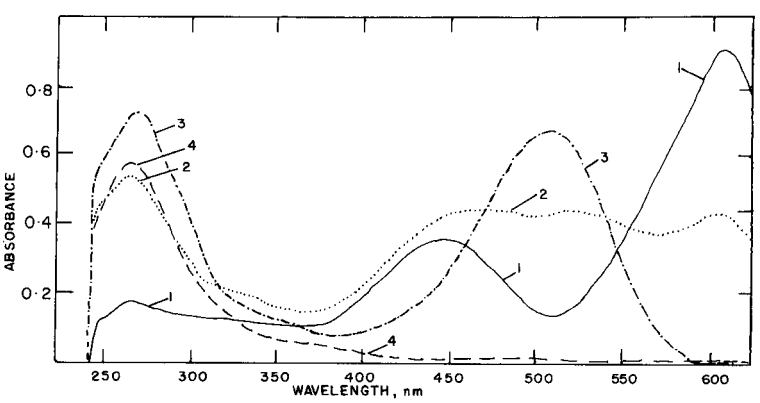

Fig. 1. The interaction of thallium(III) (4×10^{-4} M) and dithizone (2×10^{-2} M in chloroform). Absorption spectra: (1) the dithizone solution in chloroform; (2) the wine-red organic extract; (3) the pink-red organic extract; (4) the yellow organic extract.

The final yellow product has previously been identified spectrophotometrically (λ_{max} = 266 nm) [12] as the mesoionic compound (see below) and shown to be identical with the 'dehydrodithizone' prepared by oxidising dithizone with potassium hexacyanoferrate(III) [13] and other reagents. Clearly, thallium(III) (E = +1.33 V) is the effective oxidant in the reaction with dithizone and the Tl^+ formed could then itself participate in the overall reaction. Many experiments (not detailed here) showed that the oxidation of the dithizone (as evidenced by a decrease in the absorbance at its λ_{max} of 605 nm (cf. Fig. 1)) is associated with the growth of a new band (λ_{max} = 508 nm) related to a pink-red species. This is the wavelength maximum for thallium(I) dithizonate in chloroform [1—7]. This assignment to Tl(HDz) was confirmed by preparing a sample of the pink-red complex by shaking a solution of thallium(III) (2×10^{-5} M in ca. 0.1 M perchloric acid) with one of dithizone (1.7×10^{-5} M in chloroform) for 1 min and then rapidly separating the organic phase. Residual absorption at 605 nm established the presence of some unreacted dithizone and its small contribution to the total absorbance at 508 nm could be calculated from the spectrum of pure dithizone for which the molar absorptivity (ϵ) is 5900 l mol^{-1} cm^{-1} at 508 nm. If the (corrected) absorbance at 508 nm is due only to thallium(I) dithizonate (for which ϵ_{max} = 33 000 at 508 nm), the concentration of Tl(HDz) can be calculated to be 5.6×10^{-6} M. The organic phase was then reverted by equilibration with 1 M perchloric acid (reverse of Eqn. 1) and from the absorption spectrum of the resulting green dithizone solution (and allowing for the amount previously shown not to have reacted) the value $[H_2Dz] = 5.6 \times 10^{-6}$ was again found, confirming the combining of metal/dithizone ratio as 1:1. As a further check, the amount of dithizone in the aqueous phase after reversion was evaluated by raising the pH to 12 and determining the metal spectrophotometrically with dithizone [8].

Whilst the above experiments verified the formation of thallium(I) dithizonate as an intermediate product of the reaction between dithizone and an excess of thallium(III), it is noteworthy that in many experiments where the reactants were present in comparable amounts, only about a third of the dithizone appeared to be consumed in the reaction leading to the formation of Tl(HDz); the fate of the remainder was in doubt. It must also be emphasized that the presence of thallium(I) dithizonate in the organic phase cannot be ascribed to a reaction between thallium(I) in the aqueous phase and any residual dithizone in the organic phase (according to Eqn. 1) under the experimental conditions (acidic aqueous phase), for this reaction proceeds to the right only under strongly alkaline conditions [1—7]. It is thus tempting to speculate that the primary reaction between thallium(III) and dithizone leads to the formation of the thallium(III) complex, $Tl(HDz)_3$, which then disproportionates by an oxidation process in the organic phase:

$$Tl^{3+} + 3H_2Dz(org) \rightarrow Tl(HDz)_3(org) + 3H^+ \quad (2)$$

$$Tl(HDz)_3(org) \rightarrow Tl(HDz)(org) + (HDz)_2(org) \quad (3)$$

It is evident from Fig. 1 (spectrum 3) that the absorbance at about 450 nm is greater than could be expected if the mixture contained only unreacted dithizone (H_2Dz), (1), the mesoionic compound (3) and the 1:1 complex Tl(HDz). This is believed to be due to the presence of the disulphide [$(HDz)_2$, 2] which has previously been shown to be formed as the primary oxidation product of dithizone by mild oxidants such as iodine or *o*-iodosobenzoic acid [12]:

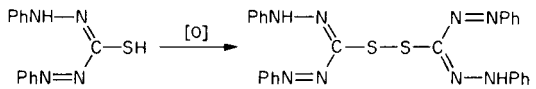

(1) (2)

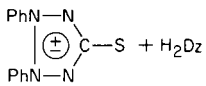

(3)

It has previously been established [12] that bis-1,5-diphenylformazan-3-yl-disulphide (2) disproportionates spontaneously to yield an equimolecular mixture of dithizone (1) and the mesoionic compound, 2,3-diphenyl-2,3-dihydrotetrazolium-5-thiolate (3). The thermal fission of the disulphide group is kinetically first-order and the rate increases with the polarity of the solvent [14]. Figure 2 shows the course of changes in the spectrum of a solution of the pure disulphide in chloroform with time. Dithizone regenerated by this reaction will, of course, react with any excess of thallium(III), according to Eqn. 2 so that the overall reaction in the presence of sufficient thallium(III) will be:

$$Tl^{3+} + H_2Dz\,(org) \rightarrow Tl^{+} + 2H^{+} + meso(\pm) \qquad (4)$$

This reaction proceeds completely to the right if the two phases are shaken together or left in contact for a sufficient length of time.

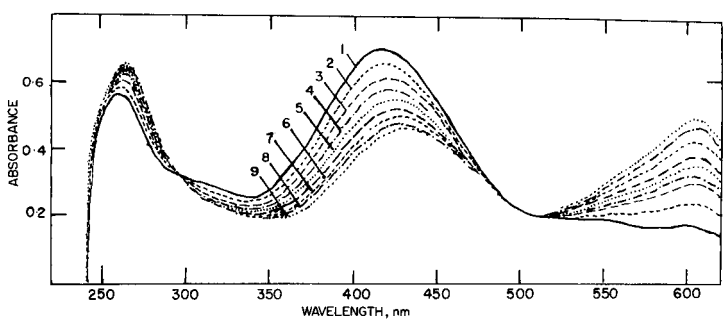

Fig. 2. The absorption spectrum of the disulphide (2) in chloroform recorded at 4-min intervals at ambient temperature.

The mesoionic compound 3 dissolves in water to give ca. 5×10^{-4} M solutions which absorb strongly in the ultraviolet region with ϵ = 2478 and 2721 l mol^{-1} cm^{-1} at 249 nm and 266 nm, respectively. However, the distribution coefficient between water and chloroform favours the organic solvent with values of 28.2 ± 0.5 at pH 6.3 and 29.7 ± 0.4 in dilute perchloric acid adjusted to ionic strength 0.1 M. As the acidity increases, compound 3 partitions increasingly into the aqueous phase as its conjugate acid but, because its acidity constant is low ($pK_a \approx -1.6$), the amount that is present in this form in an aqueous phase comprising ca. 0.1 M perchloric acid should be negligible [15, 16].

On standing, or more rapidly on shaking the organic and aqueous phases together, any thallium(I) dithizonate produced in the organic phase (e.g., by Eqns. 2 and 3) will be reverted by protons in the aqueous phase (reverse of Eqn. 1) as illustrated by the changes of spectrum shown in Fig. 3. During this process, thallium initially extracted into the organic phase returns more or less rapidly to the aqueous phase. As expected the process was shown experimentally to be accelerated by lowering the pH.

When the above reactions were examined for aqueous solutions of thallium(III) labelled with the radionuclide ^{204}Tl, equilibration with a deficiency of dithizone caused a rapid transfer of activity to the organic phase which reached a maximum as the initial red colour developed. This was followed by a slower decrease in activity as the solution in the organic phase gradually became colourless [17]. These initially puzzling phenomena are now explicable in terms of Eqns. 1–4.

The cleavage of the disulphide linkage in compound 2 has been shown to be catalyzed by cations such as Zn^{2+}, Cd^{2+}, Cu^{2+}, Pd^{2+} and phenylmercury(II) to give the corresponding primary metal dithizonate and an

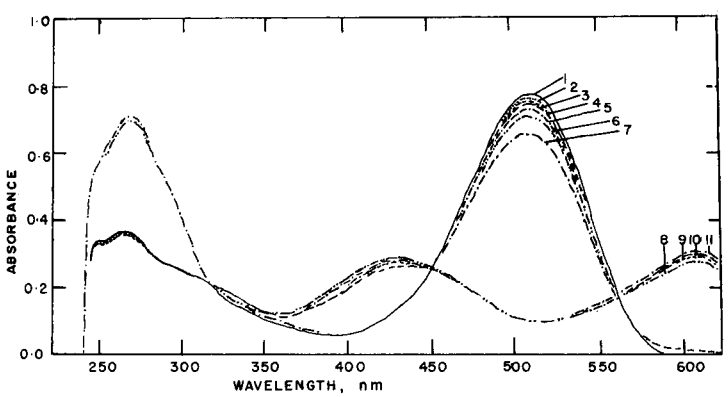

Fig. 3. Changes in time in the absorption spectrum of the organic phase produced by shaking 2×10^{-5} M dithizone in chloroform for 1 min with 4×10^{-4} M thallium(III) in 0.1 M perchloric acid. Spectra 1—7 recorded after 5, 10, 20, 30, 40, 50 and 80 min, respectively; spectra 8—11 recorded after 240, 245, 250 and 255 min, respectively.

equivalent amount of the mesoionic compound 3 [12]. In the case of mercury(II), this takes the course

$$2(HDz)_2\,(org) + Hg^{2+} \rightarrow 2H^+ + 2\ meso\ (\pm) + Hg(HDz)_2\,(org) \qquad (5)$$

By using solutions of the pure disulphide 2 in chloroform, it was shown spectrophotometrically that the spontaneous cleavage of the disulphide linkage was similarly accelerated by both Tl^+ and Tl^{3+} ions [14].

It has been known for a long time [18] that the mesoionic compound 3 forms a water-soluble complex with mercury(II) of the composition $Hg(meso)_2^{2+}$. This was later studied in detail [16] for a spectrophotometric determination of mercury(II) and ethylmercury(I): but interferences, especially by silver(I), were severe. It was clearly of importance to see whether the mesoionic compound also formed complexes with Tl^+ and Tl^{3+}, for this would produce an additional complicating feature in the reactions under discussion.

The absorption spectrum of an aqueous solution of the mesoionic compound 3 in 0.1 M perchloric acid remained unchanged on adding a solution of thallium(I) in perchloric acid, indicating the absence of complex formation under these conditions. When, however, a yellow aqueous solution of the mesoionic compound was equilibrated with increasing concentrations of thallium(III) in 0.1 M perchloric acid, and the total volume was kept constant at 20 cm^3 with the same acid solution, the colour was gradually bleached as the absorbance at 249 nm decreased to a minimum at a [mesoionic compound]/[Tl^{3+}] ratio of 2.0 and thereafter remained practically constant (Table 1). When the reverse process was examined, the absorbance at 249 nm of a mixture containing 1.453×10^{-5} M thallium(III) in 0.1 M perchloric acid to which increasing amounts of the mesoionic compound were added (Fig. 4) showed a small linear increase until the [mesoionic compound]/[Tl^{3+}] ratio was about 2:1, whereafter excess of mesoionic compound over that required for the formation of $Tl(meso)_2^{3+}$ caused a rapid linear increase in absorbance. This molar ratio was further confirmed (Fig. 5) by Job's method of continuous variations [1]. Substantially the same results were obtained when these photometric titrations were done in the presence of excess of chloride ions [16]. This would appear to rule out the participation of ion-pairs involving the complex anion $TlCl_4^-$ or the extraction of a species such as 4, which was postulated by Cox and Servant

TABLE 1

Reaction of mesoionic compound 3 (2.04×10^{-5} M) with increasing amounts of thallium(III), followed at 249 nm

Tl^{3+}	0.00	0.291	0.581	0.736	1.017	1.453	2.034	2.615
Absorbance	0.50	0.425	0.291	0.216	0.069	0.059	0.057	0.057

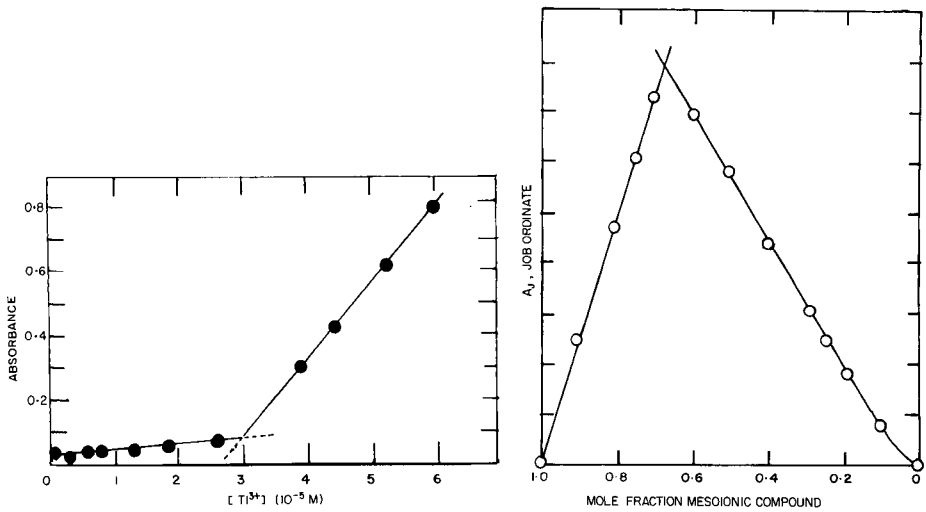

Fig. 4. Photometric titration. Absorbance at 249 nm of the mesoionic compound (2.040×10^{-5} M) measured after equilibration with various amounts of thallium(III) in a total volume of 20 ml.

Fig. 5. Job's method of continuous variations applied to mixtures of thallium(III) and the mesoionic compound 3 at a total concentration of 5.22×10^{-5} M.

[20] in the closely similar dithizone extraction of gold(III). Of course, unless added deliberately, chloride would only be produced by the photochemical oxidation of a chlorinated organic solvent.

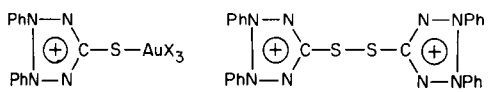

(4); X = Cl or Br **(5)**

When a solution of the mesoionic compound in chloroform was equilibrated for 25 min with an equal volume of increasingly concentrated solutions of thallium(III) in 0.1 M perchloric acid, the absorbance of the separated organic phase at 266 nm (λ_{max} for the mesoionic compound in this solvent) showed a steady decrease until the mole ratio $[Tl^{3+}]/[$mesoionic compound reacted$]$ was about 1:1.7. Thereafter there was no further decrease (Fig. 6). The residual absorbance could be explained if the bulky complex cation $Tl(meso)_2^{3+}$ previously indicated from experiments in the aqueous phase partitioned to some extent in the organic phase as the ion-pair $[Tl(meso)_2][(ClO_4)_3]$; it is noteworthy that there are progressive changes in the absorption spectra and a general shift of the (broad) maximum to 268 nm and the appearance of weaker bands at still shorter wavelengths. To test this hypothesis, the concentration of thallium was deter-

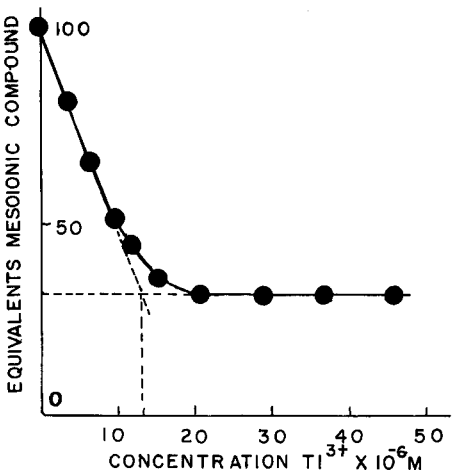

Fig. 6. The absorbance at 266 nm of 10 ml of a 2.94×10^{-5} M solution of the mesoionic compound in chloroform after equilibration with an equal volume of thallium(III) in 0.1 M perchloric acid.

mined complexiметrically in each phase. However, the mass balance (Table 2) showed a deficiency: that this must be compensated for by the presence of thallium(I) was established by differences in the results obtained for total thallium by the dithizone method after reduction of thallium(III) with sulphite.

The definite presence of thallium(I) ions shows that some or all of the thallium(III) must have oxidised the mesoionic compound 3 to a new species, possibly the dication 5. If the oxidation follows the equation

$$Tl^{3+} + 2 \text{ meso } (\pm) \rightarrow Tl^{+} + (\text{dication})^{2+} \qquad (6)$$

the stoicheiometry would be indistinguishable from the formation of the complex cation $Tl(meso)_2^{3+}$, which could of course occur as well. In all the experiments save the first listed in Table 2, there would have been sufficient thallium(III) to oxidise all the mesoionic compound according to Eqn. 6 and the product can be envisaged as partitioning between the two phases and contributing substantially to the absorption in the chloroform phase. Certainly, similar, but not completely identical, changes in the absorption spectra of solutions of the mesoionic compound in chloroform are brought about by equilibration with acidic aqueous solutions of cerium(IV) and dichromate which are oxidants comparable in redox potential to thallium(III). However, attempts to reduce the postulated dication (5) with ascorbic acid, sulphite ions, etc., did not resolve the problem while the purely analytical difficulties of obtaining precise values for the concentration of both Tl^{+} and Tl^{3+} at trace levels in both aqueous and organic phases militated against extending the data of Table 2 to a wider range of concentrations and proportions of the reactants. Clearly, if the reaction between the mesoionic

TABLE 2

Distribution of thallium after equilibrating solutions of thallium(III) in 0.1 M perchloric acid with the mesoionic compound dissolved in chloroform

Reactants (10^{-5} mol)			Products (10^{-5} mol)		
Mesoionic compound	Tl^{3+}	$[Tl^{3+}]/[meso]$	Tl^{+} (aq)[a]	Tl^{3+} (aq)	Tl^{3+} (org)
5.70	2.58	0.45	2.35 (91%)[b]	—	0.23
10.20	5.65	0.53	4.90 (81%)	0.21	0.54
5.70	5.15	0.90	2.49[c] (48%)	1.55	1.11
5.70	6.28	1.10	2.90 (46%)	2.38	1.00

[a]Value of Tl^{+} by difference. [b]The amount of thallium(I) found expressed as a percentage of the total thallium(III) taken. [c]In a redetermination, the value 2.65 was obtained.

compound and thallium(III) is neither simply one of complex ion formation nor simply one of oxidation, no unambiguous conclusions can be drawn from results shown graphically in Figs. 4—6.

More basic information on the course of the reaction between dithizone and thallium(III) in a two-phase system was obtained by replacing chloroform by carbon tetrachloride as the organic solvent. When a solution containing excess of thallium(III) (10^{-2} M) was added to one of dithizone (10^{-5} M) in carbon tetrachloride, there was no immediate colour change in the organic phase. On gentle shaking, the colour passed from green to brown and then pink, orange and finally colourless within 3 min. Equal volumes of the reactants were added to several separating funnels and, after the phases had been in contact for about 60 s, they were gently shaken together for 1, 5, 15—30, 60, 120 and 180 s, respectively. In each case, the spectrum of the separated organic phase showed that dithizone was being removed and replaced by a new species absorbing at 507 nm and to a lesser extent at 275 nm. With the passage of time, the absorbance of these two bands decreased and the absorbance at 415 nm increased with clearly defined isosbestic points at 450 and 310 nm, indicating that one species was changing into another. The changes in the separated carbon tetrachloride layer produced after the two phases had been shaken together for 1 s or 15—30 s are shown in Figs. 7 and 8, respectively.

On the basis of the above work with chloroform, it was at first thought that the prominent bands at 507 and 275 nm could be identified with Tl(HDz) and the mesoionic compound 3, respectively, subsequent changes being due to some interaction between the mesoionic compound and dithizone regenerated by the reversion of the thallium(I) complex. This hypothesis was negated by the existence of the distinct isosbestic points and by the experimental observation that dithizone does not affect the absorption spectrum of the mesoionic compound: indeed their absorbances were found to be strictly additive. Moreover, the spectrum of pure Tl(HDz)

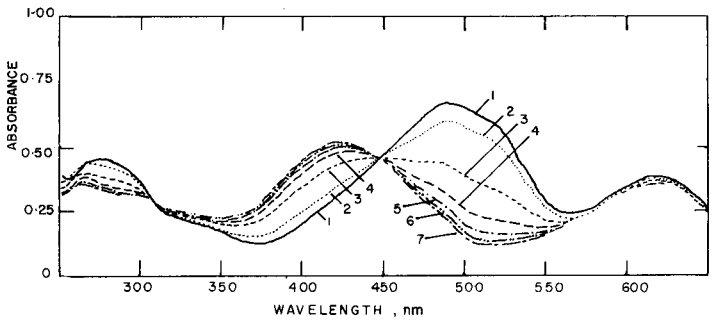

Fig. 7. Absorption spectra of a solution of dithizone in carbon tetrachloride (10^{-5} M) after gentle shaking with ca. 10^{-2} M thallium(III) in 0.1 M $HClO_4$ for 1 s. Spectra 1—7 relate to the organic phase, recorded at 10-min intervals.

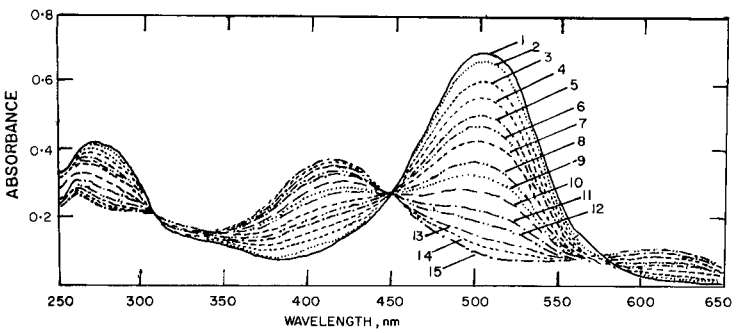

Fig. 8. Absorption spectra of a solution of dithizone in chloroform (10^{-5} M) after gentle shaking for 15—20 s with ca. 10^{-2} M thallium(III) in 0.1 M $HClO_4$. Spectrum 2 was recorded 2 min after spectrum 1 and spectra 3—15 at 10-min intervals thereafter.

prepared by extraction of thallium(I) at pH 10—12 into carbon tetrachloride comprises a major peak at λ_{max} = 513 nm (ϵ = 25,700) with a smaller band at 265 nm. It was then shown (see Experimental) that the species absorbing at λ_{max} = 507 nm was in fact the thallium(III) complex, $Tl(HDz)_3$. The absorbance at this wavelength decreased rapidly with time and the spectrum of the product corresponded to a mixture of dithizone with a species with λ_{max} = 415 nm and minor peaks at 302 and 260 nm, which was positively identified as due to the disulphide 2 by comparison of the spectrum of a pure sample in carbon tetrachloride [14].

As expected from the much lower polarity of carbon tetrachloride compared with chloroform, the rate of bond-cleavage of the disulphide is much slower in the former solvent (see Fig. 9) although independent measurements showed again that it was catalysed by both Tl^+ and Tl^{3+}.

The results obtained with carbon tetrachloride as the solvent support and extend those previously obtained with chloroform and confirm the series of reactions postulated in Eqns. 1—4. Dithizone and its metal complexes are

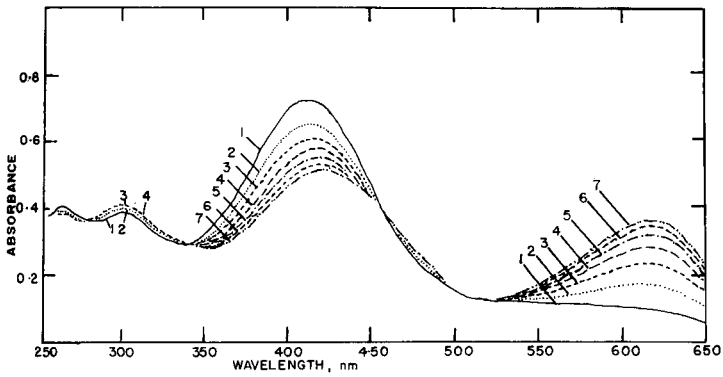

Fig. 9. Absorption spectra of a solution of the pure disulphide 3 in carbon tetrachloride (1-cm cell) recorded at hourly intervals.

known to be less soluble in carbon tetrachloride than in chloroform [1], and experiments now show that the mesoionic compound 3 is almost insoluble in the former solvent, thus it is clear that the major changes in partition coefficients will have a great influence on the detailed course and speed of reactions in which these are involved. For example, an earlier comparative study of the rate of extraction of copper and mercury(II) dithizonates into chloroform or carbon tetrachloride showed how profoundly changes in the organic solvent could affect the approach to equilibrium in these two-phase systems, and how these phenomena could be exploited analytically [21]. Similar results were found in the extraction of zinc dithizonate [22] and the kinetics of other dithizone extractions have been studied intensively by Freiser and his co-workers [23]. While these considerations certainly apply equally to the thallium(III)/dithizone system, there is an additional feature here from the solvent dependence of the kinetics of sulphur-sulphur bond cleavage in the intermediate disulphide 2.

To avoid the complications arising from the kinetic aspects of phase transfer, and in order to use stopped-flow techniques to study the early stages of the reactions between dithizone and thallium(III), the possibility of examining the reactions in a monophase prepared from a mixture of methanol, water, and chloroform was explored. However, the reaction proved to be inconveniently fast and catalytic traces of impurities in the system gave rise to unacceptable irreproducibility [19].

EXPERIMENTAL

Glassware, chemicals and solutions

All glassware, including optical cells, was scrupulously cleaned by immersion for at least 24 h in 10% Contrad, then rinsed thoroughly with deionised water, 5% (v/v) nitric acid, deionized water and finally doubly-distilled water before being allowed to dry in a dust-free environment.

Analytical-grade reagents were used and all solvents were carefully fractionated before use. Complete absence of all metallic contamination was checked by using a dilute solution of dithizone in chloroform [24]. Metal-free ammonia solutions were prepared via isopiestic distillation [25] or by passing purified ammonia gas into doubly-distilled water [24].

Dithizone was purified by standard methods [1] and had the following spectral data: (a) in chloroform, λ_{max} = 605 and 445 with ϵ_{max} = 41400 and 15900 l mol^{-1} cm^{-1} and peak ratio $\lambda_{max\,1}/\lambda_{max\,2}$ = 2.59; (b) in carbon tetrachloride, λ_{max} = 620 and 450 with ϵ_{max} = 34600 and 20000 l mol^{-1} cm^{-1} and peak ratio = 1.75. Spectra were recorded on a Varian Superscan-3 ultraviolet-visible spectrophotometer with matched 1-cm or 4-cm silica cells.

Stock solutions of thallium(III) were prepared by dissolving known masses of thallium(III) chloride (Merck) in 0.1 M perchloric acid to give 10^{-2}—10^{-4} M solutions which were diluted as required. The actual concentrations were established (a) by reducing thallium(III) to thallium(I) with sulphur dioxide and determining its concentration with dithizone by the reversion procedure [8], or (b) by titration against EDTA with thymol blue as indicator [26], a procedure which gave sharp end-points even in the presence of 0.1—0.5 M hydrobromic acid. Solutions (ca. 10^{-5} M) of thallium(I) were prepared in 0.01 M perchloric acid by dissolving known masses of thallium(I) nitrate (Hopkins and William) and standardising as above.

Procedures

The composition of the compound formed between thallium(III) and the mesoionic compound. For the photometric titration at 249 nm of the mesoionic compound 3 (2.040×10^{-5} M in 0.01 M perchloric acid) with thallium(III), the total volume was kept constant at 20 ml. The results are shown in Table 1.

For Job's method of continuous variations, the absorbances (1-cm cell) at 249 nm were measured for mixtures of x ml of thallium(III) (1.305×10^{-4} M) and (10—x) ml of the mesoionic compound (1.305×10^{-4} M) made up to 25 ml with 0.1 M perchloric acid; for absorbances less than 0.100, 4-cm cells were used. The results are listed in Table 3.

Finally, the absorbances at 266 nm were measured for solutions (10 ml) of the mesoionic compound in chloroform after equilibration with 10 ml of a solution of thallium(III) in 0.1 M perchloric acid. The concentrations taken were as follows:

Tl^{3+} (10^{-5} M)	0.00	0.628	1.26	1.57	3.14	6.28
Meso (10^{-5} M)	2.94	2.94	2.94	2.94	2.94	2.94
Absorbance	0.775	0.510	0.315	0.280	0.250	0.250

Verification of the composition of thallium(III) dithizonate. A 10^{-5} M solution of dithizone in carbon tetrachloride was shaken for 15—30 s with an equal volume of thallium(III) in 0.1 M perchloric acid (10^{-2} M; excess). The organic phase was then quickly separated and washed with

TABLE 3

Method of continuous variations

x (ml)	0	1	2	2.5	3	4	5
Absorbance	1.230	0.880	0.528	0.333	0.141	0.051	0.040
x (ml)	6	7	7.5	8	9	10	
Absorbance	0.056	0.064	0.070	0.064	0.048	0.041	

doubly-distilled water to remove any traces of thallium(III) in entrained water. The thallium/dithizone complex was reverted by shaking for 2 min with an equal volume of 0.1 M perchloric acid that had been pre-saturated with sulphur dioxide to ensure that thallium(III) was completely reduced to thallium(I) and therefore unable to oxidise the regenerated dithizone. The thallium(I) then present in the aqueous phase was determined spectrophotometrically as its dithizonate and found to be 0.553×10^{-5} M. The absorbance of the dithizone in the organic phase was 0.610, corresponding to a concentration of 1.76×10^{-5} M, whence the ratio $[HDz]/[Tl^{3+}] = 1.76: 0.533 = 3.18$, confirming the formula $Tl(HDz)_3$.

REFERENCES

1 H. M. N. H. Irving, Dithizone, Analytical Sciences Monographs No. 5, The Chemical Society, London, 1977.
2 H. M. N. H. Irving, The Analytical Applications of Dithizone, C.R.C. Crit. Rev. Anal. Chem., 1980.
3 C. W. Still and H. E. Patterson, Anal. Chem., 21 (1949) 1268.
4 A. T. Pilipenko, Zh. Anal. Khim., 5 (1950) 14.
5 R. S. Clarke and F. Cuttitta, Anal. Chim. Acta, 19 (1958) 555.
6 G. K. Schweitzer and A. D. Norton, Anal. Chim. Acta, 30 (1964) 119.
7 G. K. Schweitzer and J. E. Davidson, Anal. Chim. Acta, 35 (1966) 467.
8 D. C. Rupainwar and K. K. Kakkar, Rev. Roum. Chim., 25(2) (1980) 295.
9 H. Irving and J. J. Cox, J. Chem. Soc., (1961) 1470.
10 H. Fischer, Angew. Chem., 50 (1957) 919.
11 F. Koroleff, Merentulkimuslaitoksen Julk. Havsforskninginst. Skr., 145 (1950) 7.
12 H. M. N. H. Irving, A. M. Kiwan, D. C. Rupainwar and S. S. Sahota, Anal. Chim. Acta, 56 (1971) 205.
13 J. W. Ogilvie and A. H. Corwin, J. Am. Chem. Soc., 83 (1961) 5023.
14 A. M. Kiwan and H. M. N. H. Irving, Chem. Commun., (1970) 928; J. Chem. Soc., B: (1971) 901.
15 D. C. Rupainwar, Ph.D. Thesis, Leeds, 1969.
16 A. H. Nabilsi, Ph.D. Thesis, Leeds, 1972.
17 H. M. N. H. Irving and G. Corsweena, unpublished work.
18 S. S. Sahota, Ph.D. Thesis, Leeds, 1969.
19 C. Sacht, MSc. Thesis, Capetown, 1985.
20 J. J. Cox and D. M. Servant, Anal. Chim. Acta, 74 (1975) 200.
21 H. Irving, G. Andrew and E. J. Risdon, J. Chem. Soc., (1949) 541.
22 H. Irving, C. F. Bell and R. J. P. Williams, J. Chem. Soc., 1952, 357.
23 Full references are given in ref. 1.
24 G. Iwantscheff, Das Dithizon und seine Anwendung in der Mikro- und Spuren-analyse, 2nd edn., Verlag Chemie, Weinheim, 1972.
25 H. Irving and J. J. Cox, Analyst (London), 83 (1958) 526.
26 F. W. E. Strelow and F. von S. Torien, Anal. Chim. Acta, 36 (1966) 189.
27 A. Irving and H. M. N. H. Irving, J. Chromatogr. Spectrosc. Res., (1986) in press.

Analytica Chimica Acta, 181 (1986) 139—148
Elsevier Science Publishers B.V., Amsterdam — Printed in The Netherlands

SURFACE-ENHANCED RAMAN SPECTROMETRY WITH SILVER PARTICLES ON STOCHASTIC-POST SUBSTRATES

T. VO-DINH*

Advanced Monitoring Development Group, Health and Safety Research Division, Oak Ridge National Laboratory, Oak Ridge, TN 37831 (U.S.A.)

M. MEIER and A. WOKAUN

Physical Chemistry Laboratory, Swiss Federal Institute of Technology-ETH Zentrum, CH-8092 Zurich (Switzerland)

(Received 15th July 1985)

SUMMARY

A special type of substrate for surface-enhanced Raman scattering (s.e.r.s.) is evaluated. The substrates consist of silver particles deposited on stochastically arranged SiO_2 posts produced by plasma etching of a quartz surface using a silver island film as an etch mask. The optimization of various experimental parameters such as silver layer thickness, silver evaporation angle, and excitation energy are discussed in detail. Comparative studies with *p*-nitrobenzoic acid as the model compound indicate that this present substrate is at least one order of magnitude more effective than other common s.e.r.s. substrates, such as the silver island film and the crossed-grating surface, which were previously found to induce the strongest s.e.r.s. signals. The preparation of these silver-particle-post substrates avoids the elaborate lithographic procedures required for crossed-grating structures. The quantitation of species in a three-component mixture illustrates the selectivity of the s.e.r.s. technique.

The observation of surface-enhanced Raman scattering (s.e.r.s.) of molecules adsorbed on metallic surfaces is relatively new [1—3] and the phenomenon has stimulated extensive research efforts for the past few years. Several theoretical models have been proposed to elucidate the photophysical phenomena related to s.e.r.s. [4, 5]. More than one mechanism appears to contribute to the s.e.r.s. phenomenon. One major contribution to Raman enhancement is associated with amplified local electromagnetic fields at the surface. These fields originate from roughness-induced excitation of surface plasmons [4—11], and from the concentration of the electric field lines near high-curvature points of the surface, e.g., the tips of particles or surface protrusions; this field concentration has been termed the "lightning rod effect" [7, 8, 12]. If the adsorbate molecule is relatively close to the surface, image dipoles [4] and the modulated reflectance mechanism [4] may also contribute to Raman enhancement. This electromagnetic enhancement contribution is not molecule-specific and does not require physical contact between

0003-2670/86/$03.50

adsorbate molecule and metal surface. A second contribution to s.e.r.s. involves resonant charge-transfer excitation of surface/adsorbate complexes [13]. Special adsorption sites (adatoms) may be important for this mechanism, as they facilitate electron-hole pair excitation [4, 13—15].

In previous studies [16, 17], the effectiveness and potential of s.e.r.s. as a spectrochemical tool were investigated for quantitation of trace organic species using s.e.r.s.-active substrates based on materials coated with silver-covered microspheres; using microsphere-quartz/post-quartz substrates were also developed for s.e.r.s. [18]. Other analytical applications of s.e.r.s. have also been reported, based on stabilized colloids [19] and silver and indium island films [20]. In this work, the s.e.r.s.-active surface based on post substrates is investigated. The general applicability of s.e.r.s. with quartz substrates is extended by producing silver particles deposited on stochastic SiO_2 posts. Various experimental factors for substrate preparation including silver thickness, metal evaporation angle, and other physical parameters such as the excitation energy are described in detail. The efficiency of s.e.r.s. for multicomponent quantitation is also demonstrated by the characterization of a three-component mixture of the polyaromatic compounds, 7,8-benzoquinoline, coronene and phenanthrene.

EXPERIMENTAL

Preparation of silver-particle-post substrates

Quartz plate supports were prepared by reactive-ion etching of quartz plates in a trifluoromethane plasma, by procedures similar to those described previously [18]. Only the main features are given here. Because thermally grown silica etches much faster than fused quartz, a 500-nm layer of silica was first deposited onto a fused quartz plate by thermal evaporation. The evaporation rate of silica was set at 0.1—0.2 nm s^{-1}. The crystalline quartz resulting from silica evaporation was subsequently annealed to the fused quartz plate by heating the substrate at about 950°C for about 45 min. An etch mask was then prepared by thermally evaporating a 5-nm layer of silver onto the silica surface of the fused quartz plate. The substrate was subsequently flashed-heated at about 500°C for 20 s. The heating process caused the silver layer to bead up into small globules which served as etch masks. The quartz plates covered with stochastically positioned silver globules were then etched in a trifluoromethane plasma. The etching procedure resulted in the formation of silica posts after chemical cleaning and removal of the silver masks. The positions and diameter of the posts were determined by the imprints of the silver globules.

The additional step of substrate preparation introduced in this work consisted of producing silver particles on the posts by oblique-angle evaporation of silver at a rate of 1.5 nm s^{-1} under vacuum ($2—5 \times 10^{-6}$ Torr). Various evaporation times were used to control the amount of silver and, thus, the dimension of the particles. Different evaporation angles, θ_{Ag}, were also

used to establish the shapes of the particles by influencing the mutual shadowing of the posts. The principle of formation of isolated silver particles produced on the tops of the silica posts by oblique-angle evaporation is illustrated in Fig. 1.

Measurement procedures and instrumentation

Sample delivery. After silver evaporation on the silica-post substrate, one drop of a sample of solution was delivered on the substrate. The excess of solution on the substrate was then blown off by a stream of nitrogen, thus ensuring that the substrate surface is only covered by one monolayer of analyte molecules chemisorbed on the surface.

Instrument. Raman scattering was excited either from emission lines of an argon ion laser, or by using the output of a dye laser. Typically 10 mW of power was incident on the sample, at an angle of 70°. The scattered light was collected at 90° to the incident beam, dispersed by a model 1401 Spex double monochromator, and collected by an RCA-31034 photomultiplier tube operated in the photon-counting mode.

Metals and reagents. All compounds were purchased from Fluka at the highest purity available. Ethanol (spectroscopic grade) was used as the sol-

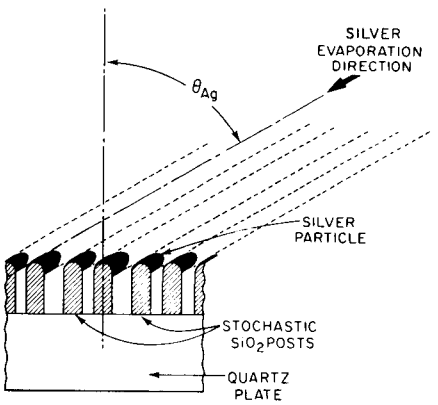

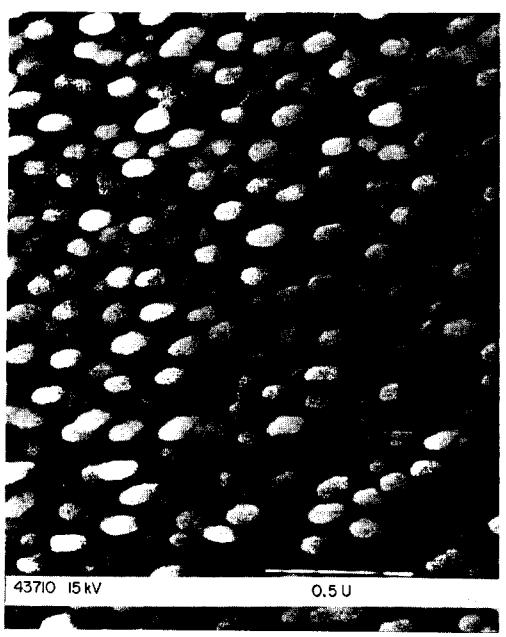

Fig. 1. Principle of formation of silver particles formed on silica posts by angle evaporation.

Fig. 2. Scanning electron microscope photograph of silver particles formed on a silica-post substrate.

vent. The concentrations of the analyte solutions used were 10^{-3} M for 7,8-benzoquinoline, coronene and phenanthrene, and 10^{-2} M for *p*-nitrobenzoic acid.

RESULTS AND DISCUSSION

S.e.r.s.-active substrates based on stochastic posts

The preparation of metal surfaces having submicron protrusions is a prerequisite for inducing s.e.r.s. in adsorbed molecules. The technique for substrate preparation investigated here is capable of producing well-separated posts distributed stochastically over the surface of the quartz plate. Measurements with a scanning electron microscope show that the posts densely cover the quartz surface, with an average center-to-center spacing of about 100—120 nm. The average sectional diameter of the posts is about 150—200 nm. The high-density arrangement of the posts and their sharp needle-like shapes are two important factors contributing to the efficacy of the substrates for maximum Raman enhancement. These two features are discussed below.

Figure 2 is a scanning electron microscope photograph of a substrate obtained after deposition of silver with a thickness of d_{Ag} = 100 nm using an evaporation angle, θ_{Ag} = 55°. The photograph shows that the silver particles are well separated from one another. The particle shape is approximately ellipsoidal with a long half axis of ca. 60 nm and a short half axis of ca. 30 nm. The surface is uniformly covered by the silver particles deposited on the top of the stochastic posts. In general, regular and well-defined microstructures are desirable for theoretical studies aimed to elucidate the various s.e.r.s. mechanisms. However, for quantitative applications, surfaces having randomly positioned protrusions could be useful when they are practical to prepare and reproducible. Reproducibility studies indicated that the stochastic-post substrates are suitable for most applications: replicate measurements for a given sample provided a relative standard deviation of ±10%, while measurements with different samples under identical conditions produced a sample-to-sample variation of ±30%.

Figure 3 shows typical s.e.r.s. spectra of 7,8-benzoquinoline, phenanthrene, and coronene. The excitation energy was the 19436 cm^{-1} laser line and the s.e.r.s. substrate used for the measurements was obtained with d_{Ag} = 100 nm at θ_{Ag} = 55°. The s.e.r.s. spectra exhibit sharp peaks emerging above a structureless continuum background covering the entire spectral range from 300 cm^{-1} to 1800 cm^{-1}. This background has a typical double-peak structure at ca. 1300 cm^{-1} and ca. 1600 cm^{-1}, which is consistent with results observed previously [17, 21, 22]. The broad double-peak feature is characteristic of many s.e.r.s. substrates and is believed to originate from graphite species produced by decomposition of carbon-containing adsorbates.

Effect of silver-coating thickness on s.e.r.s. signals

An important parameter affecting the magnitude of Raman enhancement is the size of silver particles. The optimal size range is governed by two

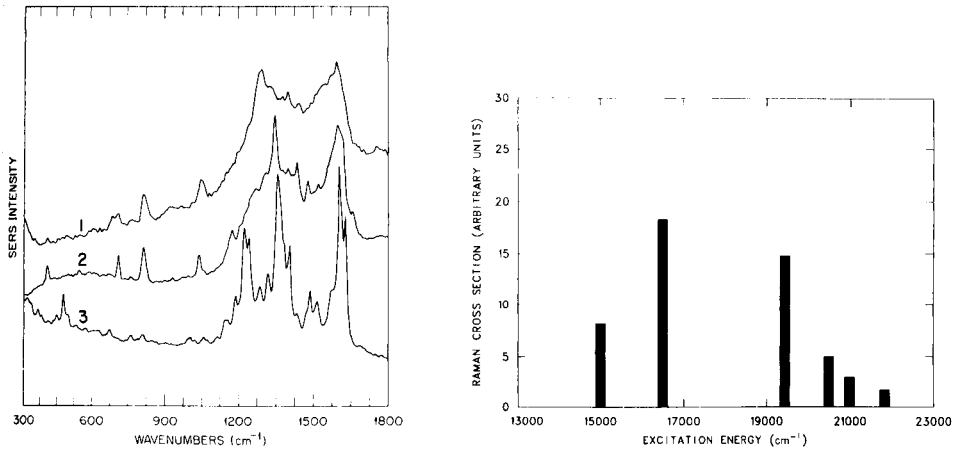

Fig. 3. Surface-enhanced Raman spectra: (1) benzoquinoline; (2) phenanthrene; (3) coronene. Samples adsorbed onto silver particles deposited on stochastic-post substrates. Experimental parameters: d_{Ag} = 100 nm, θ_{Ag} = 55°, λ_{ex} = 19436 cm^{-1}.

Fig. 4. Effect of the excitation energy on the s.e.r.s. signal of *p*-nitrobenzoic acid adsorbed on silver particles deposited on stochastic posts (θ_{Ag} = 55°).

mechanisms. The first mechanism, often referred to as the size effect, represents energy losses of the conduction electrons of the metal caused by collisions with the particle surface; this loss mechanism is caused by surface scattering and is significant for small particles, especially when the particle dimensions become equal to or less than the mean free path of the electrons in the metal. The high limit of the particle size is governed by radiation damping, which involves radiative losses of the electric particle dipole [24]. In order to establish the optimal size of the silver particles, experiments were done to vary the amounts of silver evaporated onto the quartz surface. The deposited silver thickness (as measured by a quartz crystal monitor normal to the evaporation source) was varied between 30 and 140 nm. The s.e.r.s. signals observed for adsorbed *p*-nitrobenzoic acid increased with increasing silver thickness, reaching a maximum with 100 nm of deposited silver. With silver thicknesses above 100 nm, the particles begin to coalesce upon evaporation, which results in a sharp decrease of the s.e.r.s. signal. Table 1 summarizes the results obtained corresponding to the 1597 cm^{-1} ring vibration of *p*-nitrobenzoic acid adsorbed on substrate having different thickness of silver deposition.

Theoretical calculations, taking into account the two energy-loss mechanisms previously discussed (i.e., surface scattering and radiation damping), gave an optimum diameter of ca. 35 nm for silver spheres and an optimum long axis of ca. 80 nm and optimal short axis of 20 nm for 4:1 ellipsoids [24]. The dimensions of the silver particles obtained with the substrates under study (Fig. 2) are similar to these theoretical values.

TABLE 1

Effect of the silver layer thickness (d_{Ag}) on the surface-enhanced Raman scattering intensity

Silver thickness d_{Ag}[a] (nm)	S.e.r.s. intensity[b] (photon s^{-1} mW^{-1})
30	690
50	985
70	1150
100	1530
120	1410
140	780

[a]Silver evaporation angle, 55°. [b]Laser excitation, 514.5 nm; s.e.r.s. intensity for the 1597 cm^{-1} band of *p*-nitrobenzoic acid.

Effect of silver evaporation angle

In addition to the amount of silver deposited onto the substrate, another parameter that can influence the particle shape and size is the angle of silver evaporation. Because of the dependence of the mutual shading of the protrusions on the etched quartz surface, the shape and dimensions of the silver particles can be varied by using different θ_{Ag} values. Measurements of the s.e.r.s. signal of *p*-nitrobenzoic acid (Raman band 1597 cm^{-1}) absorbed on an etched quartz substrate covered with d_{Ag} = 100 nm were made to study the effect of θ_{Ag}. The results indicated that an angle of 55° between the evaporation direction and the substrate normal axis provided the strongest s.e.r.s. signal. However, the dependence of the Raman enhancement upon θ_{Ag} was found only to be moderate (Table 2).

Effect of the excitation energy

Surface-enhanced Raman scattering is a resonance process involving amplification of both Raman emission and laser field emission [24—28]. The laser frequency used for excitation is, therefore, an important parameter in the optimization of s.e.r.s. measurements. Enhancement occurs when the

TABLE 2

Effect of the silver evaporation angle upon the s.e.r.s. signal intensity

Silver evaporation angle[a] (°)	S.e.r.s. intensity (photon s^{-1} mW^{-1})
0	1190
40	1485
55	1530
60	1350

[a]Angle between evaporation path and the normal axis of the substrate plane (θ_{Ag}).

excitation frequency or the Raman frequency is resonant with the particle plasmon. For larger particles, the plasmon resonance excitation curve is broadened by radiation damping [24] such that both excitation and Raman radiation can experience resonant enhancement if the laser frequency is suitably chosen. The effects of radiation damping, which decreases Raman enhancement, are more severe at shorter wavelengths, the radiation reaction field being proportional to λ^{-3} [24]. It is therefore of importance to establish the optimal excitation frequency for a given type of substrate and adsorbate. Figure 4 shows the results of excitation-energy-dependence studies with *p*-nitrobenzoic acid as the model compound. The substrate consisted of silver particles deposited on silica posts (using $\theta_{Ag} = 55°$ and $d_{Ag} = 100$ nm). The s.e.r.s. intensities were normalized to the average value of the 19436 cm^{-1} laser excitation energy to calculate the Raman scattering cross-section; the raw data were also normalized to eliminate the trivial ω^4_{Raman} dependence, where ω_{Raman} is the frequency of the Raman emission. The results in Fig. 4 were finally obtained by taking into account the spectral dependence of the detector sensitivity. The results indicate that the Raman cross-section depends significantly on the excitation energy.

Multicomponent quantitation and comparative studies

Figure 5 illustrates the selectivity of s.e.r.s. for the analysis of a synthetic mixture containing 7,8-benzoquinoline, phenanthrene, and coronene. The remarkable spectral selectivity of s.e.r.s. was demonstrated by the fact that most of the 30 Raman peaks of the mixture spectrum can be assigned to the individual components. The results of the spectral assignment are given in Table 3.

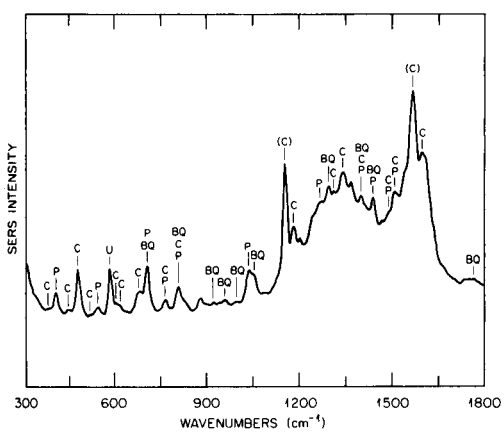

Fig. 5. Surface-enhanced Raman spectrum of a three-component mixture containing 7,8-benzoquinoline (BQ), coronene (C), and phenanthrene (P); U, unidentified peak. Experimental parameters: $d_{Ag} = 100$ nm, $\theta_{Ag} = 55°$, $\lambda_{ex} = 19436$ cm^{-1}.

TABLE 3

Spectral identification of a three-component mixture by surface-enhanced Raman scattering.

S.e.r.s. peaks in mixture (cm^{-1})	S.e.r.s. peaks for individual compounds (cm^{-1})			Blank emission (cm^{-1})
	Benzoquinoline (BQ)	Coronene (C)	Phenanthrene (P)	
		319		
		369		
		384		
408 (P)			408	
453 (C)		453		
483 (C)		483		
		499		
535 (C)		536		
546 (P)			546	
588 (U)[a]				
610 (C)		631		
		676		
688				
711 (P)			711	
811 (BQ)	815		814	813
928 (BQ)	928			
967 (BQ)	967			
1014 (BQ)	1014			
1042 (P)			1040	
	1048			
1097 (C)		1144		
1158 (BQ, C, P)	1152	1153		1155
		1176		
1185 (C)		1186		
1209				
		1219		
1240 (C)		1237		
1275 (P)			1273	
		1284		
1299 (BQ)	1296			
1315 (C, P)		1317	1314	
	1329			
147			1346	
		1354		
	1366 (P)			711
1374				

[a]U, unidentified peak on Fig. 5.

The efficacy of the silver particle-post substrates investigated in this work was evaluated by comparing them with two other common types of s.e.r.s.-active surfaces, viz., a silver island film and a cross-grating substrate. Measurements were conducted with *p*-nitrobenzoic acid as the model compound

adsorbed on the three types of substrates. For comparison purposes, the same laser line at 20487 cm^{-1} was used as the excitation energy. The island film was produced by evaporating 5 nm of silver onto a glass plate at an evaporation rate of 0.05 nm s^{-1}. The crossed-grating substrate was prepared by evaporating 100 nm of silver onto crossed quartz grating at a rate of 1.5 nm s^{-1} [29]. The comparative measurements of Raman intensity indicated that the stochastic-post substrate provides the strongest Raman intensities, about 30-fold stronger than with the island film and about 8-fold stronger than with the crossed-grating structure. The high value of the enhancement on the present stochastic-post structures is due to several factors. Compared to the oblate spheroids observed in electron micrographs of island films, the "lightning rod" enhancement contribution [7, 8] is stronger for the prolate spheroids on our samples, as seen e.g., in Fig. 1. Most importantly, the size of the particles produced in this work appears to correspond to the optimum range [24] which yields maximum enhancement. The stochastic arrangement of the posts results in a somewhat larger particle density (average center-to-center spacing of ca. 100 nm), and hence in a higher surface area available for adsorption, compared to particles on a crossed-grating substrate. For crossed-grating structures, the particle dimensions are linked to the grating period, which can be no shorter than half the wavelength of light used for the holographic exposures (grating period $\approx$ 260 nm).

In conclusion, this study shows that silver particles on silver particle-post substrates provide a new and very efficient type of s.e.r.s.-active substrate. These stochastic-post substrates provide another type of s.e.r.s.-active materials developed for analytical applications and appear to exhibit the strongest Raman enhancement reported so far. The substrate preparation technique avoids elaborate lithographic procedures required for cross-grating structures. The stochastic-post substrates require longer times to prepare than silver microsphere-coated celluloses [17] and silver island films but can be re-used many times after chemical cleaning and removal of silver particles.

This research was sponsored by the U.S. Department of the Army (Interagency Agreement Numbers DOE 40-1294-82/ARMY 3311-1450), the Office of Health and Environmental Research, U.S. Department of Energy, under contract DE-AC05-84OR21400 with Martin Marietta Energy Systems, Inc., the Swiss National Science Foundation, and The Branco Weiss Foundation.

REFERENCES

1 M. Fleischmann, P. J. Hendra and A. J. McQuillan, Chem. Phys. Lett., 26 (1974) 123.
2 D. L. Jeanmaire and R. P. Van Duyne, J. Electroanal Chem., 84 (1977) 1.
3 M. G. Albrecht and J. A. Creighton, J. Am. Chem. Soc., 99 (1977) 5215.
4 R. K. Chang and T. E. Furtak (Eds.), Surfaced-Enhanced Raman Scattering, Plenum Press, New York, 1982.

5 T. E. Furtak and J. Reyes-Corona, Surf. Sci., 93 (1980) 351.
6 M. Kerker, Acc. Chem. Res., 17 (1984) 271.
7 J. I. Gersten, J. Chem. Phys., 72 (1980) 5779.
8 A. Wokaun, in H. Ehrenreich, F. Seitz and D. Turnbull (Eds.), Solid State Physics, Academic Press, New York, Vol. 38, 1984, p. 223.
9 M. Moskovits, J. Chem. Phys., 69 (1978) 4159.
10 M. Kerker and C. G. Blatchford, Phys. Rev. B: 26 (1982) 4052.
11 T. L. Fennell, Phys. Rev., 25 (1982) 2930.
12 P. F. Liao and A. Wokaun, J. Chem. Phys., 76 (1982) 751.
13 A. Otto, in M. Cardona (Ed.), Light Scattering in Solids, Springer Verlag, Berlin, Vol. 4, 1983, p. 289.
14 B. H. Loo and Y. G. Lee, J. Electroanal. Chem., 163 (1984) 401.
15 R. K. Chang and B. L. Lawbe, CRC Crit. Rev. Solid State Mater. Sci., 12 (1984) 1.
16 J. P. Goudonnet, G. M. Begun and E. T. Arkawa, Chem. Phys. Lett., 92 (1982) 197.
17 T. Vo-Dinh, M. Y. K. Hiromoto, G. M. Begun and R. L. Moody, Anal. Chem., 56 (1984) 1667.
18 M. C. Buncick, A. J. Warmack, J. W. Little and T. L. Ferrell, Bull. Am. Phys. Soc., 29 (1984) 129.
19 C. D. Tran, Anal. Chem., 56 (1984) 824.
20 C. Jennings, R. Avoca, A. Hor and R. V. Loufyt, Anal. Chem., 56 (1984) 2033.
21 J. P. Heritage, J. G. Bergman, A. Pinczuk and J. M. Worlock, Chem. Phys. Lett., 67 (1979) 229.
22 C. Y. Chen, E. Burstein and S. Lundquist, Solid State Commun., 32 (1979) 63.
23 P. F. Liao, J. G. Bergman, D. S. Chemla, A. Wokaun, J. Melngailis, A. M. Hawryluk and N. P. Economonou, Chem. Phys. Lett., 82 (1981) 355.
24 A. Wokaun, J. P. Gordon and P. F. Liao, Phys. Rev. Lett., 48 (1982) 957.
25 P. W. Barber, R. K. Chang and H. Massouli, Phys. Rev. B: 27 (1983) 7251.
26 M. Meier and A. Wokaun, Opt. Lett., 8 (1983) 581.
27 M. Meier, A. Wokaun and P. F. Liao, J. Opt. Soc. Am., B: May (1986) in press.
28 E. J. Zeman and G. C. Schatz, in Proc. 17th Jerusalem Symposium in Quantum Chemistry and Biochemistry, Reidel, 1984.
29 H. W. Lehmann, R. Widmer, M. Ebnoether, A. Wokaun, M. Meir and S. K. Miller, J. Vac. Sci. Technol., B: 1 (1983) 1207.

Analytica Chimica Acta, 181 (1986) 149—157
Elsevier Science Publishers B.V., Amsterdam — Printed in The Netherlands

DIRECT FATTY ACID PROFILING OF COMPLEX LIPIDS IN INTACT ALGAE BY FAST-ATOM-BOMBARDMENT MASS SPECTROMETRY

MARK M. ROSS*, REX A. NEIHOF and JOSEPH E. CAMPANA*
Naval Research Laboratory, Chemistry Division, Washington, DC 20375-5000 (U.S.A.)
(Received 19th August 1985)

SUMMARY

Fast-atom-bombardment mass spectrometry (FABMS) is used for the semiquantitative determination of the fatty acids of complex lipids directly from intact algal cells, crude algal lipid extracts, and vegetable oils. Carboxylate ions, $RCOO^-$, corresponding to the fatty acid moieties of the complex lipids are detected. The relative abundances of the carboxylate fatty acid ions in the FAB mass spectra agreed with the relative percentages found by gas chromatography of the fatty acid methyl esters derived from the extracted lipids. Chemical ionization/fast-atom-bombardment mass spectrometry (CI/FABMS) is discussed with respect to enhancing the molecular ions of the fatty acids and triacylglycerols from these materials. The use of FABMS requires little sample preparation, and FABMS enables rapid fatty acid screening, directly from crude biological materials.

One application of biotechnology [1] in this laboratory is the growth of algae in heavy water to produce deuterated biological compounds, which may serve as starting compounds for synthesizing high-temperature, oxidatively stable, deuterated materials such as deuterated lubricants, polymers, and composites. For example, Navy laboratories have shown deuterated lubricants to have a greater oxidative stability in high-temperature applications than their hydrogenated analogs [2]. The biological compounds of interest in this study are long-chain fatty acids present in algae primarily as triacylglycerols (triglycerides) and phosphoglycerides, which would be suitable for synthesizing certain lubricant base stocks. The production of deuterated materials from microorganisms offers advantages over the conventional catalytic hydrogen/deuterium exchange method including lower cost, higher atom-percent deuteration, and greater product purity. The conventional method of deuteration uses high-temperature and reducing conditions that may lead to degradation products, which cannot be separated easily and economically.

The conventional method for the determination of fatty acids in the lipid-fraction of biological material is the extraction of the triacylglycerols with organic solvents, followed by the saponification and esterification or the transesterification of the triacylglycerols to form the methyl esters of the fatty acids. The fatty acid methyl esters (FAMEs) can be quantified by gas

chromatography with either flame-ionization (GC/FID) or mass spectrometric (GC/MS) detection. There have been numerous reports of mass spectrometric determinations of triacylglycerols and FAMEs including electron ionization (EI) [3], GC/EIMS [4—6], and GC/chemical ionization (CI)MS [7]. For example, the identities of the acid portions of esters in essential oils, extracted from plant roots, were determined by GC/CIMS on the esters and detecting the $[RCOO]^-$ species, produced by reaction with the OH^- negative ion chemical ionization reagent [8]. These time-consuming procedures and the large number of algal samples generated in algal growth and lipid optimization studies in this laboratory required that a faster method of fatty acid screening in algal samples be found.

This paper reports a method, based on fast-atom-bombardment mass spectrometry (FABMS), for the rapid and direct determination of fatty acids of complex lipids in intact algal cells and other crude biological matrices. (Complex lipids are those lipids containing fatty acid moieties.) This method is relevant to many general problems of a similar nature in biotechnology, environmental science, and the medical sciences. Previously, FABMS has been used to profile fatty acids from lipids, the results of which were in excellent agreement with the results of gas chromatography on the FAMEs [9—11]. However, in all of these reports, extracted and/or purified lipid compounds were used. The use of the FABMS method for profiling fatty acids directly from vegetable oils (mixed triacylglycerols) is also demonstrated here. A recent method, chemical ionization/fast-atom-bombardment mass spectrometry (CI/FABMS) [12] is shown to enhance dramatically the ion abundances of the fatty acid species as well as the triacylglycerol molecular ions.

EXPERIMENTAL

Materials

Algal cultures were grown in mineral media in glass containers at 29°C with carbon dioxide supplied in a 5% (v/v) gaseous mixture with nitrogen. The total lipid content of the alga ranged from 20 to 70% dry weight. The cultures were agitated continuously and illuminated with fluorescent lamps. For deuterated organisms, the media were dissolved in redistilled deuterium oxide (99.8 atom % deuterium; Aldrich Chemical Co.) [13]. The organisms studied were *Scenedesmus obliquus* (University of Texas cultures) and *Chlorella vulgaris* (Crespi, Argonne National Lab.). For GC determinations, the algae were concentrated by centrifugation, heated briefly in boiling water to rupture the cells, and extracted with chloroform/methanol mixtures to obtain the crude lipid [14]. The FAMEs were obtained by transesterification with boron trifluoride in methanol [15].

Mixed triacylglycerols, glyceryl-1,2-palmitate-3-stearate (PPS) and glyceryl-1,2-stearate-3-palmitate (SSP) were used (Research Plus, Bayonne, NJ). The vegetable oil triacylglycerols were household brand-name products obtained commercially.

Instrumentation and methods

Gas chromatography of the FAMEs was done on a Hewlett-Packard 5830 gas chromatograph using a 10-ft., 2-mm-i.d. glass column packed with 10% SP-2330 on 100—120 Chromosorb (Supelco, Bellefonte, PA). Helium was used as the carrier gas with flame ionization detection. The column was heated from 200 to 230°C at 2°C min^{-1} with a 1-μl injection volume from 0.01—1.0 mg ml^{-1} sample solutions. The GC data represent averages of at least three runs.

A reverse-geometry, double-focusing mass spectrometer (ZAB-2F, VG Analytical, Manchester, England) was used for the FABMS experiments. Samples were prepared in a triethanolamine (TEA; Fisher Scientific, Fair Lawn, NJ) matrix and bombarded with an 8-keV xenon atom beam. All mass spectra were obtained at a resolving power of at least 1000. The mass spectral relative ion abundances of the carboxylate ions represent averages of at least 10 scans over a mass/charge ratio (m/z) in the 50—500 range. Approximately 1—10 mg of intact dried algal cells or 50 μl of a 1—3 mg ml^{-1} crude lipid extract solution was added to 100 μl of TEA so that 1—100 μg of total lipid was deposited on the probe tip for quantitation. The triacylglycerol vegetable oils were processed as neat samples. The sensitivity of the method was not determined.

The CI/FABMS experiments were done with a specially modified, closed FAB ion source with approximately 0.1 Torr of reagent gas. The sample was sputtered with an 8-keV xenon atom beam, which passed into the source through a small aperture. A conventional electron filament was used to ionize the reagent gas. The method has been described in detail elsewhere [16].

RESULTS AND DISCUSSION

It was found that negative-ion FABMS of intact algal cells suspended in a liquid matrix yielded abundant carboxylate ions, $[RCOO]^-$, corresponding to the fatty acids from the lipid compounds. In FABMS, these very stable carboxylate ions (also observed from the free acids [17]) arise from the fragmentation of complex lipid compounds such as a triacylglycerols:

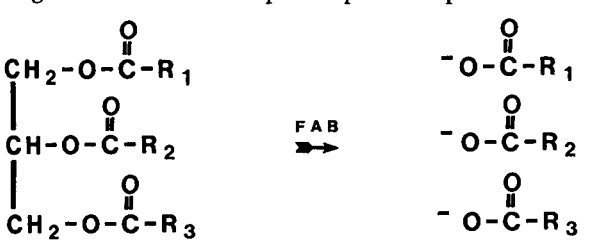

The FABMS measurement of the relative abundances of the carboxylate ions yielded semiquantitative data that compared well with results obtained by the GC/FID of the FAMEs. The FABMS determinations were done with little sample preparation resulting in a rapid procedure.

Proof of method

In order to establish if FABMS could be used for the semiquantitative determination of fatty acid moieties on triacylglycerols, the following experiments were done. The mixed triacylglycerol PPS, mixed in TEA, yielded the negative-ion FAB mass spectrum shown in Fig. 1. In addition to the ions from the TEA matrix (*m/z* 148, $[TEA - H]^-$, and *m/z* 297, $[2(TEA) - H]^-$), the carboxylate ions, $[RCOO]^-$, of the palmitate group (C_{16} with no double bonds, here labelled 16:0, *m/z* 255) and the stearate group (18:0, *m/z* 283) of the triacylglycerol PPS were observed. The ratio of the average relative abundances of these two ions (16:0/18:0) was measured to be 2.0 ± 0.2 from four experiments. This study was repeated for the triacylglycerol SSP with analogous results. The FABMS results were confirmed by GC applied to the corresponding FAMEs, and the accuracy and precision were similar to that of the FABMS result.

In addition to the $[RCOO]^-$ species observed for each acid moiety, an ion is observed at two atomic mass units below the $[RCOO]^-$ species. The abundances of these lower mass species are 5—15% of the $[RCOO]^-$ abundance, and apparently result from dehydrogenation during the FAB ionization process. The relative abundances of the fatty acid moieties reported here are not corrected for these contributions, because the semiquantitative data and correlation coefficients are not affected significantly by the correction.

It should be mentioned that the positive-ion FABMS of the triacylglycerols yielded abundant diacylglycerol ions, $[(M + H) - RCOOH]^+$, and low abundances of the ions corresponding to either the protonated triacylglycerol molecule, $[M + H]^+$, or the loss of water from the protonated molecule, $[(M + H) - H_2O]^+$. No abundant positive ions were observed from which the different fatty acid moieties could be determined directly and unambiguously. For this reason negative-ion FABMS was used for the fatty acid screening of algal lipids.

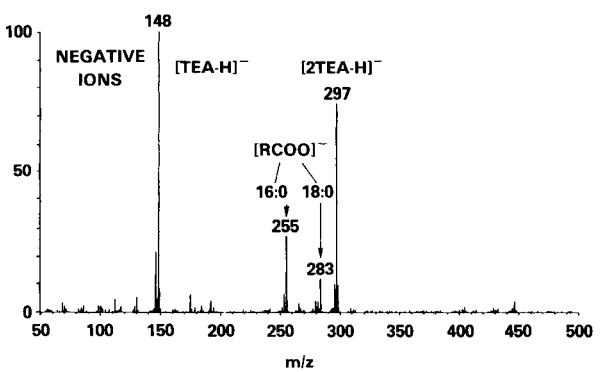

Fig. 1. Negative-ion/FAB mass spectrum of the mixed triacylglycerol, glyceryl-1,2-palmitate-3-stearate (PPS), in triethanolamine.

Algal samples

An example of FABMS of an algal sample is shown in Fig. 2. This algal sample, *Scenedesmus*, was grown in conventional water media, and the ions observed correspond to undeuterated fatty acid species. The mass spectrum obtained from the intact cells is shown in Fig. 2(a) where the most abundant carboxylate ions correspond to the oleate group (18:1, m/z 281) and the palmitate group (16:0, m/z 255). The $[2(TEA) - H]^-$ species is observed at m/z 297 also. The FAB mass spectrum of the crude lipid extract (Fig. 2b) is almost identical to that of the intact cells, indicating that no major changes in the composition of the lipids occurred by extraction (e.g., preferential extraction). The crude lipid extract provided a more concentrated sample; and consequently, greater ion abundances were observed in the FAB mass spectra (although the signal-to-noise ratio did not improve). Finally, the FAB mass spectrum of the algal residue, the material remaining after extraction, shown in Fig. 2(c) demonstrates that there is little unextracted fatty acid-containing material.

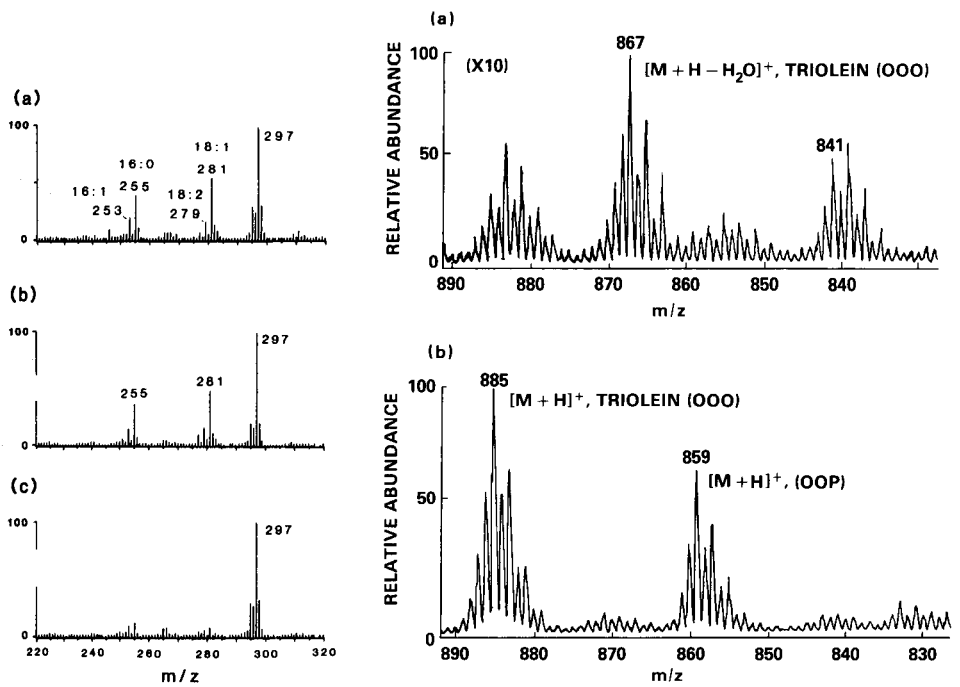

Fig. 2. Negative-ion/FAB mass spectra; (a) intact *Scenedesmus* cells in triethanolamine; (b) chloroform/methanol crude lipid extract of *Scenedesmus* cells in triethanolamine; (c) *Scenedesmus* extract residue in triethanolamine.

Fig. 3. (a) Positive-ion/FAB mass spectrum of the molecular ion region of neat olive oil. (b) Positive-ion isobutane chemical ionization/FAB mass spectrum of the molecular ion region of neat olive oil.

Deuterated algal samples were processed by FABMS in the same manner as above except that carboxylate ions were detected at m/z ratios corresponding to the deuterated analogs. Table 1 presents data obtained by FABMS of the algal cells compared with data obtained by the GC/FID of the corresponding FAMEs. These algal data represent different samples of *Scenedesmus* and *Chlorella* algal strains. Only the most abundant (>1%) fatty acid species are tabulated. Sample 1 is the only deuterated algal sample shown. It is evident from these and other data that the same fatty acids predominate [i.e., palmitate (16:0), oleate (18:1), and linoleate (18:2)] in deuterated and undeuterated samples. The correlation coefficients given in the last column indicate the excellent agreement between the data taken by the two methods.

The atom-% deuteration of the fatty acids was determined from the EI mass spectra obtained by GC/MS on the FAMEs. The atom-% deuteration of any of the fatty acids was calculated from the relative abundances of selected ions in the molecular ion region as described by Wendt and McCloskey [6]. The average atom-% deuteration for five samples was measured as 98.3 ± 0.5%.

TABLE 1

Comparison of results for fatty acids of complex lipids in various algal samples and in vegetable triacylglycerol oils

Sample	Method	Palmitic (16:0)	Hypogeic (16:1)	Stearic (18:0)	Oleic (18:1)	Linoleic (18:2)	Linolenic (18:3)	Correl. coeff.
Algal samples								
1[a]	FABMS	20	5.4	1.9	48	18	6.7	0.99
	GC/FID	18	2.0	1.4	56	16	6.2	
2	FABMS	52	9.1	2.2	5.6	19	12	0.93
	GC/FID	39	7.1	2.6	7.3	25	19	
3	FABMS	36	7.4	5.2	45	5.1	1.3	0.99
	GC/FID	35	6.2	3.1	48	4.3	3.3	
4	FABMS	39	11	2.2	21	7.8	19	0.99
	GC/FID	42	7.1	1.6	20	8.3	20	
5	FABMS	37	7.1	3.4	28	16	8.5	0.95
	GC/FID	32	3.3	2.7	32	17	13	
Vegetable oils								
Olive	GC/FID	11	1.2	2.5	70	14	1.3	1.0
oil	FABMS	12	4.1	5.9	58	17	3	1.0
	Normal[b]	16.6	4.4	3.1	57.1	18.8	—	
Corn	GC/FID	9.7	—	2.2	27	58	3.1	1.0
oil	FABMS	10	—	4.0	27	52	7.0	1.0
	Normal[b]	11.2	—	3.1	27.0	56.8	1.9	
Sun-	GC/FID	5.8	—	3.2	19	72	—	0.99
flower	FABMS	9.5	—	7.5	25	59		0.98
oil	Normal[b]	7.6	—	4.4	15.7	73.3	—	

[a]98 atom-% deuteration. [b]Conventional method [18].

The negative-ion FAB spectra of the $[RCOO]^-$ region also allowed the atom-% deuteration to be quantified, and yielded values similar to the GC/MS data. It is interesting to note that no hydrogen/deuterium exchange was observed for deuterated samples that were processed by FABMS in triethanolamine, even with extensive bombardment.

The amounts and types of fatty acids from the deuterated algal samples, including the variation of lipid production with growth conditions, will be reported elsewhere.

Triacylglycerol oils

The vegetable oils (olive, corn, and sunflower), which consist mainly of various triacylglycerols, were analyzed for fatty acids by negative-ion FABMS. These data are also presented in Table 1, where they are compared with the results of GC/FID determination of the FAMEs and with data obtained by conventional methods [18]. The positive-ion FAB mass spectra of the vegetable oils yielded abundant diacylglycerol ions, $[(M + H) - RCOOH]^+$, and low abundances of molecular-like ions. Again, negative ion FABMS yielded the abundant carboxylate negative ions, $[RCOO]^-$, which were used to determine the relative amounts of fatty acids. The data obtained by the three methods are in good agreement.

The application of the recent CI/FABMS method [12, 16] to the triacylglycerol oils is of interest. In this method, a chemical-ionization reagent gas is admitted to a closed FAB source that has an electron filament to ionize the gas to give reagent ions. The sample is bombarded with a fast xenon atom beam, and sample species (ions and neutrals) are sputtered into the CI reagent plasma where post-desorption processes such as collisional stabilization, charge-exchange reactions, and chemical ionization can occur. The chemical ionization of the abundant sputtered neutrals increases the abundance of sample ions. The use of a H_2/N_2O mixture to produce OH^- reagent ions for negative-ion CI/FABMS of olive oil has been reported [16]. The OH^- CI/FABMS experiments yielded carboxylate ions that were approximately 300 times more abundant than those in the regular FAB mass spectra.

In addition to fatty acid profiling, it is useful to determine the parent triacylglycerol compounds in the vegetable oils. Figure 3 presents a comparison of the molecular ion region of the mass spectrum obtained by FABMS vs. that obtained with isobutane CI/FABMS of olive oil. The most abundant ions in the molecular ion region of the FAB mass spectrum correspond to $[(M + H) - H_2O]^+$ species (Fig. 3a), which are observed in the EI mass spectrum [3]. The ion abundances in this FAB spectrum (Fig. 3a) have been multiplied by 10 to allow direct comparison to the CI/FAB mass spectrum. The isobutane CI/FABMS (Fig. 3b) produces abundant protonated molecular species such as $[M + H]^+$ (m/z 885) for triolein (OOO) (or glyceryl-1,2,3-oleate) and $[M + H]^+$ (m/z 859) for glyceryl-1,2-oleate-3-palmitate (OOP). The abundances of the $[M + H]^+$ species in the CI/FAB mass spectrum

are approximately 40-fold greater than the abundances in the conventional FAB mass spectrum, where observation of the $[M + H]^+$ species is questionable. In addition to using isobutane for the observation of protonated molecular species, ammonia was used to produce not only $[M + H]^+$ but also $[M + NH_4]^+$ species. Therefore, the positive-ion CI/FABMS allows the direct determination of the parent triacylglycerol species.

Conclusions

The major difference between the two methods, FABMS and GC, used for the fatty acid profiling of complex lipids in algal cultures is the time required for the analysis. Algal sample preparation for GC requires extraction, purification, and esterification to yield the FAMEs. For FABMS the algal culture need only be dried (and extracted if the crude lipid extract is required for a more concentrated sample). In general, the time needed for preparation of an algal sample for GC/FID was 3—4 times longer than that for FABMS. These FABMS procedures can be done on a less sophisticated mass spectrometer, such as a quadrupole instrument, to achieve the same results at a lower cost.

The quantitation of FAMEs by GC offers the advantages of selectivity, nanogram detection, and quantitative results. The time-consuming nature of the method is a serious drawback when a large number of samples needs to be processed, for example, in a research and development environment. The determination of fatty acids from algal lipids by FABMS is a more direct and rapid method requiring little sample preparation. Other algal cell constituents (e.g., pigments) can be determined by FABMS, making it a more flexible and versatile method than GC. In a similar application reported recently, FABMS was used for the rapid and direct (compared to GC) screening of tricothecene mycotoxins from crude fungal extracts [19].

The authors gratefully acknowledge H. L. Crespi of Argonne National Lab. for furnishing the deuterated algal cultures and for helpful advice. The authors thank the Naval Air Systems Command, the Naval Sea Systems Command, and the Air Force Wright Aeronautical Laboratories Material Laboratory (Directors Funding) for support of this program. This paper was presented in part at the 1985 Pittsburgh Conference, New Orleans, LA, February 1985.

REFERENCES

1 P. H. Abelson (Ed.), Biotechnology and Biological Frontiers, The American Association for the Advancement of Science, Washington, D.C., 1984.
2 J. E. Campana, High-Temperature Deuterated Lubricants: Additives Mechanisms and Methods, NRL Report 8779, Naval Research Laboratory, Washington, D.C., December, 1983.
3 R. A. Hites, Anal. Chem., 42 (1970) 1736.

4 T. Murata and S. Takahashi, Anal. Chem., 45 (1973) 1816.
5 T. Rezanka, J. Volkoun, J. Slavicek and M. Podojil, J. Chromatogr., 268 (1983) 71.
6 G. Wendt and J. A. McCloskey, Biochemistry, 9 (1970) 4854.
7 T. Murata and S. Takahashi, Anal. Chem., 49 (1977) 728.
8 H. Hendriks and A. P. Bruins, J. Chromatogr., 190 (1980) 321.
9 M. E. Hemling, R. K. Yu, D. Sedgewick and K. L. Rinehart, Jr., Biochemistry, 23 (1984) 5706.
10 W. D. Lehmann and J. Kessler, Chem. Phys. Lipids, 32 (1983) 123.
11 M. Arita, M. Iwamara, T. Higuchi and Y. Nagai, Biochemistry, 95 (1984) 971.
12 J. E. Campana and R. B. Freas, J. Chem. Soc. Chem. Commun., (1984) 1414.
13 W. Chorney, N. J. Scully, H. L. Crespi and J. J. Katz, Biochim. Biophys. Acta, 37 (1980) 280.
14 E. G. Bligh and W. J. Dyer, Can. J. Biochem. Biophysiol., 37 (1959) 911.
15 W. R. Morrison and L. M. Smith, J. Lipid Res., 5 (1964) 600.
16 R. B. Freas, M. M. Ross and J. E. Campana, J. Am. Chem. Soc., 107 (1985) 6195.
17 K. B. Tomer, F. W. Crow and M. L. Gross, J. Am. Chem. Soc., 105 (1983) 5487.
18 E. C. Horning, A. Karmen and G. C. Sweeley in R. T. Holman (Ed.), Progress in the Chemistry of Fats and other Lipids, Vol. VII, MacMillan, New York, 1964, p. 167.
19 J. R. J. Pare, R. Greenhalgh, P. Lafontaine and J. W. ApSimon, Anal. Chem., 57 (1985) 1470.

Analytica Chimica Acta, 181 (1986) 159—168
Elsevier Science Publishers B.V., Amsterdam — Printed in The Netherlands

PRECONCENTRATION BY DITHIOCARBAMATE EXTRACTION FOR DETERMINATION OF TRACE ELEMENTS IN NATURAL WATERS BY INDUCTIVELY-COUPLED PLASMA ATOMIC EMISSION SPECTROMETRY

MASAHITO SUGIYAMA, OSAMU FUJINO[a], SORIN KIHARA and MASAKAZU MATSUI*

Institute for Chemical Research, Kyoto University, Uji, Kyoto 611 (Japan)

(Received 15th April 1985)

SUMMARY

Preconcentration by dithiocarbamate extraction into 2-ethylhexyl acetate for simultaneous determination of trace elements in natural water is described. After 250-fold concentration, the organic phase is used directly for inductively-coupled plasma atomic emission spectrometry. Thirteen elements (As, Se, Mo, Zn, Cd, Ni, Co, Sn, Fe, Cr(VI), Pb, V and Cu) are simultaneously concentrated at pH 4.3 with the combination of ammonium tetramethylenedithiocarbamate and dibenzylammonium dibenzyldithiocarbamate and are determined in the extract; Mn and Cr(III) are also determined after preconcentration at pH 6.9 with the same chelating agents. Lake waters are analyzed by this method.

The simultaneous determination of trace elements in natural waters is not only convenient but also very useful for studies in geochemistry or environmental chemistry, because both absolute and relative concentrations among the elements can be obtained. From this point of view, inductively-coupled plasma atomic emission spectrometry (i.c.p.a.e.s.) which is capable of simultaneous multi-element determination is excellent for the determination of trace elements in natural waters. However, the concentrations of many elements are very low, and thus preconcentration techniques such as liquid-liquid extraction [1—4], coprecipitation [5, 6], chelating ion-exchange [7] or solvent evaporation [8] are required. Consequently, it is desirable to develop a simple, rapid and reliable preconcentration method which has as high an enrichment factor as possible and can be applied to as many elements as possible.

It is well known that dithiocarbamates form complexes with many elements which are extracted into an organic phase with a high distribution ratio [9—12]. Therefore, dithiocarbamates are one of the most suitable classes of chelating agents for simultaneous multi-element extraction. The

[a]Present address: Research Institute for Science and Technology, Kinki University, Higashi-Osaka, Osaka 577, Japan.

0003-2670/86/$03.50

use of a number of dithiocarbamates, e.g., sodium diethyldithiocarbamate [1, 13], diethylammonium diethyldithiocarbamate (DEADEDC) [2, 14], ammonium tetramethylenedithiocarbamate (ATMDC) [2, 4] and hexamethyleneammonium hexamethylenedithiocarbamate (HMAHMDC) [3, 4] have been reported.

In this paper, a preconcentration method with a 250-fold enrichment factor by dithiocarbamate extraction is reported. Four dithiocarbamates [DEADEDC, ATMDC, HMAHMDC and dibenzylammonium dibenzyldithiocarbamate (DBADBDC)] are examined.

EXPERIMENTAL

Apparatus and reagents

A Japan Jarrell-Ash model 96-953 inductively-coupled plasma emission spectrometer was used. Some properties of the instrumentation are shown in Table 1.

All chemicals were of reagent grade. Deionized/distilled water was used. Organic solvents were shaken twice with 1 M nitric acid and then washed a few times with pure water. Impurities in aqueous solution of DEADEDC or ATMDC were removed by shaking with 2-ethylhexyl acetate. The DBADBDC was prepared by the method of Moore [15] and dissolved in 2-ethylhexyl acetate. The HMAHMDC was dissolved in methanol and DEADEDC and ATMDC in water. Dithiocarbamates except for DBADBDC were added to the aqueous phase. Buffer solutions were prepared by mixing 1 M acetic acid and 1 M ammonia in the appropriate ratios, and were purified by ATMDC extraction into 2-ethylhexyl acetate.

Stock solutions (1000 mg l^{-1}) of the elements except for Se, Mo, Cr(VI), V, Zr and As were prepared by dissolving their salts in nitric or hydrochloric acid. Those of Se, Mo, Cr(VI), V and Zr were prepared by dissolving selenium dioxide in pure water, ammonium molybdate in pure water, potassium dichromate in hydrochloric acid, ammonium vanadate in sulfuric acid and zirconium oxychloride in hydrochloric acid, respectively. For the arsenic stock solution, arsenic(III) oxide was dissolved in sodium hydroxide solution and hydrochloric acid was added.

TABLE 1

Instrumental properties

Plasma		Spectrometer	
Frequency	27.12 MHz	Focal length	0.75 m
Nebulizer	Cross-flow type	Grating	2400 grooves mm^{-1}
		Reciprocal linear dispersion	0.53 nm mm^{-1}
		Entrance slit-width	25 μm
		Exit slit-width	50 μm

Extraction procedure

A representative procedure adopted for the determination of trace elements in lake water is as follows. In order to prevent adsorption of trace elements on the container surface, the lake water sample was acidified to pH 1.0 by the addition of nitric acid. The sample was filtered through 0.4-μm Nuclepore filters as soon as possible, in order to minimize the release of trace elements from particulate material. A 2500-ml sample was placed in a 3000-ml separatory funnel, and 25 ml of 2% (w/v) ATMDC solution was added. The pH was adjusted to the desired value (4.3 ± 0.1 or 6.9 ± 0.1) with ammonia and 25 ml of 1 M buffer solution was added. After the addition of 10 ml of 2-ethylhexyl acetate containing 5% (w/v) DBADBDC, the mixture was shaken for 1 h. The organic phase was separated after standing for 10 min and was used directly for i.c.p.a.e.s.

Measurement of extraction efficiency

The first extraction was done by the above procedure. A 2000-ml portion of aqueous phase was transferred to another separatory funnel and 8 ml of 2-ethylhexyl acetate containing 5% (w/v) DBADBDC was added. A second extraction was done under the same conditions as the first. The two organic extracts were used for i.c.p.a.e.s. Extraction efficiency, E (%), was calculated from the equation $E = 100(I_1 - I_2)/I_1$, where I_1 and I_2 are the emission intensities of the first and second organic extracts, respectively.

RESULTS AND DISCUSSION

Selection of organic solvent

The organic solvent to be used in this method should have the following characteristics. Its solubility in water should be very low, because the extraction must be done at a high volume ratio. It should be easy to introduce into the plasma, and not affect plasma stability, because the organic phase is used directly for i.c.p.a.e.s. 2-Ethylhexyl acetate, *o*-dichlorobenzene and *p*-xylene were examined. Their losses by dissolution in water in the procedure described above were about 2%, 3% and 5%, respectively.

Effect of pH on the extraction of trace elements

Figure 1 shows the effect of pH on the extraction into 2-ethylhexyl acetate with DEADEDC, ATMDC, HMAHMDC or DBADBDC alone. Seven ions (Cd, Ni, Fe(III), Mn, Cr(III), V and Cu) were studied and mixed standard solutions were prepared from individual stock solutions, each at 100 μg l^{-1}, except for the ATMDC extraction. The efficiency of ATMDC extractions decreased above 20 μg l^{-1} for each element, and concentrations of 10 μg l^{-1} were therefore used. Distribution of Cd, Ni, Fe, Mn, V and Cu reached equilibrium within 1 h in every extraction system. Equilibrium was not achieved with chromium even after 4 h. Nevertheless, the shaking time was set at 1 h.

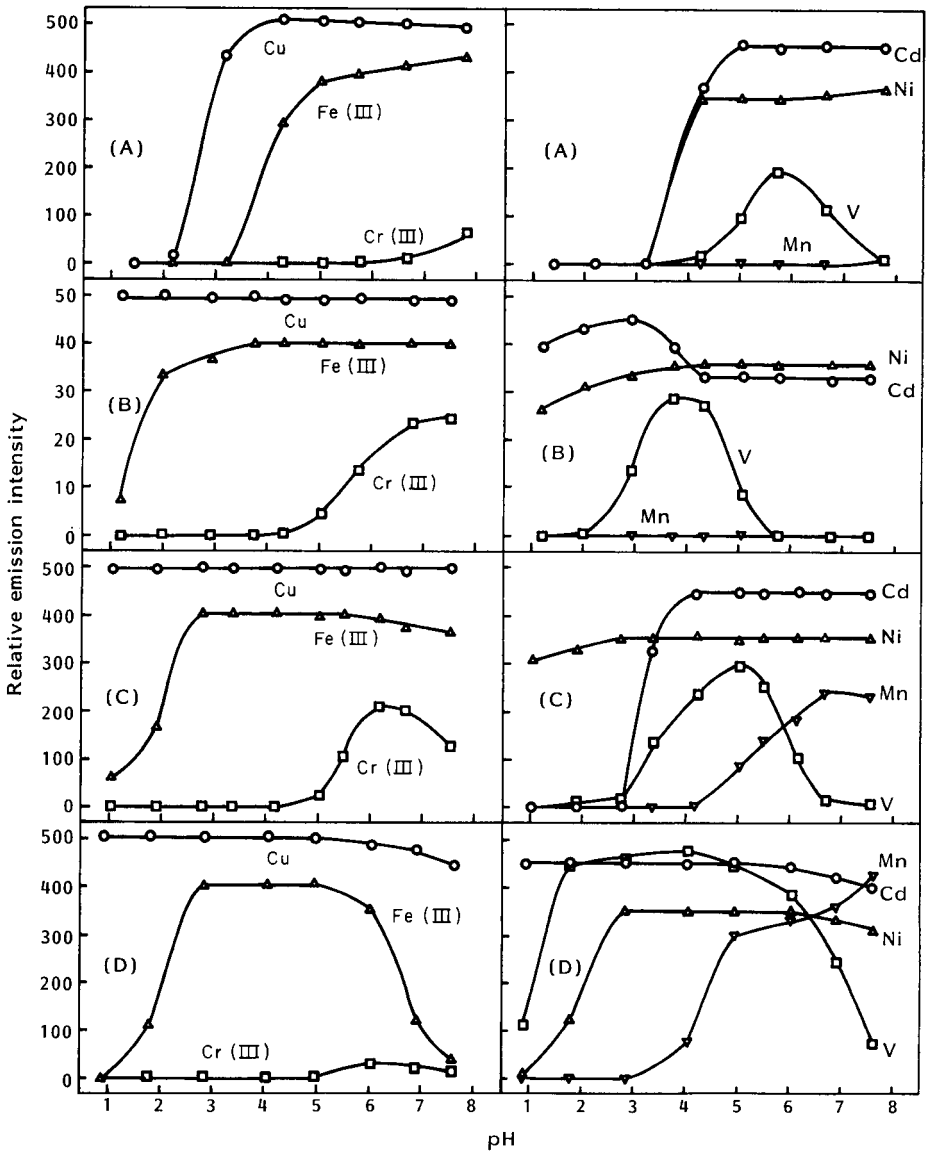

Fig. 1. Effect of pH on extraction with dithiocarbamates: (A) DEADEDC; (B) ATMDC; (C) HMAHMDC; (D) DBADBDC. Dithiocarbamate concentration: (A—C) 0.02% (w/v) in aqueous phase, (D) 5% (w/v) in organic phase. Concentration of each element: (A, C, D) 100 $\mu g\ l^{-1}$; (B) 10 $\mu g\ l^{-1}$.

As shown in Fig. 1, Cd, Ni, Fe and Cu were extracted well compared to V, Cr or Mn, and there were pH regions in which the extraction efficiencies were independent of pH. However, extractions of V, Cr and Mn were significantly affected by pH and efficiencies were poor except for V and Mn by DBADBDC extraction.

It has been reported that a combination of dithiocarbamates is effective for the quantitative extraction of a number of trace elements [2, 4, 14]. Therefore, the synergic effects of these dithiocarbamates were investigated, with the results shown in Fig. 2. A combination of ATMDC and DBADBDC was the most efficient extractant, and pH regions of constant extraction efficiency also existed for V, Mn and Cr. *o*-Dichlorobenzene and *p*-xylene were used instead of 2-ethylhexyl acetate to investigate the effect of the organic solvent, but they gave poorer extractions. Consequently, ATMDC/DBADBDC extraction into 2-ethylhexyl acetate was selected as the best system.

Figure 3 shows the effect of pH on the extraction of the other elements. Extractions of titanium and zirconium were more sensitive to pH than those

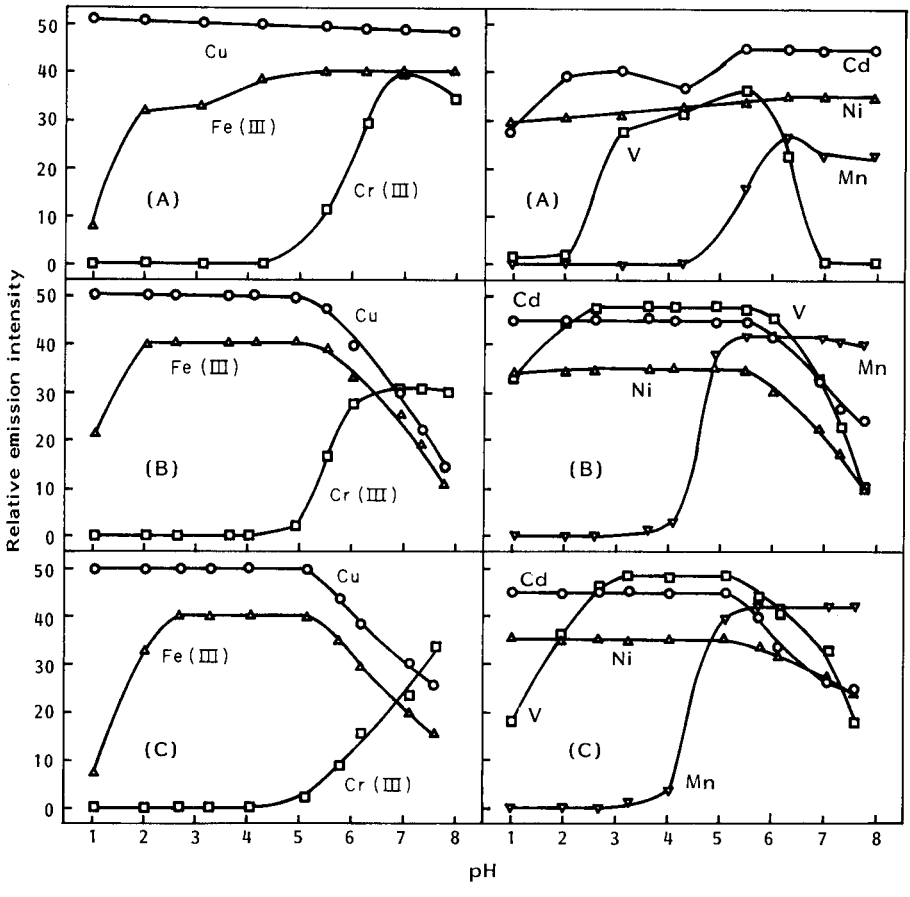

Fig. 2. Effect of pH on extractions with combinations of dithiocarbamates: (A) ATMDC/HMAHMDC; (B) ATMDC/DBADBDC; (C) HMAHMDC/DBADBDC. Dithiocarbamate concentration: ATMDC and HMAHMDC each at 0.02% (w/v) in aqueous phase; DBADBDC at 5% (w/v) in organic phase. Concentration of each element was 10 $\mu g\ l^{-1}$.

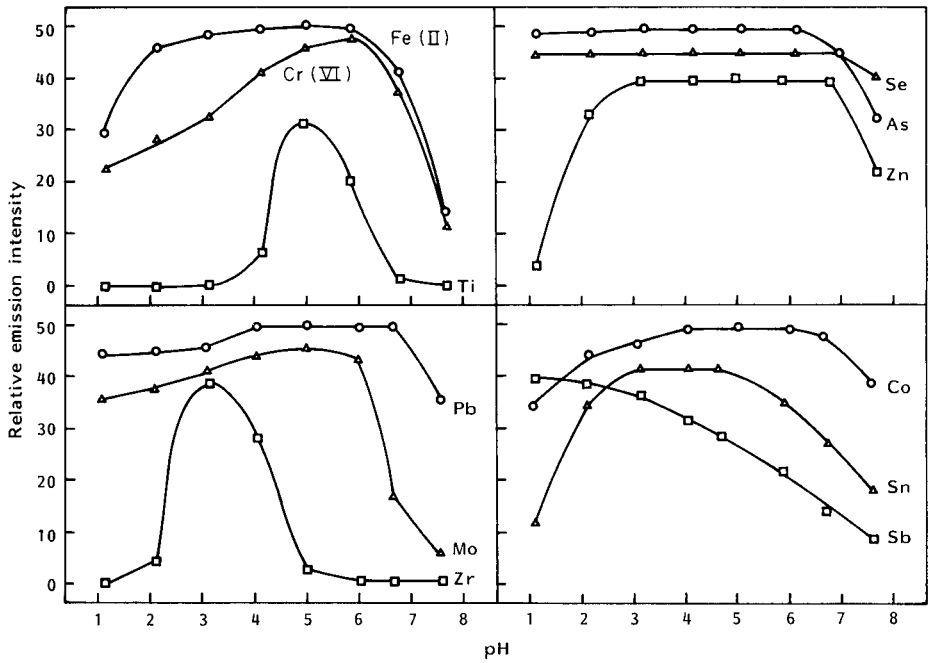

Fig. 3. Effect of pH on extractions with ATMDC/DBADBDC. Dithiocarbamate concentration: 0.02% (w/v) ATMDC in aqueous phase, 5% (w/v) DBADBDC in organic phase. Concentration of each element was 10 $\mu g\ l^{-1}$.

of the other elements, and the extraction of antimony was not satisfactory. However, for all other elements, there are pH regions where the relative emission intensities are scarcely affected by pH. The results in Figs. 2(B) and 3 indicate that thirteen elements (As, Se, Mo, Zn, Cd, Ni, Co, Sn, Fe, Cr(VI), Pb, V and Cu) are simultaneously extracted at pH 4.1—4.6, and Mn and Cr(III) are extracted at pH 6.9—7.0. Speciation of iron is not possible, because Fe(II) and Fe(III) are simultaneously extracted at pH 4.3. At pH 6.9, about 60% of Cr(VI) is extracted together with Cr(III), and thus interferes in the determination of Cr(III). Therefore, it is necessary to separate Cr(VI) at pH 4.3 before extraction of Cr(III) at pH 6.9, or to correct the Cr(III) value for the Cr(VI) concentration.

Extraction efficiencies and detection limits

Extraction efficiencies, detection limits and working pH regions for each element are listed in Table 2. Detection limits were calculated as the concentrations which gave intensities three times the standard deviation of the blank intensity on the basis of a 250-fold enrichment factor. The extraction efficiencies for all the elements except for Mn and Cr were >96%. The low extraction efficiency for Cr(III) is probably caused by its very slow exchange reactions with chelating reagents. However, if the extractions

TABLE 2

Characteristics of the analytical procedure with ATMDC/DBADBDC extraction

Species	Extraction efficiency (%)	Detection limit (ng l^{-1})	Working pH region	Species	Extraction efficiency (%)	Detection limit (ng l^{-1})	Working pH region
As	99	620	3.1—5.8	Mn	91	7	5.5—7.0
Se	99	810	3.1—6.7	Fe(II)	98	9	4.1—5.8
Mo	99	73	4.1—6.0	Fe(III)	99	5	2.1—5.0
Zn	98	63	3.1—6.7	Cr(III)	43	22	6.9—7.8
Cd	96	9	1.1—5.5	Cr(VI)	89	12	4.1—4.6
Ni	99	46	2.6—5.5	Pb	98	260	4.1—6.6
Co	99	13	4.1—6.0	V	98	5	2.6—5.0
Sn	96	93	3.1—4.6	Cu	99	2	2.1—5.0

are done under strictly controlled conditions, the accurate determination of Cr(III) is possible. The extraction efficiency for the elements was constant at all the concentrations tested, and the calibration graphs were linear from the detection limit upto at least 100 $\mu g\ l^{-1}$ for any of these elements. The log/log calibration plots for Cd, Ni, Fe(III), Cr(VI), V and Cu are shown in Fig. 4.

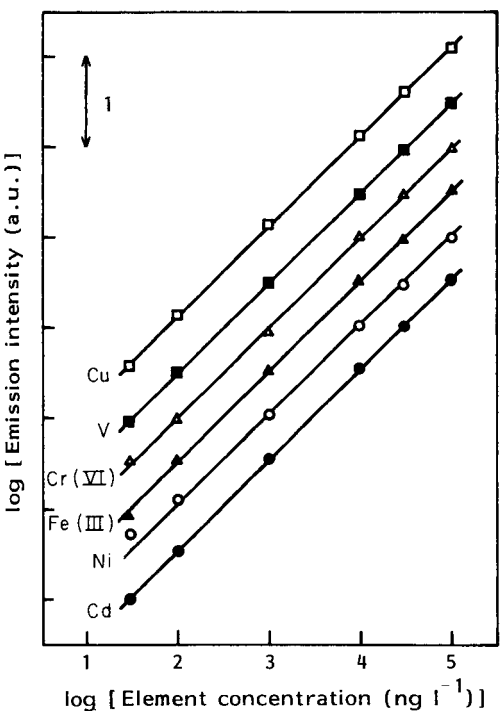

Fig. 4. Log/log calibration graphs for ATMDC/DBADBDC extraction. Intensity is given in arbitrary units.

TABLE 3

Precision of the procedure with ATMDC/DBADBDC extraction (1 $\mu g\ l^{-1}$ for each element)

Species	Cd	Ni	Fe(III)	Cr(VI)	V	Cu
Mean intensity[a]	14720	352	8470	8274	13833	11222
S.d.	54	20	92	37	85	64
R.s.d. (%)	0.4	5.7	1.1	1.0	0.6	0.6

[a]Mean emission intensity (of figure) given in arbitrary units.

The detection limits for As, Se and Pb are relatively high compared to those for the other elements. However, with reference to a previous report [16], the values in Table 2 are adequate for the determination of trace elements in lake water. To investigate the precision of this method, five samples containing 1 $\mu g\ l^{-1}$ of each element were analyzed. The results are shown in Table 3. The r.s.d. for all elements apart from nickel was ca. 1%.

Analysis of lake water

After filtration of the lake water samples collected from Lake Biwa and standard additions, the samples were analyzed by the proposed method. The results for Mo, Zn, Ni, Pb, V and Cu are shown in Fig. 5. The slopes of the standard additions plots agree very closely with that of the calibration graph obtained by extraction from distilled/deionized water. The concentra-

TABLE 4

Trace element concentrations ($\mu g\ l^{-1}$) in Lake Biwa

Species	Station 1			Stn. 2	Stn. 3	Stn. 4
	0 m[a]	40 m	80 m	0 m	0 m	0 m
As	<0.6	<0.6	<0.6	<0.6	<0.6	<0.6
Se	<0.8	<0.8	<0.8	<0.8	<0.8	<0.8
Mo	0.28	0.26	0.38	0.28	0.40	0.47
Zn	1.9	2.6	2.1	<0.06	1.4	3.8
Cd	<0.01	1.0	<0.01	<0.01	1.0	<0.01
Ni	0.25	0.27	0.33	0.18	0.37	0.52
Co	0.03	0.03	<0.01	0.09	0.33	0.70
Sn	<0.09	<0.09	<0.09	<0.09	0.16	0.25
Mn	4.7	8.4	12	4.2	22	33
Fe	13	11	5.6	14	100	160
Cr(III)	0.05	0.06	0.03	0.04	0.05	0.09
Cr(VI)	<0.01	<0.01	<0.01	0.02	0.02	0.04
Pb	0.28	<0.26	<0.26	<0.26	0.39	0.46
V	0.14	0.08	0.06	0.15	0.20	0.30
Cu	1.0	0.85	1.3	0.55	0.80	1.1

[a]Depth.

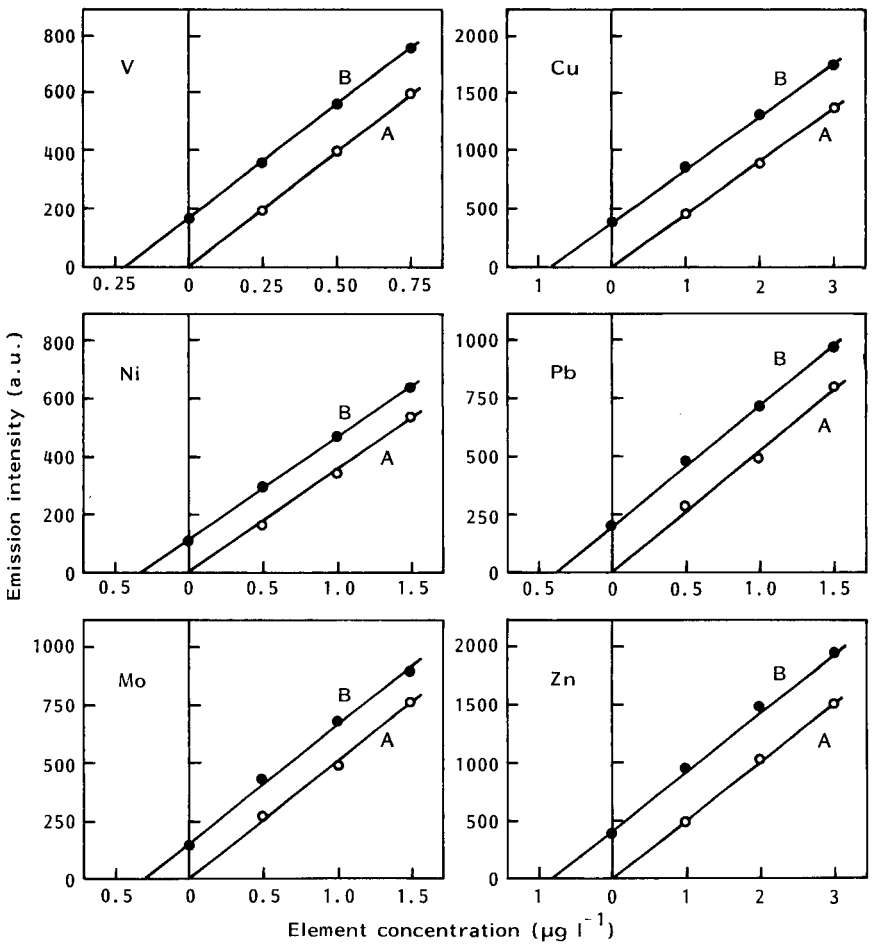

Fig. 5. Standard additions and calibration graphs for trace elements in lake water: (A) extraction from distilled/deionized water; (B) extraction from lake water (Lake Biwa).

tion obtained from the calibration graph was also in good agreement with that obtained by the standard addition method for any element. These results indicate that several trace elements in lake water can be determined easily, accurately and simultaneously by this method.

Table 4 shows the results for the trace elements in the Lake Biwa water, which generally are low compared to those in the previous report [16]. The concentrations of As and Se were below the detection limits in all the samples. The values for Zn and Co have poor reproducibility; the blank value for zinc is high compared to that for the other elements because of contamination, and the determination of cobalt is affected by the presence of abundant iron. Manganese and iron were also measured directly with i.c.p.a.e.s. The results agreed well with those listed in Table 4.

REFERENCES

1 A. Sugimae, Anal. Chim. Acta, 121 (1980) 331.
2 C. W. McLeod, A. Otsuki, K. Okamoto, H. Haraguchi and K. Fuwa, Analyst (London), 106 (1981) 419.
3 A. Miyazaki, A. Kimura, K. Bansho and Y. Umezaki, Anal. Chim. Acta, 144 (1982) 213.
4 H. Tao, A. Miyazaki, K. Bansho and Y. Umezaki, Anal. Chim. Acta, 156 (1984) 159.
5 M. Hiraide, T. Ito, M. Baba, H. Kawaguchi and A. Mizuike, Anal. Chem., 52 (1980) 804.
6 A. S. Buchanan and P. Hannaker, Anal. Chem., 56 (1984) 1379.
7 A. Miyazaki and R. M. Barnes, Anal. Chem., 53 (1981) 299.
8 M. Thompson, M. H. Ramsey and B. Pahlavanpour, Analyst (London), 107 (1982) 1330.
9 A. Hulanicki, Talanta, 14 (1967) 1371.
10 A. Wyttenbach and S. Bajo, Anal. Chem., 47 (1975) 2.
11 A. Wyttenbach and S. Bajo, Anal. Chem., 47 (1975) 1813.
12 S. J. Yeh, J. M. Lo and L. H. Shen, Anal. Chem., 52 (1980) 528.
13 O. Fujino, M. Matsui and T. Shigematsu, Mizu Shori Gijutsu, 20 (1979) 201.
14 B. Magnusson and S. Westerlund, Anal. Chim. Acta, 131 (1981) 63.
15 R. V. Moore, Anal. Chem., 54 (1982) 895.
16 A. Kurata, Umi, 20 (1982) 21.

Analytica Chimica Acta, 181 (1986) 169—178
Elsevier Science Publishers B.V., Amsterdam — Printed in The Netherlands

PYROLYTIC CARBON COATING METHOD FOR CONTOURED GRAPHITE TUBES AND THEIR USE IN FURNACE ATOMIC ABSORPTION SPECTROMETRIC DETERMINATION OF BORON AND URANIUM

ELSA NORVAL

National Institute for Materials Research, CSIR, P.O. Box 395, Pretoria, 0001 (South Africa)

(Received 2nd February 1985)

SUMMARY

Tubes are machined from rods of suitable graphite according to a modified design so that there is a recess of 20-μl capacity in the inner surface at the tube centre; this improves reproducibility and sensitivity. Pyrolytic carbon coating is accomplished independently of the atomic absorption instrument by using a simple apparatus (dimensions are given). Tube lifetimes are considerably longer than those of both coated and uncoated commercial tubes. The coated tubes described have lifetimes long enough at high atomizing temperatures to determine uranium and boron on a routine basis. The boron memory is eliminated and that of uranium successfully controlled. The addition of organic solvents to the analyte solution to enhance sensitivity for uranium is reported.

A major problem encountered in graphite-furnace atomic absorption spectrometry is inadequate tube life under severe analytical conditions. The factors which shorten tube lifetimes are elevated atomization temperatures which cause erosion, mainly by oxidation of the outer tube surface, and chemical attack by the analyte and/or its matrix, which chiefly affects the inner surface.

It is well known that many elements exhibit enhanced sensitivity with tubes having a pyrolytic coating and that this is particularly true of refractory elements. Pyrolytic carbon is hard, dense and much more resistant to oxidation and carbide formation than is graphite. This type of carbon is classified as a turbostratic carbon by Bokros, who has described it in detail [1]. As commercially coated tubes have a thin coating layer and have been observed to deteriorate rapidly under severe conditions, several coating methods have been described [2—5]. In all these cases, tubes are coated in the spectrometer with incomplete shielding from the atmosphere, and the emphasis has been more on enhancement of sensitivity for particular elements than on extension of tube lifetimes. Sturgeon and Chakrabarti [6] evaluated tubes obtained from UltraCarbon Corporation, but no particulars were given regarding the coating method.

It has been found more satisfactory to have a separate and simple apparatus for coating tubes reproducibly, and independently of the atomic absorption spectrometer. This paper describes such an apparatus, gives the dimensions of the contoured tubes used, and reports on the application of these coated tubes to determinations of boron and uranium.

EXPERIMENTAL

Coated contoured tubes and other equipment

The modified shape and the dimensions of tubes which were machined from UltraCarbon UF-4S graphite rods are given in Fig. 1. There are no ridges on the inner surface at the tube ends (such as the commercial tubes have) but at the centre there is a recess with a 20-μl capacity which prevents sample spreading. The 2.6-mm diameter sample introduction hole is larger than that of the commercial tubes.

Tubes were coated by means of resistive heating and thermal decomposition of methane. A welding transformer was used to supply 230 A for four successive 10-min periods followed by one of 250 A for 2 min. Tubes were allowed to cool and were inverted after each 10-min period. Temperatures were about 1900 and 2000°C at the tube centre, and about 250°C lower at the ends. However, the centre of the tube is the main site of erosion. The apparatus is depicted in Figs. 2 and 3. Tube ends were supported by copper and graphite holders with water cooling to prevent the copper from getting too hot at the graphite contact surface. There were two graphite supports at each end: one more solid which fitted into the copper tube and had a gas channel and a second hollow support fitting over the first one. This type of support was found to be necessary to ensure that the tube ends reached a temperature sufficiently high for deposition of an adequate coating. (The first signs of erosion always appeared around the sample introduction hole.) Sixteen small channels supplied a laminar gas flow around the outer tube surface. The graphite endpieces were easily replaceable when the contact surfaces became worn. Tube and holders were surrounded by a quartz tube which slid over two O-rings. Two streams of high-purity gas were mixed to flow through the quartz tube, one of nitrogen and one of a 10% methane/

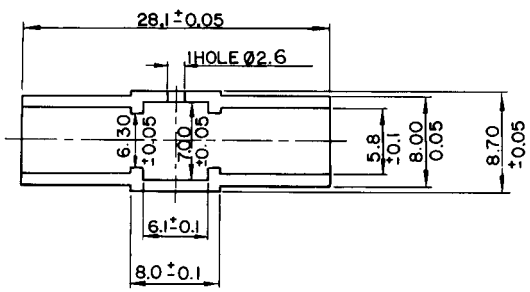

Fig. 1. Modified graphite tube (dimensions in mm).

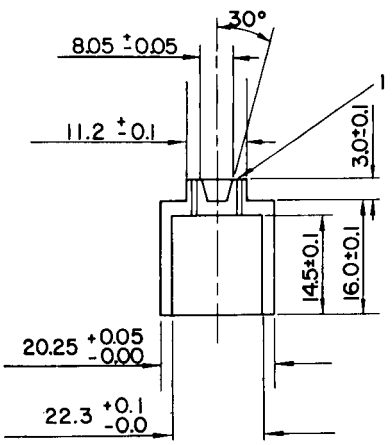

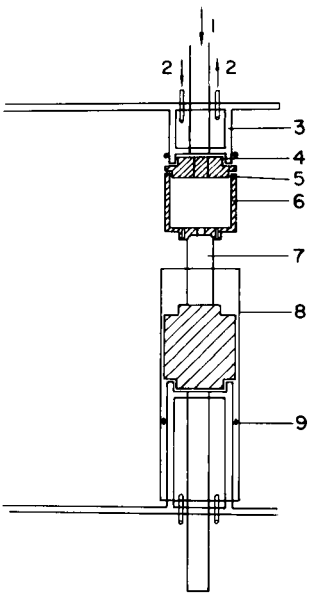

Fig. 2. Graphite endpieces for supporting the tube during coating: (1) 16 holes for laminar gas flow; diameter 0.5 mm at gas inlet and 0.75 mm at gas outlet.

Fig. 3. Pyrolytic coating apparatus: (1) gas; (2) water cooling; (3) copper; (4) press fit; (5) sliding fit; (6) graphite; (7) tube; (8) quartz tube; (9) O-ring.

90% argon mixture. Total gas flow was ca. 6 l min^{-1} and the ratio of nitrogen to methane/argon was ca. 3:1.

Under the conditions described, a total of about 170 mg of pyrolytic carbon was applied to both inner and outer tube surfaces. Masses applied were controlled by the flow of methane/argon and could be checked by weighing after each 10-min heating period. Coatings adhered less well when applied more rapidly than described above.

The results were obtained using a Perkin-Elmer AA-5000 spectrometer equipped with an HGA-500 furnace, an AS-40 sampler and PRS-10 printer. The parameters used for tube lifetime tests (copper in 10% v/v nitric acid) and for determination of boron and uranium are given in Table 1.

Preparation of samples and standards for boron determination

To 1 g of steel sample was added 15 ml of (9 + 1) H_3PO_4/H_2SO_4 mixture. Samples were heated gently and then more strongly until fumes appeared, when a further 10 ml of acid solution was added and the samples were fumed for ca. 10 min until dissolution was complete. They were cooled and diluted to ca. 40 ml with distilled water, warmed again and stirred with a polythene rod, after which they were made up to 100 ml with distilled water. One blank solution was prepared from pure iron.

TABLE 1

Instrumental parameters for determination of copper, boron and uranium[a]

Element	Dry	Ash	Atomize	Clean	Cool
Cu	110/40/10	500/10/5	2700/0/5	—	—
B	300/120/20	950/40/10	2900/0/5	—[e]/2/1	30/10/5
U/dil. acid[c]	110/150/30	—	2700/0/5 to 2900[d]	—[e]/2/1	30/10/5
U/0.2 M HCL/ 30% THF[c]	100/150/30	—	2700 to 2900[d]	—[e]/2/1	30/10/5
U/0.2 M HCL/ 30% dioxan[c]	70/180/50	—	2700 to 2900[d]	—[e]/2/1	30/10/5

[a]Under each heading of dry, ash, etc. the numbers given are temperature (°C)/ramp time (s)/hold time (s). Gas flow during atomization was 20 ml min^{-1}; background correction was used for boron determinations. [b]Atomizing temperatures were measured by optical pyrometer, and so could be up to 40° C lower than the actual temperature [7]. During the initial 50 firings, the CSIR coated tubes reached an atomizing temperature up to 250°C higher than the instrument setting. For the commercially coated tubes, the measured temperature was 50—100°C higher than the instrument setting. [c]The media used were 0.01 M HCL, 0.2 M HCL/30% tetrahydrofuran and 0.2 M HCL/30% dioxan. [d]Different temperatures were tested. [e]The cleaning temperature was the same as the atomizing temperature.

Calibration standards were prepared by adding various amounts of boron (0.5, 1 and 2 $\mu g\ ml^{-1}$) to equal aliquots of a solution of pure iron which had been taken through the above procedure, ensuring similar iron and acid concentrations.

Polyethylene laboratory ware was used as far as possible, i.e., measuring cylinders, beakers and volumetric flasks, and all chemicals used were of reagent grade.

RESULTS AND DISCUSSION

Tube lifetime tests

It had been found that the coating of commercially coated tubes was very thin and was removed too rapidly at high temperatures, after which the resultant powdery surface caused very poor reproducibility. The tubes coated at the CSIR were, therefore, compared to the commercial standard (uncoated) tubes. A large number of tests (>25) was run on each type of tube, a 0.01 μg Cu ml^{-1} solution in 10% (v/v) nitric acid being used for testing. Tubes were weighed after every 100 firings; initially the mass loss was on average 10 mg, at first increasing gradually as the tubes eroded. A sharp increase in this figure to 40 mg or more and a 50% decrease in initial sensitivity marked the end of tube life. Average lifetimes were 200 firings for the commercial tubes and 600 firings for the CSIR tubes with a number of the latter lasting for up to 1000 firings. An average three-fold sensitivity increase was obtained with the CSIR tubes compared to the commercial tubes.

Boron determination

When CSIR tubes were used with the temperature program given, the memory caused by carbide formation was eliminated, zero values being obtained for blanks. Ten determinations of 1 μg ml^{-1} boron in a medium of 0.01 M hydrochloric acid and 500 μg ml^{-1} calcium had an average absorbance of 0.18 and a relative standard deviation of 2.6%. The limit of detection was obtained with a fresh tube and taking ten absorbance readings with a blank solution (HCl/Ca). The absorbance value equal to three times the standard deviation was equivalent to 0.015 μg ml^{-1} or 0.3 ng of boron in the 20-μl sample. Table 2 gives a comparison of the performance of the three types of tubes.

As steel samples are frequently analysed for boron by inductively-coupled plasma atomic emission spectrometry, in this laboratory, this element was determined in a number of these samples, using the furnace technique and CSIR tubes. Under the conditions given and with the strongly acidic medium of the samples (20% of (9 + 1) H_3PO_4/H_2SO_4), tubes lasted for 45—50 firings, which were sufficient for analysis of the samples listed in Table 3. However, tube life can be extended by including two further steps in the temperature program: a conditioning step at 500°C with ramp time 1 s and hold time 20 s, and a pyrolysing step during which the argon flow is replaced with a 130 ml min^{-1} flow of 10% methane in argon, at 2150° C with ramp time 15 s and hold time 250 s [8]. While the latter is not recommended as a primary coating method, it can be useful, albeit time-consuming, when large numbers of samples have to be analysed. A comparison of the values obtained by the plasma and graphite-furnace techniques is given in Table 3. These tests were run with commercial tubes purchased during 1982.

TABLE 2

Comparison of the performance of three types of tube for boron determination

	Boron conc. (μg ml^{-1})	Firing numbers	Absorbance
CSIR tube	1	13—22	0.165—0.172
Commercial coated tube	1	4—15	0.083—0.044
Commercial uncoated tube	10	—	0.016

TABLE 3

Boron concentrations (μg ml^{-1}) in steel sample solutions

Method	Sample number					
	1	2	3	4	5	6
Plasma	0.28	0.36	0.24	0.28	0.30	0.33
Graphite furnace	0.24	0.34	0.22	0.29	0.45	0.39

It was found that the matrix of these samples (iron in H_3PO_4/H_2SO_4) caused a suppression of boron absorbance of about 40%. The discrepancy between the plasma and atomic absorption values might have been due to this fact. Increasing the sensitivity of the latter method through prior removal of iron by means of ion exchange should improve the accuracy. Such a step, requiring considerable sample dilution with 10 M hydrochloric acid, would not be too time-consuming, as it can be completed in a day with samples subsequently evaporating down overnight. Such a separation method was tested for synthetic boron samples in the presence of iron, and gave an average boron recovery of 97%.

Uranium determination

There is a rapidly expanding interest in uranium determinations in geological, biological and other samples. Numerous methods exist for trace uranium determination, the most suitable for routine analysis being laser-induced fluorescence, x-ray fluorescence and plasma emission spectrometry. However, the high cost of the equipment involved places these methods beyond the reach of many laboratories. Atomic absorption spectrometry is the procedure that best meets requirements of automation and cost-effectiveness. While the flame method is of modest sensitivity, an absorbance of 0.2 being obtained for 2300 μg U ml^{-1}, determination by the graphite-furnace technique has been made possible by the development of pyrolytic carbon coatings, which have a much higher resistance to carbide formation than the uncoated graphite. Sensitivity for uranium is adversely affected both by carbide formation and by the formation of a number of oxides, in particular U_3O_8 which is thermally very stable, the stoichiometrically pure compound being obtained between 800 and 900°C.

Sensitivity for uranium is critically dependent on the atomizing temperature and on the nature of the inner tube surface; an increase in atomizing temperature from 2670 to 2800°C can cause an 80—100% increase in sensitivity, and absorbance values often differ markedly from one tube to another. Inner surfaces are eroded not only by the high temperatures but also by the continual formation and dissociation of the carbide, and blank values were found to increase steadily with increase in the number of firings. In addition, it was found that the atomizing temperature dropped by an average of about 50°C after 100 firings. However, with the CSIR tubes and the temperature program in Table 1, the blank values obtained could be tolerated. For 25 μg U ml^{-1} and a 2700°C atomizing temperature, these values varied between 0.01 and 0.06 absorbance, depending on the tube lifetime.

While for about the first 25 firings, one to two firings were sufficient to clean the tube, the number of cleanings had to be increased to four and sometimes five at the end of the lifetime of a tube, which was 80 to 200 firings at atomizing temperatures of 2700 to 2750°C.

In this laboratory, ore samples are periodically analysed for uranium by means of inductively-coupled plasma atomic emission spectrometry. As these

samples (usually pyrites) are routinely put through ion-exchange columns so that quite simple sample solutions (containing the analyte and only a little iron) are obtained, it was decided to omit the ashing step in the furnace tests and merely ensure complete drying. This resulted in improved reproducibility and in fewer firings being required for cleaning. Typical sensitivity and reproducibility values obtained with CSIR tubes and with three commercially coated tubes are given in Table 4. Test solutions were 25 μg U ml^{-1} in 0.01 M hydrochloric acid and 50 μg U ml^{-1} in 0.2 M hydrochloric acid. As measurements were also to be taken with 50 μg U ml^{-1} in 0.2 M hydrochloric acid and 30% of an organic solvent, the 50 μg U ml^{-1}/0.2 M hydrochloric acid test

TABLE 4

Results of tube tests for uranium determination

Tube	Atomizing temp. (°C)	Firing numbers[a]	Average absorbance	Relative standard deviation (%)	Lifetime (number of firings)
Test solution: 25 μg U ml^{-1} in 0.01 M HCl					
Commercially[b] coated (i)	2750	6—35 (10)	0.094	5.6	60
Commercially coated (ii)	2750	19—60 (8)	0.206	16.8	60
Commercially coated (iii)	2840	4—40 (8)	0.330	11.0	40
CSIR (1)[c]	2700	29—67 (10)	0.080	7.2	237
	2700	98—120 (6)	0.063	7.3	237
	2650	140—175 (9)	0.059	7.7	237
	2700	190—212 (7)	0.067	7.1	237
	2700	237—244 (4)	0.053	4.6	237
CSIR (2)	>2900	22—44 (6)	0.262	4.9	45
CSIR (3)	2850	12—27 (5)	0.137	7.0	93
	2800	34—67 (10)	0.117	6.8	93
	2790	71—87 (5)	0.104	9.9	93
CSIR (4)	2880	17—36 (5)	0.172	2.0	70
	2850	55—70 (4)	0.139	7.9	70
Test solution: 50 μg U ml^{-1} in 0.2 M HCl					
CSIR (5)	2710	37—47 and 71—96 (9)	0.207	3.5	96
CSIR (6)	2760	33—57 (5)	0.250	2.2	70
CSIR (7)	2800	85—109 (5)	0.320	2.8	109

[a]Number of determinations in parentheses. [b]When deterioration of the commercially coated tubes had set in, it was useless to increase the temperature setting, as reproducibility steadily became much poorer. [c]After 180 firings, the supporting cylinders were cleaned and the temperature setting increased to regain a pyrometer reading of 2700°C. The absorbance readings for 10 blanks, taken after 212 firings, varied between 0.015 and 0.020.

solution was used for purposes of comparison. At the stage when measurements with the 50 μg ml^{-1} solution were made, a new hollow-cathode lamp was obtained. The fact that this source was a great improvement on the one initially used, may in part account for the improved reproducibility obtained. The 25 μg ml^{-1} solution was used with commercially coated tubes and with CSIR tubes 1—4, while the 50 μg ml^{-1} solution was used with CSIR tubes 5—7. The commercial tubes used in these tests were purchased during 1983. The detection limit at an atomizing temperature of 2750°C, calculated as for boron, was found to be 0.6 μg U ml^{-1}.

With a view to possible complexing of uranium, tetrahydrofuran and dioxan were each tested in 30% solution in 0.2 M hydrochloric acid as the medium for 50 μg U ml^{-1}. By this means a 40—50% absorbance enhancement was obtained, but this indicated little complex formation, as otherwise the enhancement would have been much greater. On cutting the tube lengthwise, a fine thin carbon layer was found to be present on the inner surface which apparently protected the tube against carbide formation to a certain extent. Underneath the layer, the surface seemed unaffected on visual inspection after 50 firings. In addition, blank values were lower and fewer cleaning firings were required. Furthermore, a very small quantity of pyrolytic carbon was deposited on the outer surface around the sample introduction hole with each firing. It was found that the organic compound had to be present in the sample solution, because sampling of a blank (organic compound/acid) immediately prior to sampling the analyte solution had no enhancing effect, and continual use of such a blank for the cleaning firings had an adverse effect on reproducibility. Tubes were therefore cleaned by one firing with only the dilute acid followed by firings with no deposition of a blank (i.e., air only). Table 5 lists typical enhanced absorbances and reproducibilities obtained.

TABLE 5

Enhancement of uranium sensitivity by addition of organic solvents to the analyte medium

Temp. (°C)	Absorbance[a]	Organic solvent	Absorbance[b]	Firing numbers[c]	R.s.d. (%)[c]
2680	0.164	Dioxan	0.249	6—31 (7)	5.6
2650	0.150	Dioxan	0.291	6—16 (4)	2.0
2750	0.237	Dioxan	0.332	94—106 (3)	2.4
2730	0.224	THF	0.312	35—68 (10)	3.5
2730	0.210	THF	0.318	50—67 (5)	1.5
2780	0.300	THF	0.459	8—28 (5)	2.2

[a]For 50 μg U ml^{-1} in 0.2 M HCl, mean of 3 determinations. [b]For 50 μg U ml^{-1} in 0.2 M HCl/30% organic solvent. [c]Results refer to uranium in 0.2 M HCl/organic solvent. The number of determinations is given in parentheses.

Apart from the enhancement found, the presence of an organic solvent also had a beneficial effect on tube lifetime. However, extreme care should be exercised with the sampling process when these solvents are used, as the lowered surface tension can cause large losses of the sample aliquot if the sampler tip or a droplet adhering to it touches that part of the tube surrounding the opening. This can result in a large portion of the sample volume being drawn out and deposited on the outer surface. In addition, the ashing stage should be closely watched. In order to prevent the formation of air bubbles in the sampling capillary caused by the dilute acid/organic solvent solution, it was found best to use chloroform as the wash liquid.

Only one or two determinations were made from one sampling cup before its replacement with another freshly filled one, in order to avoid an increase in analyte concentration by evaporation of the organic solvent.

Two tubes were given an inner surface coating of 21.7 and 22.3 mg of zirconium by sputtering, whereafter the metal was transformed to the carbide during the pyrolytic coating process. These tubes were found to give absorbance increases of 42 and 48% for 25 μg U ml^{-1} in 0.01 M hydrochloric acid at an atomizing temperature of 2790° C, i.e., average absorbances of 0.145 (12 determinations) and 0.154 (4 determinations), respectively, compared to the absorbance at the same temperature given in Table 4 for a similar uranium concentration. These tubes are not recommended for routine use, as the increase in absorbance does not justify the expense and time required to obtain the zirconium carbide coating. However, this finding is worthy of mention as it has been found in this laboratory and elsewhere [9] that the presence of zirconium carbide on the inner tube surface enhances the absorbance of elements such as phosphorus and silicon which form stable oxides. Particularly noteworthy is the good reproducibility over a large number of firings obtained with the better of the tubes (smoother inner surface and better coating adherence), i.e., 12 determinations from firing number 16 to number 74 with a relative standard deviation of 2.2%. In this respect, it should be mentioned that Schmidt and Dietl [10] reported that after removal of the major part of the iron from digested soil solutions no interferences on thallium absorbance by accompanying ions could be observed when zirconium-coated graphite tubes were used.

In conclusion, with regard to the determination of uranium, the results obtained illustrate: (i) the achievement of a diminished memory effect so that uranium can be determined routinely by means of graphite-furnace atomic absorption spectrometry; (ii) decrease in tube lifetime with increase in atomization temperature, (iii) an increase in sensitivity with increasing atomization temperature, and (iv) generally a longer lifetime of the CSIR tubes compared to commercial tubes, together with the possibility of a further extension of tube lifetime by the use of organic solvents.

REFERENCES

1 J. C. Bokros, Carbon, 15 (1977) 355.
2 D. C. Manning, F. J. Fernandez and G. E. Peterson, Ind. Res., Feb. (1977) 82.
3 S. A. Clyburn, T. Kantor and C. Veillon, Anal. Chem., 46 (1974) 2213.
4 K. C. Thompson, R. G. Godden and D. R. Thomerson, Anal. Chim. Acta, 74 (1975) 289.
5 D. C. Manning and R. D. Ediger, At. Absorpt. Newsl., 15 (1976) 42.
6 R. E. Sturgeon and C. L. Chakrabarti, Anal. Chem., 49 (1977) 90.
7 C. J. Rademeyer, PhD Thesis, 1984, Rand Afrikaans University, Johannesburg.
8 S. Schwartzer, Technikon Pretoria, 420 Church Street, Pretoria 0002 South Africa personal communication (1984).
9 H. M. Ortner and E. Kantuscher, Talanta, 22 (1975) 581.
10 W. Schmidt and F. Dietl, Fresenius Z. Anal. Chem., 315 (1983) 687.

Analytica Chimica Acta, 181 (1986) 179—186
Elsevier Science Publishers B.V., Amsterdam — Printed in The Netherlands

DETERMINATION OF URINARY ARSENIC BY ELECTROTHERMAL ATOMIC ABSORPTION SPECTROMETRY WITH THE L'VOV PLATFORM AND MATRIX MODIFICATION

DANIEL C. PASCHAL*, MARY M. KIMBERLY and GEORGE G. BAILEY

Division of Environmental Health Laboratory Sciences, Center for Environmental Health, Centers for Disease Control, Public Health Service, U.S. Department of Health and Human Services, Atlanta, GA 30333 (U.S.A.)

(Received 5th September 1985)

SUMMARY

Total arsenic can be determined rapidly and simply in urine by dilution with a matrix modifier containing nickel and magnesium nitrate in nitric acid. The background correction capability of Zeeman-effect electrothermal atomic absorption spectrometry effectively nullifies nonatomic absorption by urine concomitants. Accuracy and precision of the method were evaluated by the determination of total arsenic in the National Bureau of Standards' SRM 2670, Toxic Elements in Freeze-Dried Urine, and commercially available lyophilized urine material. Deviations of determined concentrations from expected values ranged from about 4 to 18 ng ml^{-1} with standard deviations ranging from about 5 to 31 ng ml^{-1}.

Arsenic has been the subject of intense study because of its very complex chemistry. In an early review, Talmi and Bostick [1] describe the many methods used to determine arsenic. Methods in use include spectrophotometric, x-ray, electrochemical, neutron activation, and atomic spectrometric techniques, with a variety of specimen-preparation methods. Some investigators have evaluated the chemical forms in which arsenic is present in biological or environmental specimens. Speciation of arsenic has been accomplished with chromatographic methods [2, 3], by extraction [4, 5], by electrochemical reduction [6] and by selective volatilization of the arsines produced on chemical reduction [7, 8]. Some workers have focused attention on the differential toxicity of arsenic in its various forms. Inorganic arsenic(III) and arsenic(V) compounds are generally observed to be of higher toxicity to mammals than the various organic forms [9].

The method described here is designed to evaluate total arsenic in urine or water without attempting to differentiate the various chemical species present in these media. The rationale for this approach is threefold. First, most studies that have been used to generate "normative" or baseline data for urinary arsenic have yielded data on total arsenic, so that the total arsenic content is more easily interpreted in epidemiological or emergency response

settings. Secondly, studies have shown that urinary arsenic is mostly organic, presumably because it is altered in the human system [10]. Therefore, the speciation of arsenic in urine only rarely reflects environmental exposure. Finally, methods for total arsenic are inherently simpler to operate and are more easily transferred to other laboratories. The latter point is important for the role of this laboratory in providing technology transfer to a large variety of actual or potential user laboratories and in standardizing technology among laboratories assisting in health studies. With additional steps, the method presented could be easily expanded to include simple speciation into organic and inorganic arsenic, most likely by differential extraction.

Determination of arsenic, selenium, tellurium, etc. by electrothermal atomic absorption spectrometry offers a number of attractive advantages, some of which are due to developments in this technology. With a combination of stabilized temperature-platform furnace, matrix modification, fast, low-noise electronics, and Zeeman-effect background correction, arsenic can be determined with a minimum of sample pretreatment or other processing steps. The only sample treatment required in the present method is dilution with a matrix modifier. With the simplified treatment described here, throughput is greatly enhanced and cost is reduced. Furthermore, the method provides adequate accuracy, and it is free of common interferences. Similar methods have been described for selenium and arsenic [11, 12], which illustrates the general nature of this approach to electrothermal atomic absorption.

EXPERIMENTAL

Equipment

A Perkin-Elmer Model 5000 Zeeman-effect spectrometer was used for absorbance measurements. This instrument was equipped with a Perkin-Elmer Model AS-40 autosampler and Data Station 10, with HGA graphics software for signal processing (Perkin-Elmer Corp., Norwalk, CT). The resonance-line radiation was produced by a Perkin-Elmer electrodeless discharge lamp operated at 8 W with a 0.7-nm slit width, with the 193.7-nm emission line used for absorbance measurements. Pyrolytically coated graphite furnaces and solid anisotropic graphite platforms were from Perkin-Elmer (part nos. B109-322 and 290-2311, respectively). Furnace conditions were optimized experimentally, and the manufacturer's recommended values were used as a starting point [13].

Reagents and glassware

Ultrapure nitric acid was used (G. F. Smith Chemical Co.; "Redistilled" grade). All water for reagent preparation and glassware rinsing was purified to approximately 18 mohm cm^{-1} resistance by a Milli-Q purification system. Inorganic arsenic standard was from J. T. Baker Chemical Co. Organic arsenic standards were prepared from cacodylic acid (J. T. Baker) or disodium methylarsonate (Alfa), both at 1000 mg l^{-1}. A matrix modifier was prepared

by dissolving 2.83 g of nickel nitrate hexahydrate (J. T. Baker) in a minimum amount of ultrapure water, adding 11.4 ml of ultrapure nitric acid, 0.57 ml of Triton X-100 (J. T. Baker), and 2.86 g of magnesium nitrate hexahydrate (BDH Chemicals), and diluting to 500 ml with ultrapure water.

All plasticware and glassware were cleaned by soaking the containers for 24 h in concentrated detergent (Sparkleen, Fisher Scientific) and then soaking them for 72 h in 25% (v/v) reagent-grade nitric acid. The cleaned containers were rinsed with copious amounts of ultrapure water, and dried under laminar flow hoods. Urine was diluted in 4-ml plastic scintillation vials (Beckman) cleaned as described. Autosampler cups were from Fisher Scientific and plastic pipet tips were from Rainen. Plastic vials used for dilution of urine were rinsed with ultrapure water immediately before use, as were the plastic pipet tips. Reagent blanks prepared by substituting 1% (v/v) nitric acid for acidified urine showed arsenic levels consistently below the limit of detection of the present method.

Procedures

Urine or water specimens, preserved by acidification to 1% (v/v) with ultrapure nitric acid, are diluted (1 + 7) with the matrix-modifier solution described above. This mixed modifier serves to stabilize endogenous arsenic, presumably by formation of nickel arsenide [14]. Magnesium nitrate acts as an "ashing aid" in a function similar to its use in classical methods. The particular combination of reagents used here is similar to one used for determination of urinary selenium [11].

For the preparation of intermediate and working standard arsenic solutions, the original 1000 mg l^{-1} stock arsenic was diluted with ultrapure water to 10 mg l^{-1} to provide an intermediate standard, which was prepared weekly. On a daily basis, this intermediate arsenic standard solution was further diluted with ultrapure water to prepare the four working standards of 250, 500, 750, and 1000 μg l^{-1}.

In the usual procedure, 0.50-ml amounts of urine or water are diluted with 3.50 ml of matrix modifier. Into four precleaned autosampler cups containing 20 μl of 250, 500, 750, and 1000 μg l^{-1} inorganic arsenic, 500-μl aliquots of diluted urine or water are pipetted. Unspiked, diluted urine or water is pipetted into a fifth cup. With the autosampler set to deliver 10-μl volumes, the solutions are pipetted onto the pyrolytic graphite platform and absorbances are measured in duplicate. The temperature program used for this determination is given in Table 1.

RESULTS AND DISCUSSION

Accuracy and precision

Accuracy and precision were evaluated with two different types of studies, namely, the determination of arsenic in lyophilized urine reference materials with known or certified total arsenic concentrations, and an interlaboratory

TABLE 1

Instrumental conditions for determination of arsenic

Step Function	1 Dry	2 Char	3 Atomize	4 Cool
Temp. (°C)	140	1400	2400	20
Ramp (s)	5	5	5	10
Hold (s)	20	20	5	10
Internal Ar flow (ml min^{-1})	300	300	0	300
Record			−5	
Baseline			−1	

comparison study involving two of the most commonly used techniques for arsenic, hydride generation and graphite-furnace atomic absorption.

In the first study, a series of 16 determinations was made during a one week period (four runs) of the total arsenic in National Bureau of Standards' SRM 2670, Toxic Elements in Freeze-Dried Urine, and in two pools from Fisher Scientific Co. (Urichem Level II, cat. no. 2935-80). Results of these determinations are given in Table 2. As can be seen, good agreement was obtained with the certified or reference values for these urine specimens. Overall precision, including within- and among-run/day components, is in the range of 6—8% RSD. As a further indication of method accuracy, an interlaboratory comparison was conducted by the University of Washington in connection with a health study of an arsenic-emitting copper smelter. Frozen urine specimens, containing both inorganic and organic forms of arsenic, were distributed to a series of laboratories which did routine determinations of arsenic. Methods used were mostly hydride-atomic absorption in several versions, some of which involved determination of four of the major arsenic species. Additionally, an aqueous standard containing arsenic(III and V) and

TABLE 2

Precision[a] and accuracy of urine arsenic determinations

Sample	Arsenic concentration (ng ml^{-1})		Standard deviations (ng ml^{-1})		
	Target	Determined	Within-run	Among-run	Total
Urichem Level II	132	144.9	4.6	11.3	12.2
Urichem Level II	323	304.9	9.6	19.6	21.8
SRM 2670	480	489.3	11.1	30.9	32.9

[a]As determined by analysis of variance (ANOVA).

monomethyl- and dimethyl-arsenic, all at 80 ng ml^{-1} arsenic, was processed by the present method. Results for this sample are shown in Table 3, illustrating the usefulness of the method for determination of arsenic in water. Accurate results were also obtained for a large variety of Environmental Protection Agency water samples, with results well within the 95% confidence limits published for these aqueous quality control samples.

Matrix modifier

The use of nickel as a matrix modifier has been extensively documented. Presumably, nickel forms a more thermally stable arsenide or other nickel/arsenic compound that prevents volatilization of the arsenic until concomitant compounds have been removed during the thermal pretreatment step [14]. Magnesium nitrate has been shown to be useful in the determination of urinary selenium [11] and other elements [15], so its use as a "charring aid" was investigated.

A series of experiments was conducted with a constant concentration of nitric acid, previously shown to be optimal, in which the amounts of nickel and magnesium nitrate were varied. The results of this study are illustrated in Fig. 1, from which the recommended amounts of 10 μg of nickel and 50 μg of magnesium nitrate were chosen. More nickel seriously delays the atomization of arsenic; more magnesium nitrate depresses the absorbance signal by approximately 10%.

Temperature program

To optimize the temperature program for arsenic, the manufacturer's recommended conditions were used as a starting point. Because several different species of arsenic normally appear in urine [7], any optimization process must be evaluated with all the various arsenic species. The optimized procedure should maximize sensitivity and show a minimum of interspecimen variability.

The charring temperature was evaluated by measuring the peak area of a urine specimen, with added arsenic as a function of charring temperature and with atomization temperature held constant. Previous experience with arsenic

TABLE 3

Results of interlaboratory comparison

Sample	Arsenic concentration (ng ml^{-1})		Number of determinations
	Target	Determined ± SD	
Aqueous Standard	240	235 ± 11	18
Sample C	48.0	51.7 ± 4	8
Sample B	142.0	138.2 ± 3.6	.8
Sample A	254.0	239.4 ± 8.7	8

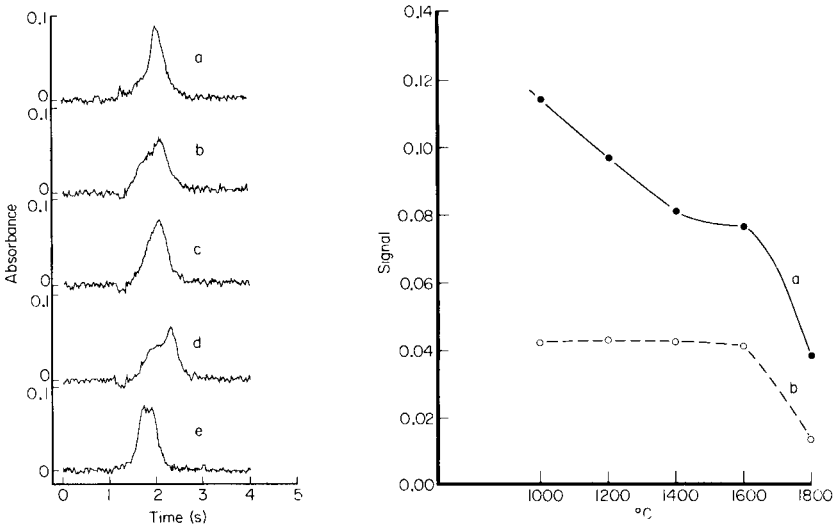

Fig. 1. Optimization of matrix modifier for diluted urine spiked with 10 ng of inorganic arsenic. (Experimental conditions as given in Procedures.) Nickel added: (a) 10 μg; (b) 15 μg; (c) 20 μg; (d) 30 μg; (e) 10 μg. Magnesium nitrate added: (a—d) 50 μg; (e) 100 μg.

Fig. 2. Optimization of thermal-pretreatment temperature (atomization temperature 2400°C): (a) Urine + 10 ng As, single beam (total absorbance); (b) Urine + 10 ng As, Zeeman a.a.s. (analyte absorbance). The signal used is integrated absorbance.

peak shapes in the presence of nickel led to the choice of 2400°C as the atomization temperature. The charring (thermal-pretreatment) temperature was varied from 1000 to 1800°C in 200°C increments. As shown in Fig. 2, the losses of arsenic are minimal up to a temperature of about 1600°C. The 1400°C charring was chosen because of the decrease in background signal, which decreases constantly as charring temperature increases. At 1400°C, most urines have background values in the 0.1—0.2 absorbance × second range, well within the correction capacity of the Zeeman system. The three species of arsenic tested (inorganic, monomethyl, and dimethyl) all exhibited similar behavior in terms of charring losses.

Spectral interferences

The Zeeman-effect background-correction system should be used in systems in which there is either high or structured background interference. Although the measured background absorbance under the experimental conditions suggested here is not excessive, measurements with deuterium arc systems suggest that overcompensation occurs at the 193.7-nm wavelength, an effect that is exaggerated with increasing slit width from 0.7 to 2.0 nm. Others have noted this effect in the determination of arsenic in urine [16] and arsenic in sea water [17]. Interferences by aluminum [18] species

(Al^{2+}, Al^{+}) on arsenic at the 193.7-nm resonance line were not observed with Zeeman-effect correction. The major contributor to nonspecific absorbance in urine specimens is sodium chloride; however, the (1 + 7) dilution and the use of nitric acid both have the effect of diminishing the residual sodium chloride present during atomization.

Sensitivity, limit of detection, calibration and interspecimen slope variability

Sensitivity of atomic absorption methods has been defined as that amount, C, causing a measured absorbance (A) of 0.0044, or 0.0044 × second if integration is used. By this definition, the sensitivity of the method is about 23 pg, which compares favorably with published values for determination of arsenic in urine [16] with Triton X-100 and nitric acid matrix modifier, which gave a calculated sensitivity of 20 pg. The limit of detection, calculated as three times the standard deviation of a "low" arsenic specimen, is about 8 ng ml^{-1} in terms of the original undiluted urine specimen.

Interspecimen variability of calibration slopes was evaluated by using the method of additions of inorganic arsenic standards as described above. Twelve urines were chosen randomly, including lyophilized, fresh, and "aged" specimens collected 1—2 years earlier. The average calibration slope, determined by linear regression of five-point calibration plots, was 2.35×10^{-4} A.s ng^{-1} ml, with a standard deviation of 2.73×10^{-5} (11.6% RSD). This variability of calibration slopes was within the limit set as a method objective, about 10% RSD.

Calibration slopes obtained from urine spiked with inorganic, monomethyl-, and dimethyl-arsenic standards were compared to document further the comparability of response of the known major species of arsenic in urine and water. Slopes varied from 94 to 107% of those obtained for the same urine with inorganic arsenic.

Conclusion

During the past year, the method has been in constant use in this laboratory in connection with epidemiological and other health studies. All of the identified species of arsenic present in urine give approximately the same absorbance values, a fact that has been verified both by calculated recoveries of cacodylic acid and monomethylarsenic acid standards (95—105% recovery) and by interlaboratory comparison of common specimens with hydride and other methods. Work is under way to fractionate urinary arsenic into inorganic and organic portions by differential extraction.

REFERENCES

1 Y. Talmi and D. T. Bostick, J. Chromatogr. Sci., 13 (1975) 231.
2 Y. Talmi and D. T. Bostick, Anal. Chem., 47 (1975) 2145.
3 T. M. Vickrey, H. E. Howell and M. T. Paradise, Anal. Chem., 51 (1979) 1880.
4 F. Puttemans and D. L. Massart, Anal. Chim. Acta, 141 (1982) 225.
5 A. W. Fitchett, E. H. Daughtvey, Jr. and P. Mushak, Anal. Chim. Acta, 79 (1975) 93.

6 D. J. Meyers and J. Osteryoung, Anal. Chem., 45 (1973) 267.
7 R. S. Braman and C. C. Foreback, Science, 182 (1973) 1247.
8 R. S. Braman, L. L. Justen and C. C. Foreback, Anal. Chem., 44 (1972) 2195.
9 National Institute of Occupational Safety and Health Criteria Document, US Dept. HEW, Publ. 79-100 (1978).
10 E. A. Crecelius, Environ. Health Perspect., 19 (1977) 147.
11 G. R. Carnrick, D. C. Manning and W. Slavin, Analyst (London), 108 (1983) 1297.
12 E. Pruszkowska and P. Barrett, Spectrochim. Acta, Part B: 39 (1984) 485.
13 Perkin Elmer Corporation, Analytical Methods for Furnace AAS, January 1984.
14 J. Koreckova, W. Frech, E. Lundberg, J. Perssonn and A. Cedergren, Anal. Chim. Acta, 130 (1981) 267.
15 S. A. Lewis and T. C. O'Haver, Anal. Chem., 57 (1985) 2.
16 U. Voellkopf and Z. Grobenski, At. Spectrosc., 5 (1984) 115.
17 Z. Grobenski, R. Lehmann, B. Radzink and U. Voellkopf, At. Spectrosc., 5 (1984) 87.
18 K. Riley, At. Spectrosc., 3 (1982) 120.

Analytica Chimica Acta, 181 (1986) 187—193
Elsevier Science Publishers B.V., Amsterdam — Printed in The Netherlands

DETERMINATION OF INORGANIC TIN AND ORGANOTIN COMPOUNDS BY GRAPHITE-FURNACE ATOMIC ABSORPTION SPECTROMETRY WITH A NEW MATRIX MODIFIER

RAOUL PINEL*, MOHAMMED ZAHER BENABDALLAH, ANNETTE ASTRUC and MICHEL ASTRUC

Laboratoire de Chimie Analytique, Université de Pau et des Pays de l'Adour, Avenue de l'Université, 64000 Pau (France)

(Received 22nd March 1985)

SUMMARY

The determination of total tin in water samples by graphite-furnace atomic absorption spectrometry is described. A matrix modifier containing 0.4% (w/v) potassium dichromate and 0.2% ammonium dihydrogenphosphate in 2% nitric acid is proposed. Interferences from major ions in natural fresh waters decreased and the sensitivity is greatly improved. The procedure is compatible with all the commercial injection devices and requires no pretreatment of the graphite furnace or use of a stabilized temperature platform. The 3σ detection limit is 0.62 ng Sn ml^{-1}, and calibration is linear up to 30 ng ml^{-1} tin.

Interest in the determination of tin at trace levels in the environment has increased in recent years because of the growing use of organotin compounds as stabilizers for PVC, biocides in antifouling paints, pesticides, fungicides, etc. [1—4]. Graphite-furnace atomic absorption spectrometry (GFAAS) appears to be the method of choice for the determination of metals and organometallic compounds at very low concentrations. This very sensitive and relatively simple method has been used by several authors for the determination of tin [5—20], but many of them have described difficulties that decrease the attractiveness of the method.

The major problems seem to be the tendency of tin to form volatile compounds, which are easily lost during the drying and ashing steps, and the interaction of tin with the carbon of the furnace wall. These two processes were studied in detail by Lündberg et al. [5], who used radioactive ^{113}Sn for monitoring the losses of tin during the temperature cycle by radioactivity measurements. To overcome these problems, several approaches have been described, which include the separation of tin from the matrix by liquid-liquid extraction [10, 14—18, 21], thus avoiding matrix interferences; pretreatment of the graphite furnace with elements that form refractory carbides (W, Ta, Zr, Mo, La) to prevent interaction with tin [10, 13, 21—24]; addition to the sample of a matrix modifier, essentially to prevent volatilization of tin before atomization, and to decrease interferences [5, 9, 10, 12, 25, 26]. The last

0003-2670/86/$03.50

method is the simplest as it requires minimal sample treatment before injection into the furnace.

Many organic and inorganic compounds have been proposed as matrix modifiers for this purpose. The most important are 10% (w/v) ascorbic acid [9], 10% (v/v) ammonia [5], 8% (w/v) citric acid in (1 + 9) hydrochloric acid [15], ammonium nitrate [10], phosphoric acid [12], 10% ascorbic acid/400 μg ml^{-1} iron(III) nitrate [26], ammonium dihydrogenphosphate [27] and ammonium dihydrogenphosphate/magnesium nitrate in (1 + 99) nitric acid [25]. All these modifers have been reported for use with manual or automatic injection of 10—50 μl of sample. A different automatic injection device is commercially available from Instrumentation Laboratory, in which the sample is introduced as an aerosol from a nebulizer into a hot furnace (typically 150°C) so that the sample is instantly dried. In this way, a large volume of sample can be injected if the matrix does not cause limitations and detection limits can be greatly improved. However, with such a device, successive injections of sample and modifier, as in the methods of Tominaga and Umezaki [9], Lündberg et al. [5] and Pruszkowska et al. [25] are not simple. Moreover, the use of a relatively concentrated solution of a solid matrix modifier (8% citric acid or 10% ascorbic acid, for example) results in the rapid deposition of these compounds on the optical windows of the furnace assembly.

In this paper, these problems are overcome by means of a new matrix modifier in solutions sufficiently dilute to be used with any injection device without the inconveniences described above. A solution of potassium dichromate, 0.04% w/v in (1 + 49) nitric acid, is shown to give better results than other modifiers when used as a stabilizer for the determination of inorganic and organic tin in aqueous solution. The addition of 0.2% diammonium hydrogenphosphate decreases the interference of sulfate.

EXPERIMENTAL

Apparatus

An Instrumentation Laboratory model 451 atomic absorption spectrometer was used with a deuterium arc background corrector and an electrothermal atomizer model IL-555 with the Fastac IL-254 automatic sampler. Settings for the spectrometer were: lamp current 5 mA, wavelength 286.3 nm, bandwidth 1.0 nm, integration time 15 s, peak height read-out, photomultiplier voltage 800 V. Settings for the controlled-temperature furnace were: nitrogen purge gas at 1.4 bar, auto-operation mode, temperature feedback ON, auto-clean OFF. The temperature program was as listed in Table 1. Only pyrolytically coated tubes were used. Settings for the auto-sampling device were: sample deposit time 20—60 s, delay 5 s, nebulizer flow 5 ml min^{-1}.

TABLE 1

Temperature program for furnace

	Dry		Char		Atomize	
Step	1	2	3	4	5	6
Temperature (°C)	0	150	750	900	2500	2500
Time (s)	0	5	20	10	0	0

Reagents

The nitric and hydrochloric acids were of Suprapur grade (Merck). All the matrix modifiers were of analytical grade. Organotin compounds were "for synthesis" quality from Merck or Fluka. All aqueous dilutions were made in Millipore 18 MΩ cm^{-1} water.

A stock solution of inorganic tin (1000 $\mu g\ ml^{-1}$) was prepared by diluting a Prolabo Normadose of 1 g of tin in 4 M hydrochloric acid. Fresh standards (10 and 1 $\mu g\ ml^{-1}$) were prepared daily by dilution in 10% (v/v) hydrochloric acid. Working standards at ng ml^{-1} levels were made by further dilution in a 0.4% (w/v) potassium dichromate/(1 + 49) nitric acid solution. Stock solutions of organotin compounds (1000 μg Sn ml^{-1}) were prepared by dissolving appropriate amounts in methanol. Standards at 10 and 1 $\mu g\ ml^{-1}$ were prepared daily in methanol and working standards at ng ml^{-1} levels were made by direct dilution in the above dichromate/nitric acid solution.

RESULTS AND DISCUSSION

Preliminary studies

Lünberg et al. [5] demonstrated that tin could be stabilized as tin(IV) oxide during the ashing step by adding ammonia to the furnace after sample injection. Such an operation is not possible with the Fastac automatic injector, so the use of oxygen donors that could be mixed to the sample prior to injection was studied. Potassium dichromate was proposed by Kirkbright et al. [28] as a matrix modifier in the determination of mercury and selenium by GFAAS. The efficiency of this modifier was tested in the GFAAS determination of tin. As shown in Table 2, it gave a considerable improvement in sensitivity compared to other modifiers.

All modifiers were tested under the ashing and atomizing conditions described by their authors. The drying step was adapted to the present injection device (5 s at 150°C after deposition at the same temperature). Ascorbic acid, citric acid and ammonium nitrate could not be tested at their most efficient concentration because of the necessity to nebulize the sample. The sensitivity obtained when potassium dichromate is used is not linked to coating of the furnace by chromium compounds as there is no persistence of the effect between consecutive sample injections if dichromate additions are stopped.

TABLE 2

Effect of some matrix modifiers on the peak height absorbance observed for 20 ng ml^{-1} solutions of inorganic tin in distilled water

Modifier	Observed peak height	Relative absorbance (%)
None	0.016	11
10% HNO_3 [25]	0.060	40
10% NH_3 [5]	0.059	39
1% tartaric acid[a]	0.070	46
2% HNO_3/0.04% $K_2Cr_2O_7$	0.152	100

[a]Suggested in the Instrumentation Laboratory manual.

The reproducibility for determinations at low concentrations of tin using the dichromate modifier was evaluated by measuring the peak heights obtained for 100 consecutive injections of the same 10 ng ml^{-1} solution of inorganic tin. The standard deviation was 0.008 absorbance (6%) of the mean peak height of 0.132 absorbance.

The temperature program proposed was optimized after a study of the effects of the charring and atomizing temperatures on the peak height of a 20 ng ml^{-1} inorganic tin solution containing dichromate. Maximum peak heights were obtained for charring temperatures from 900 to 1100°C and atomizing temperatures from 2500 to 2700°C. These observations are in accordance with the formation of tin(IV) oxide during the charring step (m.p. 1127°C, b.p. 1397°C).

The use of excessive atomizing temperatures decreases the useful lifetime of the furnace. Thus an atomizing temperature of 2500°C was chosen as a reasonable compromise compatible with 400—500 measurements with one graphite tube. This performance is in agreement with that reported by Liyi Zhou et al. [21]. But these authors had to impregnate the graphite tube with sodium tungstate to ensure 500 firings. Other workers reported much shorter lifetimes; Burns et al. [29] used tantalum carbide-coated tubes prepared by the procedure of Hocquellet and Labeyrie [10] and the lifetime of their tubes was only about 60 firings. Tominaga and Umezaki [9] using 10% ascorbic acid as matrix modifier and 2500°C as atomizing temperature, and obtained 100—150 measurements with a given graphite tube. This relatively short lifetime is probably due to the use of tubes without pyrolytic coating. The use of 10% ascorbic acid can result in other problems. Pruszkowska et al. [25] observed a heavy carbon residue built up on the tube walls when they tested the effectiveness of ascorbic acid as a matrix modifier. This residue can undoubtedly lead to erroneous results. Such a problem does not occur when a dilute modifier like 0.04% potassium dichromate solution is used. Moreover, sensitivity and long lifetime are obtained without time-consuming pretreatment of the furnace.

The responses of standard solutions of many organotin compounds (dimethyltin dichloride, tributyltin chloride, triphenyltin chloride, dioctyltin dichloride, dibutyltin dichloride and diphenyltin dichloride) were compared to those of inorganic tin standards at the same tin concentration. No significant difference was observed.

With the Fastac injector, the deposition time can be chosen from 1 to 999 s. However, with the modifier proposed, the blank signal from tin impurities in the potassium dichromate becomes too great if this deposition time exceeds 30 s or if the dichromate concentration is increased. The optimum concentration was chosen after comparing the peak heights observed for a 20 ng ml^{-1} solution of inorganic tin in solutions of various dichromate concentrations and the corresponding blank signals. The best signal-to-noise ratio was obtained for 0.04% potassium dichromate in 2% nitric acid. For 20-s sample deposition, the 3σ detection limit was 0.62 ng ml^{-1} when this modifier was used, and the calibration graph was linear up to 30 ng ml^{-1} tin. This detection limit could greatly be improved if purer potassium dichromate were available.

Interferences studies

This simplified procedure is attractive for monitoring organotin pollution in fresh water. However, in complex matrices many interferences can be encountered. Tables 3 and 4 present the results obtained with this modifier in the presence of the major ions usually found in environmental water samples. The only serious problem is due to sulfate. The effect of sulfate on the determination of tin by GFAAS is well known: many authors [6, 9, 10, 13, 30] have demonstrated that sulfate almost totally suppresses the tin atomic absorption signal. Hocquellet and Labeyrie [11] attributed this to carbon-mediated formation of volatile tin sulfide. A much smaller effect was found in the present studies with potassium dichromate as modifier suggesting

TABLE 3

Effect of anion concentration on the relative absorbance of a 20 ng ml^{-1} solution of inorganic tin in 0.04% $K_2Cr_2O_7$/2% HNO_3

Anion[a]	Relative absorbance (%)				
	Added concentration (mg l^{-1})				
	0	1	10	100	1000
NO_3^-	100	99	102	100	103
Cl^-	100	104	120	115	107
SO_4^{2-}	100	30	0	0	0
PO_4^{3-}	100	98	99	93	96
HCO_3^-	100	96	91	103	93

[a]All were added as the acid except hydrogencarbonate, for which the sodium salt was used.

TABLE 4

Effect of cations on the relative absorbance of a 20 ng ml^{-1} solution of inorganic tin in 0.04% $K_2Cr_2O_7$/2% HNO_3

Cation[a]	None	Na^+	K^+	Ca^{2+}	Mg^{2+}
Rel. abs. (%)	100	101	99	102	91

[a]100 mg l^{-1} added as nitrate.

that reduction of sulfate to sulfide is slower under these oxidizing conditions. However, the loss of sensitivity still makes it impossible to determine tin in samples containing more than a few mg l^{-1} sulfate.

An attempt was made to find an effective association of potassium dichromate with another modifier that could decrease the sulfate effect further. Ammonium dihydrogenphosphate [25] was found to be efficient at a concentration low enough to be compatible with the injection device. The effectiveness of this matrix modification on decreasing the sulfate effect is shown in Table 5.

Application to the determination of tin in fresh waters

The new matrix modifier was examined for the determination of tin in some natural fresh waters. A common tap water, a river water and some commercial bottled drinking waters were injected directly into the furnace for GFAAS determination of tin after addition of potassium dichromate, nitric acid and dihydrogenphosphate. None of these samples contained a detectable concentration of tin. The samples were spiked with 10 ng ml^{-1} inorganic tin and the standard addition procedure was used to evaluate tin recoveries. Recoveries from all samples were quantitative (94—107%).

Conclusions

The direct determination of tin added to fresh water samples by GFAAS, using potassium dichromate and ammonium dihydrogenphosphate in nitric

TABLE 5

Effect of added sulfate on the relative absorbance of a 20 ng ml^{-1} solution of inorganic tin in various modifiers

Modifier	Rel. abs. (%) with sulfate added[a]				
	0	1	10	100	1000
None	10	0	0	0	0
0.04% $K_2Cr_2O_7$/2% HNO_3	100	30	0	0	0
0.2% $(NH_4)_2HPO_4$	20	20	22	39	37
0.2% $(NH_4)_2HPO_4$/0.04% $K_2Cr_2O_7$/2% HNO_3	100	96	90	75	47

[a]0—1000 mg l^{-1} sulfate as sodium salt.

acid as matrix modifier is simple and rapid, requiring no pretreatment of the graphite furnace. The low effective concentration of the modifier makes the method compatible with any commercial injection device. Sulfate interferences are decreased enough to make possible the direct determination of tin in water samples containing a few mg l^{-1} sulfate by direct calibration. Fresh waters particularly rich in sulfate ions may be analyzed for tin by the standard addition method with a slight reduction in sensitivity. However, analysis of waters with more complex contents such as sea water requires liquid-liquid extraction of the dissolved tin species before GFAAS determination. The development of procedures including toluene extraction of inorganic tin and organotin compounds from complex matrices [31] and speciation studies using GFAAS as an automated element specific detector for liquid chromatography are in progress.

REFERENCES

1 Critères d'hygiène de l'environnement 15, Etain et organostanniques, Mise au point préliminaire O.M.S., Genève, 1981.
2 J. J. Zuckerman, R. P. Reisdorf, H. V. Ellis and R. R. Wilkinson, in F. E. Brinckman and J. M. Bellama (Eds.), ACS Symposium Series 82, Organometals and Organometalloids Occurrence and Fate in the Environment, Washington, DC, 1978.
3 C. J. Evans, Tin Its Uses, 100 (1974) 3; 101 (1974) 12.
4 C. J. Evans and P. J. Smith, J. Oil. Col. Chem. Assoc., 58 (1975) 160.
5 E. Lündberg, B. Bergmark and W. Frech, Anal. Chim. Acta, 142 (1982) 129.
6 W. B. Barnett and E. A. McLaughlin, Jr., Anal. Chim. Acta, 80 (1975) 285.
7 D. B. Ratcliffe, C. S. Byford and P. B. Osman, Anal. Chim. Acta, 75 (1975) 457.
8 G. Delmonte Tamba and N. Luperi, Analyst (London), 102 (1977) 489.
9 M. Tominaga and Y. Umezaki, Anal. Chim. Acta, 110 (1979) 55.
10 P. Hocquellet and N. Labeyrie, At. Absorpt. Newsl., 16 (1977) 124.
11 P. Hocquellet and N. Labeyrie, Analusis, 3 (1975) 505.
12 K. Ohta and M. Suzuki, Anal. Chim. Acta, 107 (1979) 245.
13 H. Fritzsche, W. Wegschneider and G. Knapp, Talanta, 26 (1979) 219.
14 J. Meranger, J. Assoc. Off. Anal. Chem., 58 (1975) 1143.
15 H. L. Trachman, A. J. Tyberg and P. D. Branigan, Anal. Chem., 49 (1977) 1090.
16 A. W. Varnes and V. F. Gaylor, Anal. Chim. Acta, 101 (1978) 393.
17 S. Kojima, Analyst (London), 104 (1979) 660.
18 M. Sano, M. Furukawa, M. Kourai and I. Tomita, J. Assoc. Off. Anal. Chem., 62 (1979) 764.
19 G. L. Everett, T. S. West and R. W. Williams, Anal. Chim. Acta, 70 (1974) 291.
20 J. Y. Marks, G. G. Welcher and R. J. Spellman, Appl. Spectrosc., 31 (1977) 9.
21 Liyi Zhou, T. T. Chao and A. L. Meier, Talanta, 31 (1984) 73.
22 T. M. Vickrey, H. E. Howell, G. V. Harrison and C. J. Ramelow, Anal. Chem., 52 (1980) 1743.
23 Y. Thibaud, Rev. Trav. Inst. Pêches Mar. (France), 44 (1982) 349.
24 V. J. Zatka, Anal. Chem., 60 (1978) 538.
25 E. Pruszkowska, D. C. Manning, G. R. Carnick and W. Slavin. At. Spectrosc., 4 (1983) 87.
26 Jin Long Zhu, At. Spectrosc., 5 (1984) 91.
27 M. L. Kaiser, S. R. Koirtyohann and E. J. Hinderberger, Spectrochim. Acta, Part B: 36 (1981) 773.
28 G. F. Kirkbright, Shan Hsiao-Chuan and R. D. Snook, At. Spectrosc., 1 (1980) 85.
29 D. T. Burns, D. Dadgar and M. Harriott, Analyst (London), 109 (1984) 1099.
30 G. D. Rayson and J. A. Holcombe, Anal. Chim. Acta, 136 (1982) 249.
31 R. Pinel, M. Z. Benabdallah, A. Astruc, M. Potin-Gautier and M. Astruc, Analusis, 12 (1984) 344.

Analytica Chimica Acta, 181 (1986) 195—201
Elsevier Science Publishers B.V., Amsterdam — Printed in The Netherlands

THE USE OF SAMPLE ADDITIVES IN FLAME EMISSION SPECTROMETRY

R. REZAAIYAAN[a], G. M. HIEFTJE* and T. HIRSCHFELD[b]
Department of Chemistry, Indiana University, Bloomington, IN 47405 (U.S.A.)
(Received 3rd January 1985)

SUMMARY

New kinds of sample additives were investigated to increase the efficiencies of desolvation and atomization in flame spectrometry. Hydrazine and nigrosin were chosen as chemical and dye additives, respectively; an enhancement in the flame-emission signal was obtained in both cases. With nigrosin, it was possible to eliminate completely the interference of phosphate on a calcium emission signal. The increase in the signal for both additives was believed initially to be due to the more rapid evaporation of droplets in the sample aerosol. Further evidence, however, suggested that enhanced vaporization is responsible for the observed signal increase. It is suggested that similar sample additives might be useful also in inductively-coupled plasma emission spectrometry.

In flame emission, absorption and fluorescence spectrometric methods, samples are introduced as sprays and are only partially converted to the free atoms that are detected. Clearly, sensitivity, precision and reduced interelement interferences would all benefit from an improvement in the efficiency with which samples are converted to free atoms.

Desolvation is the first step involved in the atomization of sample droplets. Earlier studies on desolvation [1—3] showed it to be a process controlled by heat transfer. Immediately after droplet desolvation is complete, particle vaporization occurs. Vaporization can be controlled by either mass or heat transfer [4]. Recently [5], a new model was introduced which described the generation and ionization of atoms during the vaporization of individual solute particles in a flame.

In the present study, information gained during these earlier mechanistic investigations was used in an attempt to improve the overall efficiency of atom formation, and also to investigate the practical utility of new sample additives for eliminating vaporization interferences. In this approach, selected sample additives (nigrosin and hydrazine) were added to solutions to increase direct heat gain by a droplet during desolvation and to provide

---

[a]Present address: Chemistry Department, Luther College, Decorah, Iowa 52101, U.S.A.
[b]Permanent address: Department of Chemistry, Lawrence Livermore National Laboratory, P.O. Box 808, Livermore, CA 94550, U.S.A.

0003-2670/86/$03.50

a sample matrix with lower volatility. In the case of nigrosin, a black dye, an increase in heat gain should be realized by absorption of flame background radiation. For hydrazine, a readily oxidizable substance, heat gain should occur through an exothermic chemical reaction. For both species, the effect on droplet evaporation rate and overall atomization efficiency was investigated. Surprisingly, although an enhancement in overall atom formation was observed, neither additive caused a significant increase in the evaporation rate of individual droplets.

EXPERIMENTAL

Equipment and procedures

Emission measurements. A Beckman nebulizer-burner assembly, which provides a highly turbulent flame, was used for emission measurements. In such a flame, the evaporation of large droplets is not complete [6, 7]. Therefore, chemical interferences that are sensitive to the droplet-size distribution occur to a high degree. With this burner and a hydrogen/oxygen flame, vertical spatial scans of flame emission were taken. All subsequent measurements were made at 4.5 cm above the burner top, found to be optimal for the element (Ca) studied. The applied gas pressures of hydrogen and oxygen were, respectively, 2 and 10 psig.

For the spatially resolved measurements, the flame was focused onto the entrance slit (200 μm) of a 0.35-m monochromator (model EU-700, GCA/McPherson Instruments, Acton, MA). The emission intensity of the calcium 422.7-nm line was detected by a RCA 1P28 photomultiplier tube (Pacific Photometric Instruments, Emeryville, CA) powered at 500 V, and the resulting photocurrent was measured by a picoammeter (414S, Keithley Instruments, Cleveland, OH). The picoammeter output was monitored with a strip-chart recorder (Heath/Schlumberger model SR-204). Later, emission profiles were also obtained using a pre-mixed burner-nebulizer assembly (Instrumentation Laboratory, Wilmington, MA) with a stoichiometric (fuel/oxidant = 0.13) air/acetylene flame.

Absorption measurements. A conventional atomic absorption spectrometer (Heath Atomic Absorption, Model EU-705-70) was used to measure the spatial flame absorbance profile in a stoichiometric (fuel/oxidant = 0.14) air/acetylene flame. The slit width of the monochromator was set at 126 μm and the photomultiplier tube was operated at 500 V.

Desolvation-rate measurements. A droplet generator system similar to the one described originally by Hieftje and Malmstadt [1] was selected as the sample-introduction system. This system enables one to inject uniformly-sized aerosol droplets into a flame reproducibly, and to study an individual droplet without interference from neighboring droplets.

Desolvation rates for various solutions in an air/acetylene flame were measured using an experimental technique and apparatus similar to those previously described [1, 8]. In this technique, the rate of droplet desolvation

is measured by observation of the change in droplet size with time as the droplet travels through the flame. Because droplets are introduced into the flame at a known frequency, the time between droplets is known and the droplet velocity in the flame can be deduced. Therefore, the change in droplet size with its position in the flame can be related to the variation of droplet diameter with time.

Droplet sizes were measured by the MgO impression technique [9]. A single-flash photograph of droplets entering the flame was taken with a high-intensity stroboscope and the observed height versus the residence time in the flame was obtained from the photograph.

To obtain the experimental desolvation rate, the square of the measured diameter of the droplet was plotted versus the time after its entry into the flame. The least-squares slope of the line so obtained was taken as the desolvation rate. The initial droplet diameters used were 68 ± 2 and 60 ± 2 μm for hydrazine and nigrosin solutions, respectively.

Reagents. Stock solutions of calcium (from dried reagent-grade calcium chloride), aluminum (from reagent-grade aluminum chloride), phosphate (from phosphoric acid) and nigrosin dye (MC/B, Norwood, OH) were prepared according to standard procedures [10]. Standards were prepared by suitable dilution of stock solutions and 95% hydrazine (Eastman Kodak Co., Rochester, NY 14650).

RESULTS AND DISCUSSION

Emission measurements

Because the results obtained in both absorption and emission modes were similar, only emission data are reported here.

Hydrazine. Figure 1 reveals that the emission signal of a phosphate-containing calcium solution in the total consumption burner peaks at 1.25% of added hydrazine. Because this behavior was reproducible (2% r.s.d.), this concentration of hydrazine was used in further experiments. The well known phosphate-caused depression in the calcium signal in Fig. 1 is due to the formation of a relatively non-volatile compound [11—13]. In the absence of phosphate, the initial decrease in the calcium signal by adding hydrazine could be a physical effect (e.g., change in density, viscosity and surface tension of the solution). A small change in any of these parameters alters the sample uptake rate and consequently affects the emission signal. At higher concentrations of hydrazine, vaporization or desolvation efficiency might be enhanced. In the presence of phosphate (lower curve), it is possible that hydrazine complexes with calcium only at specific concentrations (0—1.5% by weight), thus reducing the phosphate-induced signal depression.

The vertical profiles of Fig. 2 show that hydrazine does not significantly alter the emission signal of calcium alone but even at its optimal concentration only partially overcomes the signal depression induced by phosphate.

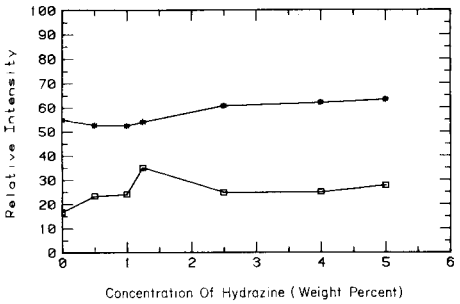

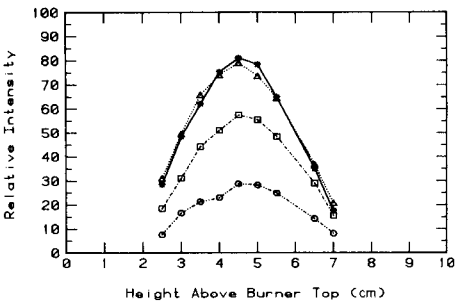

Fig. 1. Effect of hydrazine on calcium emission: (*) without phosphate; (⊡) in presence of phosphate (100 mg l^{-1}). Conditions: 4.5 cm above the burner top with a Beckman burner; 50 mg l^{-1} calcium.

Fig. 2. Vertical spatial profiles of calcium emission taken with a Beckman burner: (*) 50 mg l^{-1} Ca; (⊙) 50 mg l^{-1} Ca + 100 mg l^{-1} PO_4^{3-}; (△) 50 mg l^{-1} Ca + 12500 mg l^{-1} hydrazine; (⊡) 50 mg l^{-1} Ca + 100 mg l^{-1} PO_4^{3-} + 12500 mg l^{-1} hydrazine.

Nigrosin. Figure 3 compares the effect of nigrosin on the Ca I (422.7 nm) emission intensity, taken with a laminar flame, in the presence and absence of phosphate. It can be noted that in the absence of phosphate (upper curve) nigrosin suppresses the calcium signal at low added concentrations but enhances it at higher concentrations. A similar effect to that of hydrazine might be responsible for the observed behavior. In the presence of phosphate (lower curve), however, nigrosin restores the calcium emission signal to its original value. A comparison of phosphate interference on a calcium signal, taken with a laminar flame, in the presence and absence of nigrosin, is given in Fig. 4. Clearly, nigrosin is efficient in maintaining the calcium signal at essentially its original (no interference) value.

An attempt was made to evaluate the effect of nigrosin on the interference of aluminum on calcium. Unfortunately, because of the insolubility of nigrosin in calcium chloride solutions in the presence of an aluminum salt, an even greater depression of the signal occurred by adding nigrosin than in its absence (Fig. 5). Unfortunately, because nigrosin is a poorly characterized mixture of compounds, it is difficult to explain the cause of this insolubility. In addition, because there is little literature information on the chemistry of nigrosin with other cations, it is not known if the salts of those cations are soluble in nigrosin-containing solutions.

Desolvation studies

The observed increase in the signal with the total-consumption burner caused by the addition of hydrazine (Fig. 1) was believed to be due in part to the enhanced evaporation rate of droplets, hydrazine undergoes combustion in the flame according to the following reaction, and transfers some of its heat of reaction (ΔH_c) to the droplets:

$$NH_2NH_2 + O_2 \rightarrow N_2 + 2H_2O \quad (\Delta H_c = 125 \text{ kcal mol}^{-1}) \qquad (1)$$

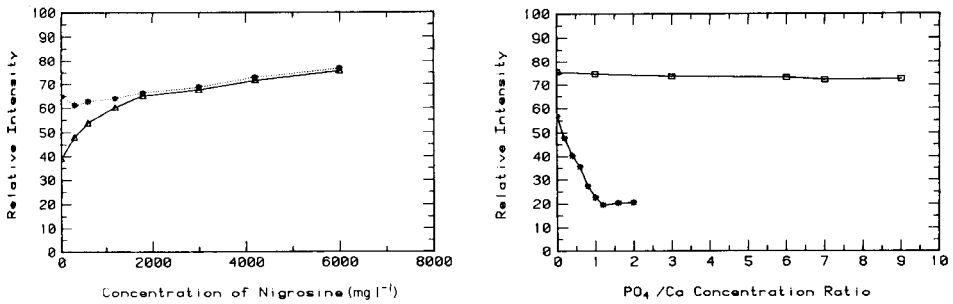

Fig. 3. Effect of nigrosin on calcium emission: (*) without phosphate; (△) in presence of phosphate (100 mg l^{-1}). Conditions: premixed burner; observation height optimized for greatest signal; 50 mg l^{-1} calcium.

Fig. 4. Effect of phosphate on calcium emission: (*) without nigrosin; (□) with nigrosin (6 g l^{-1}). Conditions: laminar air/acetylene flame; 50 mg l^{-1} calcium.

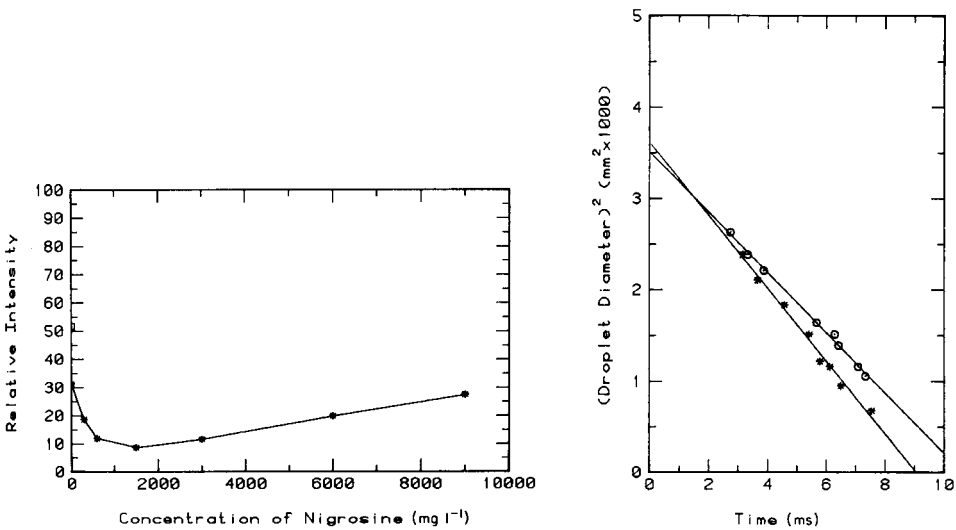

Fig. 5. Effect of nigrosine on emission from calcium (50 mg l^{-1}) in the presence of Al (100 mg l^{-1}) taken at 4.5 cm above the burner top with a Beckman burner.

Fig. 6. Desolvation plots: (*) Ca (50 mg l^{-1}); (⊙) Ca (50 mg l^{-1}) + orthophosphate (100 mg l^{-1}) + nigrosin (1200 mg l^{-1}). The regression equations for these plots are D^2 = −(0.40 ± 0.03)t + (3.61 ± 0.20) with correlation coefficient (r^2) of 0.989, and D^2 = −(0.33 ± 0.03)t + (3.51 ± 0.11) with correlation coefficient (r^2) of 0.996, respectively.

From this reaction, an aqueous solution of 14% (w/v) hydrazine would liberate enough heat upon oxidation to evaporate the solution completely. Moreover, during this reaction the generated nitrogen should evolve violently, and generate bubbles which would fragment a droplet or its desolvated particles. In both cases, hydrazine should enhance the atomization efficiency by producing smaller droplets or desolvated particles.

A different mechanism was hypothesized for the observed enhancement of a calcium signal by added nigrosin (Fig. 3). Nigrosin, a black dye, was believed to absorb flame background radiation and transfer the gained energy to an evaporating droplet; alternatively, nigrosin as an organic dye could burn in the flame once a droplet had evaporated. It would thereby generate extra energy, leave the remaining solute in a finely divided state, and thus enhance atomization.

To distinguish among these possibilities, droplet desolvation rates were measured directly [1]. Figure 6 shows desolvation plots for nigrosin-containing droplets. The desolvation rates calculated from the slopes of the desolvation plots are listed in Table 1 for nigrosin and hydrazine-containing solutions. The measured rates are all in close agreement with the value obtained previously for a simple solution [1—3]. Apparently, there is no significant effect of either additive (nigrosin or hydrazine) on the desolvation process. Therefore, an alternative explanation must be found for the enhancements observed during the emission measurements.

The mechanism by which either additive reduces the interference of phosphate on calcium might be similar to that involving EDTA, glycerol or dextrose. The work of Wirtschafter [14] showed that EDTA can be used to suppress the interference of phosphate on calcium. Pro and Mathers [15] reported that dextrose in the presence of phosphate in concentrations of 20—100 mg l^{-1} enhances the emission intensity of calcium. Finally, others [16] have used glycerol as an agent to reduce the signal-depressing effect of various anions, including nitrate, phosphate and sulfate on the emission of calcium. In all of those studies, the interference of phosphate on calcium was eliminated either by combining the metal with an anion to form a complex or compound which readily decomposes in the flame, or by dispersing the analyte in a more volatile matrix. It is likely that nigrosin and hydrazine enhance the calcium signal according to such mechanisms. However, no evidence has yet been found conclusively to support or refute this hypothesis.

TABLE 1

Desolvation rates for 50 mg l^{-1} calcium solutions containing phosphate and hydrazine or nigrosine

Species added (mg l^{-1})			Desolvation rate[a] ($mm^2\ s^{-1}$)
Phosphate	Hydrazine	Nigrosin	
—	—	—	0.37 ± 0.05
100	5055	—	0.30 ± 0.04
100	11323	—	0.32 ± 0.02
100	—	1200	0.33 ± 0.06
100	—	3000	0.28 ± 0.03

[a]Error in slopes is reported with 95% (n = 8) confidence limit.

To understand the exact mechanism of enhancement of these new sample dditives, further studies are needed. It would be useful to examine the ffect of sample additives on the interference of additional anions (e.g., sul- ate) and cations on calcium. However, the limited practical utility of these dditives indicates that further studies are not warranted.

From a practical point of view, the use of neither hydrazine nor nigrosin s recommended as a sample additive. Hydrazine solutions are not stable over xtended (hour-long) periods of time and do not eliminate completely the aporization interference. Similarly, the practical utility of nigrosin as an dditive is limited by its insolubility in the presence of some cations. Never- heless, the authors believe that the results of this study point toward the ossible utility of new kinds of sample additives for atomic spectrometry. uch additives could increase sample atomization not only by complexing r dispersing the analyte, but also by increasing the thermal energy available o the sample, by conduction or chemical reaction.

This work was supported in part by the National Science Foundation hrough grants CHE 82-14121 and CHE 83-20053 and by the Office of laval Research.

EFERENCES

1 G. M. Hieftje and H. V. Malmstadt, Anal. Chem., 40 (1968) 1860.
2 N. C. Clampitt and G. M. Hieftje, Anal. Chem., 44 (1972) 1211.
3 N. C. Clampitt and G. M. Hieftje, Anal. Chem., 46 (1974) 382.
4 G. J. Bastiaans and G. M. Hieftje, Anal. Chem., 46 (1974) 901.
5 B. D. Bleasdell, E. P. Wittig and G. M. Hieftje, Spectrochim. Acta, Part B: 36 (1981) 205.
6 A. P. D'Silva, R. N. Kniseley and V. A. Fassel, Anal. Chem., 36 (1964) 1287.
7 J. H. Gibson, W. E. L. Grossman and W. D. Cooke, Anal. Chem., 35 (1963) 266.
8 G. M. Hieftje, Ph.D. Thesis, University of Illinois, 1969.
9 K. R. May, J. Sci. Instrum., 27 (1950) 128.
0 J. A. Dean and T. C. Rains, in J. A. Dean and T. C. Rains (Eds.), Flame Emission and Atomic Absorption Spectrometry, Chap. 13, Vol. 2, M. Dekker, New York, 1971, p. 332.
1 C. Th. J. Alkemade and M. H. Voorhuis, Z. Anal. Chem., 163 (1958) 91.
2 S. Fukushima, Mikrochim. Acta, (1959) 596.
3 R. Herrmann, C. Th. J. Alkemade and P. J. Gilbert, Chemical Analysis by Flame Photometry, Interscience, New York, 1963.
4 J. D. Wirtschafter, Science, 125 (1957) 603.
5 M. J. Pro and A. P. Mathers, J. Assoc. Off. Agric. Chem., 37 (1954) 945.
6 H. B. Heeny, G. M. Ward and A. F. Willson, Analyst (London), 87 (1962) 49.

Analytica Chimica Acta, 181 (1986) 203—209
Elsevier Science Publishers B.V., Amsterdam — Printed in The Netherlands

SIMULTANEOUS DETERMINATION OF IRON(II) AND IRON(III) IN AQUEOUS SOLUTION BY KINETIC SPECTROPHOTOMETRY WITH TIRON

SHIGEKI ABE*, TAMAKI SAITO and MASAMI SUDA
Department of Applied Chemistry, Yamagata University, Yonezawa 992 (Japan)
(Received 30th July 1985)

SUMMARY

A kinetic spectrophotometric method that requires no prior measurement of rate constants is developed for the simultaneous determination of iron(II) and iron(III). The method is based on the aerial oxidation of iron(II) in the presence of tiron and acetate ions. The iron(III) formed is subsequently complexed with tiron and the absorbance/time relation is evaluated. The concentrations of iron(III) and iron(II) are obtained from the absorbance values at the start and at equilibrium, respectively, calculated by non-linear least-squares fitting. A linear calibration graph is obtained up to 12 μg ml^{-1} iron(II)/iron(III). The method is applied to iron-rich ground water.

The determination of iron in its different oxidation states present in a particular aquatic system is of great importance. There is increasing evidence that non-equilibrium processes involving iron may lead to measurable concentration of iron(II) species in natural and industrial waste waters [1]. Although various analytical techniques including u.v.-visible spectrophotometry, atomic absorption spectrometry and spectrofluorimetry have been used for the measurement of iron(II) and iron(III), only a few approaches have been developed to quantify the different oxidation state species of iron in a sample. Several electroanalytical methods, e.g., polarography [2] and voltammetry [3], have been applied to rock samples, and flow-injection procedures, with electrochemical detection, have also been used for the simultaneous determination of iron(II) and iron(III) [4, 5]. Lynch et al. [6] determined both species spectrophotometrically by synchronized sample injection into two parallel flow systems, in which iron(II) was determined with 1,10-phenanthroline and iron(III) with thiocyanate. Combinations of flow injection with two detection techniques were also reported [7, 8]. These complicated systems were simplified by incorporating a Jones reductor column before spectrophotometric detection [9] with 1,10-phenanthroline, using a single detector.

Differential rate methods are a versatile alternative for the analysis of mixtures of metal ions. Various differential kinetic methods have been reported [10] but few practical applications to real samples have been

described owing to their poor selectivity. This paper reports a rapid and inexpensive procedure for the simultaneous kinetic determination of iron(II) and iron(III). The method is based on the aerial oxidation of iron(II) and complex formation of iron(III) with tiron (sodium 1,2-dihydroxybenzene-3,5-disulfonate). In the presence of tiron and acetate buffer, aerial oxidation of iron(II) is accelerated and complete within a short time. The additional iron(III) formed is complexed to form more iron(III)/tiron chelate. The iron(II) oxidation is first order, so an appropriate kinetic equation can be used to treat the absorbance/time data to give the initial and equilibrium absorbances, which are a measure of iron(III) and total iron concentration. Rate-constant measurements are not required. This gives a simple basis for interference-free spectrophotometric determination of iron(II) and iron(III). The method has the advantage of requiring a single sample. It does not require precise control of temperature, unlike most kinetic measurements.

EXPERIMENTAL

Reagents and apparatus

All chemicals used were of analytical-reagent grade. Deionized water from a Millipore Milli-Q system was used throughout. Standard iron(II) and iron(III) solutions (500 μg Fe ml^{-1}) were prepared by dissolving weighed amounts of ammonium iron(II) sulfate and ammonium iron(III) sulfate in 0.18 M sulfuric acid. The solutions were standardized by redox titration and stored in polyethylene bottles for sequential dilution. The tiron solution (5%, w/v) was prepared in water. A 0.2 M acetate buffer solution, pH 5.3, was prepared from acetic acid and sodium acetate.

A Hitachi Model 228 double-beam spectrophotometer with 10-mm cells was used for absorbance measurements. Measurements of pH were made with a Hitachi-Horiba model M-5 pH meter. A Sharp MZ-80 B personal computer was used to evaluate kinetic data.

Procedures

Kinetic measurements were made spectrophotometrically by monitoring the absorbance of the iron(III)/tiron complex at 558 nm. Reactants were taken in the following order: the requisite volume of water to make the final volume of the reaction mixture 50 ml, acetate buffer (10 ml), and exactly 2 ml of tiron solution. The reaction was started by addition of exactly 2 ml of sample solution. For samples of low iron concentration, it is recommended first to place the sample (2—20 ml) in a volumetric flask and then to initiate the reaction by addition of tiron. Absorbance values were recorded at 1-min intervals after manual sample mixing. As the reaction was found to follow a simple exponential equation (i.e., first order), the absorbance values at the start (A_0) and at equilibrium (A_e) were calculated by nonlinear regression analysis of the data (see below). The concentrations of both

iron(II) and iron(III) were evaluated from a calibration graph of the absorbance vs. iron(III) concentration obtained by equilibrium measurements. All experiments were done at room temperature.

RESULTS AND DISCUSSION

Spectrophotometric characteristics

In weakly acidic media, tiron forms violet 1:2 iron(III)/ligand chelates, solutions of which are stable. Maximum absorbance is attained almost immediately. Oxidation of iron(II) by dissolved oxygen normally proceeds very slowly in acidic solution. No complex formation between iron(II) and tiron has been reported. Preliminary studies, however, indicated that aerial oxidation of iron(II) occurs more readily when the medium contains tiron and acetate ions. Typical absorbance/time curves for tiron/iron(II) systems are shown in Fig. 1. The rate of iron(II) oxidation is dependent on pH, the reaction proceeding faster at higher pH. The absorption spectra of the complex (λ_{max} = 558 nm) corresponds to that of the iron(III)/tiron complex, and the molar absorptivity obtained at equilibrium was the same as that of the iron(III) complex. The absorbance/time profiles for iron(II) were found to follow an exponential equation.

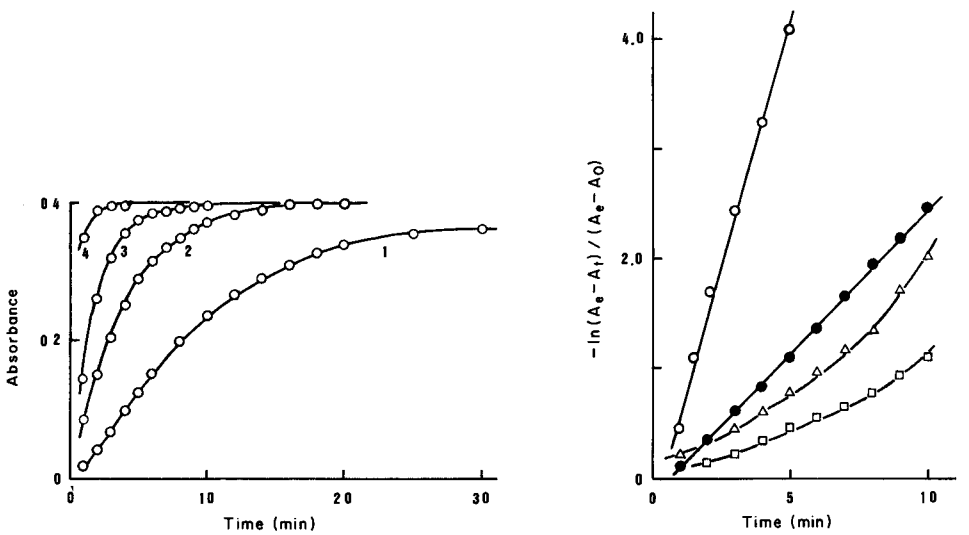

Fig. 1. Absorbance time curves for the oxidation of iron(II) in the presence of tiron; (1) pH 5.0; (2) pH 5.3; (3) pH 5.6; (4) pH 6.2. Each solution contained 5 μg ml^{-1} iron(II).

Fig. 2. Kinetic plots for iron/chromogen systems at pH 5.6: (○) 0.2% tiron (558 nm); (●) 0.08% protocatechuic acid, Na salt (565 nm); (△) 0.08% 2,3-dihydroxynaphthalene-6-sulfonic acid, Na salt; (510 nm); (□) 0.2% chromotropic acid, Na salt (640 nm). Each solution contained 5 μg ml^{-1} iron(II).

Effect of reaction variables

Some colorimetric reagents for iron(III) were evaluated as reagents for the kinetic determination. The results are shown in Fig. 2. Graphs of $\log(A_e - A_t)/(A_e - A_0)$ vs. time, indicating first-order kinetics, were linear for tiron and protocatechuic acid. Tiron was the most sensitive of the reagents investigated and had no appreciable background absorbance. The absorbance was constant above 0.05% tiron concentration.

The effect of pH is shown in Fig. 3. As a compromise between the oxidation rate of iron(II) and spectrophotometric sensitivity, pH 5.3 was chosen for the analytical measurements. The reaction was complete after ca. 10 min at room temperature. The effect of dissolved oxygen is shown in Fig. 4. Naturally, prior deoxygenation of the solution with nitrogen gas decreased the oxidation rate of iron(II). According to Stumm and Lee [11], the rate of oxidation of iron(II) in simple aqueous media is first order with respect to the partial pressure of oxygen as well as to the iron(II) concentration, at constant pH. However, slight variations in the dissolved oxygen content had no effect on the present iron determination, because a change in the rate of iron(II) oxidation did not alter the final A_e value.

Rate equation

The rate of formation of the iron(III) complex was followed by recording the absorbance/time curves at 558 nm. Under the experimental conditions of constant pH and with an excess of tiron with respect to iron(II), the semi-log plots of absorbance vs. time were linear, and indicated that the oxidation was first order with respect to iron(II) (Fig. 2). Thus, the integrated equation in absorbance terms can be written as

$$-\ln (A_e - A_t)/(A_e - A_0) = kt \qquad (1)$$

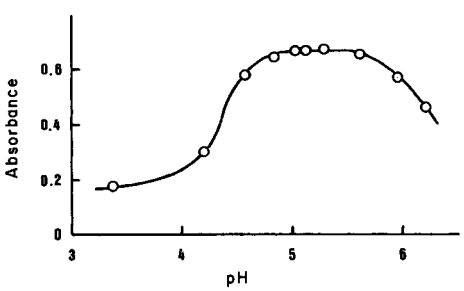

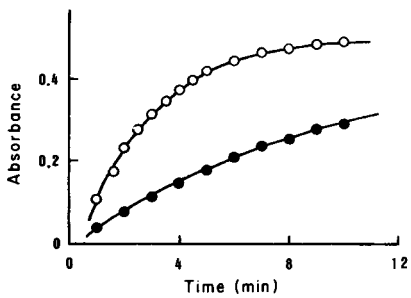

Fig. 3. Effect of pH on the absorbance of iron(III)/tiron complex, 8 μg ml^{-1} iron(III).

Fig. 4. Effect of dissolved oxygen on the rate of oxidation of iron(II) in the presence of tiron: (○) normal dissolved oxygen content; (●) after deoxygenation with nitrogen (6 μg ml^{-1} iron(II)).

where k is the conditional rate constant and A_0, A_t and A_e are the absorbances after zero time, time t, and at equilibrium, respectively. To avoid complications from deciding the exact incidence of t_0, an experimental time lag (t_ϕ) was introduced. Therefore, Eqn. 1 is modified:

$$-\ln (A_e - A_t)/(A_e - A_0) = k(t - t_\phi) \quad (2)$$

Various methods for the estimation of A_0 and A_e were considered; the technique adopted is based on non-linear regression. From Eqn. 2, $(A_e - A_t) = (A_e - A_0) \exp[-k(t - t_\phi)]$; a computer program was written to achieve the best least-squares fit of the data to this equation, and the best values of A_e and A_0 were obtained. The concentrations of iron(II) and iron(III) were obtained from a calibration graph of absorbance vs. iron(III) concentration. The A_e and A_0 values correspond to the concentration of total iron and iron(III), respectively, so that the initial iron(II) concentration can be obtained by difference. The value of A_e is highly reproducible, but changes in lag time cause errors in the A_0 value.

Calibration and interference studies

Under the experimental conditions described, the calibration graphs were identical for oxidized iron(II) and iron(III), and linear up to 12 μg ml^{-1} iron. The molar absorptivity of the iron(III)/tiron complex was 4.17×10^3 l mol^{-1} cm^{-1}. At 5×10^{-5} M iron(II) and iron(III), the relative standard deviations were 2.0 and 2.2% (n = 9), respectively.

The conventional spectrophotometric procedure for iron(III) with tiron is almost free from interferences [12]. The analytical results for spiked water samples were in good agreement, showing quantitative recovery of iron(II) and iron(III) (Table 1), indicating that the ions commonly present in ground water samples did not interfere significantly. Interferences from aluminum (<10 μg ml^{-1}) can be eliminated by very carefully controlled addition of fluoride.

TABLE 1

Recovery of iron(II) and iron(III) from spiked samples

Matrix	Iron added (μg ml^{-1})		Iron found (μg ml^{-1})	
	Fe(II)	Fe(III)	Fe(II)	Fe(III)
River water	1.00	5.00	0.99	4.83
	3.00	3.00	2.95	2.94
	5.00	1.00	4.93	0.98
Ground water	1.00	5.00	0.97	4.76
	3.00	3.00	2.86	2.91
	5.00	1.00	4.84	0.92

Reaction mechanism

Mechanistic studies of the oxidation of iron(II) have been described. Poe and Diehl [13] reported that iron(II) complexes of some dihydroxy compounds were rapidly and quantitatively oxidized by air. A spectrophotometric determination of iron with *N*,*N*-bis(2-hydroxybenzyl)ethylenediamine-*N*,*N*-diacetic acid was based on a similar reaction [14]; the iron(II) complex formed was oxidized rapidly to the red iron(III) complex. The exact mechanism of the reaction between iron(II), oxygen and tiron is not fully known; experimental evidence indicates that the iron(II) is first oxidized by dissolved oxygen to iron(III), which then reacts with tiron. The oxidation of iron(II) did not proceed appreciably in the absence of tiron. Though sulfosalicylic acid is more sensitive than tiron for spectrophotometric iron(III) determinations, iron(II) was not quantitatively oxidized to iron(III) in acetate media containing sulfosalicylic acid. This suggests that tiron acts as a catalyst for the oxidation of iron(II), as well as chromogenic complexing agent for iron(III). As shown in Fig. 2, linear plots for $\log(A_e - A_t)/(A_e - A_0)$ vs. time indicated that there is only a single rate-determining step. The role of acetate ion was significant; no enhancement of the rate of iron(II) oxidation was observed in phosphate buffer solutions of similar pH. Acetate ions are known to activate iron(III) in catalimetric spectrophotometry [15].

Analysis of ground waters

The validity of the method was tested with ground-water samples. The normal concentration level of iron in ground water collected in the Yonezawa district was below the detection limit of the present method and most samples contained <0.1 μg ml^{-1} total iron. Typical results for iron-rich samples are shown in Table 2. They were checked by atomic absorption spectrometry (a.a.s.) and u.v.-visible spectrophotometry and were in good agreement. Each sample of a particular origin was also analyzed on different days to assess the degree of iron(II) oxidation, because the collection of ground-water samples with subsequent analysis at a laboratory several

TABLE 2

Determination of iron(II) and iron(III) in iron-rich ground waters

Sample	Proposed method (μg ml^{-1})			A.a.s. (μg ml^{-1})	Spectrophotometry[b] (μg ml^{-1})
	Fe(II)	Fe(III)	Total Fe		
A	9.32	1.68	11.00	10.45	10.87
B	1.80	0.92	2.72	2.91	2.66
C	1.89	0.04	1.93	2.16	1.98
D[a]	77.48	49.12	126.0	114.8	125.0

[a]Acidic exuded water from a closed mine. [b]Measured as Fe(II) 1,10-phenanthroline complex.

days later could introduce a large variation in the iron(II)/iron(III) ratio. It is well known that iron(II) is rapidly oxidized in most surface waters, providing a simple process for iron removal [16]. This was confirmed by a marked decrease in the iron(II)/iron(III) ratio with time. Even though the sample preservation technique based on acidification with sulfuric acid was applied, the natural equilibrium concentrations of iron species present was altered during storage. At $\mu g\ ml^{-1}$ levels, about 40% of the total iron had been oxidized to iron(III) after 10 days. As sample deterioration is clearly a major problem, the collected samples should be analyzed as soon as possible for iron species.

REFERENCES

1 T. D. Waite and F. M. M. Morel, Anal. Chem., 56 (1984) 787.
2 M. E. Beyer, A. M. Bond and R. J. W. McLaughlin, Anal. Chem., 47 (1975) 479.
3 W. M. Moore, Anal. Chim. Acta, 105 (1979) 99.
4 B. P. Bubnis, M. R. Straka and G. E. Pacey, Talanta, 30 (1983) 841.
5 J. W. Dieker and W. E. van der Linden, Anal. Chim. Acta, 114 (1980) 267.
6 T. P. Lynch, N. J. Kernoghan and J. N. Wilson, Analyst (London), 109 (1984) 843.
7 J. L. Burguera and M. Burguera, Anal. Chim. Acta, 161 (1984) 375.
8 T. P. Lynch, N. J. Kernoghan and J. N. Wilson, Analyst (London), 109 (1984) 839.
9 A. T. Faizullah and A. Townshend, Anal. Chim. Acta, 167 (1985) 225.
10 D. Perez-Bendito, Analyst (London), 109 (1984) 891.
11 W. Stumm and G. F. Lee, Ind. Eng. Chem., 52 (1961) 143.
12 J. H. Yoe and A. L. Jones, Ind. Eng. Chem., Anal. Ed., 16 (1944) 111.
13 D. P. Poe and H. Diehl, Talanta, 21 (1974) 1065.
14 T. Katsuyama and T. Kumai, Bull. Chem. Soc. Jpn., 54 (1981) 1544.
15 S. Nakano, M. Odzu, M. Tanaka and T. Kawashima, Mikrochim. Acta, I (1983) 403.
16 T. M. Florence and G. E. Batley, Crit. Rev. Anal. Chem., 9 (1980) 219.

Analytica Chimica Acta, 181 (1986) 211—218
Elsevier Science Publishers B.V., Amsterdam — Printed in The Netherlands

MERCURY-COATED CARBON FIBER MICROELECTRODES
Preparation and Some Properties

JANUSZ GOŁAS[a] and JANET OSTERYOUNG*

Department of Chemistry, State University of New York at Buffalo, Buffalo, NY 14214 (U.S.A.)

(Received 15th July 1985)

SUMMARY

Carbon fiber microelectrodes were made by sealing the fibres into glass and by using heat-shrinkable tubing. The electrodes can be coated with mercury by deposition at −0.9 V vs. SCE from 0.1 M thiocyanate containing 0.05 mM mercury(II) at pH 2.5. Coulometric measurements and square-wave voltammetry were used to establish the properties of the deposit. Conditions for the deposition and stripping of cadmium are outlined.

Recent publications have described promising possibilities for electroanalytical measurements with carbon fiber microelectrodes [1—5]. Different types of electrodes have been tested but it seems that the most useful is a simple fiber microelectrode. Its length is usually about 0.5—2 mm and the diameter 8—12 μm. Other types also made from carbon fibers like brush or disk microelectrodes have disadvantages such as relatively high background current (brush) or low faradaic current disk [3].

Investigations of the behavior of simple carbon fiber electrodes under various experimental conditions are still nascent so publication of experimental observations might assist further development in this field even if the observations cannot be rationalized in detail. The very small dimensions of these fibers and their fragility cause certain difficulties in preparing microelectrodes. The procedure mainly recommended until now is based on sealing a fiber in a capillary using epoxy resin. This procedure is time-consuming and can produce artifacts associated with the epoxy resin. Accordingly, two new ways of preparing carbon fiber microelectrodes are proposed here. Investigations of the properties of mercury-coated carbon fiber microelectrodes were also done and the results are presented in this paper. Coulometric measurement during deposition of mercury was usually followed by square-wave voltammetry (SWV). Anodic SWV was also used for investigation of cadmium deposits on the mercury-coated electrode. Choice of the

[a]Permanent address: Academy of Mining and Metallurgy, Institute of Material Science, 30-059 Kraków, Poland.

0003-2670/86/$03.50

conditions for this investigation was guided by literature concerning glassy-carbon disc electrodes [6—8]. Stulikova [6] showed that mercury deposited on a glassy carbon disc exists in the form of droplets, the size and location of which depend strongly on the potential of deposition. It is probable that mercury behaves in a similar manner on the carbon fiber surface.

EXPERIMENTAL

Instrumentation and reagents

A three-electrode system in an IBM electrolytic cell was used with a PAR Model 173 potentiostat and Model 179 digital coulometer. A square-wave analyzer (ODSW) was used for all square-wave voltammetric measurements [9]. This instrument operates at a fixed frequency of 30 Hz and in all cases a square-wave amplitude of 20 mV and sweep rate of 100 mV s^{-1} were used. A saturated calomel reference electrode and a platinum wire auxiliary electrode were used. Solutions were purged with argon before measurement and blanketed with argon during measurement. All reagents were of analytical grade, and solutions were prepared with distilled water which had been passed through a Millipore Milli-Q water purification system. The working solutions were prepared just before use from the following stock solutions: 0.1 M potassium thiocyanate, 2.35 M nitric acid, 5×10^{-2} M mercury(II) nitrate, and 1×10^{-2} M cadmium nitrate.

Preparation of microelectrodes

At first, the procedure proposed by Schulze and Frenzel [3] was used: the carbon fiber was inserted into a glass disposable pipet and sealed with a resin (Buehler Epoxide with hardener). Disadvantages of this procedure were the relatively long time needed for hardening of the resin (ca. 24 h) and that proportions of hardener to resin had to be controlled precisely. Unless this condition was fulfilled, adhesion of the resin to the fiber was sometimes lost and the seal leaked. This could be observed indirectly when the electrode, after working for several hours in the solution, changed its behavior and the mercury contact inside the pipet changed color. For these reasons, improved methods were sought for making electrodes from these fibers. The carbon fiber used in all cases was Aesar (Johnson Matthey, Seabrook, NH) with a diameter of 8 μm.

For one type of electrode, a carbon fiber about 2.5-cm long was inserted into the capillary tip of a soft glass pipet which had been cut and narrowed at the tip by heating. Then the tip was put into the flame of a small burner; this burner had a special glass tube head (diameter 2.5 cm, length 10 cm) fixed onto the standard burner with a cork washer. The tip must be put into the narrow wall of flame which surrounds the edge of the tube so that the fiber is inside where it is cool. Then it is held carefully until the tip collapses. After that the electrode is taken out quickly. This procedure requires some skill, but in this way many electrodes can be made in a very short time,

even if some of them are wasted because of burning or breaking. The idea is illustrated in Fig. 1. The outside part of fiber should not be longer than about 1.5 mm. If it is longer, the fiber begins to wave in the flame and usually burns. The inside of the glass part of the electrode was filled with mercury to enable electrical connection with silver or platinum wire. The electrodes were then checked under a microscope and cut to the required length.

For another type of electrode, a micro-bore Tygon tube (0.4 mm i.d., 1.6 mm o.d., ca. 2.5 mm long) is placed inside one end of a heat-shrinkable tube (2 mm i.d., 7—8 mm long). The other end of this tube is pulled onto the tip of a disposable glass pipet which has been cut and partly sealed. The carbon fiber is threaded into the capillary through the Tygon tube. The half of the shrinkable tube surrounding the inner Tygon tube is gently heated with a soldering iron. During heating the Tygon melts and the exterior tube shrinks. It is advisable to observe the tip at that moment through a magnifying glass in order not to overheat the tubing. The procedure is illustrated in Fig. 2. After the seal has been made, the electrodes are examined and their lengths measured under a microscope. Here, in contrast with the previous procedure, the fibre can be cut to any required length. Also, in this case the fiber is not exposed to flame. One electrode can be made in 5 min. For convenience, the electrodes are denoted as G-type (sealed in glass) or T-type (sealed in Tygon).

RESULTS AND DISCUSSION

The aim of this work was to establish if these types of microelectrodes could be used as the basis for mercury-coated carbon fiber microelectrodes and to evaluate the general properties of such electrodes. Investigations were done in 0.1 M potassium thiocyanate, as there are reports on the utility of this medium for plating mercury onto glassy carbon disks and carbon fiber electrodes [3, 5, 7]. Under these conditions, 98% of the mercury in solution exists as $Hg(SCN)_4^{2-}$, and the calculated equilibrium potential at zero ionic

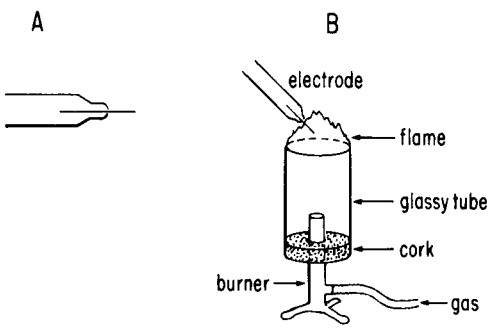

Fig. 1. Schematic diagram of procedure for making a carbon fiber microelectrode by sealing into glass: (A) carbon fiber in capillary tip; (B) sealing fiber into the tip.

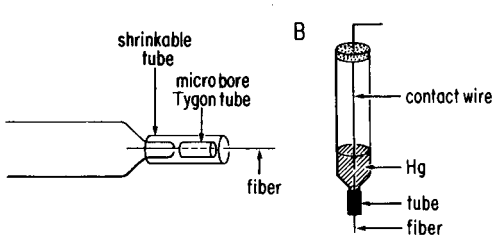

Fig. 2. (A) The assembly of the microelectrode tip; (B) Diagram of the finished microelectrode.

strength and 10^{-5}—10^{-4} M mercury(II) is in the range —0.02 to —0.05 V vs. SCE [10].

Deposition of mercury and cadmium

A G-type electrode (l = 0.75 mm) was immersed in a solution of 0.1 M KSCN, 0.05 mM Hg(II) and 0.0 mM Cd(II). The electrode was conditioned for about 10 min at +0.7 V (until the anodic current dropped below 0.1 μA), and then deposition was begun at —0.9 V for 2 min with stirring.

The magnetic stirrer was switched off 15 s before the end of the deposition and after that a square-wave voltammetric scan was done from —0.9 to +0.6 V. The positive potential limit ensures that mercury and cadmium are stripped off the electrode. The above procedure was repeated for various pH values which were obtained by adding 2.3 M nitric acid.

The peak current of oxidation of mercury increases as the pH decreases, which is opposite to the situation with cadmium. Results are presented in Table 1 and a representative curve for pH 2.00 is shown in Fig. 3. These results suggest that the optimal pH for both elements is about pH 2.5. Thus all further experiments were done in 0.1 M thiocyanate acidified with nitric acid to pH 2.48.

TABLE 1

Dependence of anodic peak current on pH for anodic stripping square-wave voltammetry of Cd and Hg co-deposited from 0.1 M KSCN (SWV; ΔE = 20 mV, sweep rate 100 mV s^{-1}) after 2 min deposition on carbon fiber microelectrode[a]

	Peak current (μA)	
pH	Hg	Cd
5.2	1.60	2.90
3.8	1.65	2.75
3.4	1.70	2.50
2.9	1.90	2.45
2.4	2.10	2.00
2.0	2.25	1.45

[a]8 μm diameter, 0.75 mm long.

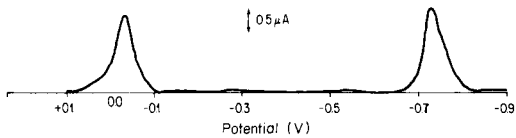

Fig. 3. Anodic-stripping SWV of Hg and Cd deposited on a carbon fiber microelectrode at pH 2.00 in 0.1 M KSCN. E_{dep} = —0.9 V, t_d = 2 min; ΔE = 20 mV, sweep 100 mV s^{-1}.

Effect of deposition potential

The behavior of the mercury deposit when the electrode is plated at different potentials was then studied. In addition to examining the square-wave anodic stripping behavior, charge/time curves were recorded during the deposition process. The electrode (G-type, l = 1.04 mm) was polarized for 2 min with stirring. Then the potential was switched off and after 15 s the anodic square-wave voltammogram was recorded. The deposition potential was set at —0.25 V, —0.50 V, —1.00 V, and —1.10 V. The first of this series of applied potentials is only slightly more negative than the anodic stripping peak (E_p = —0.1 V) and the last one is in the potential range where reduction of hydrogen ion begins. Sets of curves for each potential are shown in Fig. 4.

Some approximate calculations based on the charge consumed during deposition were done to estimate the thickness of the deposit. Of course, it seems obvious that the deposit is not a film, but more likely an array of droplets. So, in considering these numbers, it should be remembered that if the film were uniform then its thickness would be of this value; thus, it may be said that the thickness of the film was f = 16, 28, 66, 144 nm for E_{dep} = —0.25, —0.5, —1.0, —1.1 V, respectively. The most reproducible data with the simplest anodic peak were observed for a deposition potential near —1.0 V. Other experiments showed that if the charge used for deposition was so large that the apparent film thickness would exceed approximately 140 nm, then the square-wave anodic stripping peak would be strongly deformed into several peaks.

Although deposition appears to be diffusion-controlled at each potential, the number of active sites where mercury can be reduced depends strongly on potential. This is why the charge, and hence the apparent film thickness, increases with increasingly negative deposition potential. As seen in Fig. 4, if the potential is too positive (e.g., —0.25 V), the charge/time curves (Fig. 4A) are exponential and the anodic peaks are not completely reproducible. It is likely that under these conditions mercury is deposited only on the most active sites of the carbon fiber, and longer deposition time allows growth of the droplets but not the number of sites.

It was also found that when the electrode with a deposit of mercury on it was exposed to air for longer than ca. 2 min then the square-wave anodic stripping peak decreased significantly. In a typical experiment, the peak height

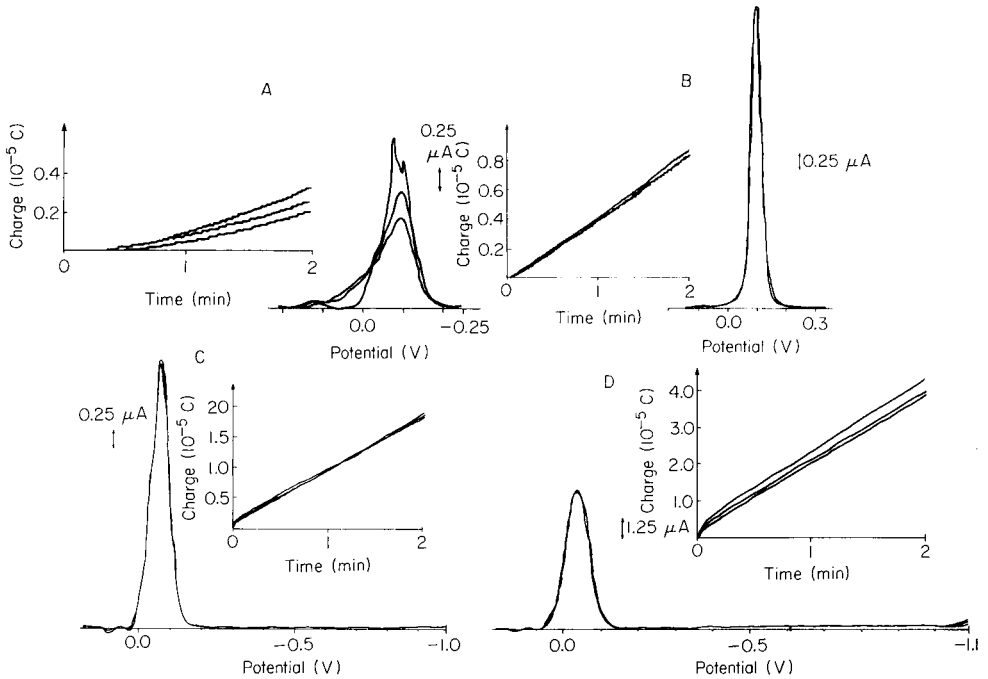

Fig. 4. Deposition of mercury on carbon fiber microelectrode (G-type, l = 1.04 mm) in 0.1 M KSCN; pH 2.48; 2 × 10^{-4} M mercury(II). Deposition potential (V); (A) —0.25; (B) —0.50; (C) —1.0; (D) —1.1. Dependence of charge on time during deposition and current on potential for anodic-stripping SWV (ΔE = 20 mV, sweep 100 mV s^{-1}). Three replicate experiments at each potential.

decreased to 27% of its initial value after exposure to air for 6 min, and to 8% after 2 h. Of course air oxidation of mercury to form HgO or other oxides is strongly favored thermodynamically. Clean, dry mercury metal undergoes this reaction only very slowly. Perhaps the freshly-deposited mercury dispersed on the fiber is oxidized more rapidly. It is possible but less likely that the deposit is partly stripped mechanically when the electrode is taken out of and put into the solution. The cause of this phenomenon may not deserve more detailed examination, but the phenomenon itself must be avoided in experiments with these electrodes.

Comparison of G- and T-type electrodes

Both electrodes were coated electrochemically with mercury by using the same quantity of charge (40 μC) at E_{dep} = —1.0 V in 0.1 M thiocyanate (pH 2.48) containing 0.2 mM Hg(II). After being plated with mercury, the electrode was transferred into a solution of the same composition but containing Cd(II) instead of Hg(II). Cadmium was deposited for 2 min and square-wave anodic stripping was applied for various concentrations in the potential range between —0.95 V and —0.4 V, in order not to destroy the mercury

deposit, but only to observe oxidation of cadmium. Also, in both cases the apparent thickness of the film was calculated. Its value was f = 75 nm for the T-type electrode (l = 1.48 mm) and f = 159 nm for the G-type (l = 0.74 mm) electrode. Curves in Fig. 5 show the dependence of stripping peak current on concentration of Cd(II) for both electrodes; each point on the curves results from five consecutive measurements. The peak current is linear in cadmium concentration up to concentrations at which the deposit is saturated with cadmium. The upper limit of linearity was near 16 μM for the T-type electrode, where the apparent film thickness was f = 75 nm, and near 32 μM for the G-type electrode where f = 159 nm.

The stripping response within the linear region is qualitatively different from that at concentrations above the linear range, as shown in Fig. 6. Square-wave anodic stripping voltammograms obtained under conditions of saturation are broadened and ill-shaped in comparison with those characteristic of the linear region. Furthermore, if the scan is continued to +0.4 V there is no sign of mercury oxidation. It seems that the deposit in this case loses its adhesive properties and mercury is stripped together with cadmium. Unusual behavior of saturated deposits on carbon disk electrodes has been mentioned by Copeland and Skogerboe [11]. Exactly the same effect was observed when the G-type microelectrodes were used. In general, there seems to be no significant difference in behavior of these two types of microelectrodes, but the fiber of the G-type electrode, which had contacted flame, was more fragile and needed longer electrochemical conditioning.

Conclusions

The two procedures proposed for preparing carbon fiber microelectrodes are relatively simple and efficient. There was no significant difference observed between the two types of electrodes, but the procedure for the T-type is

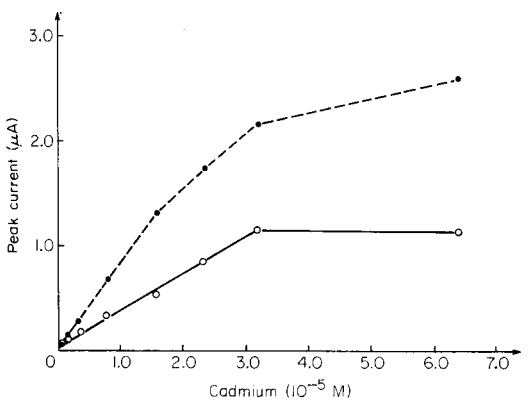

Fig. 5. Square-wave anodic stripping voltammetry. The dependence of peak height on concentration of cadmium (t_{dep} = 2 min, E_{dep} = —0.95 V, ΔE = 20 mV, sweep 100 mV s^{-1}). Electrodes: (•) T-type, l = 1.48 mm, f = 75 nm; (○) G-type, l = 0.74 mm, f = 159 nm.

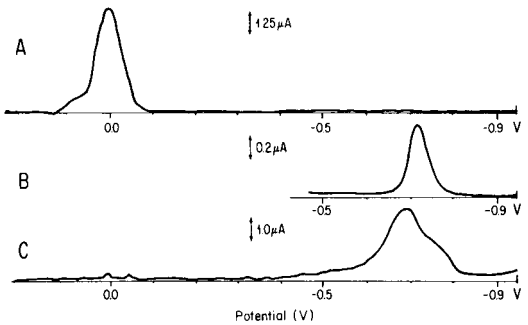

Fig. 6. Anodic-stripping SWV at a carbon fiber microelectrode (T-type, $l = 1.48$, $f = 75$ nm): (A) oxidation of Hg; (B) oxidation of Cd deposited in Hg film; (C) stripping of Cd/Hg amalgam. SWV (ΔE = 20 mV, sweep 100 mV s^{-1}); 0.1 M KSCN, pH 2.48. Concentration of Cd: (B) 8×10^{-6} M; (C) 9.6×10^{-5} M.

safer for the fiber and easier to implement. Results indicate some range of conditions over which one can expect to plate mercury films reproducibly and use those films for determination of Cd(II). The quality of the mercury deposit depends on the potential of deposition and deteriorates when the electrode is exposed. When amalgams with cadmium are too concentrated, the entire deposit can be more easily stripped off.

The authors thank Professor Z. Kowalski, Institute of Material Science, Krakow, for the suggestion of using heat-shrinkable tubing for fitting the microelectrodes. This work was supported in part by the Office of Naval Research.

REFERENCES

1 J.-L. Ponchon, R. Cespublio, F. Gonon, M. Jouvet and J.-F. Pujol, Anal. Chem., 51 (1979) 1483.
2 M. A. Dayton, J. C. Brown, U. J. Stutts and R. M. Wightman, Anal. Chem., 52 (1980) 946.
3 G. Schulze and W. Frenzel, Anal. Chim. Acta, 159 (1984) 95.
4 M. R. Cushman, B. G. Bennet and C. W. Anderson, Anal. Chim. Acta, 130 (1981) 323.
5 V. J. Jennings and J. E. Morgan, Analyst (London), 110 (1985) 121.
6 M. Stulikova, Electroanal. Chem., 48 (1973) 33.
7 L. Luong and F. Vydra, Electroanal. Chem., 50 (1974) 379.
8 R. Bilewicz, Z. Stojek and Z. Kublik, J. Electroanal. Chem., 96 (1979) 29.
9 Ch. Yarnitsky, R. A. Osteryoung and J. Osteryoung, Anal. Chem., 52 (1980) 1174.
10 P. Wrona and Z. Galus, in A. J. Bard (Ed.), Encyclopedia of Electrochemistry of the Elements, Vol. IXA, M. Dekker, NY, 1982, Chap. 1.
11 T. R. Copeland and R. K. Skogerboe, Anal. Chem., 46 (1974) 1257A.

Analytica Chimica Acta, 181 (1986) 219–225
Elsevier Science Publishers B.V., Amsterdam — Printed in The Netherlands

IMMOBILIZED ENZYME ELECTRODE FOR THE DETERMINATION OF SALICYLATE IN BLOOD SERUM

MOHAMMAD ALI NABI RAHNI, GEORGE G. GUILBAULT* and G. NETO DE OLIVEIRA[a]

Department of Chemistry, University of New Orleans, New Orleans, LA 70148 (U.S.A.)

(Received 2nd October 1985)

SUMMARY

This determination of salicylate in blood serum is based on application of an immobilized enzyme electrode. Salicylate hydroxylase (E.C.1.14.13.1) is chemically immobilized onto a pig intestine mounted on an oxygen electrode. The signals are monitored amperometrically and the resulting output voltage is read using a simple adapter. The experimental parameters and possible interferences are discussed. Samples containing 1.0×10^{-5}—1.87×10^{-3} M (1.6—300 μg ml^{-1}) salicylate were assayed with relative standard deviations between 1.3% and 6% and recoveries between 98.7 and 103%. Results obtained by the proposed method and by the established clinical method for randomly spiked pooled serum samples correlated well (r = 0.99).

Acetylsalicylic acid (aspirin) is probably the most widely used antipyretic, analgesic and anti-inflammatory drug. After ingestion, a major amount of aspirin is rapidly hydrolyzed to salicylic acid at the intestinal wall and the liver circulating in the ionized form in blood [1, 2]. Salicylate intoxication results from the easy availability of aspirin as a safe medication. Since the pharmacokinetics of salicylate metabolism is not yet understood, therapeutic overdose among children and arthritis patients is common [3]. High doses of aspirin for chronic inflammatory diseases such as rheumatoid arthritis requires control and close monitoring of serum salicylate level, because the effective therapeutic levels are very close to the toxicity stage. Therefore, the assay of serum salicylate levels is vital for clinical purposes. Salicylic acid is the main aspirin metabolite in the body, reaching its maximum level in blood serum two hours after aspirin ingestion [4]. The other aspirin metabolites are salicyluric acid, and its hydroxylated form, gentisic acid (2,5-dihydroxybenzoic acid) [5], but their formation is capacity-limited in the therapeutic dose range [6—9]. The toxicity is related to the amount of drug ingested [10—12]. Severe symptoms can be observed when doses beyond 300 mg kg^{-1} of body weight are taken.

Many methods have been reported for the assay of serum salicylate as well

[a]Present Address: Instituto de Quimica, University of Sao Paulo at Campinas, Campinas, Brazil.

as minor aspirin metabolites such as salicyluric and gentisic acids. High-pressure liquid chromatography (HPLC) has been used [13—15]. The improved HPLC method [15] is highly sensitive (50 $\mu g\ l^{-1}$), but the detector is complex and an extra extraction and preconcentration step is needed. Gas-liquid chromatography [9, 16—18], colorimetry [19] and spectrofluorimetry [20, 21] have also been used for the assay of aspirin metabolites. Of these, the Trinder test [22] is by far the most commonly used clinical method for salicylic acid. It involves the formation of a colored complex between salicylic acid and iron(III) measured at 540 nm. Unfortunately, many aliphatic enolic (e.g., acetoacetate) and phenolic (e.g., tyrosine and gentisate) compounds as well as some other drugs (e.g., phenothiazines) also exhibit color reactions similar to that of salicylate [23, 24]. Besides, background values for serum are usually high, unless salicylate is first extracted. An alternative approach is to use an enzymatic method. The hydroxylation is catalyzed by salicylate hydroxylase (salicylate 1-mono-oxygenase, EC 1.14.13.1) from *Pseudomonas cepacia* [25]:

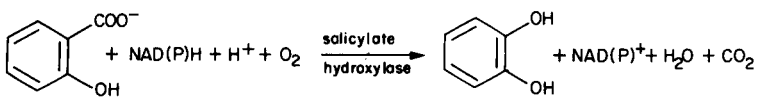

This reaction proceeds irreversibly until one of the reactants is exhausted. Either NADH or NADPH can be used, because the V_{max} is the same with either [26]. Kwan-Sa and Bittikofer [27] developed a method based on the soluble form of salicylate hydroxylase, monitoring the decrease in the absorbance of NAD(P)H at 340 nm. Their method exhibits a high reaction rate and selectivity for the substrate (salicylate), characteristic of enzymatic reactions, with no interference from serum protein. The main disadvantages are waste of the soluble enzyme and NAD(P)H for each assay, because the enzyme concentration has to be kept at well above the required level to ensure that the reaction rate is only dependent on salicylate concentration.

A more efficient method is to immobilize salicylate hydroxylase on the tip of an oxygen electrode and measure the decrease in the oxygen concentration at the steady state, which can be correlated to salicylate level in serum. No sample treatment and preconcentration step is needed.

EXPERIMENTAL

Apparatus, reagents and chemicals

A PHM 84 Research pH meter coupled to a Radiometer REC-61 Servograph Recorder through a d.c. offset module and potentiometric amplifier (Model EU-200-1 and 2, Schlumberger) was used for all the measurements. To eliminate the necessity of using a polarograph to monitor the amperometric oxygen electrode, an adapter (Model CP-960, Universal Sensors, P.O. Box 736, New Orleans, La.) was used; this device simultaneously

applies the desired potential to the amperometric enzyme electrode, and converts the resulting current to a voltage. A Radelkis combination oxygen electrode (type A) was used for the construction of the enzyme electrode.

All of the following chemicals and materials were obtained from Sigma Chemical Company: nicotinamide adenine dinucleotide (reduced form), salicylic acid (sodium salt), acetylsalicylic acid, gentisic acid, chymotrypsin from bovine pancreas (E.C. 3.4.21.1), salicyluric acid (*o*-hydroxyhippuric acid), bovine albumin, glutaraldehyde (25%, grade II), salicylate hydroxylase (E.C. 1.14.13.1), reference serum, and the salicylate kit (procedure no. 530).

Procedure

The enzyme electrode was prepared by covalent cross-linking, as described by Guilbault et al. [28, 29]. First, a pig intestine type-H membrane was mounted on the tip of the oxygen electrode. The membrane was activated by a few drops of chymotrypsin solution (0.5 mg/0.5 ml). Then, 20 μl of 5% (w/v) bovine serum albumin (BSA) solution containing 3 mg (6.9 units) of lyophilized enzyme was put on top of the pig intestine. After the enzyme had completely dissolved in the BSA, 2.5 μl of 6.25% (w/v) glutaraldehyde solution was added as cross-linking reagent, stirred rapidly by a nylon rod for 2 min and let dry at room temperature. After 3 h, the electrode was equilibrated in 0.025 M phosphate buffer pH 6.75, containing 1 mM EDTA. This buffer was used throughout the experiment.

In all measurements, the total volume was 1.5 ml (1.15 ml of 0.025 M phosphate/EDTA buffer, pH 6.75, 0.10 ml of 0.07 M β-NADH and 0.250 ml of substrate with appropriate concentration). The β-NADH solution was always prepared fresh, stored in a dark vial in a refrigerator and used within 2 h. In order to control the quality of β-NADH solution, its absorbance at 340 nm was periodically checked [30]. All solutions were left to reach thermal equilibrium (25°C) and a steady baseline potential (after about 5–10 min), before the substrate was introduced; the signal was recorded at steady state. The electrode jacket was kept at 5°C in buffer for later use.

RESULTS AND DISCUSSION

Electrode response

The Universal Sensors adaptor simultaneously applies a constant potential of −0.65 V to the oxygen electrode and converts the current output of the electrode to a potential which can then be monitored on a regular pH meter. Every 1-nA change in the current caused by an oxygen concentration change in the bulk solution is equal to a potential change of 10 mV. Therefore, a linear relationship exists between the current and/or voltage changes, and either one can be used to construct the calibration curve. The enzyme electrode was placed into the stirred buffer/NADH solution (see above) until it reached a constant signal. Substrate solution (0.25 ml) of varying concentration was then added and the initial rate of change in the limiting current and

the steady-state current were recorded. In the bulk reaction, both the initial rate of change of current and the total current change were proportional to the substrate concentration. Steady-state currents were obtained because of a steady state between the dissolved oxygen consumption by the enzymatic reaction and the supply of oxygen from the bulk solution to the enzyme layer. The oxygen content in the buffer solution was found to be relatively constant during a series of assays, owing to the slow equilibration of oxygen between buffer solution and air for these experimental conditions. This gives rise to a residual signal of about 110—130 nA (1100—1300 mV); the signal is superimposed on this background current.

Effect of experimental parameters. Figure 1 shows the optimum conditions for three of the experimental parameters. A salicylate solution of 2.60×10^{-4} M (41.7 μg ml^{-1}) was used for this comparison. Figure 1, curve A, illustrates the pH profile for the immobilized enzyme electrode. The optimum pH of the soluble enzyme has been reported to be 7.6, whereas for this immobilized enzyme electrode, the optimum pH was found to be 6.5—7.0. Therefore, a pH of 6.75 was selected for all assays. Figure 1, curve B, shows the effect of NADH concentration on the reaction. A concentration of 4—5 mM was found to be optimum; 4.7 mM was selected for use. Finally, the effects of temperature on the reaction rate were studied; from curve C, 25°C was chosen for further studies.

Calibration curve and selectivity

Figure 2, curve A, shows a calibration curve obtained for the assay of salicylate. Aliquots of stock solution were added to initiate the enzyme-catalyzed reaction; the signal was recorded at steady state. The response time was 1—3 min at low concentrations of salicylate to about 6 min at high

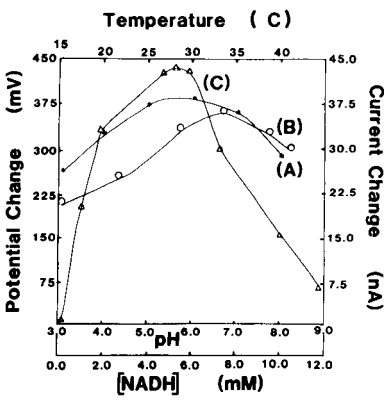

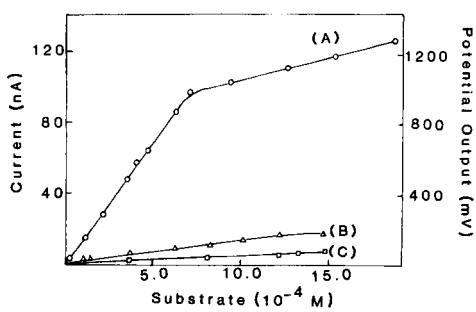

Fig. 1. (A) pH profile of the immobilized enzyme-catalyzed reaction; (B) NADH effect on the reaction; (C) effect of temperature.

Fig. 2. (A) Standard calibration curve of salicylate with immobilized salicylate hydroxylase; (B) typical response to gentisate; (C) typical response to aspirin.

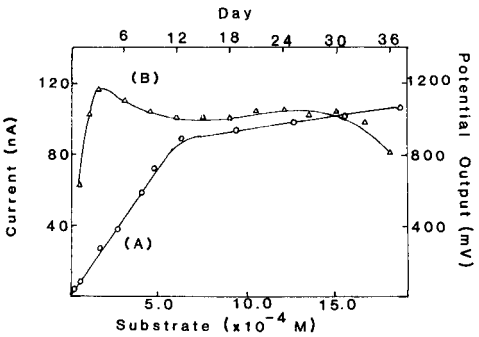

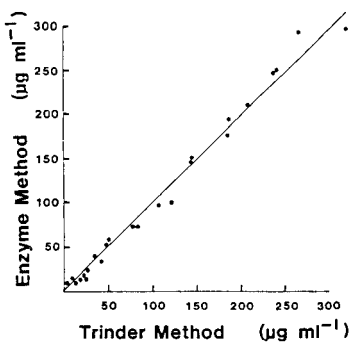

Fig. 3. Stability studies: (A) a typical calibration curve with an enzyme electrode 28 days old; (B) response of an immobilized salicylate hydroxylase electrode with time (a sample of 1.87×10^{-3} M salicylate was assayed for every data point).

Fig. 4. Comparison of the proposed enzyme electrode method and the Trinder method.

concentrations. The linear region is 1.0×10^{-5}—6.90×10^{-4} M (1.6—110.5 µg ml^{-1}); higher concentrations of the substrate (up to 1.87×10^{-3} M (300 µg ml^{-1})) can be assayed. Figure 3, curve B, shows the variation in response to 1.87×10^{-3} M salicylate over 36 days; the enzyme electrode sensitivity actually increased during the first several days, then became fairly stable for about 30 days before finally starting to decrease. Figure 3A shows a calibration curve obtained with the same electrode when it was 28 days old. Some of the sensitivity in the upper region was lost, but a useful region up to about 6×10^{-4} M still existed.

Figure 2, curve B, shows a typical response of the electrode to gentisate. It must be noted that gentisate concentration in real serum is much lower than that of the main aspirin metabolite (salicylate) and is capacity-limited in blood. Figure 2, curve C, shows a typical response of the electrode to aspirin; again 2 h after aspirin ingestion, its concentration is at a minimum, whereas the salicylate concentration reaches its peak after 2 h. Thus, the electrode should be quite selective for the assay of salicylate.

Reproducibility and recovery studies were done using randomly spiked pooled serum samples. The corresponding salicylate concentration obtained from the calibration curve was compared to the amount originally added. Table 1 shows the precision, relative error and recovery percentages of pooled serum sample containing 1.25×10^{-4}—1.87×10^{-3} M salicylate. The relative errors ranged from 0.43 to 3.0%, within-run precision ranged from ±1.3 to ±5.6, and the recoveries were from 98.8 to 103%.

Comparison of the proposed immobilized enzyme electrode and spectrophotometric methods

The Trinder method [22] is the accepted method for the assay of salicylate. A Sigma salicylate kit was used to minimize any error associated with

TABLE 1

Precision, relative errors and recoveries of salicylate added to pooled serum (n = 5).

Salicylate (μg ml^{-1})		Recovery (%)	Relative error (%)	R.s.d. (%)
Added	Found			
20	19.75	98.7	−1.3	5.6
50	51.50	103.0	+3.0	4.1
100	100.4	100.5	+0.4	1.3
150	148.3	98.9	−1.1	3.3
200	202.6	101.3	+1.3	3.1
250	252.3	101.2	+0.9	1.5
300	303.0	101.0	+1.0	3.1

reagent preparation. Random samples of spiked control serum were processed using both the established spectrophotometric and the enzyme electrode methods. Linear regression of the two sets of results showed good agreement between the two methods. Figure 4 shows a plot of the proposed enzyme electrode method (y) vs. the Trinder method (x) for 24 spiked control serum samples, ranging from 3.12×10^{-5} to 1.87×10^{-3} M (5—300 μg ml^{-1}). A straight line, defined by the equation $y = (1.016 \pm 0.015)\,x + 1.45$, with a correlation coefficient of $r = 0.99$ (n = 24) was obtained.

REFERENCES

1 J. R. Leonards, Proc. Soc. Exp. Biol. Med., 110 (1962) 304.
2 J. R. Leonards, Aust. N.Z. J. Med., 6 (1976) 8.
3 T. C. Kwong, Clin. Chem. News, 1 (1985) 14.
4 B. E. Cham, D. Johns, F. Bochner, O. M. Imhoff and M. Rowland, Clin. Chem., 25 (1979) 1420.
5 D. Schachter, J. Clin. Invest., 36 (1957) 297.
6 G. Levy and A. W. Vogel, J. Pharm. Sci., 58 (1969) 503.
7 T. Tsuchiya and G. Levy, J. Pharm. Sci., 61 (1972) 541.
8 T. Gibson, G. Zaphiropoulos, J. Grove, D. D. Berry and B. Widdop, J. Clin. Pharmacol., 2 (1975) 233.
9 L. J. Walter, D. F. Biggs and R. T. Coutts, J. Pharm. Sci., 63 (1974) 1754.
10 A. K. Done, Pediatrics, 26 (1960) 800.
11 A. K. Temple, Arch. Intern. Med., 141 (1981) 364.
12 T. C. Kowong, J. Laczin and J. Baum, Am. J. Clin. Pathol., 80 (1983) 888.
13 L. Y. Lo and A. Bye, J. Chromatogr., 181 (1980) 473.
14 B. E. Cham, D. Johns and F. Bochner, Clin. Chem., 25 (1979) 1420.
15 J. N. Buskin, R. A. Upton and R. L. Williams, Clin. Chem., 28 (1982) 1200.
16 A. J. Hoffman and H. I. Mitchell, J. Pharm. Sci., 52 (1963) 305.
17 E. B. Dechene, L. H. Booth and M. J. Caughey, J. Pharm. Pharmacol., 21 (1969) 678.
18 E. R. Blankley, Anal. Biochem., 15 (1960) 350.
19 F. Furman and L. Firberg, J. Pediatr., 70 (1967) 287.
20 G. Graham and J. Rowland, J. Pharm. Sci., 61 (1972) 1219.
21 A. Saltzman, J. Biol. Chem., 174 (1948) 339.
22 P. Trinder, Biochem. J., 57 (1954) 301.

23 E. S. Kang, T. A. Todd and M. T. Capaci, Clin. Chem., 29 (1983) 1012.
24 K. D. Mutchie, G. H. Saunders, A. S. Manissan and T. E. Pooc, J. Rheumatol., 7 (1980) 737.
25 S. C. Tu, F. A. Romero and L. H. Wang, Arch. Biochem. Biophys., 209 (1981) 423.
26 R. H. While-Stevens and H. M. Kamin, Biol. Chem., 247 (1972) 2358.
27 Y. Kwan-sa and J. A. Bittikofer, Clin. Chem., 30 (1984) 1549.
28 W. C. White and G. G. Guilbault, Anal. Chem., 50 (1978) 1481.
29 M. Mascini and G. G. Guilbault, Anal. Chem., 49 (1977) 795.
30 C. P. Fawcett, M. M. Ciotti and N. O. Kaplan, Biochim. Biophys. Acta, 54 (1961) 210.

Analytica Chimica Acta, 181 (1986) 227—234
Elsevier Science Publishers B.V., Amsterdam — Printed in The Netherlands

THE APPLICATION OF 2,4,6-TRINITROBENZENE-1-SULPHONIC ACID IN THE DIFFERENTIAL PULSE POLAROGRAPHIC DETERMINATION OF AMINES

M. A. AL-HAJJAJI

Department of Chemistry, College of Science, King Saud University, Riyadh (Saudi Arabia)

(Received 15th May 1985)

SUMMARY

The differential pulse polarographic behaviour of 2,4,6-trinitrophenyl (TNP) derivatives of several primary amines and amino acids was investigated in the presence of sulphite ion. All the derivatives produced a polarographic peak for their complexes with sulphite (1×10^{-2} M) in pH 8.0 phosphate buffer (0.05 M)/0.1 M potassium chloride. The derivatives of proteins and peptides did not give such a peak. A 5-min reaction time at room temperature (or 50°C for lysine) and pH 10.5 using 1×10^{-4} M 2,4,6-trinitrobenzene-1-sulphonic acid provides the optimal conditions for the determination of 5×10^{-6}—2.5×10^{-5} M amines. The relative standard deviation for determining 1×10^{-5} M glycine ($n = 5$) was 1%.

The determination of amines by differential pulse polarography (DPP) has been achieved directly by their anodic oxidation at a glassy carbon electrode [1]. Indirect methods have also been applied, e.g., by use of the catalytic wave of the cobalt(III)/hexamine complex in the presence of traces of protein [2] and the conversion of the irreducible amino group to a polarographically active azomethine with formaldehyde [3]. In a previous report [4] amino acids ($1—4 \times 10^{-4}$ M) were determined by d.c. polarography after their conversion to trinitrophenyl derivatives with 2,4,6-trinitrobenzene-1-sulphonic acid (TNBS). In this paper, TNBS is applied in the determination of an extended list of amines utilizing the more sensitive differential pulse polarography (DPP).

EXPERIMENTAL

Apparatus and reagents

A Metrohm Polarecord Model 506 polarograph was used to record all differential pulse polarograms at the following settings: 0.8 s drop time, —50 mV

Present address: Department of Chemistry, Faculty of Applied Sciences and Engineering, Umm Al-Qura University, Makkah Almukarramah, Saudi Arabia.

0003-2670/86/$03.50

pulse amplitude and a scan rate of 2.5 mV s^{-1}. The polarographic cell was as described before [4]. All potentials quoted are against a silver/silver chloride electrode (saturated potassium chloride).

The chemicals used were of analytical-reagent grade. The TNP-amines were prepared by the method of Okuyama and Satake [5].

Determination of amines

The trinitrophenylation reaction [6] was carried out in a 10-ml volumetric flask. A 2.5-ml portion of aqueous TNBS solution (1×10^{-3} M) was mixed with 0.125–0.625 ml of amine solution (1×10^{-3} M). At zero time the volume was completed to the mark with borate buffer (pH 10.5, 0.025 M) and the reaction was allowed to proceed for 5 min at room temperature (or 50°C for lysine). The pH was lowered to pH 8.0 with dilute hydrochloric acid, and the solution was transferred quantitatively to a 25-ml volumetric flask followed by the addition of 5 ml of sodium sulphite/potassium chloride solution (0.05 M/2.5 M). The volume was completed to the mark with phosphate buffer (0.05 M, pH 8.0) and the polarograms were recorded after deoxygenation with nitrogen for 4 min. Blanks (reagents plus double-distilled water in place of amine solution) were run similarly.

RESULTS AND DISCUSSION

The investigation was divided into two parts. The first dealt with the sensitivity and resolution of the peaks of the TNP-amines sulphite complexes [5]. The second considered the optimization of the trinitrophenylation reaction, no longer restricted by the conditions required for spectrophotometric detection [6].

The response of TNBS and its derivatives in the absence of sulphite ions was investigated. Four peaks were produced by TNBS (3×10^{-4} M) at pH 7.0 (phosphate buffer 0.05 M/0.1 M potassium chloride); TNP-histidine at the same concentration gave only three peaks under the same conditions (Fig. 1). This was also the case for all the other TNP-amines. The d.c. polarographic behaviour of TNBS was different in that only three waves were noticed [4].

A sulphite solution (1×10^{-2} M) alone in pH 7.0, 7.5 and 8.0 phosphate buffer (0.05 M, 0.1 M KCl) revealed two small peaks at pH 7.0 (peak potentials E_p = −640 mV and −1132 mV) which were decreased in height (but had the same E_p) at pH 7.5 and had disappeared at pH 8.0 (Fig. 2). These peaks should not be present according to Kolthoff and Miller [7], as the two-wave reduction of sulphurous acid should not occur at pH > 6.0, but probably the sensitivity of DPP and the high sulphite concentration (1×10^{-2} M) accounts for their appearance. Further work therefore was done at pH ⩾ 8.0 and not pH 7.0 as before [4]. The effect of sulphite concentration (4×10^{-4}–4×10^{-2} M) at pH 8.0 on the behaviour of

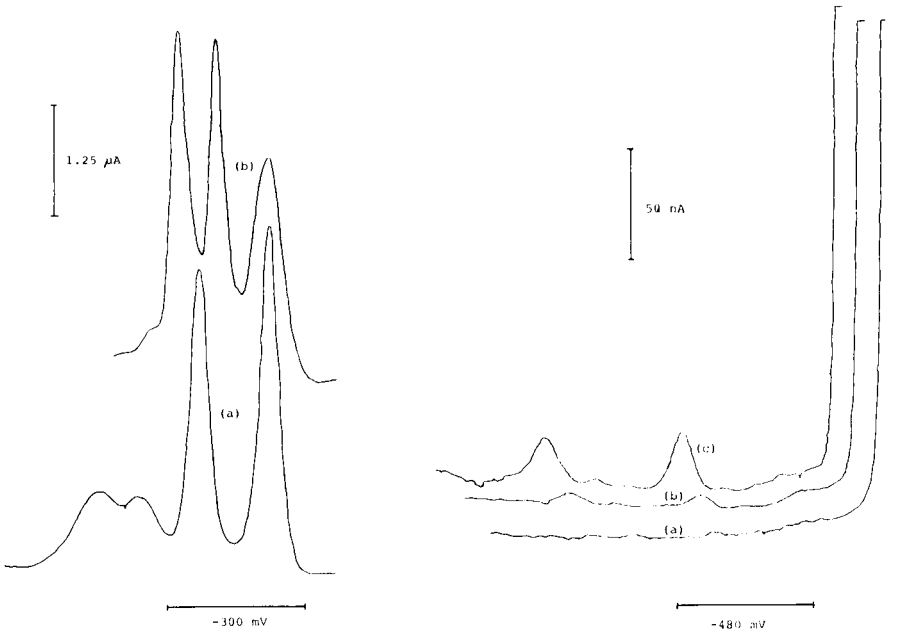

Fig. 1. Differential pulse polarograms: (a) 3×10^{-4} M TNBS; (b) 3×10^{-4} M TNP-histidine. Phosphate buffer, pH 7.0/0.1 M KCl; initial potential 0 V.

Fig. 2. Polarograms of 0.01 M sulphite at different pH: (a) pH 8.0; (b) pH 7.5; (c) pH 7.0. Phosphate buffer (0.05 M, 0.1 M KCl); initial potential 0 V.

1×10^{-5} M TNP-amines was investigated. Figure 3 shows how TNP-asparagine polarograms were affected by the formation of a well-defined peak at more negative potentials (E_p = —1132 mV) at $\geqslant 1 \times 10^{-2}$ M sulphite. This peak was also observed with most amine derivatives but not in solutions containing TNBS or picric acid. It is these peaks which were used for the determination of different amines in the presence of excess of TNBS. The TNP-proteins (yeast alcohol dehydrogenase and egg albumin) and TNP-peptides (glycylhistidine and triglycine), however, did not produce such peaks; TNP-arginine showed poor sensitivity (Table 1). The bisTNP-lysine sulphite complex showed two peaks (E_p = —992, —1200 mV) but when TNP-α-acetyllysine was used, only one peak was found (E_p = —1016 mV). Attempts to see if this behaviour was repeated with other diamines failed because of the insolubility of the derivative (bisTNP-ethylenediamine).

Methanol has been used in some procedures [8] to quench the trinitrophenylation reaction and was used in this work to dissolve some of the derivatives. Its effect on the peaks of the sulphite complexes of all the derivatives was investigated (0.04—8% v/v supporting electrolyte); only the peak height of the TNP-histidine sulphite complex was slightly decreased (15% decrease in 8% methanol) but the E_p was not altered. Polyvinyl alcohol

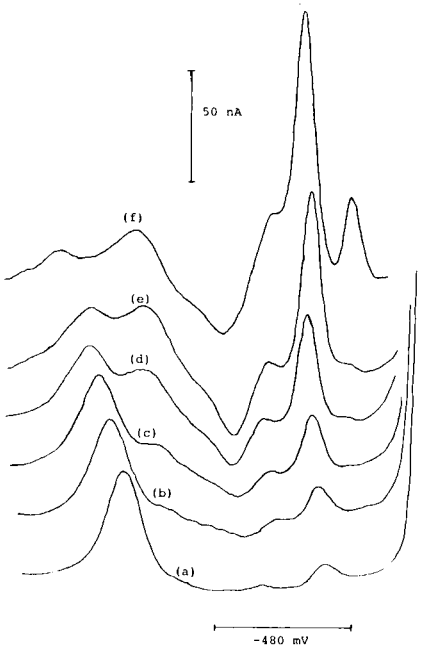

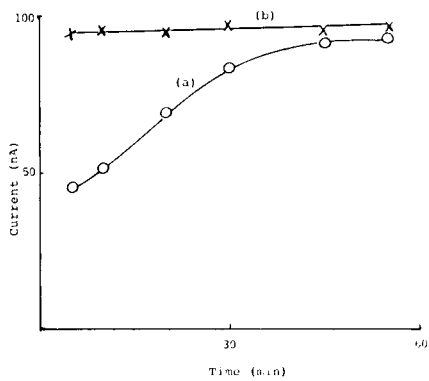

Fig. 3. Effect of sulphite concentration on TNP-asparagine (1×10^{-5} M) polarograms: (a) 4×10^{-2} M; (b) 2×10^{-2} M; (c) 1×10^{-2} M; (d) 4×10^{-3} M; (e) 2×10^{-3} M; (f) 4×10^{-4} M sulphite. Phosphate buffer, 0.05 M, 0.1 M KCl, pH 8.0; initial potential −0.1 V.

Fig. 4. Time dependence of the glycine (1×10^{-5} M) reaction with TNBS (1×10^{-4} M) at: (a) pH 9.5; (b) pH 10.5.

had a negligible effect on the peak heights and potentials at concentrations $\leqslant 0.02\%$. The peaks, however, were removed at concentrations $\geqslant 0.4\%$.

Studies of the effect of borate (0.025 M), phosphate (0.05 M), and carbonate (0.05 M) buffers (pH 8.0, 0.1 M KCl) on the peaks of the TNP-amine sulphite complexes (1×10^{-2} M sodium sulphite) showed that carbonate solutions decreased the peak heights and shifted the peak potentials towards more negative values. No peak was apparent for TNP-threonine. Borate and phosphate solutions gave similar results (Table 1). Increase of pH to 9.0 (borate buffer, 0.025 M, 0.1 M KCl) shifted the peaks to more negative potentials and decreased their heights except for TNP-serine and bisTNP-lysine. No splitting of the peaks was noticed [4]. The effect of ionic strength is also shown in Table 1. It is clear that peak currents were maximal when 0.5 M potassium chloride was present and that all peaks appear within 154 mV of each other, even the two peaks of bisTNP-lysine fused to give a slightly asymmetrical peak.

The investigation showed that the α-amino groups in amino acids gave complexes that were reduced at a more negative potential (except histidine

TABLE 1

Effects of buffer composition and pH on peak potential (E_p in mV vs. Ag/AgCl) and peak current (i_p in nA) for TNP-amine sulphite complexes (1×10^{-5} M)

Compound	Borate or phosphate[a]		Carbonate[b]		Borate[b]		Phosphate[c]	
	E_p	i_p	E_p	i_p	E_p	i_p	E_p	i_p
Histidine	−940	73	−1020	67	−1044	21	−924	77
Glycine	−1144	42	−1200	35	−1180	27	−1000	50
Serine	−1144	34	−1172	29	−1160	35	−984	48
Threonine	−1180	30	—[d]	—[d]	−1140	23	−996	52
Glutamic acid	−1220	33	−1336	24	−1304	26	−1016	52
Ethylamine	−972	73	−1136	23	−1032	61	−952	77
Asparagine	−1136	45	−1292	28	−1200	26	−1024	51
Lysine[e]	−992	21	−1016	22	−1040	19	−1016	46
	−1200	21	−1256	22	−1260	19		
Acetyllysine	−1016	47	−1048	26	−1048	36	−952	68
Histamine	−936	36	−1000	25	−1012	20	−868	55
Arginine	−976	7	−1024	9	−1020	6	−870	12

[a]0.05 M buffer pH 8.0/0.1 M KCl/0.01 M Na_2SO_3 (borate, 0.025 M). [b]As (a) but pH 9.0. [c]As (a) but 0.5 M KCl. [d]No peak observed. [e]Two peaks.

and arginine) than the primary amino groups present in aliphatic amines. This was illustrated clearly for lysine with its two amino groups.

Determination of amines

The reaction of TNBS with different amines was found to be pH-dependent, as only the unprotonated primary amino group is attacked [5, 9]. The reaction is therefore faster at higher pH values. In spectrophotometry, however, the use of a higher pH was prohibited owing to the rate of picric acid formation which increased the blank signals [9].

Peaks obtained at several concentrations of TNBS (1×10^{-4}—1×10^{-3} M) showed that higher concentrations (1×10^{-3} M) affected the resolution of the peaks of the TNP-amine sulphite complexes from those of TNBS, at the desired sensitivity. Therefore, lower concentrations of TNBS (1×10^{-4} M) should be used for the trinitrophenylation of 5×10^{-6}—2.5×10^{-5} M amines by the equilibrium method [9].

The trinitrophenylation of ethylamine, α-acetyllysine and glycine (all 2×10^{-5} M) was investigated with 1×10^{-4} M TNBS at pH 9.5 and 10.5. The peaks of the sulphite complexes were recorded as described above. The results for glycine (Fig. 4) indicate that the reaction was practically complete after 5 min at pH 10.5. It is evident that competition for TNBS by hydroxide and primary amino groups was in favour of the latter. The trinitrophenylation of lysine gave interesting results. At pH 9.5 only one peak was observed over the first 30 min of reaction. Comparison of the E_p for this peak with those of authentic bisTNP-lysine and TNP-acetyllysine

indicated that it belonged to the ϵ-amino group. A second peak was produced at more negative potential after 45 min and this peak increased as the first decreased. The two peak potentials coincided with those from authentic bisTNP-lysine. Leaving the reaction of TNBS (1×10^{-4} M) and lysine (1×10^{-5} M) to proceed for 270 min at pH 9.5 led to two equal peaks being produced which were similar to those of the authentic derivative. At pH 10.5, similar results were obtained after only 20 min. Heating of the reaction mixture (at 50°C) decreased the reaction time to 5 min. Reagent blanks showed no change in their polarographic behaviour even after being heated at 50°C for 1 h at pH 10.5.

These results seem to indicate that the ϵ-amino group of lysine was trinitrophenylated faster than the α-amino group. The difference in reactivity, however, was greater than those based on comparing the ϵ-amino group of acetyllysine with the α-amino group of glycine [10]. The presence of both amino groups on one molecule seem to be the only reason for this difference. Another peculiarity in the trinitrophenylation of lysine was the decrease of the first peak as the second peak increased. The decrease in the

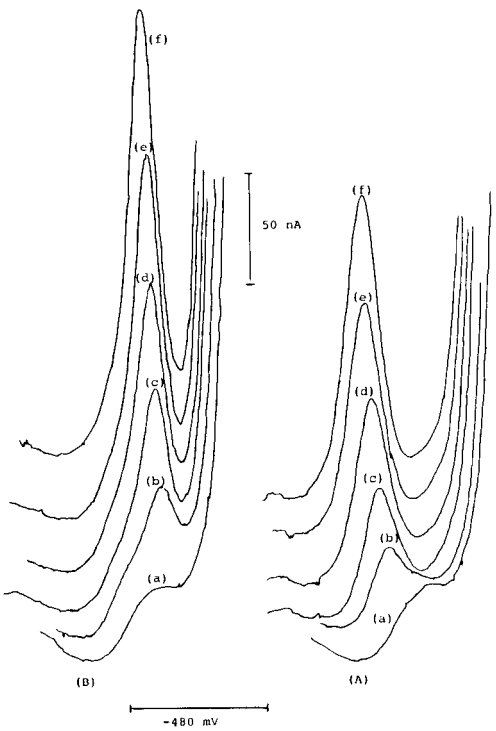

Fig. 5. Polarograms used for obtaining calibration graphs: (A) glycine; (B) ethylamine. Amine concentration: (a) 0.0 M; (b) 5×10^{-6} M, (c) 1×10^{-5} M; (d) 1.5×10^{-5} M; (e) 2×10^{-5} M; (f) 2.5×10^{-5} M. Conditions: 1×10^{-4} M TNBS and 0.01 M sulphite at pH 8.0 (0.5 M KCl); initial potential —0.8 V.

diffusion coefficient on attachment of a second TNP group could not account for such a decrease (the first peak was halved at the end of the reaction).

Calibration graphs were constructed by recording the polarograms from −800 mV. Linear calibration graphs were obtained for all the compounds investigated in the range 5×10^{-6}—2.5×10^{-5} M. Figure 5 shows typical polarograms for glycine and ethylamine. The relative standard deviation for the determination of 1×10^{-5} M glycine (5 measurements) was 1%.

Various aliphatic and aromatic compounds that contain primary amino groups react with the reagent. The resolution of peak potentials of the TNP-amine sulphite complexes is insufficient (especially at high ionic strength) to allow determinations of these compounds in the presence of each other (Table 1) although there are some exceptions when binary mixtures (at low ionic strength) are considered. Ammonia, which was found to interfere in the spectrophotometric method [11], and which can be determined by means of this reaction [11], did not interfere in the present procedure at 2×10^{-4} M. Further selectivity was obtained by applying Mokrasch's procedures [8] that took advantage of the different solubilities of TNP-amino acids and TNP-amines; 1×10^{-5} M histidine was determined in its mixture with 2×10^{-5} M histamine after extraction of the reaction mixture (pH 10.5) with three 5-ml portions of toluene, which resulted in the removal of the TNP-histamine derivative.

Conclusions

The method described is sensitive and could complement that for the spectrophotometric determination of amino acids. It is unfortunate that proteins and peptides could not be determined by this method but, therefore, they will not interfere, and the method can be used in studies of protein degradation [12]. Further studies for improving selectivity are in progress. Although the d.c. polarographic study showed the reduction of sulphite complexes to be diffusion-controlled [4], the possibility of a stripping procedure for the determination of amines is being investigated with promising preliminary results.

Mr. Khalid M. Mirza is thanked for his excellent technical assistance.

REFERENCES

1 J. Ballantine and A. D. Woolfson, Int. J. Pharmacol., 3 (1979) 239.
2 P. W. Alexender and M. H. Shah, Talanta, 26 (1979) 97.
3 J. D. McLean, V. A. Stenger, R. E. Reim, M. W. Long and T. A. Hiller, Anal. Chem., 50 (1978) 1309.
4 M. A. Al-Hajjaji, Anal. Chim. Acta, 157 (1984) 31.
5 T. Okuyama and K. Satake, J. Biochem., 47 (1960) 454.
6 S. L. Snyder and P. Z. Sobocinski, Anal. Biochem., 64 (1975) 284.
7 I. M. Kolthoff and C. S. Miller, J. Am. Chem. Soc., 63 (1944) 2819.

8 L. C. Mokrasch, Anal. Biochem., 18 (1967) 64.
9 R. Fields, in Methods in Enzymology, Vol. 25, Part B, Academic Press, New York, 1972, p. 464.
10 A. R. Goldfarb, Biochemistry, 5 (1966) 2570.
11 J. R. Whitaker, P. E. Granum and G. Aasen, Anal. Biochem., 108 (1980) 72.
12 K. M. Clegg, Y. K. Lee and J. F. McGilligan, J. Food Technol., 17 (1982) 517.

Analytica Chimica Acta, 181 (1986) 235—239
Elsevier Science Publishers B.V., Amsterdam — Printed in The Netherlands

Short Communication

THE APPLICATION OF STRONGLY OXIDIZING AGENTS IN FLOW INJECTION ANALYSIS
Part 3. Cobalt(III)

R. C. SCHOTHORST and G. DEN BOEF*

Laboratory for Analytical Chemistry, University of Amsterdam, Nieuwe Achtergracht 166, 1018 WV Amsterdam (The Netherlands)

(Received 30th July 1985)

Summary. The application of cobalt(III) as a powerful oxidizing agent in flow injection analysis is described. Cobalt(III) is electrochemically generated in the flowing system at a working electrode consisting of a packed bed of gold powder. Depending on the analyte, spectrophotometric detection is at 605 nm or 320 nm. For the oxidizable organic and inorganic substances tested, linear responses are usually obtained in ranges around 10^{-3} mol l^{-1}.

The application of cobalt(III) as a strong oxidizing agent in titrimetric analysis has always remained very limited because of the reaction of the reagent with water at room temperature. The introduction of flow injection analysis (f.i.a.) provides a new and fast quantitative application of this oxidimetric reagent. As with silver(II) [1] and manganese(III) [2], cobalt(III) can be applied by generating the reagent and conducting the analytical reactions in a flowing system.

The standard (formal) potential for the half-reaction $Co^{3+} + e^- \rightleftharpoons Co^{2+}$ in 4 mol l^{-1} perchloric acid is 1.92 V [3]. In sulphuric acid solution (0.5 mol l^{-1}), this standard potential is 1.81 V [4], indicating weak complex formation. However, in sulphuric acid medium, oxidations with cobalt(III) are often more rapid than with hydrated cobalt(III) [5, 6]. The electrochemical generation of cobalt(III) in sulphuric acid also proceeds more easily than in perchloric or nitric acid [7]. Cobalt(III) is rapidly reduced by water. The overall reaction in sulphuric acid solution can be represented by

$$4\,Co^{3+} + 2\,H_2O \rightleftharpoons 4\,Co^{2+} + 4\,H^+ + O_2$$

This reaction can be suppressed by increasing the acid concentration and by lowering the temperature.

Solutions of cobalt(III) are commonly prepared by chemical or electrochemical oxidation. For chemical oxidation of cobalt(II), the oxidizing agents applied are ozone, hydrogen peroxide, sodium perborate, or chlorine [7]. For the electrochemical oxidation of cobalt(II), the commonest preparation is that described by Swann and Xanthalsos [8] and by Bawn

0003-2670/86/$03.50

and White [9], who electrolyzed saturated solutions of cobalt(II) sulphate in 5 mol l^{-1} sulphuric acid at temperatures below 10°C. The electrolysis was followed by filtering off the cobalt(III) sulphate crystals formed. Solutions of cobalt(III) sulphate were prepared by dissolution of the solid. Blaedel and Evenson [7] generated cobalt(III) in nitric, perchloric or sulphuric acid solutions in a flow system at a platinum or carbon working electrode. Current efficiencies were low (around 20%) as were the yields (maximal 30%). Of these two sorts of preparation, only the electrochemical generation of solutions of cobalt(III) is suitable for generation in flow.

The reaction of cobalt(III) with a large number of organic and inorganic substances has been described by Šrámková and Zýka [5] and by Davies and Warnqvist [10]. Titrimetric determinations of hexacyanoferrate(II) and cerium(III) with cobalt(III) sulphate have been described by Bricker and Loeffler [11].

Detection can be done spectrophotometrically at 400 or 605 nm, the wavelengths of maximum absorption of cobalt(III) in 1.5 mol l^{-1} sulphuric acid solution [12]. At these two wavelengths, the molar absorptivity is about the same (about 40 l mol^{-1} cm^{-1}), but it is larger in the u.v. region. The present communication describes the electrochemical generation of cobalt(III) in a flow-injection system at a working electrode consisting of a packed bed of gold powder. Detection is done spectrophotometrically.

Experimental

The instrumentation and the dimensions of the flow system (Fig. 1) were identical with those used for manganese(III) [2]. Detection was done at 605 nm or 320 nm. The flow rate in each stream is indicated in Fig. 1. The cobalt(II) sulphate concentration entering the electrochemical flow-through reactor was 2.5×10^{-2} mol l^{-1} in 3.6 mol l^{-1} sulphuric acid. The sample stream was 3.6 mol l^{-1} sulphuric acid. All sample solutions were also made 3.6 mol l^{-1} in sulphuric acid. The counter and reference electrode of the electrochemical flow-through reactor are continuously rinsed (1.5 ml min^{-1}) with 3.6 mol l^{-1} sulphuric acid.

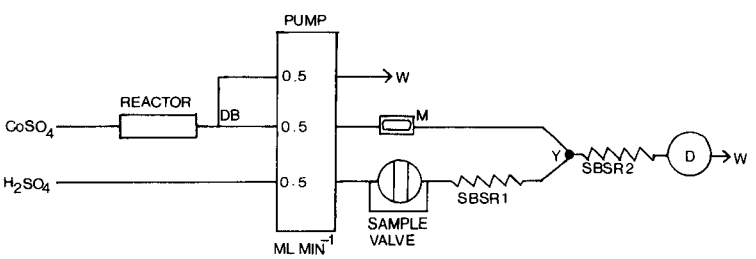

Fig. 1. Flow diagram. Length of single bead string reactors (SBSR): (1) 0.2 m; (2) 0.4 m. DB, Debubbler; D, detector; M, mixing chamber; W, waste. All connecting and SBSR tubing is polyethylene (0.75 mm i.d.); SBSRs are packed with 0.6-mm glass beads.

Preliminary experiments

The rate of the reaction of cobalt(III) with water decreases with increasing sulphuric acid concentration. However, because of the durability of the tubing and the occurrence of leakage in the connections, the sulphuric acid concentration should be as low as possible for practical applications in a flowing system. Therefore, absorption spectra resulting from a solution of cobalt(II) after passage of a fixed amount of charge in a batch procedure were recorded for sulphuric acid concentrations between 0.9 and 3.6 mol l^{-1}. For sulphuric acid concentrations up to 3.6 mol l^{-1}, the absorbance of cobalt(III) at 605 nm increased continuously, which can be ascribed mainly to increasing cobalt(III) concentration. The wavelengths of maximum absorption of cobalt(III) are not dependent on the sulphuric acid concentration. In order to make the cobalt(III) system easily interchangeable with the manganese(III) system, the same sulphuric acid concentration as for manganese(III) was chosen for further work (3.6 mol l^{-1}).

For practical applications of cobalt(III) in the flow system, generating currents of 60 mA were used; this in turn resulted in a potential of the working electrode of 2.4 V (vs. SCE). Attempts to use glassy carbon powder for the working electrode (particle diameter < 0.6 mm) were not successful.

The dependence of the peak height on the flow rate was investigated for the determination of nitrite and oxalate. Peak heights resulting from the injection of a 2.5×10^{-3} mol l^{-1} sodium nitrite solution and a 3.5×10^{-3} mol l^{-1} sodium oxalate solution were recorded at different flow rates. Between 0.5 and 1.5 ml min^{-1}, the peak height for both nitrite and oxalate was independent on the flow rate. All experiments were conducted at a total flow rate of about 1.5 ml min^{-1}.

Results

The substances examined to test the practical applicability of cobalt(III) were the same as for silver(II) [1] and manganese(III) [2]. The results for the determination of the oxidizable substances are summarized in Table 1. In addition to these compounds, formic acid, propan-1-ol, propan-2-ol, and 2-methylpropan-2-ol were examined in the range 10^{-2}—10^{-1} mol l^{-1}, but no signals were obtained. The correlations for the absorbance (A) and the concentration of the analyte in the sample solution (C) show good linearity (Table 1). The limit of determination is defined as the analyte concentration for which the absorbance change was ten times the peak-to-peak noise.

Chromium(III) could not be determined by this method, because it absorbs strongly at 405 and 605 nm. However, if the detection is done at 320 nm, chromium(III) can be determined. At this wavelength, cobalt(III) absorbs strongly (at 320 nm in 3.6 mol l^{-1} sulphuric acid, $\epsilon \approx 350$ l mol^{-1} cm) and neither chromium(III) nor dichromate, the product of the reaction with cobalt(III), absorbs at this wavelength. The same applies to nitrite and oxalate and hence determinations with detection at 320 nm were also

TABLE 1

Calibration data for the flow-injection system

Sample	Concentration range (mol l^{-1})	Regression line	Regression coefficient	Limit of determination (mol l^{-1})
Detection at 605 nm				
$NaNO_2$	10^{-3}—4×10^{-3}	$A = (10.8 \pm 0.1)C$	0.9986	9×10^{-4}
$MnSO_4$	2×10^{-3}—5×10^{-3}	$A = (9.7 \pm 0.2)C$	0.9975	1×10^{-3}
$(NH_4)_2Fe(SO_4)_2$	10^{-3}—6×10^{-3}	$A = (8.8 \pm 0.1)C$	0.9988	1×10^{-3}
$VOSO_4$	3×10^{-3}—8×10^{-3}	$A = (8.2 \pm 0.1)C$	0.9989	1×10^{-3}
$Ce(NO_3)_3$	1.3×10^{-3}—6.7×10^{-3}	$A = (7.6 \pm 0.1)C$	0.9993	1×10^{-3}
$(COONa)_2$	2×10^{-3}—4.7×10^{-3}	$A = (7.1 \pm 0.1)C$	0.9989	1×10^{-3}
KIO_3	2×10^{-2}—5×10^{-2}	$A = (0.56 \pm 0.01)C$	0.9991	1×10^{-2}
C_6H_5COOH	4×10^{-3}—7×10^{-3}	$A = (2.3 \pm 0.1)C$	0.9972	4×10^{-3}
Detection at 320 nm				
$NaNO_2$	2×10^{-4}—8×10^{-4}	$A = (32.6 \pm 0.7)C$	0.9963	3×10^{-4}
$(COONa)_2$	6.7×10^{-4}—2.7×10^{-3}	$A = (8.0 \pm 0.1)C$	0.9976	1×10^{-3}
$Cr_2(SO_4)_3$	8.5×10^{-4}—5×10^{-3}	$A = (8.6 \pm 0.2)C$	0.9977	1×10^{-3} [a]

[a] Concentration of Cr(III).

examined for these substances; the results are also presented in Table 1. The concentration of the cobalt(II) sulphate solution entering the electrochemical reactor in this case was 5×10^{-3} mol l^{-1}. For oxalate, the limit of determination is the same as for the determinations at 605 nm. For nitrite, the limit of determination is lowered by a factor of three. Most of the other substances mentioned in Table 1 cannot be determined by detection at 320 nm. Chloride interferes, because it is oxidized by cobalt(III).

Discussion

Of the three oxidimetric reagents tested, silver(II) is applicable only in nitric acid solution. In sulphuric acid solution, either manganese(III) or cobalt(III) can be applied. In hydrochloric acid solution, only manganese(III) is applicable. When the results of the determinations with silver(II), manganese(III) and cobalt(III) are compared, the conclusion is that determinations by means of silver(II) achieve lower limits of determination for all substances tested. This must be ascribed to the very high molar absorptivity of silver(II). Amperometric detection as applied in the case of the reducing agents seems impossible for these oxidimetric reagents.

With regard to the practical applications of these reagents, a very important aspect is that neither iron(III) nor copper(II) react, so that oxidizable compounds can be determined by means of any of these reagents in the presence of large amounts of these species.

As the experimental set-up is identical for silver(II), manganese(III) and cobalt(III), the reagents are easily interchangeable by changing the reagent

and the acid. The choice of the reagent depends only on the nature of the analyte under investigation and on the presence of other substances in the sample solution.

REFERENCES

1 R. C. Schothorst and G. den Boef, Anal. Chim. Acta, 169 (1985) 99.
2 R. C. Schothorst, O. O. Schmitz and G. den Boef, Anal. Chim. Acta, 179 (1985) 299.
3 D. H. Huchital, N. Sutin and B. Warnqvist, Inorg. Chem., 6 (1967) 838.
4 F. Verbeek and Z. Eechebaut, Bull. Soc. Chim. Belges, 67 (1958) 204.
5 B. Šrámková and J. Zýka, Mikrochem. J., 19 (1974) 295.
6 L. E. Bennett and J. C. Sheppard, J. Phys. Chem., 66 (1962) 1275.
7 W. J. Blaedel and M. A. Evenson, Inorg. Chem., 5 (1966) 944.
8 S. Swann and F. S. Xanthalsos, J. Am. Chem. Soc., 53 (1931) 400.
9 C. E. H. Bawn and A. G. White, J. Chem. Soc., (1951) 331.
10 G. Davies and B. Warnqvist, Coord. Chem. Rev., 5 (1970) 349.
11 C. E. Bricker and L. J. Loeffler, Anal. Chem., 27 (1955) 1419.
12 G. Hargreaves and L. H. Sutcliffe, Trans. Faraday Soc., 51 (1955) 786.

Analytica Chimica Acta, 181 (1986) 241—244
Elsevier Science Publishers B.V., Amsterdam — Printed in The Netherlands

Short Communication

PHARMACEUTICAL APPLICATIONS OF A HIGH-PERFORMANCE FLOW INJECTION SYSTEM

F. P. BIGLEY and R. L. GROB*
Villanova University, Villanova, PA 19085 (U.S.A.)
G. S. BRENNER
Merck, Sharp and Dohme Research Laboratories, West Point, PA (U.S.A.)
(Received 11th June 1985)

Summary. The flow-injection method is applied as a means of decreasing the work load associated with repetitive control determinations. The system described utilizes the design concepts used in post-column reaction with spectrophotometric detection in high-performance liquid chromatography. This equipment allows for minimal set-up and change-over time between samples and also provides the high accuracy and precision required in a testing laboratory. The system is applied to dissolution samples of hydrochlorothiazide and timolol maleate, and to combination tablets of hydrochlorothiazide, methyldopa and amiloride. Samples can be quantified at rates of up to 1200 h^{-1}.

Samples that are tested routinely in the pharmaceutical quality control laboratory generally fall into two categories: those that require a separation step prior to quantification and those that can be quantified directly. The first group of samples includes those submitted for potency and, of course, stability testing. The second group generally includes those tested to show product uniformity or dissolution rate. This second group accounts for the greatest share of the pharmaceutical analytical laboratory schedule because the samples require repetitive testing of the same sample population. For this reason, automated procedures that allow for redundant testing have generally been used.

In the studies presented in this communication, the concepts developed and used in high-performance liquid chromatography (HPLC) and in flow injection [1—4] have been merged to provide for the rapid quantification of dissolution and content uniformity. Sample rates of up to 1200 h^{-1} are possible using this equipment. In addition, these studies show that the requirements for repeatability and accuracy can easily be met.

Experimental

Equipment. The instrumentation used in support of the studies consisted of a Hewlett-Packard (Polo Alto, CA) model 1040A u.v.-visible spectrophotometer, a Spectrophysics (San Jose, CA) SP8770 isocratic pump, a Valco (Houston, TX) electronically actuated 10-port loop injector, fitted with a

0003-2670/86/$03.50

15-μl loop and 0.01-in. i.d. mixing "T", and various lengths and internal diameter 316 stainless steel tubing from Handy and Harman (Norristown, PA). The separator was manufactured to our specifications by J. L. Beemer and Co. (Philadelphia, PA).

Early in the development of the project, a six-port valve (Valco) was used to introduce the sample. When the valve was moved from one position to the other, a spike would register on the recorder that was apparently related to the stoppage of flow when the valve was between positions. To minimize this, a Valco M series ten-port valve tensioned at 1500 psi was installed. Because the rotor inside the valve has to travel a smaller distance when indexed, the flow is interrupted for a shorter period of time. Although the pulsing was diminished, it was still obviously present in many of the procedures under development. The problem was finally corrected when the grooves in the rotor were increased by 10°. With this modification, the flow is interrupted for only about 0.1 s during the cycling between the load and fill positions and the problem appears less severe. The reduced tension on the valve rotor resulted in much longer life from the valve than originally expected. A second valve was purchased when well over 20000 injections had been made on the original valve. A problem with the electronic components of the actuator overheating was corrected by removing the casing from the device and placing the injector near the cooling fan vent of the detector.

An AutoAnalyzer sampler (Technicon Corp. Tarrytown, NY) was modified so that an electronic switch closure provides the signal for the sample tray to advance one position and causes the sampling probe to extend into the sample. Plastic, disposable 10-ml sample cups are used to hold the samples. These are loaded into the circular trays mounted the sampler.

The sampling probe is connected to the loop injector by a 9-in. piece of 0.02-in. i.d. teflon tubing. Vacuum, applied from a "house" supply (about 5 Torr Hg), is applied to the valve through a 4-in. piece of 0.005-in. i.d. stainless steel tubing. The reduced inside diameter of the vacuum line produces the necessary resistance to the flow of the sample to assure that the loop is properly filled.

Both the valve and the loop injector are controlled by a PDP 11/04 computer (Digital Equipment Corp.) using a BASIC program. This program provides the switch closures necessary to extend the sampling probe, advances the valve to the load position, monitors the amount of time spent sampling, rotates the valve to the inject position, retracts the sampling probe and advances the sampler. The modifications to the sampler and the use of the M-series valve allow for a maximum sampling rate of 1200 samples h^{-1}.

Results

Using the system as described allowed the quantification of up to 1200 dissolution samples containing hydrochlorothiazide each hour. This procedure is based on the absorption of u.v. radiation by hydrochlorothiazide at 318 nm. The dissolution medium, water, is pumped through the loop injector at 2.0 ml min^{-1}.

When this flow rate and a 2-ft. section of 0.005-in. i.d. tubing were used, data were collected at different sampling rates for hydrochlorothiazide. Samples were injected at the rate of 360, 720 and 1200 per hour (Fig. 1). Each sample was injected in triplicate and four concentrations were studied (25, 50, 75 and 100% of claim). The results show that the peak height vs. concentration relationship is linear at each of the three injection rates studied (all correlation coefficients $\geqslant 0.99$). In fact, the data further show that the same results were obtained at each sampling rate. That is, the peaks reach baseline and do not overlap. The repeatability of this procedure was studied at 360 and 1200 samples h^{-1} for the 100% standard. The relative standard deviations for ten repetitions were 0.77% and 0.64%, respectively. These experiments showed that the intensity and bandwidth of the samples are a function of tubing diameter. In addition they showed that once the bandspread has been identified, conditions can be optimized.

The optimized conditions generated for hydrochlorothiazide were used to design a procedure to quantify dissolution samples containing timolol maleate with 0.1 M hydrochloric acid as carrier at 2.0 ml min^{-1}. Standards ranging from 25% to 100% of claim were determined at a sampling rate of 720 h^{-1}. This sampling rate was used because it generated less heat in the sampling valve actuator and was still approximately sixty times faster than doing the procedure manually. The results of the linearity studies produced a linear response with a correlation coefficient of 0.999. The 100%-of-claim standard was used to evaluate the repeatability of the procedure. The relative standard deviation obtained was 1.16%. The effect of carry-over was examined in the middle of the run. Five samples of 0.1 M hydrochloric acid that did not contain timolol maleate were injected following the fifth 100%-of-claim sample. No carry-over was observed.

In a related series of studies, combination tablets containing hydrochlorothiazide, methyldopa and amiloride were quantified following dissolution-rate testing in 750 ml of 0.1 M hydrochloric acid. Examination of the u.v. spectra of these compounds showed that methyldopa absorbs strongly at about 280 nm, hydrochlorothiazide absorbs at 280 nm and 318 nm and

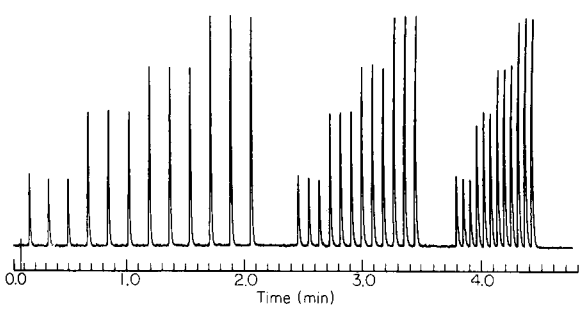

Fig. 1. Hydrochlorothiazide standards injected at a rate of 360, 720 and 1200 h^{-1} with the high-performance flow injection system.

amiloride has absorbance maxima at 280 nm and 360 nm. Because the spectra are significantly different, the compounds are easily resolved mathematically when the absorbance at these three wavelengths is recorded.

To test this approach, standard samples containing each of the three compounds were injected at a rate of 450 h^{-1}. These were followed by a series of synthetic samples prepared by diluting various amounts of the three stock standards to the working standard volume. The results obtained with these samples are shown in Table 1. As the statistical analysis shows, this approach can provide for rapid and precise quantification of this type of sample.

In an attempt to show that chemical reactions can also be used with this simplified approach, solutions containing methyldopa were reacted with iron(II) tartrate solution to produce a purple derivative that absorbs at 533 nm. A flow-injection system was constructed using the basic direct inlet approach. The 1.0% (w/v) iron(II) tartrate solution was pumped as the carrier solvent at a flow rate of 2.0 ml min^{-1} through a 2-ft. long section of 0.01-in. i.d. tubing into the spectrophotometer. Because the reaction is essentially instantaneous, an incubation period was not required. With this approach, samples of methyldopa were quantified with excellent linearity and repeatability at a rate of 450 h^{-1}. The correlation coefficient for the linearity study was 0.999. The repeatability study using the 100% standard generated an RSD of 1.0%.

TABLE 1

Results obtained for synthetic Aldoretic samples at a rate of 450 h^{-1}

	Amiloride	Hydrochlorothiazide	Methyldopa
Intercept (%)	1.35	2.49	0.61
Slope	0.97	0.94	0.96
Corr. coeff.	0.999	0.998	0.994

REFERENCES

1 J. Růžička and E. H. Hansen, Flow Injection Analysis, Wiley-Interscience, New York, 1981.
2 J. Růžička and E. H. Hansen, Anal. Chim. Acta, 99 (1978) 37.
3 J. Růžička, Anal. Chem., 55 (1983) 1040A.
4 K. K. Stewart, G. R. Beecher and P. E. Hare, Anal. Biochem., 70 (1976) 167.

Analytica Chimica Acta, 181 (1986) 245—251
Elsevier Science Publishers B.V., Amsterdam — Printed in The Netherlands

Short Communication

PHOTOCHROMISM OF SILVER(I) AND MERCURY(II) DITHIZONATES
Effect of Excess of Free Ligand on the Return to Ground State and Effect of Silver(I) Dithizonate on the Return of Mercury(II) Dithizonate

S. R. VARMA and HORACIO A. MOTTOLA*
Department of Chemistry, Oklahoma State University, Stillwater, OK 74078-0447 (U.S.A.)
(Received 29th August 1985)

Summary. The energy of photons producing highest yield in the photochromic excitation of both silver(I) and mercury(II) dithizonate is shown to be centered around 520 nm. The effect of silver(I) dithizonate on the return of the excited form of mercury(II) dithizonate to the ground state is described. The accelerating effect of the silver complex is interpreted by an empirical kinetic model that takes into consideration the concurrent excitation and relaxation of both complexes. As observed in the photochromism of mercury(II) dithizonate, the presence of excess of ligand proportionally hastens the relaxation of silver(I) dithizonate to the ground state.

This communication presents results of part of a study of different factors affecting the photochromism of metal dithizonates. These studies are motivated by a two-fold interest with analytical implications. First, there is need for a more detailed understanding of the photochromic process itself as it concerns the photometric determinations of metallic species [1]. Because different metal dithizonates relax to ground state at different rates depending on the central metal ion [2], the second point of interest lies in the possibility of kinetic-based determinations of more than one metallic species in a single dithizone extract.

As part of these studies, the dependence of the rate coefficient for the photochromic relaxation of mercury(II) dithizonate on the excess of free ligand present with benzene as solvent was recently reported [3]. More recently, Grummt et al. [4] studied the photochromism and thermochromism of dithizone itself in hexane, acetone, and acetonitrile. Both these studies point to the complexity of the photochromic phenomena in these systems and the need for gathering further basic experimental information. The present contribution reports work aimed at determining the energy of the photons producing highest yields in the photochromic excitation of silver(I) and mercury(II) dithizonate, the effect of free ligand on the return to ground state of the silver(I) dithizonate, and the effect of silver(I) dithizonate on the return to ground state of the mercury(II) dithizonate.

0003-2670/86/$03.50

Experimental

Apparatus. The equipment used was described previously [3]. Interference filters (Alpkem Corporation, Clackamas, OR) were used to isolate narrow wavelength bands. The nominal wavelengths passed by the filters were 480, 500, 520, 540 and 560 nm with band widths of 14.5, 11.0, 12.1, 12.5 and 14.0 nm, respectively.

Reagents and solutions. All the chemicals used, including benzene, were of analytical-reagent grade. Deionized water was further distilled in a borosilicate glass still equipped with a quartz immersion heater. Commercially available dithizone (White Label; Eastman-Kodak) was purified as described by Irving [5]. Solutions of mercury(II) dithizonate were prepared by dissolving the commercially available solid (Eastman-Kodak) in benzene. The presence of uncomplexed mercury(II) in solution was indicated during the photometric titration of the complex with dithizone and a correction had to be made to obtain stoichiometric ligand/metal concentrations.

Solutions containing excess of free ligand were prepared by adding a known amount of free dithizone to a solution of mercury(II) dithizonate. Two sets of experiments were done with excess of metal in solution. The first was extraction of mercury from aqueous solutions of mercury(II) perchlorate in perchloric acid (0.010 M) with solutions of dithizone in benzene. After equilibrium was reached, the benzene layer was filtered through a hydrophobic filter paper (Macherey-Nagel), collected in amber-colored bottles, and allowed to stand overnight. The second set involved similar extractions from aqueous solutions of mercury(II) chloride. The extracts were filtered and stored as before. Silver(I) dithizonate solutions were prepared by extraction from aqueous solutions of silver nitrate in 0.010 M nitric acid with benzene solutions of dithizone. The extracts were filtered and collected in amber bottles. Solutions containing excess of metal or dithizone were prepared by the same procedure used for mercury(II) dithizonate.

Cleaning and conditioning of the glassware used were found to be critical. Reproducibility was achieved by following the procedure of Goodwin and Mottola [3].

Procedure. Samples were irradiated with light passed through the filters to provide the required wavelength range. Irradiation was for 30 s, initially, and the photochromic relaxation of mercury dithizonate from the excited (blue) to the ground state (orange) was monitored at 605 nm. The irradiation time was increased until a steady state was reached and the maximum absorbance was noted. The same procedure was repeated with various filters. Experiments were also conducted with solutions containing an excess of ligand or mercury.

The same procedure was used to study the photochromism of silver dithizonate. Steady state was achieved with 180-s irradiation. The photochromic relaxation of the excited species was followed at 605 nm.

The photochromic relaxation of mixtures of mercury and silver dithizonate was similarly studied. The concentration of mercury dithizonate was

kept constant and the silver dithizonate concentration was varied. Samples were irradiated for 180 s to reach the steady state. The maximum absorbance was measured to study the effect of silver dithizonate on the relaxation rate of mercury dithizonate.

Results and discussion

Energy of photons producing the highest yield of photochromic excitation. The photochromic relaxation of mercury(II) dithizonate was monitored at 25.0 ± 0.2°C, using the interference filters already described, and in the following experimental situations: (1) stoichiometric metal/ligand ratio, (2) excess of free ligand, and (3) excess of free metal ion. Solutions with excess of metal ion were examined in the presence of different anions as potential ligands in mixed ligand complexes (i.e., perchlorate and chloride).

Measurements with the stoichiometric ratio of mercury(II) and dithizone were performed with solutions of the complex with a concentration of 2.0×10^{-5} M. As shown in Fig. 1, a maximum average value for the absorbance of the excited species appears at about 520 nm. Because different interference

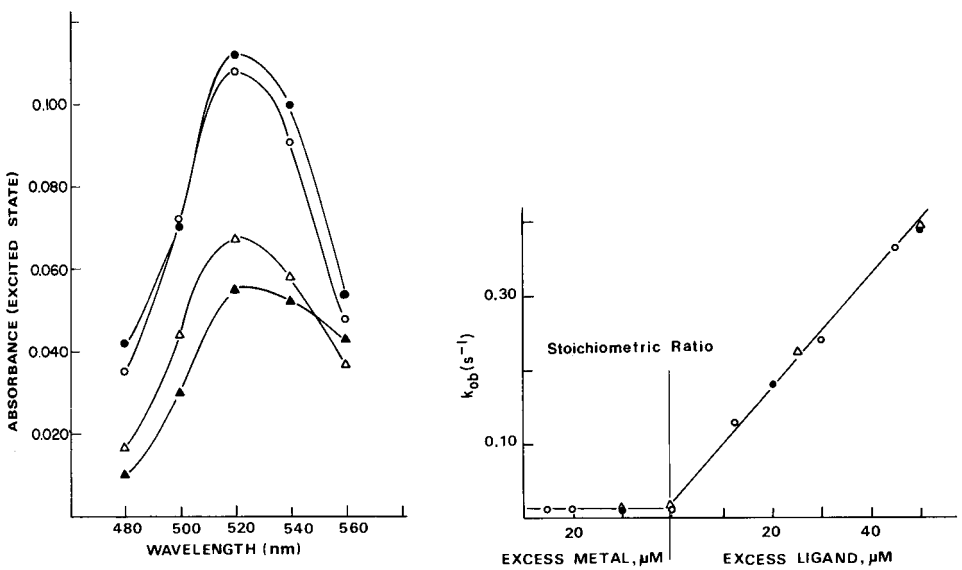

Fig. 1. Effect of wavelength of irradiation on the absorbance of the excited state of mercury(II) dithizonate. (•) Stoichiometric ligand/metal ratio (metal chelate concentration 2.0×10^{-5} M). (○) Excess of metal ion in perchlorate solutions [2.0×10^{-5} M metal chelate, 3.8×10^{-6} M excess of Hg(II)]. (▲) Excess of metal ion in chloride solutions [2.0×10^{-5} M metal chelate, 8.2×10^{-6} M excess of Hg(II)]. (△) Excess of free ligand (2.0×10^{-5} M metal chelate, 7.0×10^{-6} M excess of dithizone). Irradiation time for each nominal wavelength (s): 480 nm, 120; 500 nm, 180; 520 nm, 240; 540 nm, 120; 560 nm, 240.

Fig. 2. Effect of ligand/metal ratio on the rate coefficient for the relaxation of silver(I) dithizonate. Silver complex concentration: (○) 7.5×10^{-5} M; (•) 1.00×10^{-4} M; (△) 1.5×10^{-4} M.

filters have different thicknesses, the radiant energy transmitted by each is not the same. To compensate for this and to normalize the data, the irradiation time at each wavelength (see legend of Fig. 1) corresponds to that at which the absorbance of the excited state reached a constant value. The same absorbance value for the steady state was obtained with different filters of the same nominal wavelength but at different irradiation times.

Solutions 2.0×10^{-5} M in mercury(II) dithizonate containing an excess of about 7.0×10^{-6} M dithizone were used to establish the range of wavelength most effective for excitation in the presence of excess of free ligand. As shown in Fig. 1, the maximum irradiation effect was observed at 520 nm and the faster relaxation observed in the presence of excess of dithizone [3] was confirmed and reflected in lower values for the absorbance of the excited state in corresponding solutions.

As expected, because of the weak complexing characteristics of perchlorate, no difference was observed in measurements done at stoichiometric metal/ligand ratios and with an excess of mercury(II) ion in perchlorate solutions (Curve B, Fig. 1). When chloride solutions were used instead of perchlorate, a broader range of wavelengths produced the maximum and the decrease at higher wavelengths was not as pronounced as in the previous cases (Curve D, Fig. 1). Photons in the 520—540 nm range appear equally effective in this case. It should be mentioned that the mixed-ligand complex of mercury(II) dithizonate with chloride ion has been reported also as photochromic [6].

Attempts to perform a parallel set of experiments using silver(I) dithizonate failed because the interference filters available did not transmit sufficient radiant energy to produce an adequate population in the excited state in the time devoted to the experiments.

Effect of excess of free ligand or free metal on the relaxation of photochromically excited silver dithizonate. Solutions 7.5×10^{-5} M in silver(I) dithizonate were irradiated with unfiltered light at 20.0°C for different periods of time. An irradiation time of 180 s was needed to reach the constant ground-state and excited-state populations. Experiments done with an excess of metal ion, at the stoichiometric metal/ligand ratio (1:1), and with excess of free ligand showed the same qualitative trend previously observed for mercury(II) dithizonate [3]. This trend for silver(I) dithizonate is illustrated in Fig. 2, which shows the variation of the first-order observed rate coefficient, k_{ob}, at different ligand/metal ratios and for solutions containing different concentrations of the metal chelate. With metal/ligand ratios larger than 1:1, little or no effect was observed; k_{ob} had practically the same value as that obtained at the 1:1 ratio. As the excess of dithizone increased and the metal/ligand ratio decreased, a dramatic increase in the value of k_{ob} occurred. Also as in the case of mercury(II) dithizonate, the concentration of the metal chelate itself does not affect the value of the rate coefficient. The percent increase in rate coefficient correlates with the concentration of free ligand, as was observed for the same effect for mercury(II) dithizonate [3].

Relaxation to ground state of mercury(II) dithizonate in the presence of silver(I) dithizonate. For these experiments, the solutions contained constant mercury(II) dithizonate concentration (1.0×10^{-5} M) and varied concentrations (from 1.0×10^{-5} to 1.0×10^{-4} M) of silver(I) dithizonate. The excited states of both the metal dithizonates have absorption maxima at 605 nm but their times of relaxation to ground state are different [2, 7]. Values of rate coefficients characterizing the return to ground state for both metal complexes in different solvents and at different temperatures are presented in Table 1. In benzene, and at 20°C, the silver(I) complex relaxes about 3.5 times faster than the mercury(II) complex, and in all measurements the ratio of concentrations of silver to mercury complex is $\geqslant 1$. From a kinetic viewpoint this represents conditions under which a logarithmic extrapolation procedure would yield large errors in the concentration of the slower-reacting component and would consequently also affect the value for the faster-reacting one, because it is derived by difference from the total concentration of both components [8]. First-order plots of $-\ln (A_\infty - A_t)$ vs. relaxation time (A_∞ is the absorbance when relaxation has been completed and A_t the absorbance at any time during the relaxation process) yielded straight lines with increasing slopes as the concentration of silver(I) dithizonate was increased, and extrapolation of these lines beyond the zero extrapolation time resulted in all the lines intersecting at a common point close to 100 s, in the negative direction, in the relaxation time scale. This plot suggested that, empirically, the data can be treated as if a single component is contributing to the overall rate and the second is affecting the value of the rate coefficient of the slower reacting species. Moreover, the value for the absorbance of the excited-state population at the point of crossing for first-order plots was close to the value for the mercury(II) complex alone (0.295 compared to 0.279, with a silver(I) dithizonate contribution of 0.058 for a 1.0×10^{-4} M concentration); this points again to the possibility of an empirical data treatment, considering that the silver(I) complex affects the rate of return of mercury(II) dithizonate. This scheme is

TABLE 1

Rate coefficients for the return to ground state of Hg(II) dithizonate and Ag(I) dithizonate

Metal ion	Solvent	Temp. (°C)	Rate coefficient (s^{-1})	Ref.
Hg(II)	Benzene	25	2.7×10^{-3}	2
			$(2.7 \pm 0.4) \times 10^{-3}$	3
		24	0.5×10^{-3}	6
		20	$(2.7 \pm 0.3) \times 10^{-3}$	This work
Ag(I)	Tetrahydrofuran	11.5	1.1×10^{-2}	2
		11.5	1.7×10^{-2}	6
	Benzene	20	$(1.02 \pm 0.07) \times 10^{-2}$	This work

then similar to the one used to explain the increase in return rate for the mercury(II) complex when it is present with excess of free ligand [3]. By the same reasoning, the following mechanism is proposed for the relaxation of mercury(II) dithizonate in the presence of silver dithizonate:

$$Hg(HDz)_2 \underset{k_{ob}}{\overset{h\nu,AgHDz}{\rightleftharpoons}} Hg(HDz)_2^* \quad (1)$$

$$d[Hg(HDz)_2]/dt = k_{ob}\,[Hg(HDz)_2^*]$$

$$k_{ob} = k_{Hg} + k[AgHDz] = (2.7 \pm 0.3) \times 10^{-3}\ s^{-1} + (63.2 \pm 3.7)\ s^{-1}\ M^{-1}$$

$$[AgHDz]$$

$$A_t = A_\infty + A_0\ \{\exp - t(k_{Hg} + k[AgHDz])\} \quad (2)$$

where k_{ob} is the observed rate coefficient, k_{Hg} is the rate coefficient for the relaxation of Hg(II) dithizonate, and k is a constant accounting for the effect of the Ag(I) complex; [AgHDz] is the analytical concentration of Ag(I) dithizonate, A_0 the absorbance corresponding to the experimental zero relaxation time (for the excited species), and $[Hg(HDz)_2^*]$ is the concentration of the excited form of Hg(II) dithizonate.

If the model advanced to explain the effect of dithizone on the relaxation of mercury(II) dithizonate is also applied to the effect of silver(I) dithizonate on the relaxation of the mercury(II) complex, the absorbance at any given time, A_t, can be calculated from Eqn. 2. Figure 3 compares the calculated and experimental data and gives credibility to the mathematical model proposed.

This work was supported by the National Science Foundation (Grant No. CHE-8312494).

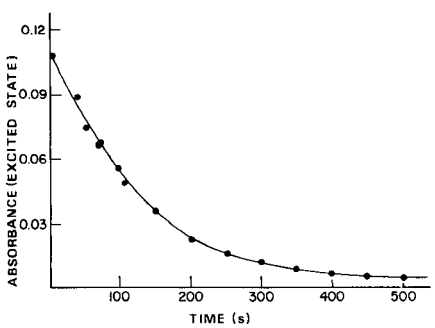

Fig. 3. Relaxation profile for 1.0×10^{-5} M Hg(II) dithizonate in presence of 1.00×10^{-4} M Ag(I) dithizonate: (—) curve calculated from Eqn. 2 (see text); (•) experimental points.

REFERENCES

1 G. Robisch and R. Dietel, Mikrochim. Acta, (1984) 447.
2 L. S. Meriwether, E. C. Breitner and C. L. Sloan, J. Am. Chem. Soc., 87 (1965) 4441.
3 A. E. Goodwin and H. A. Mottola, Anal. Chem., 55 (1983) 329.
4 U. W. Grummt, H. Langbein, R. Noske and G. Robisch, J. Photochem., 27 (1984) 249.
5 H. M. N. H. Irving, Dithizone, The Chemical Society, Burlington House, London, 1977, p. 67.
6 G. B. Briscoe and B. G. Cooksey, J. Chem. Soc. A: (1969) 205.
7 C. Geosling, A. W. Adamson and A. R. Gutierrez, Inorg. Chim. Acta, 29 (1978) 279.
8 L. J. Papa, in H. B. Mark, Jr. and G. A. Rechnitz (Eds.), Kinetics in Analytical Chemistry, Wiley-Interscience, New York, 1968, Chap. 7, pp. 196—201.

Analytica Chimica Acta, 181 (1986) 253—258
Elsevier Science Publishers B.V., Amsterdam — Printed in The Netherlands

Short Communication

ROUTINE METHOD FOR THE DETERMINATION OF THE OPTICAL CONSTANTS OF LIQUIDS

JENNIFER A. BARDWELL[a] and MICHAEL J. DIGNAM*
Department of Chemistry, University of Toronto, Toronto, Ontario M5S 1A1 (Canada)
(Received 25th July 1985)

Summary. A modification of the Kramera-Kronig method is used to obtain the spectra of the absorption and refraction indices, k and n, of benzene, chloroform and carbon tetrachloride from their infrared attenuated total-internal-reflectance spectra. The existing software of the Fourier-transform infrared spectrometer is applied for the calculation. For medium-strength bands with k between 0.004 and 0.3, agreement with earlier values is within a few percent, whereas for strong bands, the present k values are about 20% lower.

The absorption spectrum of a material is most easily obtained from a measurement of its transmission spectrum Unfortunately, the two spectra are simply related only in the case of dilute solutions for which an appropriate reference sample can be used to correct for reflection losses. In other cases, e.g., strongly absorbing or bulk materials or thin films on absorbing substrates, this technique cannot be used easily. In such cases, the specular reflection spectrum can be used instead, but the calculation is not as straightforward as for transmission spectra. This paper describes a rapid, routine method for the determination of the absorption spectrum from the specular reflection spectrum. The method is illustrated for infrared spectroscopy, but in principle is applicable to any spectral region. It has the further advantage that it yields information about the properties of anisotropic materials.

First, examples are presented which illustrate the reasons for using these techniques. Consider the specular reflection from an interface between a transparent window with refractive index n_0 and a sample characterized by a complex refractive index $\hat{n} = n - ik$ with the radiation incident from the window side. Here $i = (-1)^{1/2}$, n is the real part of the refractive index and k is the absorption index, related to the base 10 absorption coefficient, β, by the expression, $\beta = 4\pi k/(2.303\lambda)$, where λ is the wavelength. Figure 1 shows a synthetic spectrum of k and the corresponding n calculated as described previously [1] for an imaginary sample. Figure 2 shows the

[a]Present Address: Natural Research Council of Canada, Metallic Corrosion and Oxidation Section, Montreal Road, Ottawa, Ontario K1A 0R6, Canada.

0003-2670/86/$03.50

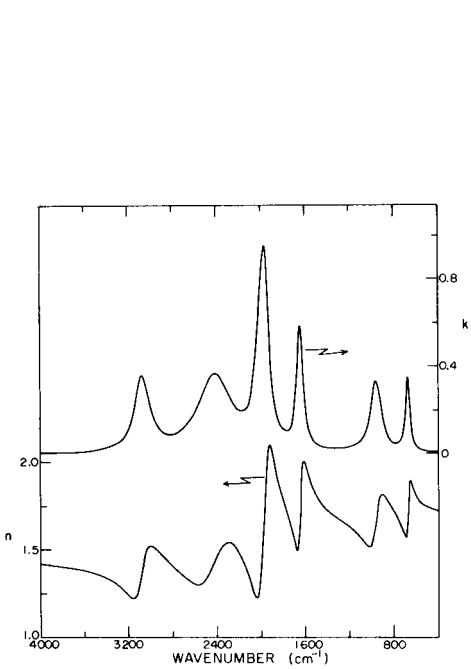

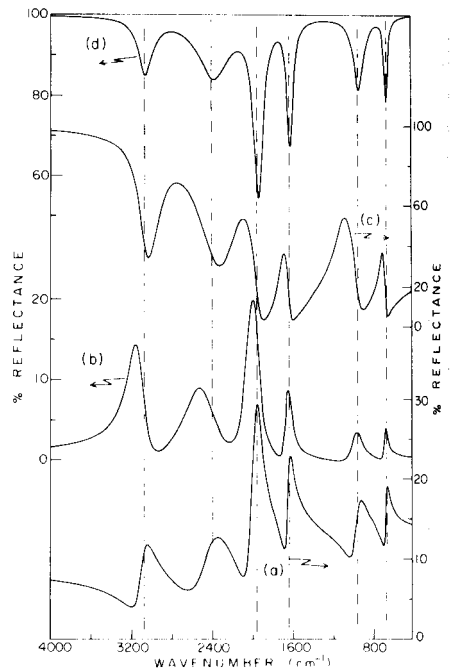

Fig. 1. Synthetic spectra of n and k for an example in the infrared range.

Fig. 2. Reflectance spectra calculated for a reflection from the interface between the material used for Fig. 1 and a window material of refractive index n_0. The dotted lines show the positions of the maxima in k. Spectra: (a) $n_0 = 1$, air or vacuum; (b) $n_0 = 1.59$, NaCl; (c) $n_0 = 2.25$, KRS-6; (d) $n_0 = 4$, Ge.

reflectance spectra which would be obtained from this material using s-polarized light (electric vector perpendicular to the plane of incidence) incident at 45°, when the window material is varied. Here the reflectance is defined as the ratio of the reflected to incident intensity. For no window ($n_0 = 1$, Fig. 2, curve a) the spectrum resembles but is not superimposable on the spectrum of n. For a NaCl window ($n_0 = 1.59$, curve b), the spectrum resembles the absorption spectrum, but there are large distortions in the band strengths and positions, particularly at the high energy end. For a KRS-6 window ($n_0 = 2.25$, curve c) features of both n and k occur in the reflectance spectrum. Finally, for a Ge window ($n_0 = 4$, curve d), attenuated total internal reflection occurs and the spectrum resembles quite closely the spectrum of k; however, even here, quantitative information cannot be obtained directly from the reflectance spectrum.

Clearly, the specular reflectance, R, is in general a complicated function of both the refractive and absorption indices. The problem at hand is to extract both n and k from measurements of R. For the case of s-polarized light incident from a vacuum, this problem is solved by use of the Kramers-

Kronig (KK) relationship [2]. The reflectance can be written as the square of the amplitude term of the complex Fresnel coefficient, $r = R^{1/2} \exp(i\theta)$, where θ is the phase. The basis of the KK technique is a relationship linking the reflectance to the phase:

$$\theta(\bar{\nu}) = (2\bar{\nu}/\pi) P \int_0^\infty \{\ln [R(\bar{\nu}_0)]^{1/2} \, d\bar{\nu}_0/(\bar{\nu}_0^2 - \bar{\nu}^2)\} \quad (1)$$

where P implies taking the Cauchy principal value. Together, the spectra of R and θ provide sufficient information to calculate n and k.

Although a cursory examination of Eqn. 1 would indicate that the phase at a frequency, $\bar{\nu}$, depends on the reflectance at every frequency, $\bar{\nu}_0$, between zero and infinity, the denominator of the integrand introduces a local character, and thus for example the phase in the infrared will depend on the reflectance in the infrared but will depend only weakly on its value in the ultraviolet.

Another relationship which is mathematically equivalent to the KK relation is the Fourier-transform (F.t.) relation [3, 4]:

$$\theta(\bar{\nu}) = -4 \int_0^\infty d\delta \, \sin(2\pi\bar{\nu}\delta) \int_0^\infty \ln [R(\bar{\nu}_0)]^{1/2} \cos(2\pi\bar{\nu}_0\delta) \, d\bar{\nu}_0 \quad (2)$$

Although this relationship might appear to require more computing time than Eqn. 1 because of fast Fourier-transform techniques, it actually requires only 1/630 of the time for 8192 points covering the band width (from $\bar{\nu} = 0$ up to the selected upper frequency, $\bar{\nu}_u$) [3]. In addition, commercial F.t.i.r. spectrometers include the software necessary to compute Eqn. 2 on a routine basis. In F.t.i.r., the interferogram, I, a function of the optical path difference δ, is transformed to obtain the real and imaginary single-beam spectra, S_r and S_i:

$$S_r(\bar{\nu}) = C \int_0^\infty I(\delta) \cos(2\pi\bar{\nu}\delta) d\delta \, ; \, S_i(\bar{\nu}) = C \int_0^\infty I(\delta) \sin(2\pi\bar{\nu}\delta) d\delta$$

To compute Eqn. 2 using the existing software, the spectrum of ln R must be treated as an interferogram, and then the result of the first Fourier transform must be made to look like another interferogram, details have been described previously [5]. Bertie and Eysel [6] used the Fourier transform to calculate n from k or vice versa, by means of the software of an F.t.i.r. spectrometer.

As noted, the KK and F.t. relationships are valid for s-polarized light, incident from a vacuum at an arbitrary angle. The extension to samples covered by window materials has been discussed [1]. An important case is that of attenuated total internal reflection (ATR) from an organic material; it was shown that the Fourier transform yields almost the correct phase and the necessary added constant correction can be determined from a knowledge of n at one point in the spectral range where $k \approx 0$. This com-

munication presents some results for ATR on organic solvents as an illustration of the ease with which this method can be applied to such systems.

Experimental

Spectra were collected on a Nicolet 8000 series F.t.i.r. spectrometer with a 7199 computer. Computer programs to compute Eqn. 2 and to calculate n and k from ATR data are available from the authors. A KBr beam splitter, a HgCdTe detector cooled with liquid nitrogen, and a globar source were used. A PLC-SIM liquid internal reflection cell with ZnSe prism (Harrick Scientific) was placed at the focal point. Two wire-grid polarizers (Perkin Elmer part no. 186-0240) were placed before and after the cell. They were driven by stepping motors with one step corresponding to 0.015°. Although only one polarizer is necessary, use of two polarizers reduced the error from polarizer imperfections and aided in alignment. The radiation coming from the beam splitter is highly polarized, so care was needed to determine the principal axes of the polarizer with respect to the plane of incidence of the reflection cell accurately; the method will be described elsewhere. For this application, precise alignment is not highly critical: a deliberate ± 2° error in the setting of the principal axes did not introduce a significant error in the results.

Organic solvents were spectral grade. Values of n at a point where $k \approx 0$ were taken from the data of Jones and co-workers [7, 8]. The refractive index of the ZnSe prism was calculated using the dispersion equation recommended by Li [9]. With the polarizers both aligned in the s position, 300 scans were collected and averaged at a resolution of 2 cm^{-1}. Although the problem does not arise in this instance, for certain conditions the reflectance, R, can approach zero [5] and hence lead to negative R when noise is included. To avoid this problem at the outset, the single-beam spectra were phase-corrected by using the "power" algorithm in which all noise is positive. The usable wavenumber range was 4200—600 cm^{-1}. Spectra were recorded for the full and empty reflection cell. The ratio of the full to empty single-beam spectra corresponds to R for the interface between the ZnSe window and the sample. In regions where $k \approx 0$, R should be close to 100%. In some of the runs, this was not the case, and these spectra were baseline-corrected. In no case was the correction greater than 3%. The correction was similar in shape in all runs corrected, suggesting a systematic error, most likely a small change in position of the liquid cell in the spring-loaded optical mount caused by the weight of the top plate used to seal the liquid in the filled cell.

Results and discussion

As outlined above, KK or Fourier transformation of ATR data yields the correct phase to within an additive constant. This constant, E, is evaluated [1] from

$$E = -\pi + 2 \arctan \left[(n_0^2 \sin^2\alpha - n^2)^{1/2}/n_0 \cos\alpha\right] - \theta' \qquad (3)$$

where α is the angle of incidence and θ' is the result of the F.t. calculation at the point where n is known. Then n and k are calculated from the corrected phase, $\theta'' = \theta' + E$, and the following equations [1]:

$$\epsilon_1 = n^2 - k^2 = n_0^2 + n_0^2 \cos^2\alpha \,[-8R + 4R^{1/2}\,(1+R)\cos\theta'']/[1+ + R - 2R^{1/2}\cos\theta'']^2$$

$$\epsilon_2 = 2nk = -4n_0^2 \cos^2\alpha\, R^{1/2}\,(1-R)\sin\theta''/(1+R-2R^{1/2}\cos\theta'')^2$$

$$n = 2^{-1/2}\,[\epsilon_1 + (\epsilon_1^2 + \epsilon_2^2)^{1/2}]^{1/2} \text{ and } k = \epsilon_2/2n$$

While the mean angle of incidence was fixed at 45° by the geometry of the ATR attachment, the i.r. beam was focused through a face of the ATR right-angle prism onto its hypotenuse, resulting in a range in α there of about ± 2°. As α is 15° or more removed from the critical angle, this range in α is not very serious, though for very precise work one should choose optics to minimize it.

Figure 3 shows spectra of n and k obtained as described above for benzene, chloroform and carbon tetrachloride. The results presented here are in general agreement with those of Jones and co-workers [7, 8]. For medium strength bands, $0.004 < k < 0.3$, the average discrepancy is 2.7% in k and 0.5% in n, with maximum discrepancies of 5.6% and 1.5%, respectively. For strong bands, $k > 0.9$, the values of k obtained here are significantly lower, by about 20%, than the literature values. These bands correspond to regions where R is < 6%, and thus is expected to be subject to greater experimental

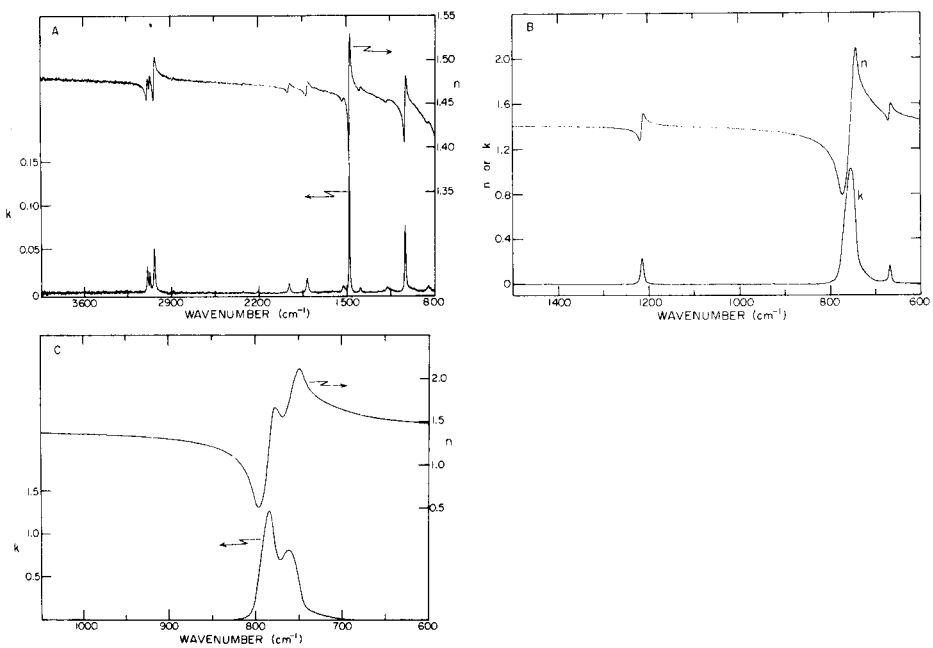

Fig. 3. Spectra of n and k: (A) benzene; (B) chloroform; (C) carbon tetrachloride.

error. Two possible sources of systematic error are the baseline correction and the use of the "power" phase-correction routine, both of which act to increase R and thus decrease k in these regions. The generally good agreement is satisfying considering the simplicity of the technique. In comparison to the method of Bertie and Eysel [6], the method used here has the advantage of needing no iteration to obtain results for n and k, but the disadvantage of requiring a polarizer. Both methods require some prior knowledge of n. However, a 5% error in this value of n introduces only a 5% error in the absorption parameters [1]. The method of Jones and co-workers [7, 8] also requires prior knowledge of n, as well as an iterative procedure to obtain n and k. An advantage of the present method is that a wide range of band strengths can be measured without changing the path length, as is required in transmission studies. For weaker bands, the sensitivity can be increased by using a multiple reflection ATR cell.

In conclusion, it is noted that this method can be applied to anistropic materials such as Langmuir-Blodgett films and liquid crystals, and results will be reported on these.

The authors thank the Natural Sciences and Engineering Research Council of Canada for supporting this work. They are also grateful to Professor Bertie for providing an early proof of his article.

REFERENCES

1 J. A. Bardwell and M. J. Dignam, J. Chem. Phys., 83 (1985) 5468.
2 M. Cardona, in S. Nudelman and S. S. Mitra (Eds.), Optical Properties of Solids, Plenum, New York, 1969, p. 137—151.
3 M. G. Sceats and G. C. Morris, Phys. Stat. Sol., 14 (1972) 643.
4 C. W. Peterson and B. W. Knight, J. Opt. Soc. Am., 63 (1973) 1238.
5 J. A. Bardwell and M. J. Dignam, Anal. Chim. Acta, 127 (1985) 101.
6 J. E. Bertie and H. H. Eysel, Appl. Spectrosc., 39 (1985) 392.
7 J. P. Hawranek and R. N. Jones, Spectrochim. Acta, Part A: 32 (1976) 111.
8 T. G. Golpen, D. G. Cameron and R. N. Jones, Appl. Spectrosc., 34 (1980) 657.
9 H. H. Li, Cindas Report — 64, May, 1982.

Analytica Chimica Acta, 181 (1986) 259—264
Elsevier Science Publishers B.V., Amsterdam — Printed in The Netherlands

Short Communication

INFRARED SPECTROMETRIC STUDIES OF THERMALLY INDUCED CHANGES IN LIGAND/SURFACE INTERACTIONS FOR CYANOALKYL GROUPS IMMOBILIZED ON SILICA

B. R. SUFFOLK and R. K. GILPIN*
Department of Chemistry, Kent State University, Kent, OH 44242 (U.S.A.)
(Received 6th September 1985)

Summary. The nitrile stretch regions for 2-cyanoethyldimethyl- and 5-cyanopentyldimethyl-silanized silica were studied under dry-state conditions by Fourier-transform infrared spectrometry. Deconvolution of each of the resulting broad asymmetric bands produced a doublet with high- and low-frequency assignments correct respectively for a population of ligands which hydrogen-bonds with free silanols and a population which is sterically hindered from the surface by adjacent groups. These results are consistent with previous observations for the same materials in contact with a non-polar liquid (n-hexane). Thermally induced changes in band contour, integrated intensity and frequency were observed, indicating a decrease in cyano/silanol interaction with increasing temperature. When similar physically coated materials were examined, the nitrile band, although broad, was substantially more symmetrical than that obtained for the chemically altered surfaces.

Currently over half of all high-performance liquid chromatographic (HPLC) separations are done in the reversed-phase mode with bonded linear hydrocarbon phases. Next in popularity are the more polar cyano and amino materials which are prepared by immobilizing the functional groups a few carbon atoms from the surface. These latter materials are suitable for both normal-phase and reversed-phase separations. Within the last few years various spectrometric techniques [1—6] have been used to characterize the chemical and physical properties of bonded phases. However, most of the work has been concerned with linear hydrocarbon phases [3]. In the case of polar surfaces, a much smaller amount of data has been acquired.

In a previous investigation, the behavior of cyano-bonded phases in liquids of differing polarity was studied by Fourier-transform infrared spectrometry (FTIR) [1]. In n-hexane, extremely broad and asymmetrical bands were observed for the nitrile stretch region. Deconvolution of these gave partially resolved doublets with a higher and lower frequency band assignable respectively to cyano groups which form hydrogen bonds with free surface silanols and to those which are sterically hindered from the surface by adjacent groups. These results were rationalized in terms of a non-uniform reaction model and the formation of at least two different distributions of attached ligands. When spectra are acquired from these same surfaces in contact with a polar liquid (1-butanol), the nitrile band was broad but symmetrical.

0003-2670/86/$03.50

To extend this earlier work [1], two of the above surfaces (i.e., 2-cyanoethyl and 5-cyanopentyl) were examined under dry-state conditions. Significant changes in the nitrile band occur as a function of both temperature and method of immobilization (i.e., chemical vs. physical). These data provide information in terms of distribution and orientation of the groups on the surface.

Experimental

Materials. All surface modifications were done on LiChrosorb Si-60 silica (mean particle size 10 μm and surface area of 550 m^2 g^{-1}; Merck). The 2-cyanoethyl- and 5-cyanopentyl-derivatized silicas were prepared from their corresponding monochlorosilanes under toluene reflux conditions as reported previously [1]. Subsequently, these materials were dried overnight at 110°C and then stored in a desiccator. The amounts of bound carbon were 5.8 and 8.6% for the cyanoethyl and cyanopentyl surfaces, respectively [1].

Stabilized 2-cyanoethyltrimethylsilane was synthesized from 2-cyanoethyltrichlorosilane by treatment with methylmagnesium iodide in sodium-dried diethyl ether [7]. The physically coated material was prepared by combining 0.43 g of this stabilized silane with 3.0 g of silica in ether and removing the solvent with a rotary evaporator.

Spectrometry. Spectra were collected with a Nicolet model 7199 FTIR spectrometer equipped with a MCT detector and set to give 1 cm^{-1} resolution. 2-Cyanoethyltrimethylsilane was prepared as a smear between two KCl disks (absorbance 0.5). Both the chemically modified and physically coated silicas were pressed into pellets using a Perkin-Elmer 13-mm pellet die. The cell was evacuated for 4 min and then 30 000 pounds pressure was applied for 2 min while maintaining the vacuum. Generally each pellet broke into several pieces when the die was opened. The largest piece from each preparation was used in subsequent steps.

The pellet prepared from the physically coated silica was mounted in a 2-mm aperture holder and placed in a Harrick Scientific Corporation 4X beam condenser. A ratio of 250 sample to 100 nitrogen background scans was taken (absorbance 0.1).

Temperature studies were done on the chemically modified materials as follows. Each pellet piece was mounted between two 25-mm diameter KBr disks. Apertures used ranged from 2 mm to 5 mm and areas not covered by the pellet were masked with aluminum foil. The pellet mounting was loaded into a Barnes Analytical high-temperature cell assembly which was regulated to ±1°C with a Love Controls Corporation controller. Ratios of 1000 sample to 250 nitrogen background scans were taken. The absorbances of the nitrile band maxima varied from 1.4 to 1.6 and 1.0 to 1.2 for the 2-cyanoethyl- and 5-cyanopentyl-modified materials, respectively. Band intensity integrations and Fourier self-deconvolution [8] were performed with Nicolet software [9].

Results and discussion

In the current investigation, two types of experiments were done: (1) the influence of temperature on the shape and intensity of the nitrile stretch was studied for chemically immobilized ligands, and (2) the effect of chemical vs. physical attachment on the C≡N band contour was examined for similar bonded and sorbed ligands. The results reported in Table 1 and Figs. 1—4 are representative of the data obtained from a number of repeated experiments.

Thermal studies. Infrared spectra were collected as a function of increasing temperature (29—237°C) from both the 2-cyanoethyldimethyl (2-CEDM) and 5-cyanopentyldimethyl (5-CPDM) modified materials. A representative set of spectra covering the nitrile stretch region (i.e., 2280 to 2200 cm^{-1}) appears in Fig. 1 for the 2-CEDM surface. Values for band position, integrated intensity, symmetry and width are summarized in Table 1 along with data from the 5-CPDM surface. In the case of this latter surface, slightly poorer

TABLE 1

Band intensities and maxima, peak width at half height (PWHH), and band asymmetry values as a function of temperature for C≡N stretch bands of cyanoalkyldimethyl ligands immobilized on silica

Chemically bonded silica surface	Temp. (°C)	Integrated band intensity (Absorbance)	Band maximum	PWHH (cm^{-1})	a/b[a]
2-Cyanoethyldimethyl	29	5.93	2228.8	20.4	2.3
	55	5.62	2228.8	18.8	1.8
	75	5.44	2228.8	18.0	1.8
	95	5.25	2228.3	18.0	1.9
	130	4.94	2227.8	17.0	1.7
	200	4.02	2226.8	16.4	1.6
	237	3.38	2225.9	15.4	1.4
5-Cyanopentyldimethyl	29	1.93	2250.9	25.0	2.3
	55	1.80	2250.4	23.4	1.9
	75	1.67	2250.4	23.2	1.7
	95	1.54	2249.5	21.4	1.8
	130	1.49	2250.0	21.2	1.4
	180	1.26	2247.1	20.8	2.0
	237	1.03	2247.1	19.4	1.4
5-Cyanopentyldimethyl	29	1.51	2250.0	24.6	2.3
	55	1.19	2250.0	23.2	2.3
	75	1.35	2251.4	23.6	1.5
	95	1.19	2249.5	22.0	1.9
	130	1.05	2249.0	20.6	1.7
	180	0.90	2248.0	19.0	1.5
	237	0.87	2246.6	20.0	1.3

[a]Band asymmetry (see [1]).

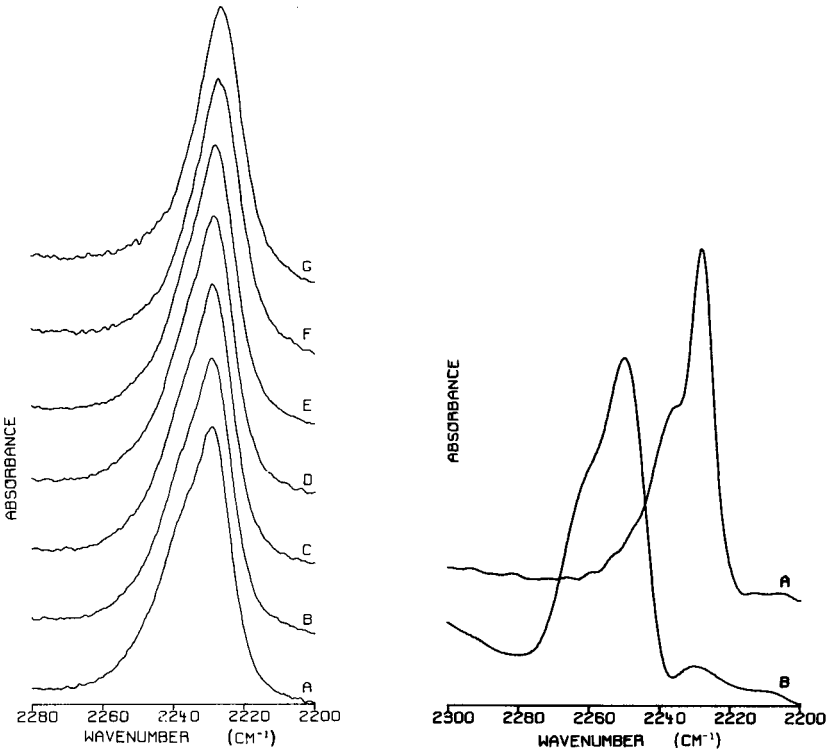

Fig. 1. FTIR spectra of the nitrile stretch bands of 2-cyanoethyl-silanized silica as a function of temperature. Temperatures in °C: (A) 29; (B) 55; (C) 75; (D) 95; (E) 130; (F) 200; (G) 237. For graphical purposes all bands are scaled to give the same height. Band height (absorbance): (A) 0.278; (B) 0.268; (C) 0.263; (D) 0.253; (E) 0.246; (F) 0.208; (G) 0.173.

Fig. 2. Fourier self-deconvolution spectra of nitrile stretch bands at 29° C of: (A) 2-cyanoethyl and (B) 5-cyanopentyl-silanized silica.

signal-to-noise was observed. Experimental reproducibility also is illustrated in Table 1 as a second entry of data for the 5-cyanopentyl surface acquired from pellets pressed and scanned on two different days.

Overall trends were similar for both the 2-CEDM and 5-CPDM modifications. Decreases in the width and asymmetry of the nitrile band were observed with increasing temperature (Fig. 1 and Table 1). Likewise, at 239°C the integrated intensity of the band was approximately half the value observed at 29°C. As noted further from the data in Table 1, a slight low frequency shift in the band maximum (V_{max}) was observed at elevated temperature. This corresponded to a change of 3 to 4 cm^{-1} for both surfaces when the low- and high-temperature data were compared.

Changes in the infrared band contour and integrated intensity similar to those observed in the current work are typically found for various degrees of hydrogen bonding in A—H (where A = O, N, S, F, Br, I, or Cl) proton donor

compounds [10—12]. For the C≡N band, White and Thompson [13] and Rochester and co-workers [14, 15] have observed increased intensity as well as small shifts to higher frequency as the result of hydrogen bonding. In a similar fashion, the current spectral changes are indicative of decreasing cyano/silanol interaction with increasing temperature and agree with results from previous work [1].

Fourier self-deconvolution of the nitrile stretch region for both immobilized ligands produced unresolved doublets as shown in Fig. 2. The higher frequency component is due to groups which form hydrogen bonds with free surface silanols, whereas the lower frequency band arises from immobilized groups which are sterically hindered from the surface by adjacent chains [1]. Deconvoluted spectra for the 2-CEDM surface are shown in Fig. 3 as a function of temperature. At 29°C, about a third of the integrated band intensity (i.e., higher frequency band) is due to hydrogen-bonded ligands. With increasing temperature the relative number of these decreases and at 237°C the higher frequency band is almost absent.

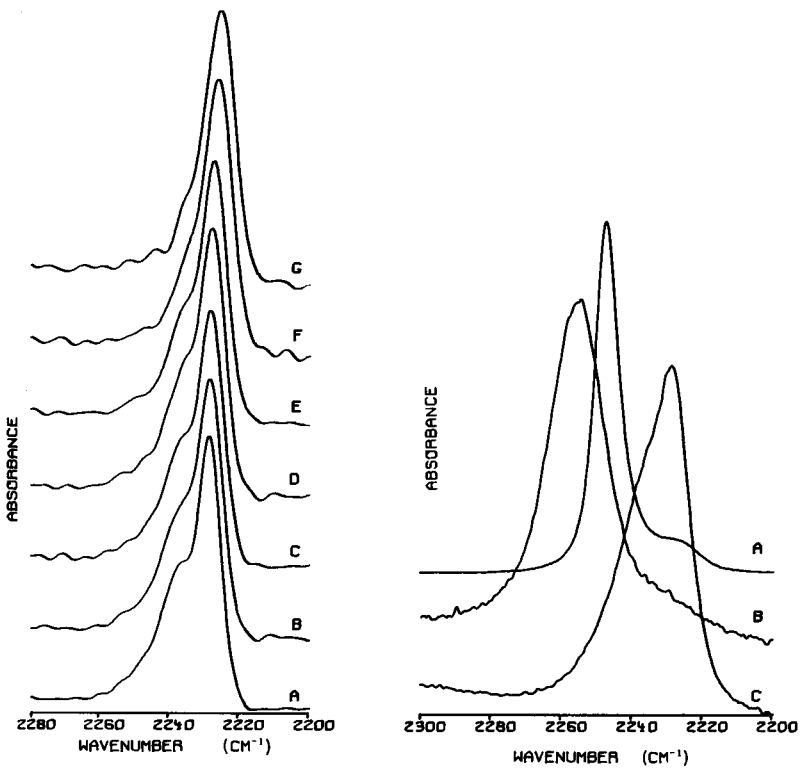

Fig. 3. Fourier self-deconvolution spectra of bands shown in Fig. 1.

Fig. 4. FTIR spectra of the nitrile stretch bands of: (A) 2-cyanoethyltrimethylsilane; (B) 2-cyanoethyltrimethylsilane physically sorbed on silica; (C) 2-cyanoethyldimethylchlorosilane chemically reacted with silica. For graphical purposes all bands are scaled to give the same height. Band height (absorbance): (A) 0.444; (B) 0.068; (C) 0.278.

Sorption studies. Infrared spectra of the nitrile region for chemically and physically immobilized 2-cyanoethyl groups are shown in Fig. 4. The latter material was prepared on the same silica base material from the stabilized monomer, 2-cyanoethyltrimethylsilane. Also included for reference purposes is a solution spectrum of the stabilized monomer.

The nitrile band for sorbed 2-cyanoethyltrimethylsilane was considerably broader (peak width at half height, PWHH = 19.3) than the corresponding solution spectrum (PWHH = 8.1) and was shifted 6.8 cm^{-1} higher in frequency (V_{max} = 2254.3 cm^{-1}). Again both of these changes are due to cyano/silanol interaction [14, 15]. However, the shape of the nitrile band for the physically coated material compared to the chemically derivatized surface is significantly more symmetrical (a/b = 1.4 vs. 2.3). These results suggest a more uniform distribution of sorbed molecules compared to those chemically anchored.

The shift of the nitrile band of 2-cyanoethyldimethyl-silanized silica 18.7 cm^{-1} lower than the stabilized monomer is consistent with previous observations [1] and is due to changes in the electronic environment surrounding the β-carbon (i.e., two methyl groups and one oxygen atom attached to the silicon for immobilized ligands vs. three methyl groups for the stabilized monomer) [1].

REFERENCES

1 B. R. Suffolk and R. K. Gilpin, Anal. Chem., 57 (1985) 596.
2 M. L. Miller, R. W. Linton, S. G. Bush and J. W. Jorgenson, Anal. Chem., 56 (1984) 2204.
3 R. K. Gilpin, J. Chromatogr. Sci., 22 (1984) 371.
4 R. K. Gilpin and M. E. Gangoda, Anal. Chem., 56 (1984) 1470.
5 R. K. Gilpin and M. E. Gangoda, J. Chromatogr. Sci., 21 (1983) 352.
6 D. E. Leyden, D. S. Kendall, L. W. Burggraf, F. J. Pern and M. DeBello, Anal. Chem., 54 (1982) 101.
7 A. M. El-Abbady and L. C. Anderson, J. Am. Chem. Soc., 80 (1958) 1737.
8 J. K. Kauppinen, D. J. Moffatt, H. H. Mantsch and D. G. Cameron, Appl. Spectrosc., 35 (1981) 271.
9 D. A. C. Compton, Spectral Lines, 5 (1983) 4. Reprinted as Nicolet FT-IR Application Note 8311.
10 S. N. Vinogradov and R. H. Linnell, Hydrogen Bonding, Van Nostrand, New York, 1971, pp. 11 and 53.
11 G. C. Pimentel and A. L. McClellan, The Hydrogen Bond, W. H. Freeman, San Francisco, 1960, pp. 70 and 196.
12 L. J. Bellamy, The Infrared Spectra of Complex Molecules, Vol. 2, 2nd edn., Chapman and Hall, New York, 1980, p. 241.
13 S. C. White and H. W. Thompson, Proc. R. Soc. A: 291 (1966) 460.
14 C. H. Rochester and D. A. Trebilco, Chem. Ind., (1978) 127.
15 C. H. Rochester and G. H. Yong, J. Chem. Soc., Faraday Trans. I: 76 (1980) 1466.

Analytica Chimica Acta, 181 (1986) 265—270
Elsevier Science Publishers B.V., Amsterdam — Printed in The Netherlands

Short Communication

A SIMPLE PROCEDURE FOR HYDRODYNAMIC INJECTION IN FLOW INJECTION ANALYSIS APPLIED TO THE ATOMIC ABSORPTION SPECTROMETRY OF CHROMIUM IN STEELS

E. A. G. ZAGATTO, O. BAHIA Fº, M. F. GINÉ and H. BERGAMIN Fº*

Centro de Energia Nuclear na Agricultura, Universidade de S. Paulo, Caixa Postal 96, 13400 Piracicaba, S. Paulo (Brasil)

(Received 25th June 1985)

Summary. The proposed technique for hydrodynamic injection is based on commutation in a simple flow-injection system with only one peristaltic pump. Precise results (usually r.s.d. < 1%) are attained even when injected volumes are small (1—10 μl). Dead-volume effects are associated with the mechanical flexibility of the system and with diffusion; differences between effective sample size and the dimensions of the injection duct are emphasized, particularly for small volumes. The proposed technique is checked for a spectrophotometric model system and confirmed by the atomic absorption spectrometry of chromium in steels. With a sampling rate of 120 h^{-1}, the precision is better than 99% for chromium contents in the 0.0—30.0% (w/w) range. The results agree well with those obtained by i.c.p./a.e.s. and conventional a.a.s.

Hydrodynamic injection was proposed by Růžička and Hansen [1] as an alternative injection procedure in flow injection analysis (f.i.a.) [2]. The distinctive feature is that the injected volume is well defined without the need for injection valves. Yet, despite its inherently favourable characteristics, hydrodynamic injection has not been widely used in routine analyses. This communication presents a new way of doing hydrodynamic injections. The approach, based on commutation, requires only a simple flow-injection system with one peristaltic pump operating continuously, and is, therefore, suitable for large-scale routine analyses.

The potential and limitations of the approach are investigated for spectrophotometric model systems. The dead volume arising from hydrodynamic pressure gradients and diffusion is kept constant by using an electronically operated commutator. The feasibility of this kind of injection in routine analysis is demonstrated for the determination of chromium in steels by atomic absorption spectrometry (a.a.s.), which involves a high degree of sample dilution.

Experimental

Materials. All solutions were prepared with analytical-grade chemicals and distilled-deionized water. The dye solutions (bromocresol green) used in the model systems and the sodium tetraborate carrier solution were prepared

as described previously [3]. The chromium standard stock solution was prepared by dissolving 2.700 g of chromium metal in 20 ml of aqua regia (by heating for 20 min at about 90°C) and diluting to 500 ml with water. Working standards, in the range 0.0—540.0 mg Cr l^{-1}, were also 0.12 M in hydrochloric acid. The steel samples were prepared as reported earlier [4].

The components of the flow-injection system, including the electronically operated commutator, the spectrophotometer and accessories were the same

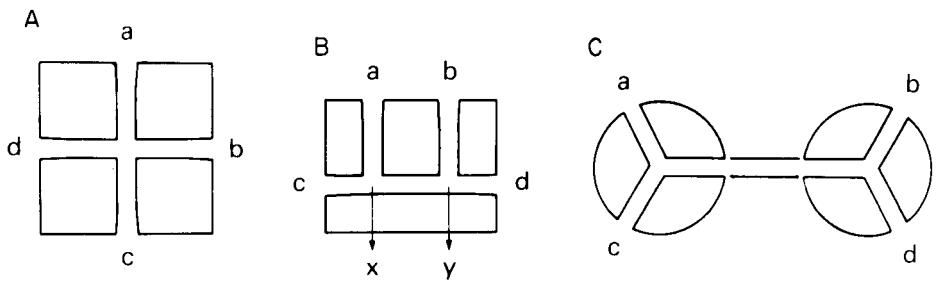

Fig. 1. Cross-sections (out of scale) of the volume-selecting devices. The inner diameter of all channels is 0.7 mm. The length of the connecting tube in Fig. 1C is 100 cm. For details, see text.

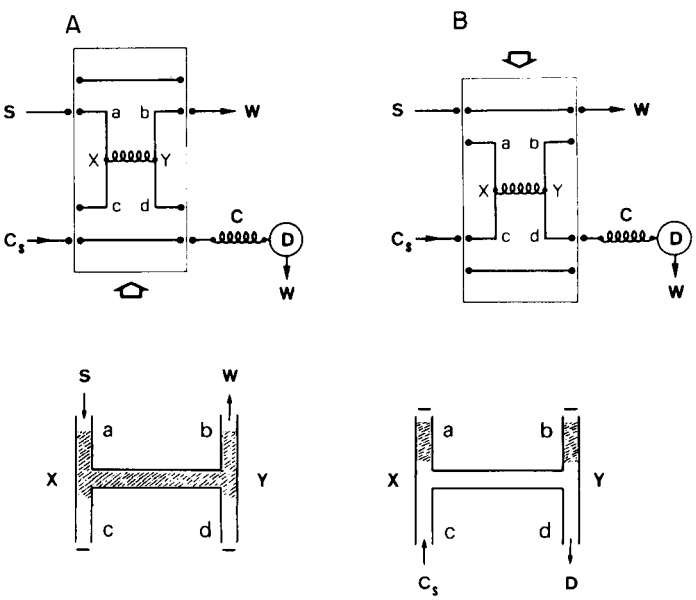

Fig. 2. Flow diagram of the proposed commutator system in the sampling (A) and injection (B) positions. S, sample; W, waste; C_s, sample carrier stream; C, coil; D, detector; a, b, c and d, duct arms; xy, injected volume selector. The large arrows indicate the direction of displacement of the central sliding bar of the commutator. The interaction between sample and carrier solutions is emphasized in the lower part of the figure. For details, see text.

as previously used [3] except for the occasional use of a Micronal flow-injection analyzer. The components used for the actual injection were made by drilling channels in perspex blocks (Fig. 1A, B) or by assembling together two Y-shaped connectors with a polyethylene tube (Fig. 1C).

Hydrodynamic injection is efficiently achieved by commutation as follows. When the commutator is in the position specified in Fig. 2A, the sample is aspirated through the **a** and **b** arms, filling the **xy** duct. Portions of the carrier solution are trapped inside the **c** and **d** arms, producing contact between the flowing sample and the trapped solutions. The carrier stream flows through the analytical path. After commutation (Fig. 2B), the solution in the **c** and **d** arms flows, transporting the sample through the analytical path. Again, the flowing carrier stream and the sample solution trapped inside the **a** and **b** arms are in contact. Replacement of samples is done when the commutator is in this position.

In the model systems with dye solutions, the carrier solution was pumped at 3.9 ml min^{-1}, the sample aspiration rate was 2.5 ml min^{-1}, the lengths of the duct arms were 25 cm, the coil (C) was 130 cm long and the wavelength was set at 617 nm. When the system was used with the Perkin-Elmer model 306 atomic absorption spectrometer, the rotation rate of the peristaltic pump was doubled to provide a total flow rate at the inlet of the nebulizer higher than the pneumatic aspiration rate of the spectrometer under the conditions specified by the manufacturer. A 2-μl duct with 5-cm long arms was selected to provide the volume of steel sample introduced into the water carrier stream. The coil length was 150 cm. The manifold was connected to the spectrometer as reported earlier [5]. For chromium measurements, maximum sensitivity was attained with air and acetylene flow rates of 21 and 5 l min^{-1}, respectively. Sampling and injection times were 10 and 20 s, respectively. A damping factor of 1.3 s (TC 2 setting) was chosen in accordance with the measurement frequency of 120 h^{-1}.

Procedures. Initially, several ducts with inner volumes ranging from 0.5 to 500 μl were tested in the model systems. Bromocresol green concentrations in the 10—1000 mg l^{-1} range were needed because of the widely differing dispersions involved. For each situation, the dispersion coefficient was evaluated [2]. The reproducibilities of the selected volumes were evaluated in terms of relative standard deviation of the recorded peak heights corresponding to ten successive injections. In this experiment, the sampling and injection times were 20 and 30 s, respectively.

The effect of sampling time was investigated over the range 0.5—40 s. The commutation cycle was kept at 60 s.

The proposed procedure was not compared with that originally devised for hydrodynamic injection [1] because of difficulties in obtaining the two identical flow rates required.

The accuracy of the injection procedure was assessed for the determination of chromium in steels. The results obtained by the proposed approach were compared with those obtained by i.c.p./a.e.s. [4] and by conventional

a.a.s. The latter procedure required a 50-fold manual sample dilution with water before measurement.

Results and discussion

A slight sacrifice in reproducibility was reported when hydrodynamic injection was first suggested [1], mainly because of the small sample volume injected (25 μl). The technique proposed here permits more precise definition of the amount injected. When 500-μl volumes were injected, the differences between results were not measurable and good reproducibilities were also attained when **xy** ducts with inner volumes of 7.5, 2, 1 and 0.5 μl were used (Fig. 3).

The almost linear relationship between the inner volume of the **xy** duct and the measured signal expected for small injected volumes [2], does not hold for the injection approach described here. As the inner volume of the duct is diminished, the difference between the expected and effective injected amounts increases, the sample size becoming less dependent on the duct inner volume (Fig. 3). It should be reported as an extreme example that, when the 1-μl duct of Fig. 1B was replaced by that of Fig. 1A (inner volume, 0.5 μl), similar results were obtained. This phenomenon is due to dead-volume effects associated with the mechanical flexibility of the flow-injection system and with diffusion. It was more visible when the 1000 mg l^{-1} dye solution was used to simulate a sample. During the sampling time (Fig. 2A), the boundaries between the flowing sample and the trapped carrier solutions slowly moved towards the interior of the **a** and **b** arms; simultaneously, the contrast between the solutions became less defined because of diffusion. Therefore, the volume of sample became larger than that related to the inner volume of the duct. Fortunately, this has little

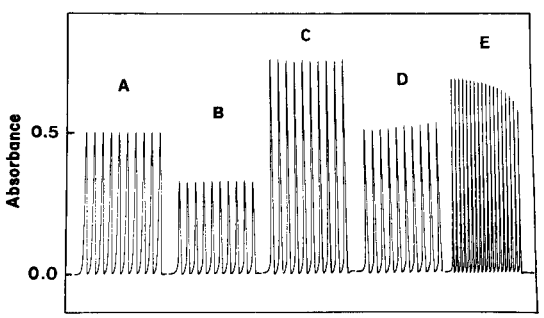

Fig. 3. Performance of some volume-selecting devices. Each set of ten successive recorded peaks is associated with duct inner volume (μl), bromocresol green concentration (mg l^{-1}), dispersion coefficient [2], r.s.d. (%) and volume-selecting device (Fig. 1) as follows: (A) 500, 10, 1.44, <0.3, Fig. 1C; (B) 7.5, 100, 22.0, 0.56, Fig. 1B; (C) 2, 1000, 95.6, 0.65, Fig. 1B; (D) 1, 1000, 138, 1.47, Fig. 1B. Set E is associated with injection times of 17.5, 16.5, 15.5 ... 2.5, 1.5 and 0.5 s, a total commutation cycle of 60 s, dye concentration of 200 mg l^{-1} and **xy** duct of 7.5 μl; the paper speed was halved.

effect on the measured signal for large sample volumes; with a 500-μl volume, differences in measurements caused by variations in sampling time from 5 to 35 s, were not detectable. In this situation, manual operation of the commutator is possible. For small volumes, however, this effect becomes more relevant (Fig. 3) because its percentage contribution to the selected volume of sample becomes significant. Electronic operation of the commutator is then required to guarantee a constant dead volume.

This phenomenon also occurs during the resting time of the commutator in the injection position (Fig. 2B). As the boundaries between sample and carrier solutions are moved, the possibility of the trapped sample reaching the flowing carrier stream decreases, thus minimizing carryover. This effect is not beneficial under conditions of negative hydrodynamic pressure. This was confirmed in preliminary tests with the f.i.a./a.a.s. system, if the aspiration rate used was higher than the flow rate reaching the spectrometer; the boundary displacements were reversed, leading to increased carryover.

The proposed f.i.a./a.a.s. system is remarkably stable. After three hours of continuous operation, only negligible variations (<2%) were observed in the coefficients of the calibration equations. These variations reflect mainly a slight drift in the a.a.s. parameters. The relative standard deviations shown in Table 1 are more related to uncertainties in the a.a.s. than to the hydrodynamic injection. The data presented in Table 1 also allow an assessment of the accuracy of the proposed technique.

Further applications

The hydrodynamic injector proposed here can be regarded as a "twin injector". When the commutator is moved to the position specified in

TABLE 1

Percentages of chromium (w/w) in standard steels as determined by the proposed procedure (f.i.a.), by atomic emission spectrometry (i.c.p./a.e.s.), and by conventional a.a.s. (Number in parentheses indicates the relative standard deviations (%) of three measurements of the same digest.)

Sample	F.i.a.[a]	I.c.p./a.e.s.[a]	A.a.s.[b]
ASTM A-217 Gr CA15	14.57 (0.26)	15.24 (0.23)	14.87 (0.60)
ASTM A-351 Gr CN7M	26.69 (0.92)	25.38 (0.75)	26.66 (0.39)
ASTM A-217 Gr C5	6.49 (0.77)	6.98 (0.65)	6.56 (0.75)
ASTM A-351 Gr CD4MCU	30.10 (1.20)	29.98 (0.37)	29.70 (0.68)
ASTM A-297 Gr HE	30.00 (0.90)	30.72 (0.73)	29.57 (0.40)
G-X50 CrMo 292	31.09 (1.07)	30.50 (0.98)	30.45 (0.28)
AISI 329	29.71 (1.12)	29.48 (1.19)	29.22 (0.25)
ASTM A-351 Gr CF8	20.68 (0.66)	20.89 (0.68)	20.80 (0.39)
ASTM A-217 Gr WC9	2.80 (2.69)	3.38 (0.38)	2.85 (2.66)
ASTM A-351 Gr CF8M	23.79 (0.83)	23.25 (0.15)	22.82 (0.51)

[a]F.i.a. and i.c.p./a.e.s. results were obtained by using the same digests. [b]After a 50-fold manual dilution of the solution with water; integration period 10 s.

Fig. 2B, the sample is injected into the carrier solution; the next commutation causes the carrier solution, or a reagent, to be introduced into the undispersed flowing sample. Therefore, both the normal [2] and reverse [6] f.i.a. configurations can be achieved with a single system. Studies on this point are in progress.

The approach can be used in confluence systems. In contrast to the procedure proposed earlier [1], the carrier stream flows continuously through the analytical path so that the flow-injection system is maintained under steady conditions. The proposed procedure is also attractive in connection with zone sampling [7].

Partial support of this research by CNPq (Conselho Nacional de Desenvolvimento Científico e Tecnológico) and by FINEP (Financiadora de Estudos e Projetos) is greatly appreciated. The authors express their gratitude to F. J. Krug and B. F. Reis for their constructive comments, and to Z. Z. Marcos for his assistance with the original manuscript.

REFERENCES

1 J. Růžička and E. H. Hansen, Anal. Chim. Acta, 145 (1983) 1.
2 J. Růžička and E. H. Hansen, Flow Injection Analysis, Wiley-Interscience, New York, 1981.
3 F. J. Krug, H. Bergamin Fº and E. A. G. Zagatto, Anal. Chim. Acta, 179 (1985) 103.
4 F. J. Krug, O. Bahia Fº and E. A. G. Zagatto, Anal. Chim. Acta, 161 (1984) 245.
5 A. O. Jacintho, E. A. G. Zagatto, H. Bergamin Fº, F. J. Krug, B. F. Reis, R. E. Bruns and B. R. Kowalski, Anal. Chim. Acta, 130 (1981) 243.
6 K. S. Johnson and R. L. Petty, Anal. Chem., 54 (1982) 1185.
7 B. F. Reis, A. O. Jacintho, J. Mortatti, F. J. Krug, E. A. G. Zagatto, H. Bergamin Fº and L. C. R. Pessenda, Anal. Chim. Acta, 123 (1981) 221.

Analytica Chimica Acta, 181 (1986) 271—275
Elsevier Science Publishers B.V., Amsterdam — Printed in The Netherlands

Short Communication

SENSITIVITY ENHANCEMENT FOR INDUCTIVELY-COUPLED PLASMA ATOMIC EMISSION SPECTROMETRY OF CADMIUM BY SUCTION-FLOW ON-LINE ION-EXCHANGE PRECONCENTRATION

TAKAHIRO KUMAMARU* and HIROSHI MATSUO

Department of Environmental Science, Faculty of Integrated Arts and Sciences, Hiroshima University, 1-1-89 Higashisenda-machi, Naka-ku, Hiroshima 730 (Japan)

YASUAKI OKAMOTO

Institute of Environment and Public Health of Okayama Prefecture, Uchio, Okayama 701-02 (Japan)

MASAHIKO IKEDA

Engineering Department, Nippon Jarrel-Ash Co. Ltd., 28 Joshungamae-cho, Shimotoba, Fushimi-ku, Kyoto 612 (Japan)

(Received 10th July 1985)

Summary. A column of iminodiacetate chelating resin is used to preconcentrate cadmium by a factor of 25-fold for a 5-ml sample. The sampling rate was 25 h^{-1}, and the detection limit 0.05 ng Cd^{2+} ml^{-1}. The r.s.d. for 0.1 μg Cd^{2+} ml^{-1} was 2.2% (n = 10). This technique was applied to the determination of cadmium in certified biological reference materials and waste-water samples.

Recent reports discussed on-line suction-flow extraction for inductively-coupled plasma atomic emission spectrometry (i.c.p./a.e.s.) with a teflon membrane for the separation of cadmium ions [1], and the determination of selenium by atomic absorption spectrometry (a.a.s.) with a miniaturized suction-flow hydride generator and an on-line chelating resin column for removing transition metal interferences [2]. The ion-exchange resin used had several advantages such as good selectivity, and easy handling and regeneration. Flow-injection i.c.p./a.e.s. with an on-line preconcentrating ion-exchange column filled with chelating resin has already been reported by Hartenstein et al. [3]. This communication describes an economical on-line preconcentration system with a chelating resin column for sensitive suction-flow i.c.p./a.e.s. applied to cadmium determination.

Experimental

Apparatus. Kyoto-Koken Model UOP-1S and Nippon Jarrell-Ash Model ICAP-575 (Kyoto, Japan) inductively-coupled plasma atomic emission spectrometers were used. The flow system was composed of a 2-channel variable-speed peristaltic pump (Nippon Jarrel-Ash), a teflon-PTFE suction cup, a

resin column and a T-joint. The other parts of the flow system were connected with 1-mm i.d. teflon-PTFE tubing. The assembly is shown in Fig. 1. The dimensions of the teflon suction cup were as reported previously [1, 2, 4]. Pipetman P-1000 and P-5000 (Gilson International, Villers-le-Bel, France) digital pipettes were used. Double-vessel digestion bombs [5] were used for the decomposition of biological materials. The bombs consisted of a teflon-PFA (perfluoroalkylvinyl ether) Tuf-Tainer vial (Pierce Chemical, Rockford, U.S.A.), a teflon-PTFE vessel and a stainless steel jacket (San'ai Science, Nagoya).

Reagents. All chemicals were of analytical-reagent grade. Pure water from an Organo Miniclear DC-610 system (Organo, Tokyo) was used. Muromac A-1 (Muromachi Chemicals, Tokyo), styrene-divinylbenzene copolymer matrix containing iminodiacetate ions was used as the chelating resin. The buffer solution (pH 5.0) used was 0.1 M sodium citrate. The standard stock solution of cadmium was prepared as previously reported [1].

Procedure. A sample solution, usually 5 ml, was added to the teflon suction cup from the digital pipette. As shown in Fig. 1, the sample solution was merged into the buffer line, and mixed. Cadmium ions were then adsorbed on the resin column. The effluent was continuously introduced into the nebulizer. Hydrochloric acid (1 M) was sucked in and the adsorbed ions were eluted. The transient emission signal was recorded on a strip-chart recorder and the peak height was measured. The optimum operating conditions are shown in Table 1. The emission peak appeared within 10 s of introducing the acid; 1 ml of water was sucked in after each elution for rinsing. The timing of the cycle is shown in Fig. 2.

Results and discussion

Optimization of conditions. The previous report [1] stressed the importance of matching the pumping rate to the specified nebulizer rate for obtaining optimum sensitivity. The system used had an optimum feed rate of 4.7 ml min^{-1}. The effect of the inner diameter of the column on the signal

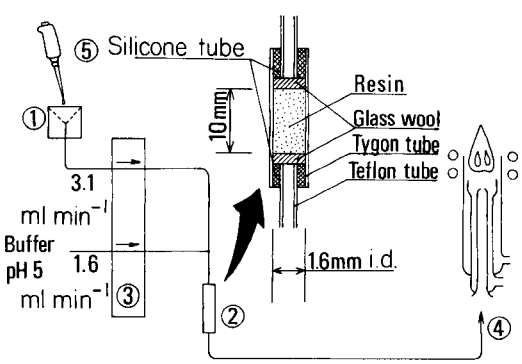

Fig. 1. Flow diagram: (1) suction cup; (2) column; (3) peristaltic pump; (4) i.c.p.; (5) digital pipette.

TABLE 1

Recommended operating conditions

I.c.p. atomic emission spectrometer	
R.f. power	1.0 kW
Argon gas flow rates	
Outer gas	10 l min^{-1}
Intermediate	0.7 l min^{-1}
Nebulizer	0.4 l min^{-1}
Observation height	12 mm above load coil
Photomultiplier	800 V
Response (time constant)	1 s
Analytical line	214.438 nm (Cd II)
Suction-flow preconcentration system	
Sample volume	5 ml
Eluent (1 M HCl) volume	250 µl
Rinse water volume	1 ml
Flow rates	
Sample	3.1 ml min^{-1} (1.6 mm i.d., 4.8 mm o.d.)
Buffer (0.1 M sodium citrate)	1.6 ml min^{-1} (1.0 mm i.d., 2.0 mm o.d.)
Column size	1.6 mm i.d., 10 mm long (resin 10 mg)
Ion-exchange capacity	ca. 0.3 mg Cu^{2+}

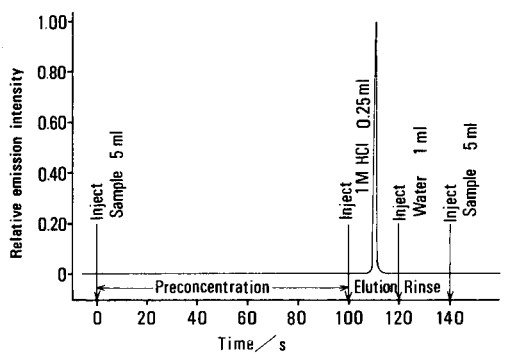

Fig. 2. Time sequence of the solution flow.

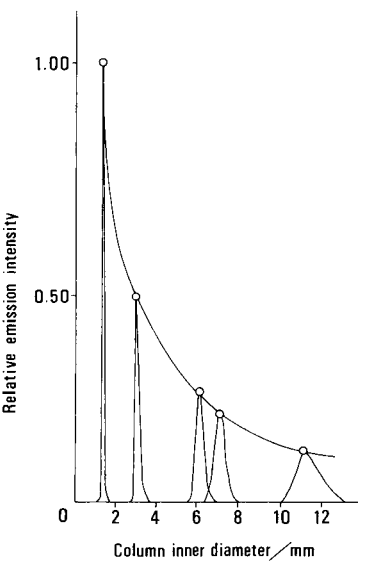

Fig. 3. Peak profile of cadmium as a function of inner diameter of ion-exchange column (10 mm long).

shape is shown in Fig. 3. The sharpest, highest peak was obtained with a column of 1.6 mm i.d. Increasing the inner diameter decreased the peak heights. The effect of column length is shown in Fig. 4. The sharpest peak was obtained with a 10-mm column.

In this work, 1 M hydrochloric acid was used as the eluent. The amount of eluent was important. The highest sensitivity was obtained with 0.25 ml of the acid (Fig. 5). It was also found that the sample acidity should be less than ca. 0.01 M in hydrochloric acid so as to collect cadmium ions quantitatively on the resin.

Sensitivity and precision. Under the operating conditions summarized in Table 1, a linear calibration graph was obtained for cadmium up to 1 μg ml^{-1}. The 3σ detection limit was 0.05 ng ml^{-1}. The sensitivity and detection limit were both about 25-fold better than those obtained by direct aspiration of the aqueous solution. The relative standard deviation for 10 replicate measurements of 0.1 μg Cd ml^{-1} was 2.2%; 25 samples could be analyzed per hour.

The emission line of platinum (214.423 nm) interferes spectrally with the cadmium line (214.438 nm). In the proposed method, however, such interference was greatly decreased because platinum(IV) (as $PtCl_6^{2-}$) was not retained by the column.

Application to practical samples. The accuracy of the method was examined by analyzing the NBS standard reference material, Bovine Liver, the NIES (National Institute for Environmental Studies, Environmental Agency of Japan) certified reference material, Pepperbush, and waste-water samples. The digestion procedure for the biological samples in the pressure vessel was adapted from the literature [5]. Briefly, up to 300 mg (dry weight) of sample was digested with 3 ml of nitric acid in the pressure vessel for 2 h at 90°C and for 4 h at 140°C. After cooling and appropriate rinsing, the digest was adjusted to pH 3 with dilute ammonia water and then diluted as required.

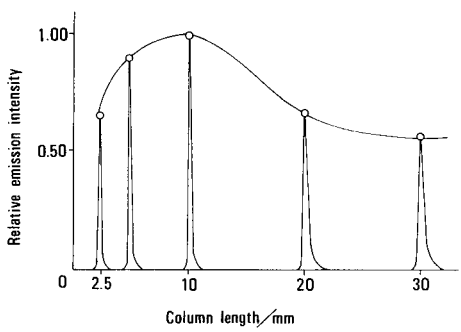

Fig. 4. Influence of length of ion-exchange column (1.6 mm i.d.) on emission signal of cadmium.

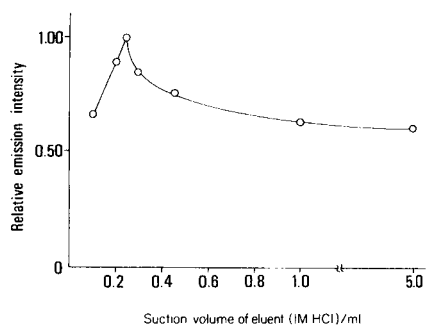

Fig. 5. Dependence of cadmium peak height on the volume of 1 M hydrochloric acid used as eluent.

TABLE 2

Results for cadmium

Sample	Cadmium found ($\mu g\ g^{-1}$)	Certified value ($\mu g\ g^{-1}$)	A.a.s. ($\mu g\ ml^{-1}$)
Bovine Liver (NBS SRM 1577)	0.24 ± 0.01	0.27 ± 0.04	—
Pepperbush (NIES CRM No. 1)	6.1 ± 0.1	6.7 ± 0.5	—
Waste-water A	0.011 ± 0.001	—	0.012 ± 0.001
Waste-water B	0.0030 ± 0.0001	—	0.0035 ± 0.0001

Waste-water samples taken at the inlet of the Waste-water Treatment Facility in Okayama prefecture were immediately filtered through a No. 2 filter paper (Toyo Filter Paper, Tokyo, Japan). The filtrates were acidified with hydrochloric acid and stored at pH 1. The pH of the samples was also adjusted to 3 with a dilute ammonia water.

The results, given in Table 2, show good agreement with the certified values or the values which were obtained by graphite-furnace atomic absorption spectrometry (a.a.s.).

REFERENCES

1 T. Kumamaru, Y. Nitta, F. Nakata, H. Matsuo and M. Ikeda, Anal. Chim. Acta, 174 (1985) 183.
2 M. Ikeda, Anal. Chim. Acta, 170 (1985) 217.
3 S. D. Hartenstein, J. Růžička and G. D. Christian, Anal. Chem., 57 (1985) 21.
4 M. Ikeda, F. Nakata, H. Matsuo and T. Kumamaru, Bunseki Kagaku, 33 (1984) 416.
5 K. Okamoto and K. Fuwa, Anal. Chem., 56 (1984) 1758.

Analytica Chimica Acta, 181 (1986) 277—282
Elsevier Science Publishers B.V., Amsterdam — Printed in The Netherlands

Short Communication

SINGLE-COLUMN ION CHROMATOGRAPHY OF WEAK INORGANIC ACIDS FOR MATERIALS AND PROCESS CHARACTERIZATION

C. McCRORY-JOY

AT and T Bell Laboratories, 600 Mountain Avenue, Murray Hill, NJ 07974 (U.S.A.)

(Received 22nd July 1985)

Summary. Single-column ion chromatography allows the separation and direct conductometric detection of anions of weak inorganic acids. Mixtures containing borate, silicate, germanate, fluoride and chloride can be resolved by using a resin-based anion-exchange column and a 0.06 $g\,l^{-1}$ sodium hydroxide/2.5×10^{-5} M sodium benzoate eluent. Judicious selection of sample preparation and of eluent composition is important. Glasses are analyzed for boron and fluoride by fusion with sodium hydroxide, suitable dilution and use of a benzoate eluent. Results on standard glasses are in good agreement with certified values. The separation of arsenite and arsenate in a gold plating bath is outlined.

Ion chromatography is very valuable for the rapid separation and detection of ionic species in solution [1—3]. Conductometric detection is the most general means of quantitative measurements; however, detection of weakly dissociated samples having $pK > 7$ may require special consideration. Anions of weak acids (e.g., borate and cyanide) pass through the detector as the weakly dissociated acids as a result of the suppressor reaction used in dual-column ion chromatography [2, 4]. Attempts made to overcome this limitation for borate include preconcentration and measurement of boron as the tetrafluoroborate [5] or the use of reagents such as mannitol to form a complex acid exhibiting greater conductivity [6]. Each of these procedures has some disadvantage in time required or constraints on sample or eluent preparation. Supplementary amperometric or u.v.-visible detectors might be considered for weakly dissociated substances, but neither approach is sufficiently general. Eluent composition may impose limitations on the detection of samples exhibiting suitable activity in other media.

The development of resin-based anion-exchange columns for single-column ion chromatography which are compatible with alkaline eluents such as sodium hydroxide facilitates the separation and detection of the anions of weak inorganic acids. Alkaline conditions promote dissociation of weak acids, allowing resolution of weak acid mixtures and direct conductometric detection. This is useful in principle for the characterization of materials which may be solubilized and have constituents which exist as weak acids in aqueous solution.

0003-2670/86/$03.50

Water-insoluble samples such as glasses represent a challenge to ion chromatography methods because reagents required for sample decomposition may introduce interfering ions [7—9]. The conditions existing as a result of fusion of glass samples with sodium carbonate have been considered, as well as those resulting from dissolution in hydrofluoric acid. These are the procedures most commonly used for the decomposition of glasses, and both present obstacles to subsequent quantitation by ion chromatography. An alternative procedure, fusion with sodium hydroxide in nickel crucibles [8], produces a melt closely matched to the sodium hydroxide eluents used and one which is free of interfering ions introduced by the other reagents. Standard (NBS) glass samples were processed to assess the accuracy of the determination of boron and fluoride in these materials.

Speciation of arsenite and arsenate in a gold plating bath used to prepare x-ray masks is also demonstrated. Anion-exclusion separation of these ions with acidic eluents requires either a supplementary amperometric detector for the determination of arsenite [10] or prior oxidation of arsenite to arsenate for conductometric detection [11].

Experimental

Apparatus. The single-column ion chromatograph was assembled with a Waters M-45 solvent-delivery system, a Wescan 213A electrical conductivity detector, and a Hewlett-Packard 680 or a Fisher Recordall strip-chart recorder. The Wescan resin-based anion column and precolumn were used. A Rheodyne 7125 sample injection port with a 100-μl sample loop served for all sample injections.

Reagents. Reagent-grade sodium hydroxide, sodium benzoate, *p*-hydroxybenzoic acid, and sodium tartrate were used to prepare eluents. All solutions were prepared with 16-Mohm deionized water. Standards were prepared from Alfa ultrapure materials except for the phosphate standard which was prepared from reagent-grade sodium phosphate. Alfa atomic absorption standards were used in some cases.

Procedure. Samples of NBS standard glasses SRM 91 and 93a, weighing 0.2 g each, were prepared by fusion with 1.2 g of sodium hydroxide in nickel crucibles for 30 min at 500°C, dissolution of the melt in deionized water, followed by filtration and dilution to an appropriate volume. Diluted samples of NBS SRM 91 were pretreated by passing 5 ml through a Bio-Rad AG-50N-X8 cation-exchange cartridge. Plating-bath samples were prepared by dilution to an appropriate volume with deionized water. Appropriate standards were prepared for each sample. Data for calibration and quantitation were obtained by measurement of peak heights. Background corrections were made using results obtained for blanks.

Results and discussion

Formulation of eluents. Sodium hydroxide can be used as eluent for the separation of ions such as silicate, borate, and fluoride, but used alone, hydroxide is too weak a displacing agent to be generally useful with the

Wescan anion/R column, as stated by the manufacturer. Application is extended to more strongly retained ions by the addition of reagents such as sodium benzoate, *p*-hydroxybenzoic acid, or sodium tartrate which exhibit greater displacing power. These formulations are advantageous for achieving practical retention times for more strongly retained anions as well as improving peak shape. Eluents containing sodium hydroxide (0.6 g l^{-1}) and small concentrations (e.g., 1 mM) of either sodium benzoate or *p*-hydroxybenzoic acid can be used for the resolution of simple and complex mixtures containing anions such as silicate, borate, germanate, fluoride, and chloride (Fig. 1). Improved peak shape for anions such as germanate and arsenite can be achieved by increasing the concentration of tartrate or benzoate, at the expense of resolution of silicate, fluoride and borate which elute even more rapidly under such conditions. Sodium citrate and sodium oxalate are also useful eluent components. Strong acid anions such as phosphate and chloride have longer retention times for a given set of operating conditions. Sulfate exhibits a particularly strong affinity for the column, requiring cleaning with a sodium benzoate solution (5 mM) after repeated injections of sulfate-containing samples such as the Sel-Rex BDT-200 gold plating bath.

The sensitivity of detection of the weak acid anions in single-column ion chromatography is improved to within 100—10 μg l^{-1} by increasing the sample size and adjusting the sensitivity range of the detector. Silicate and hypochlorite in high-purity water are detectable at levels of 20 and 5 μg l^{-1}, respectively, using a sodium hydroxide eluent [12].

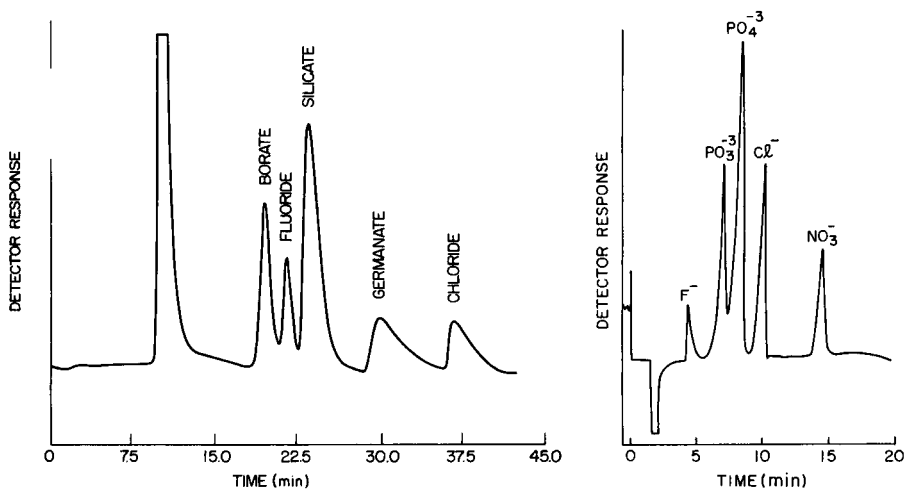

Fig. 1. Chromatogram of 10 mg l^{-1} boron, 10 mg l^{-1} fluoride, 70 mg l^{-1} silicon, 80 mg l^{-1} germanium, and 20 mg l^{-1} chloride (0.6 g l^{-1} NaOH; 2.5 × 10^{-5} M sodium benzoate, 0.5 ml min^{-1}; 100 μmho sensitivity).

Fig. 2. Chromatogram of 40 mg l^{-1} fluoride, 40 mg l^{-1} phosphite, 40 mg l^{-1} phosphate, 80 mg l^{-1} chloride and 80 mg l^{-1} nitrate (2 mM phthalic acid eluent, 0.5 ml min^{-1}; 100 μmho sensitivity).

Phthalic acid, an eluent recommended for use with silica-based anion separation columns, can also be used with resin-based columns (Fig. 2). The weaker oxy-acids are eluted rapidly and are not detected using the acidic eluent.

Optimization of sample preparation. Two commonly used procedures for the decomposition of glasses (i.e., fusion with alkali metal carbonates, and dissolution with hydrofluoric acid) present problems for subsequent steps in the proposed scheme. Carbonate may not be completely eliminated by the customary neutralization with hydrochloric or nitric acid. The neutralization step in turn introduces chloride or nitrate which could interfere in some determinations if not completely removed. Hydrofluoric acid, in addition to introducing fluoride and producing volatile substances which may result in loss of sample constituents, produces fluoro-anions in solution which undergo hydrolysis at different rates to produce a mixture of the original anion, fluoride, and the corresponding oxy-anion complicating determination of the sample constituents [13].

Fusion of glass samples with sodium hydroxide offers an alternative decomposition procedure with the advantages of a soluble melt closely matched to the sodium hydroxide eluent background, lower fusion temperatures and decreased sample loss relative to alkali carbonate fusion [8]. Advantages over hydrofluoric acid are obvious for the present purpose.

Applications. The boron content of NBS standard glass 93a, determined as B_2O_3, was 12.55 ± 0.18% compared to the standard value of 12.65% B_2O_3. Other characterizations of glasses by ion chromatography have dealt with the determination of boron and phosphorus in VLSI glasses [14] and boron in borosilicate glasses [15] using dual-column methods.

The proposed determination of fluoride in SRM 91 containing 5.73% F and 10.49% CaO required pretreatment of diluted samples by passing 5 ml through a cation-exchange cartridge to remove interfering calcium present in the original sample. Quantitation of fluoride in four samples gave a result of 5.59 ± 0.13%. By dual-column ion chromatography, the fluoride content was found to be 5.65 ± 0.06%. Low results may be attributed to residual calcium interference.

The Sel-Rex BDT-200 gold electroplating process utilizes added arsenic(III) to maintain a desirable grain size for the deposit. A procedure is required to monitor arsenic(III) so as to indicate when arsenic(III) should be replenished in the bath. Figure 3 illustrates the resolution of arsenite and a considerable concentration of accumulated arsenate in the used bath. These species have customarily been resolved and detected by using conductometric anion-exclusion chromatography of arsenate with amperometric detection of arsenite [10], or following oxidation of arsenite to arsenate [11]. The use of anion-exchange resins and alkaline eluents overcomes the large difference in strength of arsenic and arsenious acid and promotes dissociation of the weaker acid to make possible simultaneous conductometric detection of both oxidation states. A relatively inexpensive single-column ion-chromatographic

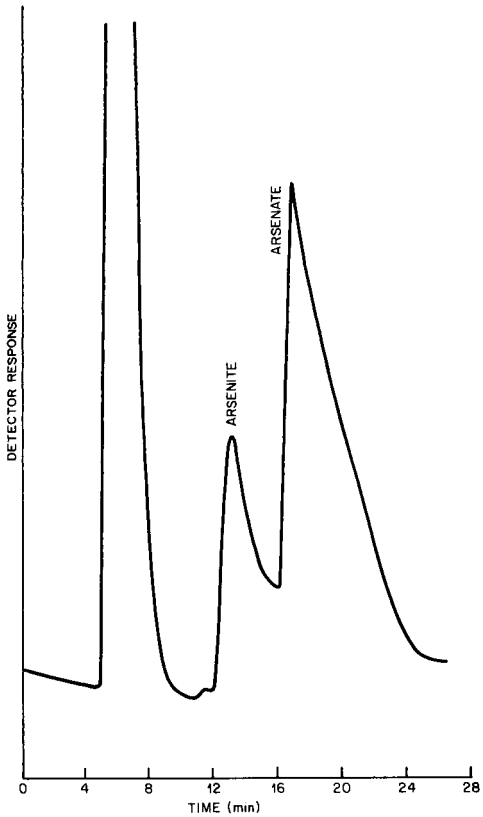

Fig. 3. Chromatogram of a Sel-Rex BDT-200 plating bath (0.5 ml/100 ml dilution; 0.6 g l^{-1} NaOH, 1 mM sodium tartrate, 0.2 ml min^{-1}; 100 μmho sensitivity).

apparatus might be used to monitor the bath. The capability for speciation of oxidation states extends to other oxy-anion systems such as tellurate and tellurite. Speciation of oxidation states by single-column and dual-column ion chromatography is important to the characterization of process solutions, particularly plating baths.

REFERENCES

1 J. S. Fritz, D. T. Gjerde and C. Pohlandt, Ion Chromatography, Huthig Verlag, New York, 1982.
2 F. C. Smith and R. C. Chang, The Practice of Ion Chromatography, Wiley, New York, 1982; C.R.C. Crit. Rev., Anal. Chem., 9 (1980) 197.
3 D. T. Gjerde, J. S. Fritz and G. Schumacher, J. Chromatogr., 186 (1979) 509.
4 S. A. Wilson, E. S. Yeung and D. R. Bobbitt, Anal. Chem., 56 (1984) 1457.
5 C. J. Hill and R. P. Lash, Can. Res., 13 (1980) 53.
6 D. R. Eubanks, L. Avgers and A. W. Fritchett, Paper presented at 25th Rocky Mountain Conf. on Anal. Chem., Denver, Colorado, 1983.

7 F. D. Snell and L. S. Ettre, Ed., Encyclopedia of Industrial Chemical Analysis, Vol. 13, Glass and Glass-Ceramics, Interscience, New York, 1971.
8 R. Bock, A Handbook of Decomposition Methods in Analytical Chemistry, Wiley, New York, 1979.
9 J. Dolezal, P. Povondra and Z. Sulcek, Decomposition Techniques in Inorganic Analysis, Elsevier, Amsterdam, 1966, p. 91.
10 Dionex Corp., Electrochemical Detector, Sunnyvale, California, February 1981.
11 L. D. Hansen, B. E. Richter, D. K. Rollins, J. D. Lamb and D. J. Eatough, Anal. Chem., 51 (1979) 633.
12 C. McCrory-Joy, Paper presented at Pittsburgh Conference, New Orleans, 1985.
13 A. M. Bond and G. T. Hefter (Eds.), International Union of Pure and Applied Chemistry, Chemical Data Series No. 27, Critical Survey of Stability Constants and Related Thermodynamic Data of Fluoride Complexes in Aqueous Solution, Part A, Pergamon Press, Oxford, 1980.
14 J. E. Tong, K. Schertenbeib and R. A. Carpio, Solid State Technology, Jan. (1984) 161.
15 J. G. Smith, in W. S. Lyon (Ed.), Anal. Chem. Nucl. Technol., Proc. Conf. Anal. Chem. Energy Technol. 25th, Meeting Date 1981, 63-7, Ann Arbor Sci., Ann Arbor, MI, 1981.

Analytica Chimica Acta, 181 (1986) 283—285
Elsevier Science Publishers B.V., Amsterdam — Printed in The Netherlands

Short Communication

A SIMPLE INJECTION VALVE FOR FLOW INJECTION ANALYSIS

J. R. CHIPPERFIELD and P. J. WORSFOLD*
Department of Chemistry, University of Hull, Hull HU6 7RX (Great Britain)
(Received August 6th 1985)

Summary. A novel sample introduction valve, based on a modified glass syringe, is described for flow injection analysis. Sample volumes of 1.4 μl or more can be injected manually or automatically, by driving with a 12-V solenoid. The valve has advantages of freedom from maintenance and long lifetime.

One of the fundamental aspects of flow injection analysis is the reproducible introduction of a fixed volume of sample into a continuously flowing carrier stream [1]. The commercial systems currently available, and indeed most purpose-built manifolds, use some form of rotary PTFE injection valve which is prone to wear. Alternative non-valve sample introduction techniques include direct aspiration of the sample [2] and hydrodynamic injection [3]. This communication describes an alternative valve design based on a syringe with ground-glass contact, which is easy to operate automatically and has excellent wear characteristics.

Experimental

Injection valve design. The valve was constructed from a Segma 1-ml interchangeable all-glass syringe (Fig. 1). The syringe piston has a 0.5-mm hole, A, drilled through it, and two 10 mm × 1 mm × 1 mm slots, B and C, cut in it (Fig. 2a). The barrel has six 1.0 mm holes (D—I) drilled in it. PTFE tubes (0.5 mm i.d.) are glued to the barrel with epoxy cement (Fig. 2b), and the whole barrel and tubes are encased in EM306PA embedding resin (Trylon, Thrift St., Wollaston, Northants, NN9 7QJ). A sketch of the assembled valve is shown in Fig. 3. The piston is moved between its two positions by a 12 V solenoid (RS 349-709), and a peg, J, moving in slot K prevents piston rotation. In position 1, the main liquid stream passes in through G, along A and out through F, while the sample loop between H and E can be loaded (in through I, along C, out via H to loop, back via E, along B and out through D). In position 2, the flow goes in through G, along C, out through H to the sample loop, back through E, along B and out through F.

Flow-injection manifold. The valve was fitted with a 100-μl sample loop and incorporated in a single-line manifold. A carrier stream of distilled water was pumped through PVC pump tubing at 1.4 ml min^{-1} by a peristaltic pump (Ismatec Mini S-840). Plastic tubing (Tygon S-54-HL; 0.5 mm i.d.) was

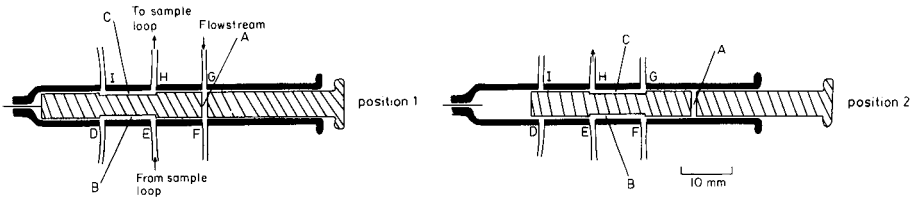

Fig. 1. Cross-section of the glass syringe-based injection valve showing the load (position 1) and inject (position 2) positions.

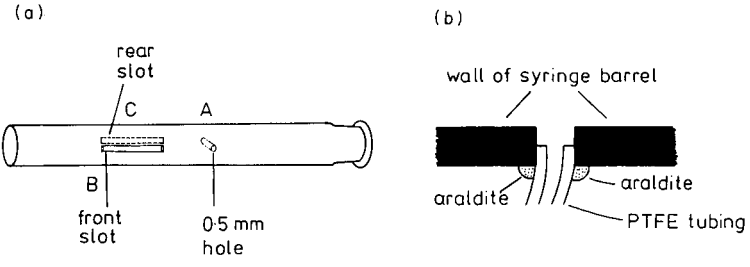

Fig. 2. (a) The syringe piston; (b) the PTFE tubing to glass syringe barrel connections.

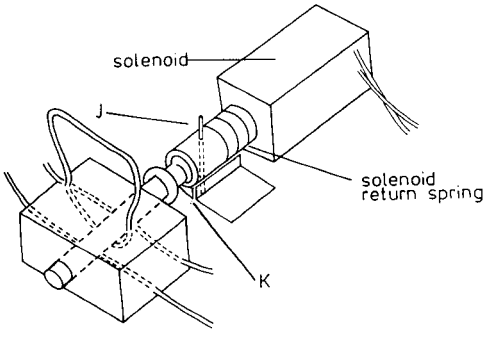

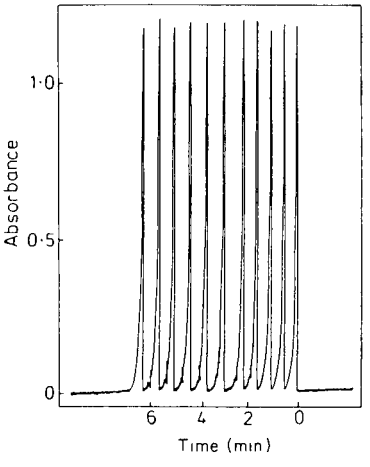

Fig. 3. The assembled injection valve.

Fig. 4. A typical detector response for repeated injections of a dye.

used throughout the remainder of the system; the distance from the injection valve to the detector was 30 cm. The detector was a single-beam spectrophotometer (Cecil CE-373), equipped with an 18-μl flow cell, set at 462 nm. A stock solution of methyl orange (0.06 g l^{-1}) was used for all injections.

Results and discussion

The detector response for eleven repeat injections of methyl orange is shown in Fig. 4. The valve was switched to the load position when the detector signal had returned to 5% of the maximum signal, and the next sample was injected when the signal returned to 1% of the maximum. The relative standard deviation on the peak height at a sampling rate of 90 h^{-1} was 1.0% for eleven injections. The spikes at the base of each peak are electrical noise from the valve returning to the load position and could be removed by appropriate shielding. The dispersion of the manifold at this stage was found to be 2.9. This was changed to 4.9 by increasing the length of the mixing coil; for nine repeated injections the relative standard deviation was again 1.0%.

The key feature of the injection valve is the ground-glass contact between the syringe piston and the syringe barrel. With a small amount of lubrication (e.g., a water film) the contact provides a low-friction, leak-free seal. The load/inject action therefore requires very little torque and the valve can be driven by a 12-V solenoid which can be activated manually, or automatically via a microcomputer. One of the limitations to the increased use of flow injection analysers for high sample throughput is the wearing of PTFE rotary injection valves, but the use of a glass-to-glass joint provides a maintenance-free alternative with a long lifetime. The valve is easy to construct from readily available glass syringes and the concept can be extended to more complex valve designs, e.g., multiple injection and merging zones, simply by drilling more holes and grooves in the required length of the ground-glass rod. The design can also accommodate variable sample volumes, and the smallest sample size (1.4 μl in this case) is limited only by the diameter of the internal ground-glass rod.

The authors are indebted to Mr. M. Bailey and Miss M. Shanaa for technical assistance.

REFERENCES

1 J. Růžička and E. H. Hansen, Flow Injection Analysis, Wiley, New York, 1981.
2 C. Riley, L. H. Aslett, B. F. Rocks, R. Sherwood, J. D. M. Watson and J. Morgon, Clin. Chem., 29 (1983) 332.
3 J. Růžička and E. H. Hansen, Anal. Chim. Acta, 145 (1983) 1.

Analytica Chimica Acta, 181 (1986) 287—291
Elsevier Science Publishers B.V., Amsterdam — Printed in The Netherlands

Short Communication

THE RESOLUTION OF OVERLAPPING CHROMATOGRAPHIC PEAKS BY EVOLVING FACTOR ANALYSIS

MARCEL MAEDER* and ANDREAS D. ZUBERBUEHLER

Institute of Inorganic Chemistry, University of Basel, Spitalstrasse 51, 4056 Basel (Switzerland)

(Received 29th October 1985)

Summary. A completely model-free method for the resolution of overlapping chromatographic peaks is presented. Evolving factor analysis enhances the power of classical factor analysis by exploiting the additional information contained in the response data through the intrinsic order of the elution time. The results are the elution profiles and the normalized spectra of the components.

There is a very high probability of overlapping peaks in a real chromatogram [1] and this problem is of more or less universal concern in the practice of analytical separations [2]. There are two possible ways of overcoming the problem: either the resolution can be improved by optimizing the chromatographic parameters (e.g., by extending the length of the column) or the overlapping peaks can be deconvoluted by the means of a software approach [3]. A method of the second type is proposed here. The method is capable of deconvoluting severely overlapping chromatographic peaks without any assumptions concerning the elution profile or response. The only requirement is a multidimensional detection system such as F.t.i.r., mass or u.v.-visible spectrometry [4], instruments which are readily available in the modern analytical laboratory. The method, for which the term Evolving Factor Analysis (e.f.a.) is appropriate, is based on factor analysis [5] and makes exhaustive use of the additional information contained in the data set through the ordered nature of the data matrix.

Completely model-free, e.f.a. avoids all difficulties associated with the selection of a satisfactory, but never perfect, peak-shape function in attempts to achieve a nonlinear least-squares fit of the data [6]. The only assumption concerning elution profile or absorption spectrum is the non-negativity of the concentrations. Self-modelling curve resolution, the only other model-free approach, is based on factor analysis and the positiveness of the absorptivities but is basically restricted to two-component systems [7]. The method found application in different fields [8, 9] but its extension to systems with three and more components is hampered by the necessity of additional assumptions such as maximum disparity [10] or minimum envelope [11] of the calculated spectra.

In a multiwavelength chromatogram across an overlapping peak of s com-

0003-2670/86/$03.50

ponents, n spectra are measured at w wavelengths as a function of the elution time. They are arranged row by row into a $n \times w$ data matrix **Y**. In the cases where the Beer-Lambert law holds (i.r. spectra have to be evaluated as absorption spectra), **Y** can be expressed as $\mathbf{Y} = \mathbf{C}\,\mathbf{A}$, where $\mathbf{C}(n \times s)$ is formed by the concentration profiles of the s components and $\mathbf{A}$ $(s \times w)$ contains their individual absorption spectra. In classical factor analysis, the unknown number s of components or factors of **Y** is calculated as the number of nonzero eigenvalues of the second moment matrix $\mathbf{M} = \mathbf{Y}^t\,\mathbf{Y}$ [5, 12].

In a chromatogram, however, the spectra are recorded in the fixed sequence of progressing elution. The intrinsic order in which the rows of **Y** are arranged contains information which is not exploited in traditional factor analysis. In the new approach, factor analysis is applied in succession to the submatrices $\mathbf{Y}_i$ formed by the first $1,2,..,i,..n$ spectra by calculating the eigenvalues of $\mathbf{M}_i = \mathbf{Y}_i^t\,\mathbf{Y}_i$. These are plotted subsequently in an e.f.a. plot as a function of the elution time (Fig. 1). With the elution of a new absorbing species, a new significant eigenvalue evolves concomitantly and therefore is easily detected and the total number of components is also an obvious result.

Naturally, the ith eigenvalue is not a direct measure of the concentration of the ith species. The eigenvalues are strongly dependent on the dissimilarity of the absorption spectra and the elution profiles. Nevertheless, Fig. 1 clearly shows the appearance of new species at the times 10, 15 and 20. These values compare well with the rise of the concentration profiles used to generate the model data (the dotted lines in Fig. 3).

It is straightforward to repeat the e.f.a. calculation from the opposite end

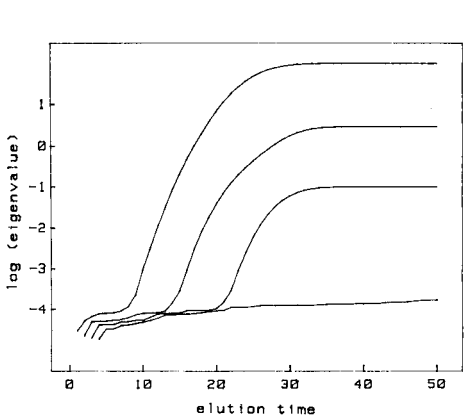

Fig. 1. Logarithmic plot of the evolving eigenvalues (factors) as function of the elution time.

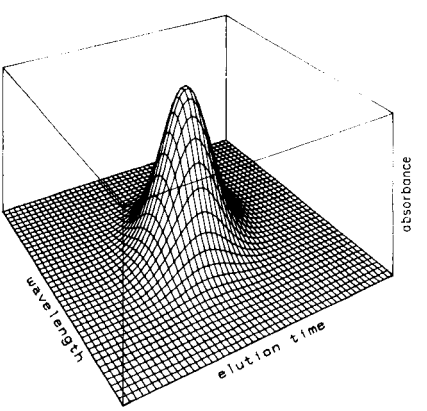

Fig. 2. Perspective projection of the model chromatogram, showing no sign of overlapping bands.

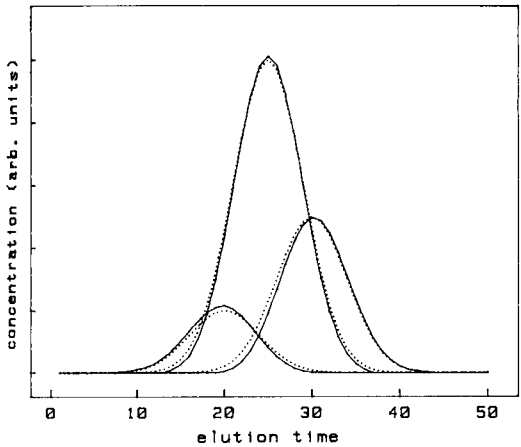

Fig. 3. Concentration profiles: (——) the result of the e.f.a. calculation; (· · · ·) the underlying model data.

by analyzing the submatrices formed by the last 1,2,... n spectra. These plots show the disappearance of the eluted species. Connecting the rising part of the ith forward curve with the falling part of the $(s + 1 - i)$th backward curve results in a rough estimate of the concentration profile of the ith component of the overlapping peak, as in primary e.f.a. which was introduced for spectrophotometric titrations [13]. All s resulting curves are arranged into the columns of the concentration matrix **C**. An iterative process is then started by calculation of the least-squares estimate **A** of the absorption spectra by a simple linear regression

$$\mathbf{A} = (\mathbf{C}^t\,\mathbf{C})^{-1}\,\mathbf{C}^t\,\mathbf{Y} \qquad (1)$$

The resulting absorption spectra are normalized; there is obviously no way of getting absolute concentrations without any knowledge of the absorptivities. Then a new concentration matrix **C** is computed by

$$\mathbf{C} = \mathbf{Y}\,\mathbf{A}^t\,(\mathbf{A}\,\mathbf{A}^t)^{-1} \qquad (2)$$

which in turn yields a new **A** by Eqn. 1 and so on. This iterative procedure converges to excellent fits if two precautions are taken: all elements of the concentration matrix **C** in the region where the primary e.f.a. results do not differ significantly from zero as well as all negative elements are set to zero in each iterative cycle.

To demonstrate the practicability of e.f.a., several chromatograms were constructed with highly overlapping elution profiles and absorption spectra. A three-component model calculation (from high-performance liquid chromatography with u.v.-visible detection) is discussed here. The resulting chromatogram was completed with a random error of 0.001 absorbance (Fig. 2). Visual inspection shows no shoulder or any other obvious sign of overlapping peaks but the fully automatic e.f.a. calculation yields con-

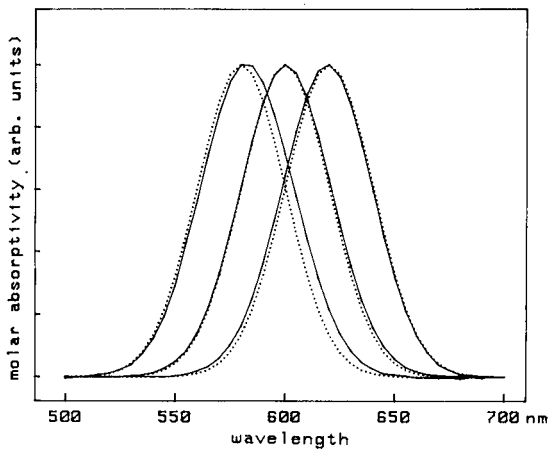

Fig. 4. Absorption spectra based on molar absorptivities: (——) e.f.a.; (· · ·) model data.

centration profiles and absorption spectra (the full lines in Figs. 3 and 4), which fit almost exactly the underlying model data (the dotted lines in Figs. 3 and 4). Both concentration and absorption maxima are very close, and the shapes are only marginally distorted. These model data were generated with severely overlapping Gaussians for both concentrations and spectra; in real cases, the spectra are usually much less similar. The calculations were done on a HP 9000/216 desk computer. Program listings in BASIC are available on request.

Evolving factor analysis achieves a completely model-free deconvolution of overlapping chromatographic peaks. There are no fundamental restrictions about the number of components. The challenge expressed by Delaney [3] is fully met: "The ultimate goal of curve resolution would be to be able to determine the number of components in an overlapping chromatographic peak as well as the spectrum and concentration profile of each compound, without assumptions regarding peak shape, location, or identity." Further, it should be mentioned that the use of evolving factor analysis is not restricted to chromatography. It will find use in all areas where factor analysis is applicable and some sort of specified order is contained in the data set.

This work was supported by the Swiss National Science Foundation, Grant No. 2.021-0.83.

REFERENCES

1 J. M. Davis and J. C. Giddings, Anal. Chem., 55 (1983) 418.
2 S. D. Frans, M. L. McConnell and J. M. Harris, Anal. Chem., 57 (1985) 1552.
3 M. F. Delaney, Anal. Chem., 56 (1984) 261R.
4 C. L. Wilkins, Science, 222 (1983) 291.
5 E. R. Malinowski and D. G. Howery, Factor Analysis in Chemistry, Wiley-Interscience, New York, 1980.

6 J. Grimalt, H. Iturriaga and X. Tomas, Anal. Chim. Acta, 139 (1982) 155.
7 W. H. Lawton and E. A. Sylvestre, Technometrics, 13 (1971) 617.
8 M. A. Sharaf and B. R. Kowalski, Anal. Chem., 54 (1982) 1291.
9 D. W. Osten and B. R. Kowalski, Anal. Chem., 56 (1984) 991.
10 A. Meister, Anal. Chim. Acta, 161 (1984) 149.
11 B. Vandeginste, R. Essers, T. Bosman, J. Reijnen and G. Kateman, Anal. Chem., 57 (1985) 971.
12 E. R. Malinowski, Anal. Chem., 49 (1977) 606, 612.
13 H. Gampp, M. Maeder, C. J. Meyer and A. D. Zuberbühler, Talanta, 32 (1985) 1133.

Analytica Chimica Acta, 181 (1986) 293—296
Elsevier Science Publishers B'V., Amsterdam — Printed in The Nethrlands

Book Reviews

Maximum Concentrations at the Workplace and Biological Tolerance Values for Working Materials 1983. Verlag Chemie, Weinheim, 1983, xi + 75 pp. Price DM 20.

This Report No. XIX of the Commission for the Investigation of Health Hazards of Chemical Compounds in the Work Area supersedes all previous reports of the Commission, and provides a useful collection of tolerance values and hazard warnings. There is an extensive tabulation (34 pp.) of MAK (maximum allowable concentration values) arranged aphabetically, with indication of sampling frequency, cutaneous absorption, sensitization and vapour pressure, as well as a list of substances for which MAK values have not yet been established. There are also lists of carcinogens, those proven carcinogenic to humans, those proven carcinogenic only in animal experiments, and suspected carcinogens, with some Technical Guiding Concentrations (TRK). Dusts and special materials such as peroxides and gasoline are discussed, and some Biological Tolerance Values (BAT) are also given. The book concludes with 11 pages of additions to the main tabulated material. The booklet provides a clear and concise description of the essential features of tolerance limits, and the tabulated material will be of great value to those charged in ensuring a safe working environment.

A. Townshend

D. Brune, B. Forkman and B. Persson, *Nuclear Analytical Chemistry.* Chartwell-Bratt Ltd., Bromley, 1984, 556 pp. Price £24.60.

This book is divided into four sections. Section A deals with the fundamentals of nuclear processes, reactions, radiation sources and the interaction of radiation with matter. Section B discusses nuclear detectors, principles, electronic measurements, statistical methods and radiation detection methods. Part C, on p. 326, gets down to analytical matters with a review of activation analysis by neutrons, by charged particles and by photons. Part D deals with sample preparation and chemical separation, and some reviews of applications in biological and medical research, criminology, environmental science and geology. Finally some twenty pages are devoted to radiation protection.

The book appears to be a recent, careful review of the field. There is no discussion of alternatives to nuclear methods so there is a danger that the student will not realise that superior analytical methods exist. More worrying to the reviewer was the large number of minor errors and inconsistencies, typified by the first page of the book proper, p. 18. Here the comma is used

as a decimal point but in a following line the decimal point is used. There are also various unconventional mathematical symbols. In the section on electronics "cirquits" are described and there is a large number of similar typographical errors throughout the book. To a reviewer who had something of an intellectual steeplechase in trying to read the book, one compensation was the title for Fig. 3-13 "Giant resonance width as a function of A. P. Carlos et al., Nuclear Physics A219 (1974) 61".

Not to be recommended!

R. B. Moyes

Hans-Peter Angelé, *Dictionary of Chromatography*, 2nd edn. Hüthig, Heidelberg, 1984 (ISBN 3-7785-0926-8), 132 pp. Price DM 54, $27.

The terms, about 3500 in all, are first listed in alphabetical order of their English versions, with French, German and Russian translations alongside. Separate lists of the French, German and Russian words, in their respective alphabetical orders, refer the reader to the appropriate term in the master list. The terms include most, if not all, of those commonly encountered in the various types of chromatography, together with a host of others, many of which do not seem to have any particular chromatographic relevance (e.g., kinetics, labile, dithizone, inorganic salt, instrumental analysis, freeze drying, tap water, tear gas, to name but a few). Some curiosities were noted, such as froth fractionation instead of foam fractionation, chromometer or tintometer for the well-known comparator, and one doubts the usefulness of ancient terms such as caustic potash lye, and ethoxythane (diethyl ether)! Otherwise the book will be useful for all chromatographers and scientific editors.

A. Townshend

H. Wagner, S. Bladt and E. M. Zgainski, *Plant Drug Analysis: A Thin Layer Chromatography Atlas.* Springer-Verlag, Berlin, 1984 (ISBN 3-540-13195-7, ISBN 0-387-13195-7), xiv + 320 pp. Price DM 169, $63.10.

This is a brilliantly conceived and executed text which stands in direct line of descent from the first illustrated Herbals of medieval times, except in the present case the illustrations refer to visualisation of the chemical content of the plant extracts in order to identify or characterise the materials. The book is divided into 15 chapters, each relating to groups of drugs with common features, e.g., alkaloid drugs, coumarin drugs, flavanoid drugs, cardiac glycoside drugs. Each chapter follows a consistent format; extraction, thin layer chromatography, detection, list of drugs within the group, structural formulae of main constituents, colour photographs and discussion of chromatograms.

For most groups of compounds results are shown for a range of solvent systems and visualisation reagents. At the end of the book a system is described for the identification of an unknown plant drug. The whole book took over 10 years of photographic work to produce pictures that are representative and technically excellent. The book is of obvious value to pharmacists, drug importers and forensic analysts but is also or will be of interest and stimulation to natural product chemists. The reviewer's colleagues will confirm the immense pleasure the book has given him and them, and that it is much coveted as an almost infinite source of student projects apart from the visual beauty of the text itself.

D. Thorburn Burns

J. C. Touchstone and J. Sherma, *Techniques and Applications of Thin Layer Chromatography*. Wiley, New York, 1985 (ISBN 0-471-88017-5), xiv + 395 pp. Price £88.65.

This volume contains the papers presented at the "3rd Biennial Symposium on Thin Layer Chromatography" held in Parsippany, New Jersey in December 1982. Thus it is a Nell Gwynne "pot pouri" or Cromwellian "warts and all" publication dependent on your view of life; on balance it is the former as it provides a deal of interest and pleasant academic stimulation. The authorship is international and the topics wide ranging both on the technique itself and its applications. A deal of useful advice can be gleaned on stationary phases, modes of operation, optimisation, quantitative methods and applications which range from nitrite in saliva to Cephalosporium mutants. The book is well produced via camera-ready copy and hence it is overpriced particularly as the material is now at least 3 years old.

D. Thorburn Burns

G. A. Olah, G. K. S. Prakash and J. Sommer, *Superacids*. Wiley-Interscience, New York, 1985, xvi + 372 pp. Price £67.00.

Although many chemists consider concentrated sulphuric acid to be one of the strongest acids, in recent years still stronger acids have been discovered. These "Superacids" are defined as being better proton donors than 100% sulphuric acid, and include systems which are up to 10^{19} as strong as sulphuric acid. Examples of such superacids are H_2SO_4/SO_3 and HSO_3F/SbF_5, the latter known as "magic acid". Use of superacids as solvents makes it possible to study ions which would not be stable in other, less acidic, media. Compounds such as alkanes, which are usually unreactive, can undergo reactions such as alkylation and carboxylation in superacid solvents. The list of chapter headings "Superacid systems", "Carbocations in Superacids", "Heterocations in

Superacids" and "Superacid Catalysed Reactions" shows the scope of the subject. In this book there is no separate discussion of analytical applications of superacids, but spectroscopic techniques, principally n.m.r., but also i.r., Raman and e.s.c.a., are used in the characterisation of chemical species in superacids.

Professor Olah and his coworkers have been leaders in this field for many years and this thorough account is written from first-hand knowledge. It should quickly become a standard reference work for this area of chemistry.

J. R. Chipperfield

K. Beyermann, *Organic Trace Analysis.* Horwood, Chichester, 1984 (ISBN 0-85312-638-0), 365 pp. Price £35.00.

This is another monograph in the Ellis Horwood series in Analytical Chemistry edited by R. A. Chalmers and M. Masson and is a translation and update of the original 1982 German language text. The aim of the book is to introduce the reader to all aspects of trace organic analysis, from general and statistical matters, through sampling, sample storage and sample pretreatment (separation and concentration), to instrumental methods and special topics. The breadth of material presented means that some areas, e.g., statistical methods, luminescence techniques and the use of biochemical reagents, are only superficially covered, but the book contains many comprehensive and up to date tables summarising the most important information and cites nearly three thousand references. It therefore serves as a very useful primary source for all aspects of trace organic analysis. The chapter on separation methods and concentration steps is a particularly informative one for the practising analytical chemist dealing with trace organic analysis of water, air or biological samples.

This is a timely publication in the light of current awareness of environmental and health problems associated with trace levels of organic compounds, because this is ultimately reflected by legislation, which in turn necessitates analytical investigation. On balance, the total analytical approach of the text is a successful one and the lack of detail is more than compensated for by the exhaustive tables and reference list.

P. J. Worsfold

Analytica Chimica Acta, 181 (1986) 297
Elsevier Science Publishers B.V., Amsterdam — Printed in the Netherlands

Erratum

J. J. Harrow and J. Janata, Heterogeneous Samples in Flow-Injection Systems. Part 2. Standard Addition.

Anal. Chim. Acta, 174 (1985) 123—132.

The section "Note Added in Proof" should read:

Gran plot in f.i.a. In the original paper the concentration of analyte in the carrier stream has been ignored which has resulted in a propagating error in Eqns. 3—7 and 12. The correct derivation is given below.

The potential of an electrode in dispersed (D) sample of initial concentration, C_0, is

$$E = E^0 + S \log [n_0 + (D-1)V_0C_C]/[V_0 + (D-1)V_0] \quad (1)$$

where $(D-1)V_0$ is the volume added due to dispersion and C_C is the concentration of the analyte in the carrier stream. When a volume, V_A, of the standard addition solution containing n_A moles of analyte is added, the final potential after dispersion is

$$E' = E^0 + S \log [n_0 + n_A + (D-1)V_0C_C]/(V_0D + V_A) \quad (2)$$

Equation 1 is subtracted from Eqn. 2 and the result is expressed in exponential form yielding

$$10^{(E-E')/S} = \Omega = \frac{[V_0C_0 + (D-1)V_0C_C + Q_At_AC_A]V_0D}{(V_0D + Q_At_A)[V_0C_0 + (D-1)V_0C_C]} \quad (3)$$

Because $D \geqslant 1$ and V_A is small compared to V_0, $(Q_At_A \ll V_0D)$,

$$\Omega = 1 + Q_At_AC_A/[V_0C_0 + (D-1)V_0C_C] \quad (4)$$

For $\Omega = 0$ at t_A^0,

$$C_0 = -[Q_At_A^0C_A + (D-1)V_0C_C]/V_0 \quad (5)$$

which is the correct form of Eqn. 7 in the original paper.

In the presence of hematocrit (volume fraction h), Eqn. (5) becomes

$$C_0 = -[Q_At_A^0C_A + (D-1)(1-h)V_0C_C]/(1-h)V_0 \quad (6)$$

which is the correct form of Eqn. 12 in the original paper.

0003-2670/86/$03.50

Analytica Chimica Acta, 181 (1986) 298
Elsevier Science Publishers B.V., Amsterdam — Printed in The Netherlands

Corrigendum

K. Ohshita, H. Wada and G. Nakagawa, Synthesis of Bidentate Pyridylazo and Thiazoylazo Reagents and the Spectrophotometric Determination of Copper in a Flow-Injection System.

Anal. Chim. Acta, 176 (1985) 41—60.

The last paragraph on p. 48 should read:

The results (0.94 mg l^{-1} for S_1, 1.12 mg l^{-1} for S_2) shown in Fig. 6 were in good agreement with the certified values (0.93 ± 0.10 mg l^{-1} for S_1, 1.24 ± 0.19 mg l^{-1} for S_2). A sample throughput of 60 h^{-1} was possible.

0003-2670/86/$03.50

Analytica Chimica Acta, 181 (1986) 299—300
Elsevier Science Publishers B.V., Amsterdam — Printed in The Netherlands

Announcement

IIND INTERNATIONAL SYMPOSIUM ON QUANTITATIVE LUMINESCENCE SPECTROMETRY IN BIOMEDICAL SCIENCES

An international symposium on quantitative luminescence spectrometry in biomedical sciences, sponsored by the Faculty of Pharmaceutical Sciences of the State University of Ghent, the National Foundation of Scientific Research (N.F.W.O.—F.N.R.S.), and the Ministry of Education, will be held in Ghent, Belgium, from Monday, 11th May to Thursday, 14th May 1987, at the Farmaceutisch Instituut.

The scope of the symposium will be similar to that of the first meeting held in Ghent, 1984, and will cover current research on all aspects of luminescence analysis.

The scientific program will consist of plenary and invited lectures, submitted research papers and posters.

Six plenary lectures will be presented by outstanding specialists in the field of quantitative luminescence spectrometry: U. A. Brinkman (Free University of Amsterdam): luminescence detection in HPLC; L. J. Cline Love (Seton Hall University, New Jersey): luminescence in micellar and cyclodextrin media; J. C. Hummelen (State University of Groningen): thermochemiluminescence techniques; L. J. Kricka (Queen Elisabeth Medical Centre, Birmingham): chemiluminescence enzyme immunoassays; S. G. Schulman (University of Florida): fluorescence techniques; O. S. Wolfbeis (Karl-Franzens University, Graz): fiber optical sensors.

Contributed papers (20 minute lectures or poster communications) will cover the following topics: drug and bioanalysis via fluorescence and phosphorescence (LTP, RTP, micellar); fluorescence and chemiluminescence immunoassays; detection techniques in chromatography (fluorescence, RTPL, ...); solid surface luminescence methods; thermochemiluminescence techniques; chemical derivatization methods; use of fluorescence labels; luminescence applications and drug metabolism, clinical chemistry, biochemistry, pharmacokinetics, toxicology, ecology, protein tagging.

The Conference language will be English. There will be an exhibition of commercial instruments for luminescence analysis.

As with the earlier symposium, the Proceedings will be published in a special issue of Analytica Chimica Acta (Editor Dr. A. M. G. Macdonald, Birmingham). Information for authors will be provided in later announcements. Authors who wish to present papers (oral or poster) should submit abstracts before 31st December, 1986.

The symposium registration fee will be about US $110 or 5.500 BF. This fee includes a copy of the final program, an abstracts volume; a copy of the Proceedings; part of the social events and refreshments during the breaks. Wagons-Lits Tours, Cantersteen 41, B-1000-Brussels has been appointed the Official Travel Agent.

All correspondence should be sent to:

DR. W. BAEYENS (Symposium Chairman)
Laboratory of Pharmaceutical Chemistry and Drug Analysis
State University of Ghent
Harelbekestraat 72
B-9000-Ghent
(Belgium)

ANALYTICA CHIMICA ACTA, VOL. 181 (1986)

AUTHOR INDEX

ACA announcements

ANNOUNCEMENTS OF MEETINGS

3rd SYMPOSIUM ON HANDLING OF ENVIRONMENTAL AND BIOLOGICAL SAMPLES IN CHROMATOGRAPHY, PALMA DE MALLORCA, SPAIN, OCTOBER 8–10, 1986

The organisation of this third event – the first was held in Lausanne, Switzerland in November 1983, the second in Freiburg, F.R.G., in October 1985 – is in hands of the International Association of Environmental Analytical Chemistry and the University of Palma de Mallorca and sponsored by national bodies. A strong industrial participation is planned. It is the intention to bring together specialists in this field who can give a good account of the state-of-art in their respective specialty and to present first-hand experience in sample handling. Robotics, continuous flow extraction techniques, solid surface sample handling with pre-column technology (on-line and off-line) pre-chromatographic use of derivatization techniques, colum switching methodology for handling of complex samples are some of the topics that will be treated and extensively discussed. Special emphasis will be placed on techniques with automation potential and actually automated procedures suitable for routine handling of larger series of samples. Much of this methodology and "philosophy" can be applied to different types of matrices and problem solving but it is the intention to concentrate on applications to biological (urine, blood, tissue, plant material) and environmental samples (water, waste water, air) with drugs (pharmaceuticals) and priority pollutants as the analytes.

For further information and for submission of contributions contact: Prof. Dr. R.W. Frei, Department of Analytical Chemistry, Free University, De Boelelaan 1083, 1081 HV Amsterdam, The Netherlands. Tel.: (020) 5485379.

4th SYMPOSIUM ON LC–MS AND MS–MS, MONTREUX, SWITZERLAND, OCTOBER 22–24, 1986

This symposium will feature invited and contributed lectures and posters on the latest developments in this field. Fundamental, instrumental and application papers will be considered. Panel discussions will deal with various parts of LC–MS, SFC–MS and MS–MS coupling.

An instrument exhibition is planned and proceedings of the workshop will be published as a special issue in the *Journal of Chromatography*. The symposium will be preceded by a 2-day short course (lecturers Dr. Dai Games and Dr. Jack Henion).

For further information and for submission of contributions contact: Prof. Dr. R.W. Frei, Department of Analytical Chemistry, Free University, De Boelelaan 1083, 1081 HV Amsterdam, The Netherlands. Tel.: (020) 5485379.

HPLC '87, 11th INTERNATIONAL SYMPOSIUM ON COLUMN LIQUID CHROMATOGRAPHY, AMSTERDAM, THE NETHERLANDS, JUNE 28–JULY 4, 1987

HPLC '87 will be held at the International Congress Centre RAI, Amsterdam, The Netherlands, from June 28–July 4, 1987.

The symposium will cover all fundamental aspects, instrumental developments and applications of column liquid chromatography (HPLC) and related methods such as field flow fractionation, supercritical fluid chromatography and column electrophoresis. Special attention will be given to: automated sample preparation, chromatography–spectrometry combination, computerized optimiza-

tion, derivatization, enantiomer separations, ion chromatography, miniaturization, preparative LC, separation of biopolymers. The symposium language will be English.

The symposium will be held in Amsterdam at the International Congress Centre RAI which conference centre is easily accessible by air, rail and road and has an efficient public transport to the centre of the city. Hotels and a park are within walking distance. A full social programme will be included.

Further information and full details of the symposium can be obtained from: Organisatie Bureau Amsterdam bv, Europaplein, 1078 GZ Amsterdam, The Netherlands. Tel.: (31) 20-44 08 07, telex: 13499 raico nl.

31st IUPAC CONGRESS, SOFIA, BULGARIA, JULY 13–18, 1987

The Organizing Committee of the 31st International Congress of Pure and Applied Chemistry has the honour of announcing that the 31st IUPAC Congress will be held on July 13–18, 1987 in Sofia at the National Palace of Culture. The Bulgarian Academy of Sciences will be responsible for the organization of the congress.

The scientific programme will include the following topics on analytical chemistry: new theoretical developments, new instrumentation and techniques in electroanalytical chemistry, automation, application of microcomputers, solubility, biotechnology, medicinal, pharmaceutical, food and environmental analysis, microchemical and trace analysis, etc.

Other sections will deal with: education, engineering chemistry, industrial chemistry, inorganic chemistry, organic chemistry, physical chemistry, polymers and clinical chemistry.

Further details are available from the Secretariat, c/o Dr. R. Vlahov, Institute of Organic Chemistry, Bulgarian Academy of Sciences, 1113 Sofia, Bulgaria. Telex: 22729 ECHBAN BG.

EUROANALYSIS VI, EUROPEAN CONFERENCE ON ANALYTICAL CHEMISTRY, PARIS, FRANCE, SEPTEMBER 7–11, 1987

On behalf of the Working Party on Analytical Chemistry (WPAC) of the Federation of European Chemical Societies (FECS) the Presidium of EUROANALYSIS VI and the French organizing societies invite you to attend, to make oral or poster contributions to the conference, to display instruments, products, or books, on the exhibition stands at EUROANALYSIS VI. The French organizing societies include: Groupement pour l'Avancement des Méthodes Spectroscopiques et Physico-chimiques d'Analyse (G.A.M.S.), Société Française de Chimie (S.F.C.), Groupe d'ingénierie analytique de la Société de Chimie Industrielle (S.C.I.), Société Française de Métallurgie (S.F.M.), with cooperation from l'Association Technique de la Sidérurgie (A.T.S.), and the sponsorship of Comité Français de Chimie.

EUROANALYSIS conferences cover all aspects of analytical sciences. In Paris emphasis will be on the most modern techniques and advances, with the aim of demonstrating their possibilities to the widest audience. Lectures will be given on the use of lasers in analytical techniques, electrochemical detectors, ion equilibria for ion chromatography, atomic spectroscopy, trace analysis of organic mixtures, chemometrics, ultraclean laboratories, etc. Special sessions are planned on: the use and construction of analytical probes; applications of analytical methods for solving environmental problems; analysis of solid state samples; new methods of teaching analytical subjects.

The conference will consist of invited plenary and keynote lectures and contributed papers presented orally or as posters. Detailed instructions will be sent to participants wishing to contribute with the second circular (fall 1986), which will also provide details of Social Events, Visits and Excursions.

For further information, contact: G.A.M.S., 88 Boulevard Malesherbes, 75008 Paris, France.

ACCURACY IN TRACE ANALYSIS – ACCOMPLISHMENTS, GOALS, CHALLENGES, GAITHERSBURG, MD, U.S.A., SEPTEMBER 28–OCTOBER 1, 1987

This symposium will focus on current trends in quantitative trace analytical chemistry and will provide perspectives on future challenges. The first day will be devoted to a plenary session that will review the history of quantitative trace analysis, the present situation from academic and industrial

viewpoints, and future directions. Key issues will be highlighted in individual talks. Topics will include the following: biomolecules in trace analysis, robotics, chemometrics, process analytical chemistry, expert systems, and reference materials for the future. The remainder of the symposium will consist of parallel sessions dealing with considerations of the measurement process; quantitation in environmental, clinical, and nutrient analyses; and advances in analytical techniques. Sessions directed to the measurement process will specifically consider industrial needs for quality assurance and efficient sample throughput.

For further information contact: Harry Hertz, A309 Chemistry Building, National Bureau of Standards, Gaithersburg, MD 20899, U.S.A. Tel.: (301) 921 2851.

FLOW ANALYSIS IV, AN INTERNATIONAL CONFERENCE ON FLOW ANALYSIS, LAS VEGAS, NV, U.S.A., APRIL 18–21, 1988

The 4th International Conference on Flow Analysis will be held in Las Vegas, NV, U.S.A., April 18–21, 1988. It will be organized by Dr. Gilbert Pacey, Department of Chemistry, Miami University, Oxford, OH 45056, U.S.A.

The scope of the conference will be similar to that of the Flow Analysis conferences held in Amsterdam, 1979, Lund, 1982, and Birmingham, 1985, and will cover current research on all aspects on continuous flow analysis. The topics will include: instrumentation for flow injection analysis and for continuous segmented and unsegmented flow analysis, including approaches to total automation; new detector systems and hybrid systems; theory of flow analysis; applications in the separation techniques of flow analysis; use of flow analysis in process control; use of flow analysis in electrochemical detection.

The scientific programme will consist of plenary and invited lectures, submitted research papers and posters, and working demonstrations. Authors who wish to present papers should submit abstracts before November 30, 1987. The conference language will be English. There will be an exhibition of commercial instrumentation for flow analysis.

As with the earlier conferences, the proceedings will be published in a special issue of *Analytica Chimica Acta*. Information for authors will be provided in later announcements.

The conference will be held in the beautiful Tropicana Resort Hotel in Las Vegas, NV, U.S.A. The conference registration fee will include meals, social events, and a copy of the Proceedings. For further information contact Dr. Gilbert E. Pacey, Department of Chemistry, Miami University, Oxford, OH 45056, U.S.A.

SCIENTIFIC SOFTWARE

SOFTWARE AVAILABLE FROM AUTHORS

A new section of this journal has started, which will give authors of computer programs the opportunity to announce software that they are willing to share with their colleagues. The aims of the section have been outlined in an Editorial (*Anal. Chim. Acta*, 173 (1985) 1). The programs offered will be listed in this section of the journal, as information becomes available.

Further details and forms for entry are available from Professor J.T. Clerc, Universität Bern, Pharmazeutisches Institut, Baltzerstrasse 5, CH-3102 Bern, Switzerland.

CALENDAR OF FORTHCOMING MEETINGS

May 18–23, 1986 San Francisco, CA, U.S.A.	**HPLC '86. New Frontiers in HPLC. 10th International Symposium on Column Liquid Chromatography** Contact: Ms. Shirley Schlessinger, 400 E. Randolph Drive, Chicago, IL 60601, U.S.A. (Further details published in Vol. 169.)

May 26–29, 1986 Lerici, Italy	**III CAC – Meeting of the Chemometrics Society** Contact: Prof. M. Forina, Istituto di Analisi e Tecnologie Farmaceutiche ed Alimentari, Via Brigata Salerno (ponte), I-16147 Genova, Italy. Tel.: (010) 3993656. (Further details published in Vol. 172.)
May 27–30, 1986 Brussels, Belgium	**2nd International Symposium on Drug Analysis** Contact: Mrs. C. van Kerchove, c/o Société Belge des Sciences Pharmaceutiques, Rue Stévinstraat 137, B-1040 Brussels, Belgium. Tel: (02) 230 26 85, ext. 33. (Further details published in Vol. 175.)
June 2–6, 1986 Raleigh, NC, U.S.A.	**1986 Joint Symposium on Dry Sulfur Dioxide and Simultaneous SO_2/NO_x Control Technologies** Contact: Jack H. Greene, Symposium Coordinator, MD-60, U.S. EPA, AEERL, Research Triangle Park, NC 27711, U.S.A. Tel.: (919) 541 2903, or J. Pekar, tel.: (919) 541 3995. (Further details published in Vol. 178, No. 2.)
June 3–6, 1986 Munich, F.R.G.	**Analytica 86, 10th International Trade Exhibition and 10th International Conference 'Biochemical Analytics'** Contact: Dr. Rosemarie Vogel, Nymphenburgerstrasse 70, D-8000 München 2, F.R.G.
June 10–12, 1986 Dublin, Ireland	**Electroanalysis na h'Eireann** Contact: Dr. Malcolm R. Smith, School of Chemical Sciences, National Institute for Higher Education, Glasnevin, Dublin 9, Ireland.
June 12–13, 1986 Gaithersburg, MD, U.S.A.	**25th Annual Technical Symposium of the Washington, D.C., Chapter of the Association for Computer Machinery and the National Bureau of Standards Distributed Information Systems: Emerging Uses and Technology** Contact: Wilma M. Osborne, B266 Technology Building, National Bureau of Standards, Gaithersburg, MD 20899, U.S.A. Tel.: (301) 921 3545.
June 16–18, 1986 Salt Lake, City, UT, U.S.A.	**1st Symposium on Pattern Recognition Methods in Analytical Spectroscopy** Contact: Melinda Van, Conference Secretariat, Biomaterials Profiling Center, University of Utah, Salt Lake City, UT, U.S.A. Tel.: (801) 581-8431, telex: GRAPHNET 3789459 UNIV UTAH SLC. (Further details published in Vol. 178, No. 2.)
June 23–24, 1986 Gaithersburg, MD, U.S.A.	**Workshop on Quantitative X-Ray Diffraction Analysis** Contact: Leslie Struble, B348 Research Building, National Bureau of Standards, Gaithersburg, MD 20899, U.S.A. Tel.: (301) 921 2845.
June 23–27, 1986 Copenhagen, Denmark	**Modern Trends in Activation Analysis, 7th International Conference** Contact: Dr. K. Heydorn, General Chairman MTAA-7, Risø National Laboratory, Post Box 49, DK-4000 Roskilde, Denmark. (Further details published in Vol. 169.)
June 25–27, 1986 Verona, Italy	**International Conference on Developments in Analytical Methods in Pharmaceutical, Biomedical and Forensic Sciences** Contact: Dr. Alberto Frigerio, Italian Group for Mass Spectrometry in Biochemistry and Medicine, via Eustachi 36, 20129 Milan, Italy.
July 7–10, 1986 Bordeaux, France	**2nd International Meeting on Chemical Sensors** Contact: Dr. Claude Lucat, 2nd International Meeting on Chemical Sensors, Université de Bordeaux I, 351, cours de la Libération, 33405 Talence, Cedex, France.

July 14–17, 1986 Ottawa, Canada	**10th International CODATA Conference** Contact: Mrs. Lois Baignée, Executive Secretary CODATA '86, Conference Services, National Research Council of Canada, Montreal Road, Ottawa, K1A OR6 Canada. (Further details published in Vol. 172.)
July 20–26, 1986 Bristol, U.K.	**SAC 86 – International Conference and Exhibition on Analytical Chemistry** Contact: Miss P.E. Hutchinson, Royal Society of Chemistry, Analytical Division, Burlington House, London W1V 0BN, U.K. Tel.: (01) 734-9971, (Further details published in Vol. 169.)
Aug. 10–17, 1986 Ottawa, Canada	**6th International Congress of Pesticide Chemistry** Contact: T.H.G. Micheal, Chemical Institute of Canada, 151 Slater Street, Suite 906, Ottawa, Ontario, Canada K1P 5H3. Tel.: (613) 233-5623. Telex: 053-4306 AIC.
Aug. 17–21, 1986 Seattle, WA, U.S.A.	**6th International Conference on Methods in Protein Sequence Analysis** Contact: MPSA, Conference Management, GH-22 University of Washington, Seattle, WA, U.S.A. Tel.: (206) 543-2300, telex: (910) 474 0096 UW UI.
Aug. 17–23, 1986 The Hague, The Netherlands	**15th International Symposium on the Chemistry of Natural Products** Contact: Dr. G.J. Koomen, Secretary, 15th IUPAC International Symposium on the Chemistry of Natural Products, Laboratorium voor Organische Scheikunde, Universiteit van Amsterdam, Nieuwe Achtergracht 102, 1018 WS Amsterdam, The Netherlands.
Aug. 25–29, 1986 Antwerp, Belgium	**10th International Symposium on Microchemical Techniques** Contact: Dr. R. Dewolfs, University of Antwerp, Department of Chemistry, Universiteitsplein 1, B-2610 Wilrijk, Belgium. Tel.: 03/828.25.28 (ext. 204). Telex: 33646. (Further details published in Vol. 169.)
Aug. 26–27, 1986 Antwerp, Belgium	**3rd International Laser Microprobe Mass Spectrometry Workshop 1986** Contact: L. Van Vaeck, UIA-University of Antwerp, Department of Chemistry, Universiteitsplein 1, B-2610 Wilrijk, Belgium. Tel.: (03) 828 25 28, telex: 33646.
Aug. 26–29, 1986 Dunedin, New Zealand	**10th Conference of the Australian and New Zealand Society for Mass Spectrometry** Contact: Dr. J. Cutfield, Department of Biochemistry, University of Otago, Box 56, Dunedin, New Zealand. (Further details published in Vol. 175.)
Aug. 31–Sept. 5, 1986 Eugene, OR, U.S.A.	**10th International Conference on Raman Spectroscopy** Contact: Prof. Warner L. Peticolas, Department of Chemistry, University of Oregon, Eugene, OR 97403-1210, U.S.A.
Sept., 1986 Graz, Austria	**4th Conference on Computer Based Analytical Chemistry** Contact: Dr. Wolfhard Wegscheider, Institut für Analytische Chemie, Mikro- und Radiochemie, Technische Universität, Technikerstrasse 4, A-8010 Graz, Austria. Tel: (0316) 7061-8300/8301. (Further details published in Vol. 172.)
Sept. 8–10, 1986 Freiburg, F.R.G.	**4th International Symposium on Bioluminescence and Chemiluminescence** Contact: Dr. J. Schölmerich, Medizinschi Universitätsklinik, D-7800 Freiburg, F.R.G.

Sept. 9–12, 1986 London, U.K.	**5th Meeting of the International Electrophoresis Society, "Electrophoresis '86"** Contact: Dr. M.J. Dunn, Muscle Research Unit, Royal Postgraduate Medical School, DuCane Road, London W12 0HS, U.K., Tel.: 01-743-2030 ext. 338.
Sept. 9–12, 1986 Preveca, Greece	**2nd International Symposium on Kinetics in Analytical Chemistry** Contact: Prof. N. Evmirides, Laboratory of Analytical Chemistry, Chemistry Department, University of Ioannina, Ioannina, Greece.
Sept. 15–18, 1986 Houston, TX, U.S.A.	**22nd International Symposium on Advances in Chromatography** Contact: Professor A. Zlatkis, Chemistry Department, University of Houston, Houston 77004 TX, U.S.A. Tel.: (713) 749 2633. (Further details published in Vol. 178, No. 2.)
Sept. 15–19, 1986 Reading, U.K.	**7th International Symposium on Analytical and Applied Pyrolysis** Contact: Dr. C.S. Gutteridge, Cadbury Scheppes Plc, The Lord Zuckerman Research Centre, The University, Whiteknights, P.O. Box 234, Reading RJ6 2LA, U.K.
Sept. 29–Oct. 3, 1986 St. Louis, MA, U.S.A.	**FACSS '86, Federation of Analytical Chemistry and Spectroscopy Societies 1986 Meeting** Contact: Dr. Marshall Fishman, U.S. Department of Agriculture, 600 E. Mermaid Lane, Wyndmoor, PA 19118, U.S.A. Tel.: (215) 233-6450. (Further details published in Vol. 178, No. 2.)
Oct. 6–8, 1986 Mátrafüred, Hungary	**Bioelectroanalytical Symposium 1986** Contact: Organizing Committee of Bioelectroanalytical Symposium 1986, Institute for General and Analytical Chemistry, Technical University, Gellért tér 4, 1502 Budapest, Hungary.
Oct. 7–11, 1986 Seattle, WA, U.S.A.	**5th International Symposium on New Spectroscopic Methods for Biomedical Research and Short Courses on Biomedical ESCA and Biomedical FTIR** Contact: Buddy D. Ratner, Ph.D., Department of Chemical Engineering, BF-10, University of Washington, Seattle, WA 98195, U.S.A. Tel.: (206) 545 1005.
Oct. 8–10, 1986 Palma de Mallorca, Spain	**3rd Symposium on Handling of Environmental and Biological Samples in Chromatography** Contact: Prof. Dr. R.W. Frei, Department of Analytical Chemistry, Free University, De Boelelaan 1083, 1081 HV Amsterdam, The Netherlands. Tel.: (020) 5485379.
Oct. 19–22, 1986 Boston, MA, U.S.A.	**4th International Symposium on Laboratory Robotics** Contact: Gerald L. Hawk, Ph.D. and Janet Strimaitis, Zymark Corporation, Zymark Center, Hopkinton, MA 01748, U.S.A. Tel.: (617) 435-9501.
Oct. 20–22, 1986 Baden-Baden, F.R.G.	**6th International Symposium on High-Performance Liquid Chromatography of Proteins, Peptides and Polynucleotides** Contact: Secretariat 6th ISPPP, P.O. Box 3980, D-6500 Mainz, F.R.G.
Oct. 20–24, 1986 New York, NY, U.S.A.	**The Silver Jubilee Eastern Analytical Symposium** Contact: Dr. S. David Klein, EAS Publicity, 642 Cranbury Cross Road, North Brunswick, NJ 08902, U.S.A. Tel.: (201) 846-1582. (Further details published in Vol. 178, No. 2.)

Oct. 22–24, 1986 Montreux, Switzerland	**4th Symposium on Liquid Chromatography–Mass Spectrometry and Mass Spectrometry–Mass Spectrometry** Contact: Professor Dr. R.W. Frei, Department of Analytical Chemistry, Free University, De Boelelaan 1083, 1081 HV Amsterdam, The Netherlands. Tel.: (020) 5485379.
Nov. 11–13, 1986 Stockholm, Sweden	**International Symposium on Immunoassays – Present Status and Future Perspectives** Contact: The Swedish Academy of Pharmaceutical Sciences, P.O. Box 1136, S-111 81 Stockholm, Sweden.
Nov. 17–20, 1986 Gaithersburg, MD, U.S.A.	**Scientific Software for Supercomputing** Contact: Francis E. Sullivan, A151 Technology Building, National Bureau of Standards, Gaithersburg, MD 20899, U.S.A. Tel.: (301) 921 3395.
Nov. 18–20, 1986 Teddington, U.K.	**4th International Conference on Quantitative Surface Analysis, Techniques and Applications and VAMAS Workshop** Contact: Conference Secretary, Dr. G.C. Smith, Division of Materials Applications, National Physical Laboratory, Teddington, Middlesex, TW11 OLW, U.K. Tel.: (01) 977 3222, telex: 262344. (Further details published in Vol. 178, No. 2.)
April 6–9, 1987 Cardiff, U.K.	**International Symposium on Electroanalysis in Biomedical, Environmental and Industrial Sciences** Contact: Short Courses Section, UWIST, P.O. Box 68, Cardiff CF1 3XA, Wales, U.K. Tel.: (0222) 42588, ext. 2213. (Further details published in Vol. 178, No. 2.)
April 28–May 1, 1987 Sydney, Australia	**9th Australian Symposium on Analytical Chemistry** Contact: The Secretary 9AC, Mr. John Eames, P.O. Box 137, North Ryde, N.S.W. 2113, Australia. Tel.: (02) 887-8688. (Further details published in Vol. 178, No. 2.)
May 11–14, 1987 Ghent, Belgium	**2nd International Symposium on Quantitative Luminescence Spectrometry in Biomedical Sciences** Contact: Dr. W. Baeyens, State University of Ghent, Laboratory of Pharmaceutical Chemistry and Drug Quality Control, Harelbekestraat 72, B-9000 Ghent, Belgium. (Further details published in Vol. 178, No. 2.)
May 17–22, 1987 Tokyo, Japan	**CHEMRAWN VI, World Conference on Advanced Materials Needed for Innovations – Energy, Transportation and Communications** Contact: Mr. H. Hamada, Executive Director, The Chemical Society of Japan, 1-5 Kanda-Suragadi, Chiyoda-ku, Tokyo, Japan.
June 17–19, 1987 Fort Collins, CO, U.S.A.	**Conference on Chemically Modified Surfaces** Contact: W. Collins, Mail Stop C41C00, Dow Corning Corporation, Midland, MI 48686-0994, U.S.A.
June 21–26, 1987 Toronto, Canada	**XXV Colloquium Spectroscopium Internationale** Contact: Mr. L. Forget, Executive Secretary XXV CSI, National Research Council of Canada, Ottawa, K1A 0R6 Canada. Tel.: (613) 993-9009, telex: 053-3145. (Further details published in Vol. 172.)

June 28–July 4, 1987 Amsterdam, The Netherlands	**HPLC '87, 11th International Symposium on Column Liquid Chromatography** Contact: Organisatie Bureau Amsterdam bv, Europaplein, 1078 GZ Amsterdam, The Netherlands. Tel.: (31) 20-440807, telex: 13499 raico nl.
July 13–18, 1987 Sofia, Bulgaria	**31st IUPAC Congress** Contact: Dr. R. Vlahov, Institute of Organic Chemistry, Bulgarian Academy of Sciences, 1113 Sofia, Bulgaria. Telex: 22729 ECHBAN BG.
Aug. 24–28, 1987 Vienna, Austria	**6th International Conference on Fourier Transform Spectroscopy** Contact: Interconvention, P.O. Box 80, A-1107 Vienna, Austria. Tel.: (222) 57 63 05, 57 62 88, telex: 11 12 10.
Aug. 25–30, 1987 Beijing, China	**8th International Conference on Computers in Chemical Research and Education** Contact: Cheng Qian, 345 Lingling Road, 200032 Shanghai, China. Telex: 33354 SIOC CN.
Aug. 30–Sept. 4, 1987 Amsterdam, The Netherlands	**EUCMOS XVIII, 18th European Congress on Molecular Spectroscopy** Contact: EUCMOS XVIII, c/o Municipal Congress Bureau, P.O. Box 2289, 1000 CG Amsterdam, The Netherlands. Tel.: (3120) 552 3459, telex: 16460 anal. chem.
Sept. 7–11, 1987 Paris, France	**Euroanalysis VI, European Conference on all Aspects of Analytical Sciences** Contact: G.A.M.S., 88 Boulevard Malesherbes, 75008 Paris, France.
Sept. 28–Oct. 1, 1987 Gaithersburg, MD, U.S.A.	**Accuracy in Trace Analysis – Accomplishments, Goals, Challenges** Contact: Harry Hertz, A309 Chemistry Building, National Bureau of Standards, Gaithersburg, MD 20899, U.S.A. Tel.: (301) 921 2851.
April 18–21, 1988 Las Vegas, NV, U.S.A.	**Flow Analysis IV, An International Conference on Flow Analysis** Contact: Dr. Gilbert E. Pacey, Department of Chemistry, Miami University, Oxford, OH 45056, U.S.A.

Now Available

IQUID CHROMATOGRAPHY DETECTORS

Second, completely revised edition

/ **R.P.W. SCOTT,** *Perkin-Elmer Corporation, Instrument Group, Main Avenue, Norwalk, CT, U.S.A.*

rnal of Chromatography Library - Volume 33

renaissance of liquid chromatography, provoked by the ctacular development of gas-liquid chromatography, took ce in the late 1960's and early 1970's. The first edition of book published in 1977 describes the detectors that were ilable at that time and which provided a performance iching that of the contemporary equipment with which they e associated. It is interesting to note that the most popular ectors then, the UV detector, the refractometer detector, fluorescence detector and the electrical conductivity ector are still the most commonly used detectors today, rly a decade later. Detector design, however, has changed y significantly over the intervening years. Modern high-ciency columns provide very narrow peaks and very fast arations, and thus the physical design of the detectors had hange to meet these new challenges. In 1977, there was real understanding of the important role played by the ector in the overall function of the chromatographic system although some of the factors were pointed out in the first tion of this book, in retrospect they appeared to be little lerstood.

s second edition gives an entirely new presentation of the ject of liquid chromatography detectors. It contains tions dealing with the fundamental aspects of the inter-on between columns and detectors and the interaction ween ancillary equipment and the detector. It brings the der up-to-date with new designs and novel detecting tems that have been developed since 1977 and extends nificantly the subject of the association of the liquid chro-tography detector with spectroscopic techniques. In par-ilar the book now explores the association of liquid chro-tography with nuclear magnetic resonance spectroscopy, ared spectroscopy and atomic absorption spectroscopy. s book not only gives a comprehensive treatment of the ject of liquid chromatography detectors and provides a onal procedure for defining their performance and so mit valid comparisons, but also discusses detector per-mance in relation to the whole of the chromatographic tem.

e the first edition, this book is expected to be well received.

CONTENTS. Chapter 1. History, Function and Classification of Detectors. History and Function. Classification of Detectors. **2. Performance Criteria of Liquid Chromatography Detectors.** Principal Detector Characteristics. The Nature of the Detector Output. Units Employed in Detector Specifications. The Dynamic Range of a Detector. Detector Linearity. Detector Response. Detector Noise. Detector Sensitivity. The Total Detecting System Dispersion. Extra Column Dispersion. Connecting Tube Form, Dimensions and Volume. Cell Dimensions and Cell Volume. Overall Detector Time Constant (Sensor and Electronics). The Time Constant of the Recorder. Pressure Sensitivity. Flow Sensitivity. Temperature Sensitivity. Summary of Detector Criteria. **3. Bulk Property Detectors.** The Refractive Index Detector. The Electrical Conductivity Detector. The Dielectric Constant Detector. Additional Bulk Property Detecting Systems. **4. Solute Property Detectors.** The UV Absorption Detector. The Fluorometric Detector. Transport Detectors. The Electrochemical Detector. The Atomic Spectroscopic System as an Element Specific Detector. The Radioactivity Detector. Additional Solute Property Detectors. **5. Special Detector Techniques.** Multi-functional Detectors. Chemical Derivatization as a Sensitivity Enhancement Technique. The Differential Detector. Integral Detection. Vacancy Chromatography. **6. Spectroscopy in Conjunction with Liquid Chromatography to Identify Solute Structure.** The Combination of the Liquid Chromatograph with the Nuclear Magnetic Resonance Spectrometer. The Combination of the Liquid Chromatograph with the Mass Spectrometer. The Combination of the Infrared Spectrometer with the Liquid Chromatograph. **7. Liquid Chromatographic Data Acquisition and Computer Processing.** Data Acquisition. Transmission of the Data to the Computer. Data Processing and Reporting. Data Processing. Data Acquisition Parameters and Chromatograph Control. Presentation of Chromatograms. **8. The Selection of the Appropriate Detector.** The UV Detector. The Refractive Index Detector. The Fluorescence Detector. The Electrical Conductivity Detector. Summary. Practical Hints on Detector Operation. Quantitative and Qualitative Analysis. Manual Measurement of Chromatographic Data. Computer Data Processing. Qualitative Analysis. Precision as an Alternative to Resolution. Quantitative Analysis. Some Physical Properties of Solvents in Common Use in Liquid Chromatography. List of Symbols. Appendix. Synopsis and References are included at the end of each chapter.

March 1986 xvi + 272 pages
Price: US $ 64.75 / 175.00 Dutch guilders
ISBN 0-444-42610-8

REVIEW

"This book . . . is a well-balanced, practical review of modern LC detectors. This first comprehensive book devoted to LC detectors . . . valuable to workers in academic and industrial laboratories who desire a clear understanding of the principles of detection in order to choose a detector suitable for their research needs." (Journal of the American Chemical Society)

"It is recommended to any liquid chromatographer who desires to have a thorough knowledge of detection principles, who would like to get the most information from his available detectors, or who is interested in pursuing development of a new detector." (Analytical Chemistry)

To Elsevier

Please supply ..... copy(ies) of
Liquid Chromatography Detectors 2nd edition
by R.P.W. Scott
Price: US $ 64.75 or 175.00 Dutch Guilders

☐ I enclose my cheque
☐ Please charge my ..... card
No ..... Valid until .....

Name .....
Full address .....
.....
..... Postal code .....

Signature

ELSEVIER

Elsevier Science Publishers
P.O. Box 211
1000 AE Amsterdam
The Netherlands

Elsevier Science Publishing Co., Inc.
P.O. Box 1663
Grand Central Station
New York, NY 10163, USA

7352

Advantages of Mass Spectrometry in Protein Chemistry *(P. Roepstorff)*. Column Techniques in the Preparation of Biological Samples of Gas Chromatography-Mass Spectrometry *(J. Sjövall)*. Analysis of Glucuronides Using Condensed Phase Ionization Techniques *(C. Fenselau)*. Analysis of Acylcarnitines in Human Metabolic Disease by Thermospray Liquid Chromatography/Mass Spectrometry *(D. J. Liberato et al.)*. Mass Spectrometry and Stable Isotopes in the Study of Mechanistic Aspects of Metabolic Pathways *(T. A. Baillie)*. Structure Elucidation of Biopolymers by FAB-MS *(H. R. Morris et al.)*. Application of Negative Ion FABMS to the Structural Elucidation of Glycolipids Including Gangliosides and Synthetic Glycoglycerolipids *(M. Iwamori et al.)*. Potentials of Fast Atom Bombardment Mass Spectrometry in the Analysis of Glycoconjugates *(H. Egge, J. Peter-Katalinić)*. Chemical Diagnosis of the Inherited Metabolic Diseases by Gas Chromatography-Mass Spectrometry - Differential Chemical Diagnosis of Lactic Acidosis *(I. Matsumoto et al.)*. The Bioavailability Study of Phenytoin in Epileptic Patients During Long Term Therapy *(Y. Kasuya et al.)*. Study of Metabolism and Prenatal Diagnosis of Inborn Metabolic Disorders Using Stable Isotopes *(K. Tanaka et al.)*. Clinical Applications of Steroid Conjugate Analysis by Liquid SIMS *(C. H. L. Shackleton, W. Chai)*. Progesterone Metabolism in $T47D_{co}$ Human Breast Cancer Cells *(P. V. Fennessey et al.)*. Mass Spectrometry of Nucleic Acid Constituents and Related Compounds *(J. A. McCloskey)*. Mass Spectrometric Identification of DNA Adducts Formed by Carcinogenic Aromatic Amines *(R. K. Mitchum et al.)*. Characterization of Nucleoside and Nucleotide Covalent Adducts of Dehydroretronecine by Liquid Secondary Ion Mass Spectrometry *(M. L. Deinzer, A. L. Burlingame)*. Mass Spectrometry in Molecular Design *(L. Grotjahn, H. Steinert)*. Poster Sessions. List of Participants. Indexes.

Electroanalysis

Theory and Applications in Aqueous and Non-Aqueous Media and in Automated Chemical Control

Dahmen, E. A. M. F.

(Techniques and Instrumentation in Analytical Chemistry)

1986 About 250 p.
ISBN 0-444-42534-9
In preparation

Since the appearance of the well-known books by Kolthoff, Lingane and Delahay in the early 1950s thousands of papers in the field of electroanalysis have been published; however, up-to-date comprehensive textbooks on electroanalysis are scarce. This book aims to fill the gap to a certain extent, viz. by presenting, on the one hand, a systematic treatment of electroanalysis and its most frequently-used techniques on an explanatory basis, and by illustrating, on the other hand, the practical application of these techniques to chemical control in industry and to the health and environmental sciences. As today such a control involves more and more automation and computerization, electroanalysis with its direct input and/or output of electrical signals is often advantageous over other techniques, especially because recent progress in electronics and computerization has greatly stimulated new developments of the electroanalytical techniques themselves, not only on the level of pure research, but also in the availability of commercial apparatus.

Contents: Preface. General Introduction. **Part A. Electroanalysis (systematic treatment).** 1. Introduction. 2. Non-faradaic methods of electrochemical analysis. 3. Faradaic methods of electrochemical analysis. **Part B. Electroanalysis in non-aqueous media.** 4. Introduction. **Part C. Electroanalysis in automated chemical control.** 5. Introduction. References are included at the end of each chapter. Appendix. Indexes.

Mass Spectrometry of Large Molecules

(Lectures of a Course held at the Joint Research Centre ISPRA (Italy), 5-9 Sept. 1983)

Facchetti, S. *(editor)*

1985 xii + 322 p.
US $ 85.25 Dfl. 230.00
ISBN 0-444-42456-3

The lectures in this volume were given at a course on mass spectrometry of large molecules, organised within the framework of the Training and Education programme of the Joint Research Centre of the European Communities. Although first presented in 1983 most of the lectures have since been updated by their authors. This volume considers the

most important ionization techniques in current use and illustrates the latest developments in the instrumentation in high molecular weight mass spectrometry. The greater part of the book, however, has been dedicated to the identification of the molecules of biological and biomedical interest, and of polymers, as well as the use of mass spectrometry in the study of structural problems and in research for applications.

Contents: Classification of biological macromolecules. A survey for macromolecular analysis in mass spectrometry *(F. Campagnari)*. Instrumentation in high molecular weight mass spectrometry *(A. J. H. Boerboom)*. Simultaneous ion detection *(A. J. H. Boerboom)*. Simultaneous ion detection *(A. J. H. Boerboom)*. Direct inlet systems for identification of labile and/or large molecules *(P. Traldi et al.)*. Structure and elucidation of "large" biological molecules *(D. H. Williams)*. Mass spectrometry of intermediate molecular weight (1000 <m/z <10,000 d) labile biological substances *(A. L. Burlingame)*. Perspective on problems in biomolecular mass spectrometry *(H. R. Morris et al.)*. New biomedical applications of mass spectrometry *(H. R. Morris et al.)*. Modification of peptides for mass spectrometry *(R. Self et al.)*. Structural studies on peptides by mass spectrometry *(D. H. Williams)*. Mass spectrometric analysis of bile acids in neonatal liver diseases *(J. O. Whitney, A. L. Burlingame)*. The potential of fast atom bombardment mass spectrometry in food and agricultural science *(R. Self et al.)*. Negative ion chemical ionization mass spectrometry *(M. Oehme)*. Application of negative ion mass spectrometry to medium-size and large molecules *(M. Oehme)*. Pyrolysis mass spectrometry *(A. J. H. Boerboom)*. Direct mass spectrometry of polymers *(S. Foti, G. Montaudo)*. The mass spectrometer as synthetizer-analyser device in polymer chemistry: the polymerization of cyclophosphazenes *(P. Traldi et al.)*. Subject Index.

CHECK WITH YOUR LIBRARY THAT THESE BOOKS ARE AVAILABLE TO YOU

Advances in Steroid Analysis '84

(Proc. of the Symp., Szeged, Hungary, 12-14 June 1984)

Görög, S. *(editor)*

(Analytical Chemistry Symposia Series, 23)

1985 xii + 604 p.
US $ 139.00 Dfl. 375.00
ISBN 0-444-99533-1

This volume comprises the Proceedings of the 2nd Symposium on the Analysis of Steroids which was attended by leading experts, from 17 countries, who in their contributions covered the analysis of all important groups of steroids: hormones and other steroid drugs, sterols, vitamins D, bile acids, cardiac glycosides, sapogenins.

As in the case of the first symposium, which was held in 1981, the general aim of this recent meeting was again to provide an international forum of publication for steroid analysts working in biochemical, clinical, pharmaceutical and industrial laboratories, to present an overview on the state-of-the-art and current methodology of steroid analysis. As the programme of the symposium was methodology-oriented, the main chapters of this volume have been compiled in a manner to cover primarily individual analytical techniques. Some papers, which are not methodology-oriented, are collected into a "General" chapter. This is followed by a short chapter dealing with protein-binding and receptor-binding studies. The most comprehensive chapter is concerned with immunological (RIA, EIA etc.) methods. Gas chromatography (mainly in conjunction with mass spectrometry) and high-performance liquid chromatography are equally well presented. This volume is concluded with a chapter containing miscellaneous methods, such as thin-layer densitometry, photometry, enzymatic assays, and CD spectroscopy.

Contents: General *(8 papers)*. Protein - Binding and Receptor - Binding Studies *(4 papers)*. Immunological Methods. Radioimmunoassays *(16 papers)*. Enzyme Immunoassays and Related Techniques *(4 papers)*. Chromatography. Gas Chromatography *(7 papers)*. Gas Chromatography - Mass Spectrometry *(8 papers)*. High-Performance Liquid Chromatography *(11 papers)*. Other Chromatographic Techniques *(3 papers)*.

Miscellaneous. Enzymatic and Non-Enzymatic Photometric and Luminescence Methods *(4 papers)*. Other Methods *(3 papers)*. Subject Index.

Gradient Elution in Column Liquid Chromatography

Theory and Practice

Jandera, P. and J. Churáček

(Journal of Chromatography Library, 31)

1985 xx+510 p.
US $ 90.75 Dfl. 245.00
ISBN 0-444-42124-6

Written for workers using HPLC for separating and analysing complex sample mixtures, this is a comprehensive discussion of the very powerful technique of gradient elution. The theory of gradient elution liquid column chromatography is presented in detail and in a unified way that makes possible the calculation of retention characteristics and optimization of the profile of gradients in various liquid chromatographic systems.

Much of the book is devoted to practical applications of gradient elution LC in the separation of a wide variety of compounds. In the section on instrumentation, the various commercially available devices used to prepare the gradients of mobile phase concentrations are systematically classified, compared and discussed.

Contents: Part I. Isocratic Elution Chromatography. II. Theory of Chromatography with Programmed Composition of the Mobile Phase. III. Instrumental and Other Practical Aspects of Chromatography with Programmed Composition of the Mobile Phase. IV. Applications of Gradient Elution in Liquid Chromatography. Appendices. Subject Index.

New Approaches in Liquid Chromatography

(Proc. of the 2nd Ann. American-Eastern European Symp. on Advances in Liquid Chromatography, Szeged, Hungary, 16-18 June 1982)

Kalász, H. *(editor)*

(Analytical Chemistry Symposia Series, 16)

1984 x+292 p.
US $ 64.75 Dfl. 175.00
ISBN 0-444-99642-7

This volume contains the full texts of the twenty-three papers presented at the 2nd Annual American-Eastern European Symposium by scientists from the U.S.A., the U.S.S.R., Czechoslovakia, Germany, Hungary and Poland. The topics covered include: HPLC of peptides and proteins; displacement chromatography using mathematical modelling of separation techniques; displacement mode of development on thin-layer plates and the effect of the length of development; sample size and position of spots in the separation of structurally related compounds; the characterization of the stationary phases for HPLC; optimization of HPLC and gel chromatography; novel results in TLC; and results of analytical and preparative separations of amino acids, peptides and proteins.

Contents: High-Performance Liquid Chromatography *(4 papers)*. Displacement Chromatography *(2 papers)*. Characterization of Liquid Chromatographic Stationary Phases *(5 papers)*. Thin-Layer Chromatography *(2 papers)*. Analysis of Amino Acids *(4 papers)*. Analytical and Preparative Separation of Peptides and Proteins *(6 papers)*. Index.

ASK YOUR LIBRARY FOR THESE BOOKS

Basic GC/MS - Principles and Techniques

Karasek, F. and Clement R.

1986 About 300 p.
In preparation

This book describing the basic principles and techniques of gas chromatography and mass spectrometry is accompanied by software designed to provide rapid access to current information in the area of gas chromatography/mass spectrometry. As well as providing a useful supplement to the book it may be used as an independent reference.

The software, by F. Settle and M. Pleva, consists of two parts: files containing information and the program which allows the information to be quickly extracted from the files. Each file is designated by a 5-chapter (2 letters, 3 digits) file code, for example GM120. A number of special purpose files are included in the module: a module index, a glossary, and a list of keywords.

Microcolumn High-Performance Liquid Chromatography

Kucera, P.

(Journal of Chromatography Library, 28)

1984. 1st repr. 1985 xvi+302 p.
US $ 61.00 Dfl. 165.00
ISBN 0-444-42290-0

The distinguished research workers and university professors who have contributed to this important work have adopted a textbook-type approach to the discussion of the theoretical aspects of new microcolumn techniques. The practical coverage includes instrumentation, design, columns, detectors, injectors, connecting tubing, gradient elution and special analytical techniques, LC-MS, derivatization, etc., and applications are described using various compounds (e.g. drugs, substances of biological origin, proteins, nucleotides, industrial extracts).

Contents: Chapter 1. Narrow-Bore and Microbore Columns in Liquid Chromatography *(G. Guiochon and H. Colin).* 2. Design of a Microbore Column Liquid Chromatograph *(P. Kucera).* 3. Theory and Practice of High-Speed Microbore HPLC *(R. A. Hartwick and D. D. Dezaro).* 4. Special Analytical Techniques *(P. Kucera and G. Manius).* 5. Chemical Derivatization Techniques Using Microcolumns *(P. Kucera and H. Umagat).* 6. Applications of Microbore HPLC *(P. Kucera and R. A. Hartwick).* 7. Liquid Chromatography in Columns of Capillary Dimensions *(M. Novotny).* 8. Micro LC/MS Coupling *(J. Henion).* Subject Index.

Analytical Spectroscopy

(Proc. of the 26th Conf. on Analytical Chemistry in Energy Technology, Knoxville, TN, 11-13 Oct. 1983)

Lyon, W. S. *(editor)*

(Analytical Chemistry Symposia Series, 19)

1984 xiv+394 p.
US $ 72.25 Dfl. 195.00
ISBN 0-444-42312-5

These Proceedings present detailed, state-of-the-art discussions on two rapidly expanding areas of analytical chemistry - laser spectroscopy and mass spectrometry. Of particular interest will be the articles on: resonance ionization mass spectrometry (RIMS), a new technique that makes high sensitivity elemental analyses possible; new and improved techniques and applications of plasma spectroscopy, including hot cell operations; and advances in nuclear techniques and gamma spectrometry.

Contents: Lasers *(15 papers).* Mass Spectrometry *(14 papers).* Plasma *(8 papers).* Nuclear *(11 papers).* Other Spectroscopic Techniques *(16 papers).* Index.

CHECK WITH YOUR LIBRARY THAT THESE BOOKS ARE AVAILABLE TO YOU

Topics in Forensic and Analytical Toxicology

(Proc. of the Ann. Eur. Meeting of the Int. Assoc. of Forensic Toxicologists, Munich, 21-25 Aug. 1983)

Maes, R. A. A. *(editor)*

(Analytical Chemistry Symposia Series, 20)

1984 x+214 p.
US $ 55.50 Dfl. 150.00
ISBN 0-444-42313-3

In this volume are the invited and selected papers from the Annual European Meeting of the International Association of Forensic Toxicologists which was attended by many distinguished participants.

Among the topics covered in the book are: drugs and driving; drugs of abuse; toxicological analysis of drugs, their metabolites and their clinical and forensic implications; mass spectrometry in toxicology; combination methodology in toxicological analysis; systematic toxicological analysis; and toxicology in developing countries. The round table discussions on quality control and documentation and on postgraduate education in forensic toxicology are also included.

For the modern forensic toxicologist, today's demands for analyses with a high degree of accuracy, sensitivity and precision make it essential that he keep abreast of this fast-moving field. The papers in this volume will provide much useful and interesting information and, it is hoped, will help lead to some new approaches to problems in forensic toxicology.

Evaluation and Optimization of Laboratory Methods and Analytical Procedures

Massart, D. L., L. Kaufman and A. Dijkstra

(Techniques and Instrumentation in Analytical Chemistry, 1)

1978. 2nd repr. 1984 xvi+596 p.
US $ 68.50 Dfl. 185.00
ISBN 0-444-41743-5

The purpose of this book is to provide detailed treatment, in a single volume, of formal methods for optimization in analytical chemistry. All aspects of optimization are discussed, from the simple evaluation of procedures to the organization of laboratories or the selection of optimal complex analytical programmes. Quantitative discrete analysis as well as qualitative and continuous measurement techniques are evaluated.

"It is a comprehensive and practical handbook. All aspects of optimization are discussed ..."

Laboratory Equipment

ASK YOUR LIBRARY FOR THESE BOOKS

Microcolumn Separations

Columns, Instrumentation and Ancillary Techniques

Novotny, M. V. and D. Ishii *(editors)*

(Journal of Chromatography Library, 30)

1985 xii+336 p.
US $ 64.75 Dfl. 175.00
ISBN 0-444-42429-6

Edited by two of the pioneers of microcolumn chromatography and written by recognized experts in the field, this timely book summarizes new advances in microcolumn liquid chromatography, capillary supercritical fluid chromatography and microelectrophoresis. Its unique combination of expert knowledge from leading laboratories in the U.S.A., Japan and Switzerland, results in a particularly in-depth yet comprehensive coverage of the various aspects of microcolumn separation methods. It is recommended to chromatographers and all analytical chemists who share an interest in the advantages of miniaturized separation systems.

Contents: **Column Studies.** Open-tubular micro-HPLC *(D. Ishii, T. Takeuchi).* Analytical characteristics of packed capillary columns *(M. Novotny).* Microcolumn size-exclusion HPLC *(S. Mori et al.).* High resolution reversed-phase LC with a packed glass micro-capillary column *(Y. Hirata, K. Jinno).* **Miniaturized Systems.** Sources of extracolumn band-broadening in microcolumn LC *(J. C. Gluckman, M. Novotny).* Component miniaturization in HPLC *(D. Ishii, T. Takeuchi).* Fast analysis by microbore HPLC *(R. A. Hartwick, R. F. Meyer).* Capillary supercritical fluid chromatography *(M. Novotny).* Capillary zone electrophoresis *(J. W. Jorgenson, K. D. Lukacs).* **Spectroscopic Detection.** Optical detectors for microcolumn LC *(E. S. Yeung).* Laser-based chromatographic detectors *(T. Imasaka).* The combination of micro-HPLC/IR spectroscopy *(K. Jinno et al.).* Principles and applications of flame-based detection in microcolumn LC *(V. L. McGuffin, M. Novotny).* New approaches to interfacing LC and MS *(S. Tsuge).* Instrumentation and applications of micro-LC/MS *(J. Henion).* **Electrochemical Detection.** Miniaturized ion chromatography *(S. Rokushika, H. Hatano).* Femtoliter cell volume potentiometric detector for open-tubular column LC *(A. Manz et al.).* Miniaturized voltammetric detectors *(M. Goto).* Subject Index.

Instrumental Liquid Chromatography

A Practical Manual on High-Performance Liquid Chromatographic Methods. 2nd Rev. Ed.

Parris, N. A.

(Journal of Chromatography Library, 27)

1984. 1st repr. 1985 xiv+432 p.
US $ 83.25 Dfl. 225.00
ISBN 0-444-42061-4

A necessary acquisition for HPLC users, this practically oriented, easy-to-follow guide enables the reader to select appropriate instrumentation, injectors, columns, etc. Applications of liquid chromatography are described as well as the technique's potential for qualitative, quantitative and trace analysis and for preparative application. Numerous applications are tabulated and cross-referenced to sections on the optimization procedure of the particular methods.

It is the new edition of a book published in 1976, twice reprinted, and described as *"...one of the more useful and successful texts on HPLC... a most readable book packed with valuable information and advice... strongly recommended."* (Laboratory Practice). The format of the original is unchanged, but some 45% of the material is new or completely revised to bring the column technology and applications data up-to-date. Written for workers involved with the application or development of LC methods, it will also be of great value to those wishing to establish if methods for their particular interest have been reported or are feasible.

Contents: **Fundamentals and Instrumentation:** 1. Introduction and historical background. 2. Basic principles and terminology. 3. The chromatographic support and column. 4. Liquid chromatographic instrumentation. 5. Liquid chromatographic detection systems. 6. Modern electronic technology and its impact on LC automation. **Factors Influencing Chromatographic Selectivity:** 7. Nature of the mobile phase. 8. Liquid-solid (adsorption) chromatography. 9. Liquid-liquid (partition) chromatography. 10. Bonded-phase chromatography. 11. Ion-exchange and ion-pair chromatography. 12. Steric exclusion chromatography. **Uses of Liquid Chromatographic Procedures:** 13. Qualitative analysis. 14. Quantitative analysis. 15. Practical aspects of trace analysis. 16. Practical aspects of preparative liquid chromatography. **Applications of Liquid Chromatography.** 17. Published LC applications. Appendices. Subject index.

Contemporary Practice of Chromatography

Poole, C. F. and S. A. Schuette

1984. 1st repr. 1985 x+708 p.
US $ 59.00 Dfl. 159.00
ISBN 0-444-42410-5
Paperback
1984. 1st repr. as a paperback edition 1985
US $ 37.50 Dfl. 110.00
ISBN 0-444-42506-3

Written not for physical chemists, but for the many scientists in a wide variety of disciplines who use chromatography as an analytical tool, this book covers all areas of gas, liquid, and thin-layer chromatography; no other book offers the same scope. The authors have had considerable experience teaching graduate-level courses and the material presented here has been tried and tested, having formed the basis for short courses taught to industrial chemists.

Emphasis is on the practice of chromatographic methods, including "how to" sections and numerous examples of calculation methods. Extensively illustrated (especially the sections on instrumentation, column separations, thin-layer chromatography, and routine test methods), it also contains numerous tables of all useful constants, materials and formulas frequently used by chromatographers. Valuable features are the chapters on sample preparation for chromatographic analysis, and on instrumental methods for sample identification.

Indispensable for chemists, clinical chemists, biologists, pharmacists, environmental scientists, instrument manufacturers and many more. It is an ideal text for: graduate-level students; professional institutes offering short courses in chromatography; and chromatographers wishing to keep up to date with the field.

Contents: 1. Fundamental Relationships of Chromatography. 2. The Column in GC. 3. Instrumental Requirements for GC. 4. The Column in LC. 5. Instrumental Requirements for HPLC. 6. Preparative-Scale Chromatography. 7. Sample Preparation for Chromatographic Analysis. 8. Hyphenated Methods for Identification after Chromatographic Separation. 9. High Performance Thin-Layer Chromatography. Subject Index.

Ion-Selective Electrodes, 4

(Proc. of the 4th Symp., Mátrafüred, Hungary, 8-12 Oct. 1984)

Pungor, E. and I. Buzás *(editors)*

(Analytical Chemistry Symposia Series, 22)

1985 xvi+766 p.
US $ 168.50 Dfl. 455.00
ISBN 0-444-99553-6

This book contains the full text of the 51 lectures given at the symposium at which was raised a number of important issues in the field of Ion-Selective Electrodes. The questions and comments raised after the lectures are also mentioned in the book.

Recent scientific research on the working mechanisms of the ion-selective electrodes, the theory, selectivity and dynamic properties of ion-selective membranes are only the highlights of the papers delivered. At this highly successful symposium the most important topics dealt with were surveys on the development, mechanism and preparation of novel-ion-selective membranes, different types of chemically sensitive field effect transistors, their application in analytical and physical chemistry; the liquid membrane ion-selective eletrodes, their selectivity properties and their application to flow analysis; the chemically modified electrode sensors for biocomponents as well as flow injection analysis and monitoring of enzyme based reactions.

Numerous contributions appear on the application of ion-selective electrodes in practical fields such as in clinical analysis, in industrial analysis with computer interpretation of data, and the investigation of interference in measurements with ion-selective electrodes.

This publication will be useful to experts working in this rapidly developing field of analytical chemistry and enhancing and updating their knowledge on these sensors and therefore raising problems to be studied in the future and discussed at the next symposium in 1988 on Ion-Selective Electrodes.

Contents: **Plenary Lectures.** Chemical Sensor Mechanisms. A progress report *(R. P. Buck).* Polarization Studies with Ion-Selective Electrodes *(K. Cammann, G. A. Rechnitz).* Selectivity Properties of Ion-Selective Liquid Membrane Electrodes and their Application to Flow Analysis *(N. Ishibashi et al.).* Membrane Technological Optimization of Ion-Selective Electrodes Based on Solvent Polymeric Membranes for Clinical Applications *(U. Oesch et al.).* **Keynote Lectures.** Chemically Modified Electrode Sensors *(R. A. Durst).* Chemically Sensitive Field Effect Transistors: their Application in Analytical and Physical Chemistry *(J. Janata).* Bis(Crown Ether) Based Ion-Selective Electrodes *(K. Kimura, T. Shono).* Theoretical Treatment of the Dynamic Behaviour of Precipitate Based Ion-Selective Membrane Electrodes in the Presence of Interfering Ions *(E. Lindner et al.).* New Developments and Consequences of Theory of Ion-Selective Membranes *(W. E. Morf et al.).* Continuous Analysis with Ion-Selective Electrodes: Flow-Injection Analysis and Monitoring of Enzyme-Based Reactions *(J. D. R. Thomas).* Bis(Crown Ether)s for Potassium Ion-Selective Electrodes *(K. Tóth et al.).* Ion-Selective Field Effect Transistors: Different Types and Problems *(F. G. Vlasov).* **Discussion Lectures.** (37 papers). **Round Table Discussion on the Problems of Standards in Work with Ion-Selective Electrodes.** Further Studies of Ionic Activity Scales. Introductory Lecture *(R. G. Bates).* Determination of Mean Activity Coefficients with Ion-Selective Electrodes *(E. Lindner et al.).* **Subject Index.**

tinued from outside back cover)

CONTENTS

(Abstracted, Indexed in: Anal. Abstr.; Biol. Abstr.; Chem. Abstr.; Curr. Contents Phys. Chem. Earth Sci.; Life Sci.; Index Med.; Mass Spectrom. Bull.; Sci. Citation Index; Excerpta Med.)

(continued on inside back